MULTIVARIATE DATA-BASED SAFETY ANALYSIS IN DIGITALIZED PROCESS SYSTEMS

by

© Md. Tanjin Amin

A thesis submitted to the

School of Graduate Studies

in partial fulfilment of the requirement for the degree of

Doctor of Philosophy

Faculty of Engineering and Applied Science

Memorial University of Newfoundland

May 2022

St. John's Newfoundland and Labrador

Dedication

This thesis is dedicated to two noblewomen. The first one sacrificed her post-graduation due to my arrival on this earth and cherished me to complete the goal she had and could not achieve to secure my healthy childhood. The second one sacrificed her whole medical career to be with me during this entire journey. I am truly blessed to get you in my life!

Nirzhor

Abstract

Chemical process industries are vulnerable to accidents due to their inherent hazardous nature, complex operations, and growing size. Although the control system works as the first safety layer and is designed to maintain the setpoint within the safety limit, it cannot suppress all the deviations. Therefore, a warning system is used above the control layer to provide alarm(s) to the operators about unpermitted process deviations that cannot be negated by the controllers. Data-based process fault detection and diagnosis (FDD) and dynamic risk assessment (DRA) tools play a pivotal role to ensure that any significant process deviation is efficiently captured and necessary maintenance has been done to restore the process to normal operating mode. Besides, these tools can provide a detailed analysis of failure paths which are significant to prevent a fault from propagating into an accident.

Conventional univariate monitoring is easier to implement and comes as standard with distributed control systems (DCS). This conventional approach is unsuitable in digitalized process systems due to increased close loop control, large process dimension, and complex interaction among variables. Modern process industries require techniques that can handle the complexity and scale of process plants. Timely detection of faults, diagnosis of root cause(s) of faults that affect multiple variables, and predicting a quantitative measure of consequence is vital to ensure process safety and reliability. The thesis deals with multivariate data-driven FDD and DRA for digitalized process systems. This research aims to reduce the technological gaps between the current methods and prerequisites of automated FDD and DRA tools for multivariate safety analysis.

This thesis looks at improving all aspects of FDD and DRA methods, starting from data pre-processing to consequence analysis due to fault(s). First, the effect of data pre-processing is investigated in the context of multivariate FDD. Multivariate exponentially weighted moving

average (MEWMA) is found to be an effective way of filtering process data without adversely affecting their correlation structure. The MEWMA is combined with PCA-BN, and a new method called MEWMA-PCA-BN is proposed. The developed framework can detect and diagnose the fault earlier than many contemporary multivariate process monitoring models. In this work, a novel methodology has been proposed to construct the BNs from historical fault symptoms. Second, the selection of the principal components (PCs) for the PCA-BN method is made automated; the correlation dimension (CD) is used in this regard. Also, a new methodology is proposed for developing BNs from continuous process data.

Third, the prediction of the consequences of a fault has been adapted for multivariate process systems. A novel data-driven framework has been proposed for concurrent FDD and DRA using the naïve Bayes classifier (NBC), BN, and event tree analysis (ETA). This work utilizes a multivariate fault probability from NBC for dynamic failure prediction. It overcomes the limitation of using univariate probability in DRA. Finally, this thesis looks into improving the FDD performance by capturing the correlation structure of process variables and considering the consequence analysis. The R-vine copula is used to demystify the correlation structure accurately while the ETA predicts the consequences. Unacceptable deviation of risk is used as an indicator of a fault, and subsequently, root cause(s) diagnosis is performed using density quantile analysis (DQA). Industrial, experimental, and simulated datasets are used to test and validate the performance of the developed models. This thesis is an important step for multivariate data-driven FDD and DRA research.

Acknowledgement

At first, I would like to thank the almighty Allah for everything in my life. I suffered a terrible car accident on the Trans-Canada Highway during my PhD that has costed me only three months rather than my whole life. This is a second life for me, bestowed by Allah.

I want to express profound indebtedness to my supervisors, Dr. Faisal Khan, Dr. Salim Ahmed, and Dr. Syed Imtiaz. I got the foremost help from them in any situation. Their motivational feedbacks, research ideas, and patience were the key to reaching my goal. Dr. Khan kept believing in my abilities that was always motivational for me. Even at the late nights, he never ignored my emails; this accelerated the pace of my work. I am truly blessed to be supervised by a person like Dr. Khan. Dr. Ahmed was always helpful with his pinpointed feedback and critical remarks.

I was in a grave after a horrible journey in my undergraduate program. Dr. Imtiaz provided me with the opportunity to complete a master degree under his supervision, even with my less competitive profile; this was the turning point for me. If Dr. Imtiaz did not consider my request to get admitted to Memorial University, I would not be the person who is writing this thesis.

I would also like to remember the sacrifice of my beloved parents, sister, and wife. My wife is always supportive; words are not enough to show my gratitude to her. My parents cherished their son to be completing the PhD degree. Their desire pushed me to go for a higher degree, and I am happy they did so. My sister is the one who has taken care of my parents in this entire abroad journey. My in-laws are always supportive; their support is commemorative. I would like to remember my grandmothers, as well. Both of them left for heaven during this journey. I will always be guilty for being unable to be with them in their last few days. My son, Farees is the one who came to my world in the midst of this program; his lovely smiles are always peace of joy to me. Again I am thankful to Allah that the accident did not take me away from my son forever.

During the PhD program, I met some excellent souls: Dr. Mohammad Aminul Islam Khan, Dr. Ahmed Elruby, Abu Hena, Arko Ghosh, Musab Habib, Abul Hossain, M M Baset Oli Mishkat, Ahmed Hossain, Ripon Karmaker, Shailen Saha, Harunur Roshid, Khaled Salauddin, Colleen Mahoney, Nicole Parisi, Tina Dwyer, Moya Crocker, Angela Doyle, and Anton Blizzanikov. Their support in my day-to-day life can never be forgotten.

I have met many excellent colleagues in the Centre for Risk, Integrity and Safety Engineering (C-RISE) in the past three years. I would like to thank all of them. Especially, I must recognize Dr. Sidum Adumene, Mohammad Zaid Kamil, Mohammed Alauddin, Rajeevan Arunthavanathan, Dr. Mohammed Taleb-Berrouane, Dr. Sunday Adedigba, and Dr. Md. Samsur Rahman. I will be missing these guys whenever I will take a coffee.

I would also like to thank the Natural Sciences and Engineering Research Council (NSERC) for the Alexander Graham Bell Canada Graduate Scholarships-Doctoral Program (CGS D) scholarship, Canada Research Chair (Tier I) Program in Offshore Safety and Risk Engineering, Department of Process Engineering, and School of Graduate Studies (SGS) for providing the fund to complete this research.

I would like to express my profound gratitude to the unanimous peers who reviewed the published works that have formulated the basis of this thesis. Also, I am thankful to the examiners for spending their valuable time examining this thesis.

Table of Contents

ABSTRACT I

ACKNOWLEDGEMENT III

LIST OF FIGURES X

LIST OF TABLES XIV

LIST OF ABBREVIATIONS XVI

LIST OF SYMBOLS XXII

CHAPTER 1: INTRODUCTION 1

1.1. BACKGROUND AND MOTIVATION 1

1.2. OBJECTIVES 5

1.3. NOVELTIES AND CONTRIBUTIONS 7

1.4. OUTLINE OF THESIS 8

1.5. CO-AUTHORSHIP STATEMENT 11

CHAPTER 2: LITERATURE REVIEW 12

2.1. MULTIVARIATE DATA-BASED FDD TOOLS 12

2.2. BN-BASED FDD TOOLS 17

2.3. RISK-BASED FDD TOOLS 20

2.4. IDENTIFIED KNOWLEDGE GAPS 21

CHAPTER 3: ROBUST PROCESS MONITORING METHODOLOGY FOR DETECTION AND DIAGNOSIS OF UNOBSERVABLE FAULTS 23

PREFACE 23

ABSTRACT 24

3.1. INTRODUCTION 25

3.2. PROPOSED METHODOLOGY 32

3.3. APPLICATION OF THE METHODOLOGY TO THE TE CHEMICAL PROCESS 41

3.4. RESULTS AND DISCUSSION 59

3.5. CONCLUSION 63

CHAPTER 4: A DATA-DRIVEN BAYESIAN NETWORK LEARNING METHOD FOR PROCESS FAULT DIAGNOSIS 66

PREFACE 66

ABSTRACT 67

4.1. INTRODUCTION 68

4.2. PROPOSED METHODOLOGY 74

4.3. APPLICATIONS OF THE PROPOSED METHODOLOGY 81

4.3.1. CONTINUOUS STIRRED TANK HEATER (CSTH) 81

4.3.1.1. FAULT SCENARIO A1 (STEAM VALVE STICTION) 85

4.3.1.2. FAULT SCENARIO A2 (STEP CHANGE IN COLD WATER VALVE) 88

4.3.2. BINARY DISTILLATION COLUMN 91

4.3.2.1. FAULT SCENARIO B1 (RANDOM VARIATION IN REFLUX FLOWRATE) 94

4.3.2.2. FAULT SCENARIO B2 (STEP CHANGE IN FEED RATE) 96

4.4. RESULTS AND DISCUSSION 99

4.5. CONCLUSION 103

CHAPTER 5: A NOVEL DATA-DRIVEN METHODOLOGY FOR FAULT DETECTION AND DYNAMIC RISK ASSESSMENT 105

PREFACE 105

ABSTRACT 106

5.1. INTRODUCTION 107

5.2. PRELIMINARIES 113

5.2.1. NAIVE BAYES CLASSIFIER (NBC) 113

5.2.2. BAYESIAN NETWORK (BN) 116

5.2.3. EVENT TREE ANALYSIS (ETA) 116

5.3. METHODOLOGY 117

5.4. APPLICATIONS OF THE PROPOSED METHODOLOGY 119

5.4.1. A BINARY DISTILLATION COLUMN 119

5.4.2. THE RT 580 EXPERIMENTAL SETUP 131

5.5. CONCLUSION 136

CHAPTER 6: RISK-BASED FAULT DETECTION AND DIAGNOSIS FOR NONLINEAR AND NON-GAUSSIAN PROCESS SYSTEMS USING R-VINE COPULA 138

PREFACE 138

ABSTRACT 139

6.1. INTRODUCTION 140

6.2. R-VINE COPULA 142

6.3. PROPOSED METHODOLOGY 146

6.3.1. DATA PRE-PROCESSING 147

6.3.2. R-VINE CONSTRUCTION 149

6.3.3. MULTIVARIATE DENSITY QUANTILE DEVELOPMENT 150

6.3.4. FAILURE PROBABILITY ESTIMATOR 151

6.3.5. FAULT DIAGNOSIS MODULE 152

6.3.6. ONLINE MONITORING 152

6.4. APPLICATIONS OF THE PROPOSED METHODOLOGY 154

6.4.1. BENCHMARKING USING THE TENNESSEE EASTMAN (TE) CHEMICAL PROCESS 154

6.4.2. THE RT 580 EXPERIMENTAL SETUP 162

6.4.3. THE INDUSTRIAL ISOMER SEPARATOR UNIT 168

6.5. CONCLUSION 172

CHAPTER 7: SUMMARY, CONCLUSIONS, AND FUTURE WORK SCOPES 174

7.1. SUMMARY 174

7.2. CONCLUSIONS 175

7.2.1. DEVELOPMENT OF AN EARLY FAULT DETECTION AND DIAGNOSIS MODEL 175

7.2.2. DEVELOPMENT OF A DATA-DRIVEN AND AUTOMATED FAULT DIAGNOSIS TOOL 176

7.2.3. DEVELOPMENT OF A FRAMEWORK FOR SIMULTANEOUS FDD AND DRA ... 176

7.2.4. DEVELOPMENT OF A RISK-BASED ABNORMAL SITUATION MANAGEMENT FRAMEWORK 177

7.3. FUTURE WORK SCOPES 177

7.3.1. TUNING PARAMETER SELECTION FOR MEWMA-PCA 178

7.3.2. AUTOMATED PC SELECTION FOR MEWMA-PCA 178

7.3.3. APPLICATION OF ADVANCED MACHINE LEARNING ALGORITHMS IN DRA 178

7.3.4. SENSOR FAULT DETECTION MODULE 178

7.3.5. MULTIMODAL PROCESS HANDLING 179

7.3.6. R-VINE COPULA-BASED BN TOPOLOGY LEARNING 179

7.3.7. DYNAMIC LOSS MODELLING 179

7.3.8. INTEGRATION OF INTENTIONAL AND NATURAL THREATS 179

7.3.9. IMPERFECT DATA TREATMENT 180

REFERENCES 181

List of Figures

Figure 1.1: Conventional vs digitalized process system. 3

Figure 1.2: Research objectives. 6

Figure 1.3: Thesis structure and related publications. 10

Figure 3.1: Flowchart of the proposed methodology. 34

Figure 3.2: Flowchart of the BN development technique. 35

Figure 3.3: (A) Construction of a simple BN of four symptoms and two fault types (B) illustration of fault diagnosis scheme. 37

Figure 3.4: PFD of the Tennessee Eastman chemical process. 42

Figure 3.5: PCA based monitoring of IDV 3, IDV 9, and IDV 15. 44

Figure 3.6: BN for T^2 control chart. 45

Figure 3.7: Fault detection and diagnosis by MEWMA-PCA-BN for IDV 3 (A) T^2 control chart, (B) SPE control chart (earlier detection), (C) SPE contribution plot, (D) updated SPE-based BN, and (E) fault diagnosis using percentage increase in the faulty state. 48

Figure 3.8: Fault detection and diagnosis by MEWMA-PCA-BN for IDV 9 (A) T^2 control chart, (B) SPE control chart, (C) SPE contribution plot, (D) updated SPE-based BN, and (E) fault diagnosis using percentage increase in the faulty state. 51

Figure 3.9: Fault detection and diagnosis by MEWMA-PCA-BN for IDV 15 (A) T^2 control chart (earlier detection), (B) SPE control chart, (C) T^2 contribution plot, (D) updated T^2-based BN, and (E) fault diagnosis using percentage increase in the faulty state. 55

Figure 3.10: Fault detection and diagnosis by MEWMA-PCA-BN for IDV 3 & 15 (A) T^2 control chart, (B) SPE control chart (earlier detection), (C) SPE contribution plot, (D) updated SPE-based BN, and (E) fault diagnosis using percentage increase in the faulty state. 58

Figure 3.11: Effect of MEWMA and CUSUM on original data. 63

Figure 4.1: The proposed methodology for FDD. 76

Figure 4.2: The continuous stirred tank heater (modified and redrawn from (Thornhill et al., 2008)). 82

Figure 4.3: BN for the CSTH. 85

Figure 4.4: Monitoring results for steam valve stiction (A) PCA-T^2 control chart, (B) PCA-SPE control chart, (C) PCA-T^2 contribution plot, (D) updated BN, and (E) root cause diagnosis by percentage change in the faulty state. 88

Figure 4.5: Monitoring results for step change in cold water valve demand (A) PCA-T^2 control chart, (B) PCA-SPE control chart, (C) PCA-T^2 contribution plot, (D) updated BN, and (E) root cause diagnosis by percentage change in the faulty state. 91

Figure 4.6: A binary distillation column (modified and redrawn from (Skogestad, 1997)). 92

Figure 4.7: BN for the binary distillation column. 93

Figure 4.8: Monitoring results for random variation in reflux flowrate (A) PCA-T^2 control chart, (B) PCA-SPE control chart, (C) PCA-SPE contribution plot, (D) updated BN, and (E) root cause diagnosis by percentage change in the faulty state. 96

Figure 4.9: Monitoring results for step change in feed rate (A) PCA-T^2 control chart, (B) PCA-SPE control chart, (C) PCA-SPE contribution plot, (D) updated BN, and (E) root cause diagnosis by percentage change in the faulty state. 99

Figure 5.1: A conceptual illustration of the proposed dynamic risk assessment framework. 111

Figure 5.2: Flowchart of the proposed methodology. 118

Figure 5.3: Schematic diagram of a binary distillation column (modified and redrawn from (Skogestad, 1997)). 120

Figure 5.4: BN for the RPB. 125
Figure 5.5: BN for the DPB. 125
Figure 5.6: BN for the IPB. 126
Figure 5.7: BN for the EPB. 126
Figure 5.8: BN for the EMFPB. 127
Figure 5.9: BN for the HFPB. 127
Figure 5.10: BN for the OFPB. 127
Figure 5.11: Pathway realization of a fault to failure. 128
Figure 5.12: Fault assessment in a binary distillation column using an NBC. 130
Figure 5.13: Prognosis of catastrophic accidents for (A) fault A1 and (B) fault A2. 131
Figure 5.14: Schematic diagram of the RT 580 experimental setup (modified from (Ghosh et al., 2019)). 132
Figure 5.15: Fault assessment in the RT 580 experimental setup using an NBC. 134
Figure 5.16: Prognosis of catastrophic accidents for (A) fault B1 and (B) fault B2. 135
Figure 5.17: Water level in the process tank (%) for fault scenario B2. 136
Figure 6.1: An illustrative example of four-dimensional D, C, and R-vine models. 145
Figure 6.2: Conceptual framework of the proposed risk-based FDD framework. 146
Figure 6.3: Proposed risk-based FDD model development phases. 147
Figure 6.4: Online process monitoring using the proposed risk-based FDD model. 153
Figure 6.5: A schematic diagram of the TE chemical process (modified and redrawn from (Downs and Vogel, 1993)). 156
Figure 6.6: The failure prediction model for the TE chemical process. 157

Figure 6.7: Monitoring results in the TE process for simultaneous A feed loss and step change in A/C feed ratio (A) fault probability estimation, (B) failure prognosis through C8, and (C) fault diagnosis. 160

Figure 6.8: Root causes diagnosis of simultaneous A feed loss and step change in A/C feed ratio by (A) PCA-SPE contribution plot, (B) PCA-T^2 contribution plot, and (C) transfer entropy.... 161

Figure 6.9: Schematic diagram of the RT 580 experimental setup (modified from (Ghosh et al., 2019)). 163

Figure 6.10: Monitoring results in the RT 580 fault finding setup (A) fault probability estimation, (B) failure prognosis through C8, (C) fault diagnosis, and (D) failure prognosis through C8 without considering joint dependence. 167

Figure 6.11: Schematic diagram of the isomer separator unit. 168

Figure 6.12: Monitoring results in the industrial separator unit (A) fault probability estimation, (B) failure prognosis through C8, and (C) fault diagnosis. 172

List of Tables

Table 3.1: A list of works that have reported lower detection rates for IDV 3, IDV 9, and IDV 15. 29

Table 3.2: CPT for DN 1..... 37

Table 3.3: CPT for DN 2..... 37

Table 3.4: Comparison of out-of-control average run length (bold implies the best performance). 60

Table 3.5: Comparison of ARL_{OC}, average FDR, and accurate diagnosis capacity for all fault cases in the TE chemical process (bold implies the best performance). 61

Table 4.1: Fault description in the CSTH. 81

Table 4.2: Confusion matrix for the CSTH. 83

Table 4.3: A comparison of Kendall's rank correlation coefficient for different data sources. ... 84

Table 4.4: Fault description in the binary distillation column. 92

Table 4.5: Confusion matrix for the binary distillation column. 93

Table 4.6: Fault detection performance comparison of distinct tools (bold implies the best performance). 100

Table 4.7: Root cause diagnosis performance comparison of distinct tools (bold implies the best performance). 102

Table 5.1: A comparison of the multivariate fault detection and dynamic risk assessment methods. 112

Table 5.2: Mean and standard deviation of the variables for all classes..... 115

Table 5.3: Fault descriptions in a binary distillation column..... 120

Table 5.4: Event description and assigned probabilities for safety barriers. 121

Table 5.5: Failure probability of the safety barriers. 129

Table 5.6: Fault descriptions in the RT 580 experimental setup. 133

Table 6.1: Kendall's τ values for illustrative four variable process. 150

Table 6.2: Description of monitored variables in the TE chemical process (Downs and Vogel, 1993). 155

Table 6.3: Failure probability of safety barriers (Amin et al., 2020; Yu et al., 2015a). 157

Table 6.4: Diagnostic performance comparison of proposed method, PCA, and transfer entropy. 162

Table 6.5: Monitored variables in the RT 580 setup. 164

Table 6.6: Variable description and fitted distributions in the separator unit. 169

List of Abbreviations

AIC: Akaike information criterion

AKPCA: Adaptive kernel principal component analysis

ALI: Abnormality likelihood index

ANN: Artificial neural network

ARL_{OC}: Out-of-control average run length

ASPCA: Adaptive sparse principal component analysis

BIC: Bayesian information criterion

BN: Bayesian network

BT: Bow-tie

BWPCA: Principal component analysis with Bayesian weighted fusion strategy

CBN: Copula Bayesian network

CC-ICA: Class-conditional independent component analysis

CD: Correlation dimension

CDF: Cumulative density function

CL: Control limit

CPT: Conditional probability table

CPV: Cumulative percentile variation

CSTH: Continuous stirred tank heater

CUSUM PCA: Cumulative sum principal component analysis

CUSUM: Cumulative sum

DBAI: Dynamic Bayesian anomaly index

DBCI: Dynamic Bayesian contribution index

DBN: Dynamic Bayesian network

DD: Detection delay

DICA: Dynamic independent component analysis

DPB: Dispersion prevention barrier

DPCA: Dynamic principal component analysis

DPCA-DR: Dynamic principal component analysis-distance correlation

DQA: Density quantile analysis

DR: Detection rate

DRA: Dynamic risk assessment

DT: Decision tree

EEMD: Ensemble empirical mode decomposition

EMFPB: Emergency management failure prevention barrier

EMRQ: ExxonMobil Research Qatar

EPB: Escalation prevention barrier

ET: Event tree

ETA: Event tree analysis

EWMA: Exponentially weighted moving average

FAR: False alarm rate

FCCU: Fluid catalytic cracking unit

FDA: Fisher discriminant analysis

FDD: Fault detection and diagnosis

FDR: Fault detection rate

FSN: Fault semantic network

FT: Fault tree

FTA: Fault tree analysis

FTE: Family transfer entropy

G-Copula: Gaussian copula

GMM: Gaussian mixture model

HAZOP: Hazard and operability study

HFPB: Human failure prevention barrier

HPS: High-pressure separator

IC: Independent component

ICA: Independent component analysis

ICA-AO: Independent component analysis and adjusted outliers

IKICA: Improved kernel independent component analysis

IPB: Ignition prevention barrier

ISVM: Independent support vector machine

JPDF: Joint probability density function

KDE: Kernel density estimator

KF: Kalman filter

KICA: Kernel independent component analysis

KLD: Kullback-Leibler divergence

KPCA: Kernel principal component analysis

LCS: Location cumulative sum

LPS: Low-pressure separator

MBTE: Multiblock transfer entropy

MCS: Monte Carlo simulation

MEWMA-PCA: Multivariate exponentially weighted moving average principal component analysis

MI: Mutual information

MICA: Modified independent component analysis

MKOPSC-Q: Mary Kay O'Connor Process Safety Center - Qatar

MPLS: Modified partial least squares

MSPM: Multivariate statistical process monitoring

MWKPCA: Moving window kernel principal component analysis

NBC: Naïve Bayes classifier

NLGBN: Nonlinear Gaussian belief network

NOC: Normal operating condition

OFPB: Organizational failure prevention barrier

PAD: Probability absolute difference

PC: Principal component

PCA: Principal component analysis

PCEG: Possible cause and effect graph

PDF: Probability density function

PID: Proportional-integral-derivative

PLS: Partial least squares

PPCA: Probabilistic principal component analysis

PSO-ICA: Particle swarm optimization independent component analysis

PSVM: Proximal support vector machine

PULSE: Process unit life safety evaluation

PVCDD: Pruning Vine copula-based dependence description

RBF: Radial basis function

RBF-GA: Radial basis function with genetic algorithm

RNPCA: Robust nonlinear principal component analysis

RPB: Release prevention barrier

SAP: Subspace aided approach

SB: Safety Barrier

SCS: Standard cumulative sum

SDG: Sign digraph

SePCA: Semiparametric principal component analysis

SISO: Single-input and single-output

SNBC: Semi-naïve Bayesian classifier

SOM: Self organized map

SPA: Statistical pattern analysis

SPCA: Sparse principal component analysis

SPE: Squared prediction error

SSVM: Selective support vector machine

SVM: Support vector machine

TAN: Tree augmented network

TE: Tennessee Eastman

TPLS: Total projection to latent structure

TVCDD: Truncated vine copula-based dependence description

VCDD: Vine copula-based dependence description

WT: Wash water tank

List of Symbols

b: Number of PCs

C: Copula function

c: Copula probability density function

C_u: Point correlation in correlation dimension

d: Number of safety barriers

D_{KL}: Kullback-Leibler divergence estimate

H: Heaviside function

h: Kernel bandwidth

I: Identity matrix

$K(.)$: Kernel function

k: Multiplier for standard deviation

K: Number of parameters in a distribution

L: Likelihood function

m: Number of variables

n: Number of samples/observations

P_l: PCA loading

P: Probability

P_w: Occurrence of each failure path

q: Number of points within the hypersphere radius in correlation dimension

Q: Quantile

T: PCA score

t: Time-step

u: Quantile number

Λ: Diagonal matrix

w: Number of safety barriers for each path

X: Data matrix

Y: Evidence

Z: MEWMA space

λ: Tuning parameter for MEWMA

μ: Mean

σ: Standard deviation

τ: Kendall's rank correlation coefficient

Chapter 1: Introduction

1.1. Background and Motivation

Process industries play a pivotal role in global economic growth. A list of the world's top 500 largest companies in 2021 includes many process industries such as ExxonMobil, Chevron, and Dow, to name a few (Fortune, 2021). The role of adequate safety assurance is instrumental behind this success, as an accident can lead to enormous financial damage and more importantly, reputation loss, which has a long-lasting impact on a company's investment portfolio and operational success. Although less frequent, indeed process industries experienced catastrophic accidents in the past century (Khan and Abbasi, 1999) and are still experiencing in this century (Mannan et al., 2016); this indicates that the current safety technologies need to be continually reviewed and improved to avoid any undesired event (Amin et al., 2019a; Talebberrouane et al., 2016).

Continuous monitoring and preventive actions are the keys to avoiding abnormal situations and accidents (Khan et al., 2016). Thus, fault detection and diagnosis (FDD), the core elements of process monitoring, are paramount in ensuring process safety (Chiang et al., 2000). A fault can be defined as an unwanted deviation of at least one of the variables from the acceptable operational range. A fault initiates an abnormal event or accident. If it goes unmitigated, eventually, a process can be led to catastrophic failure. Therefore, nullifying faults in process operations is one of the primary operational tasks to enhance safety and reliability (Vathoopan et al., 2018). An early fault detection gives a lead time to the operators, while an accurate root cause diagnosis saves a significant amount of time when an alarm is noticed (Isermann, 2005).

The current era is often termed the Fourth Industrial Revolution or Industry 4.0, characterized by the automation and digital transformation of industries (Reis and Kenett, 2018). According to Khan et al. (2021), process digitalization integrates digital technologies in process operations for achieving greater efficiency and increased product quality. An effort is ongoing to upgrade the existing chemical plants harmonious to the Industry 4.0 requirements. Along with process digitalization, data-driven automated abnormal event management and predictive monitoring are critical mandates of the current industrial revolution (Pandey et al., 2020).

Figure 1.1 compares a traditional and a digitalized process system from the control and monitoring perspectives; a tank filling system has been considered. In earlier days, operator(s) used to monitor the level of the tank to protect against any potential overfilling. The complete control and monitoring mechanisms were manually done. On the other hand, with the advancement of sensor technologies and control and automation, this practice has been shifted to automated control (Moshgbar and Hammond, 2010). A sensor can monitor the level inside the tank, and the inlet flow controller can use this information to increase or decrease the flowrate to maintain the level, thereby protect overflow. The FDD module is equally crucial to both process systems. Nonetheless, the expected mode is different. In a digitalized process system, automated FDD is expected due to the complexity of close loop operations (Khan et al., 2021). The algorithms used for process monitoring should provide a detailed diagnostic report that the operators can utilize to take necessary actions in case of an abnormal situation.

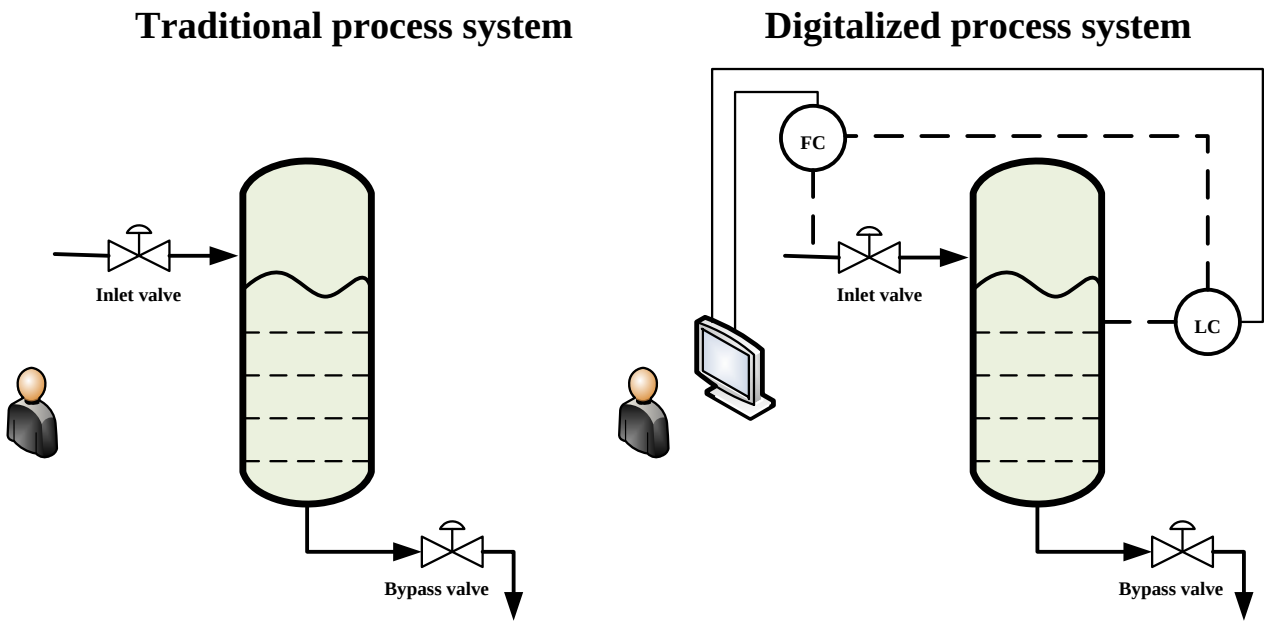

Figure 1.1: Conventional vs digitalized process system.

Although a faulty condition affects plant safety significantly, it alone does not directly measure safety since it needs to pass through several physical (e.g. emergency shutdown valve) and non-physical (e.g. controller) safety barriers to turn into an accident. Safety cannot be measured directly; it can be perceived from the assessment of risk, which is mathematically defined as the product of the probability of failure and severity of consequence (Khan et al., 2020). Process operations are dynamic; therefore, dynamic risk assessment (DRA) provides detailed plant safety information considering process state (i.e. probability of fault) and safety barriers' performance.

During the emergence of process monitoring, model-based tools were widely used for FDD. These tools rely on the first principal methods, which need detailed plant information (Venkatasubramanian et al., 2003b). A significant time is required to build the models. Also, uncertainty affects the performance of these tools significantly. In this context, the data-based statistical tools provide a more flexible mean, using available process data to develop monitoring

models. These tools can be divided into univariate and multivariate techniques (Venkatasubramanian et al., 2003c).

The univariate tools use a dedicated control chart for each variable. Although these are easier to implement, monitoring a high-dimensional process with these control charts becomes tedious and stressful for operators. The multivariate tools overcome this limitation since they use fewer control charts for the entire process (Kresta et al., 1991). Additionally, these tools can provide an early fault detection than the univariate counterparts, as they consider the correlation among process variables (Neogi and Schlags, 1998).

Nevertheless, accurate diagnosis is a significant problem for multivariate tools (Vedam and Venkatasubramanian, 1999). Operators' experience often becomes a vital resource in fault diagnosis. The personnel in the control room can predict the root cause by analyzing the variable trend plots or contribution plots (Miller et al., 1998). This is a time-consuming process and may entail errors, given the fact that symptoms often become more sensitive to a fault rather than the root cause (Liu, 2012). Furthermore, multivariate FDD tools need user opinion in captured variance to develop the monitoring model. Detecting faults earlier is another issue that continuously gets researchers' attention (Amruthnath and Gupta, 2018).

The knowledge-based tools have been used for fault diagnosis, as well. These tools necessitate expert knowledge. Nonetheless, one cannot guarantee the accuracy of the developed model due to knowledge uncertainty and human error (Gharahbagheri et al., 2017b). Recently, many researchers have developed knowledge-based tools from process data (Gharahbagheri et al., 2017b; Meng et al., 2019; Yang et al., 2014). However, the majority of these tools use process knowledge to develop models.

One of the significant limitations of the current multivariate FDD tools is their inability to capture dynamic risk profiles. Although a few articles are available in the existing literature that has addressed simultaneous FDD and DRA using multivariate process data (Yu et al., 2016; Yu et al., 2015a; Zadakbar et al., 2015, 2013, 2012), these works estimate risk from a univariate fault probability. In addition to this, the majority of them lack robust fault diagnosis and failure prognosis characteristics.

While there is progress in multivariate data-based FDD and DRA, several semi-automated aspects of these tools are the major issues that need cautious attention. The contemporary technology focuses on enhanced use of multivariate data; still, human intervention is required for model development and online performance. The current process monitoring and safety analysis tools need to be multivariate and automated, especially considering the growing complexity and required parameters to be handled in a digitalized process system (Khan et al., 2021). Hence, the motivation of this research is to bridge the main technological gaps between the existing methods and the requirements of an automated FDD and DRA method by using available process data to reduce human dependency, ensure accurate fault diagnosis, and enhance process safety.

1.2. Objectives

The main goal of this work is to develop data-based FDD and DRA tools for multivariate safety analysis in digitalized process systems. Instead of using prior knowledge, available process data are used to develop the monitoring models. Different data characteristics, such as linearity, nonlinearity, Gaussianity, and non-Gaussianity, have been considered. This work attempts to provide answers to the following questions.

i. Can the monitoring system reliably determine the system state?

ii. Can the developed system detect fault early?

iii. Where has the fault(s) likely occurred in a process?

iv. What is the likelihood of a fault transforming to a failure through different paths?

v. How can multivariate process data be utilized for predictive FDD and DRA?

Having the research questions in mind, the objectives of this research (Figure 1.2) are:

i. To develop a multivariate tool for early fault detection and diagnosis in linear and Gaussian process systems.

ii. To develop a data-driven and automated fault diagnosis tool for linear and Gaussian process systems.

iii. To develop a framework for simultaneous FDD and DRA in Gaussian and nonlinear process systems.

iv. To develop a risk-based FDD model for nonlinear and non-Gaussian process systems.

v. To test and verify the developed models with simulated and real-life case studies.

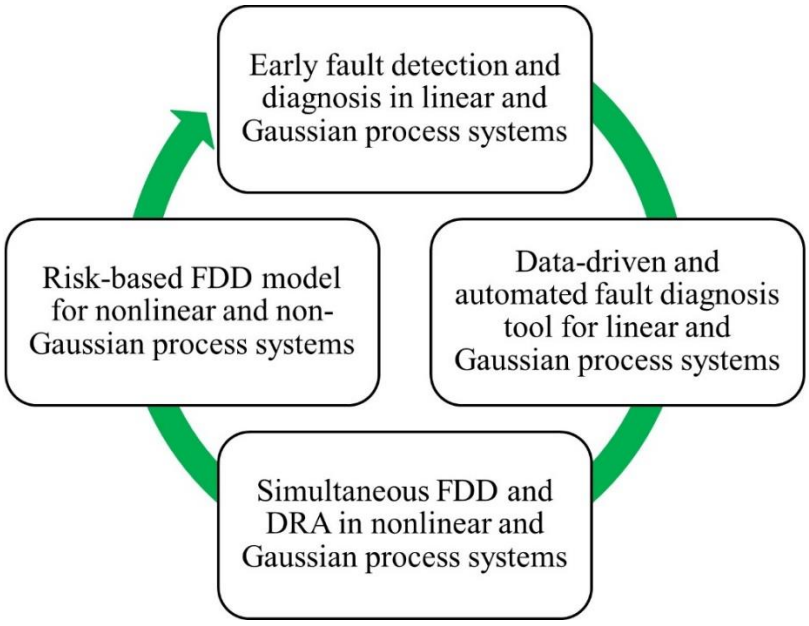

Figure 1.2: Research objectives.

1.3. Novelties and Contributions

This doctoral research's main novelties and contributions are fault detection, diagnosis, and dynamic risk assessment in process industries. The highlights of these contributions are stated below:

- An improved version of PCA for early fault detection. The multivariate exponentially weighted moving average (MEWMA) model has been integrated with the PCA. The developed MEWMA-PCA model can detect fault earlier than many contemporary fault detection tools.
- A novel data-driven BN learning method. The BNs are developed from historical fault symptoms using a supervised learning technique.
- An automated principal component (PC) selection technique for process FDD using correlation dimension (CD). It eliminates the need for human interference in PCA model development.
- An innovative data-driven BN learning algorithm using the Kullback-Leibler divergence (KLD), vine copulas, and Bayes' theorem. The proposed algorithm adopts an unsupervised learning method and is found efficient in fault diagnosis.
- A method to estimate high-dimensional conditional probabilities from continuous process data. It relaxes the necessity to discretize continuous data at the cost of information loss.
- A multivariate simultaneous FDD and DRA methodology. This work can show the failure paths using the event tree analysis (ETA). Additionally, a dynamic risk profile is developed using a multivariate probability estimator, the naïve Bayes classifier (NBC), and thus, it eliminates the existing univariate probability-based dynamic risk computation.

- A methodology to compute multivariate fault probability by an unsupervised learning method that is used for risk assessment. The R-vine copula model has been used in this context.
- A model-free simultaneously active multiple fault diagnosis module using the density quantile analysis (DQA).

1.4. Outline of Thesis

This thesis contains seven chapters and is written in a manuscript-based format. The overall outcomes of this thesis are published in four peer-reviewed journal papers. Figure 1.3 shows the organizational structure of this thesis. Chapter 1, 2, and 7 are the introduction, literature review and conclusions, respectively. Chapters 3 to 6 of this thesis are developed based on the papers published in peer-reviewed journals.

The first chapter demonstrates the motivations and objectives of the research. Chapter 2 presents a brief overview of the available literature and identified knowledge gaps. Chapters 3, 4, 5, and 6 discuss the technical outcomes based on the objectives mentioned in Section 1.2.

Chapter 3 reviews the current progress in FDD and proposes an MEWMA-PCA-BN model for fault detection and diagnosis. An algorithm is also proposed to develop BNs from historical fault symptoms. This algorithm follows a supervised learning method where all fault information needs to be available. On the contrary, the fault is detected using the MEWMA-PCA in an unsupervised manner. This work has been published in the Industrial & Engineering Chemistry Research journal.

Chapter 4 proposes a data-driven BN learning algorithm. This work relaxes the necessity of historical fault symptoms to build a BN and adopts an unsupervised learning technique. The KLD

has been used for determining BN topology, and the prior and conditional probabilities are estimated using the vine copula and Bayes' theorem. This work also proposes a CD-based automated PC selection method to eliminate user-opinion requirements in PCA model development. This work has been published in Process Safety and Environmental Protection journal.

Chapter 5 reviews the current simultaneous FDD and DRA methods and proposes a new concept in the context of DRA, where failure probability is estimated using multivariate fault probability. The NBC is used for FDD in a supervised manner. It generates a multivariate probability of each fault type which is fed into the ETA for failure prediction. This work has been published in The Canadian Journal of Chemical Engineering.

Chapter 6 proposes a risk-based FDD framework. It also uses multivariate probability for failure prediction. However, the fault probability is estimated in an unsupervised manner using the advantage of the R-vine copula. The diagnosis technique developed in this framework is found sensitive to multiple faults. This work has been published in Process Safety and Environmental Protection journal.

Chapter 7 reports the summary of this thesis and the main conclusions drawn through the technical works. Recommendations for future work are also presented at the end of this chapter.

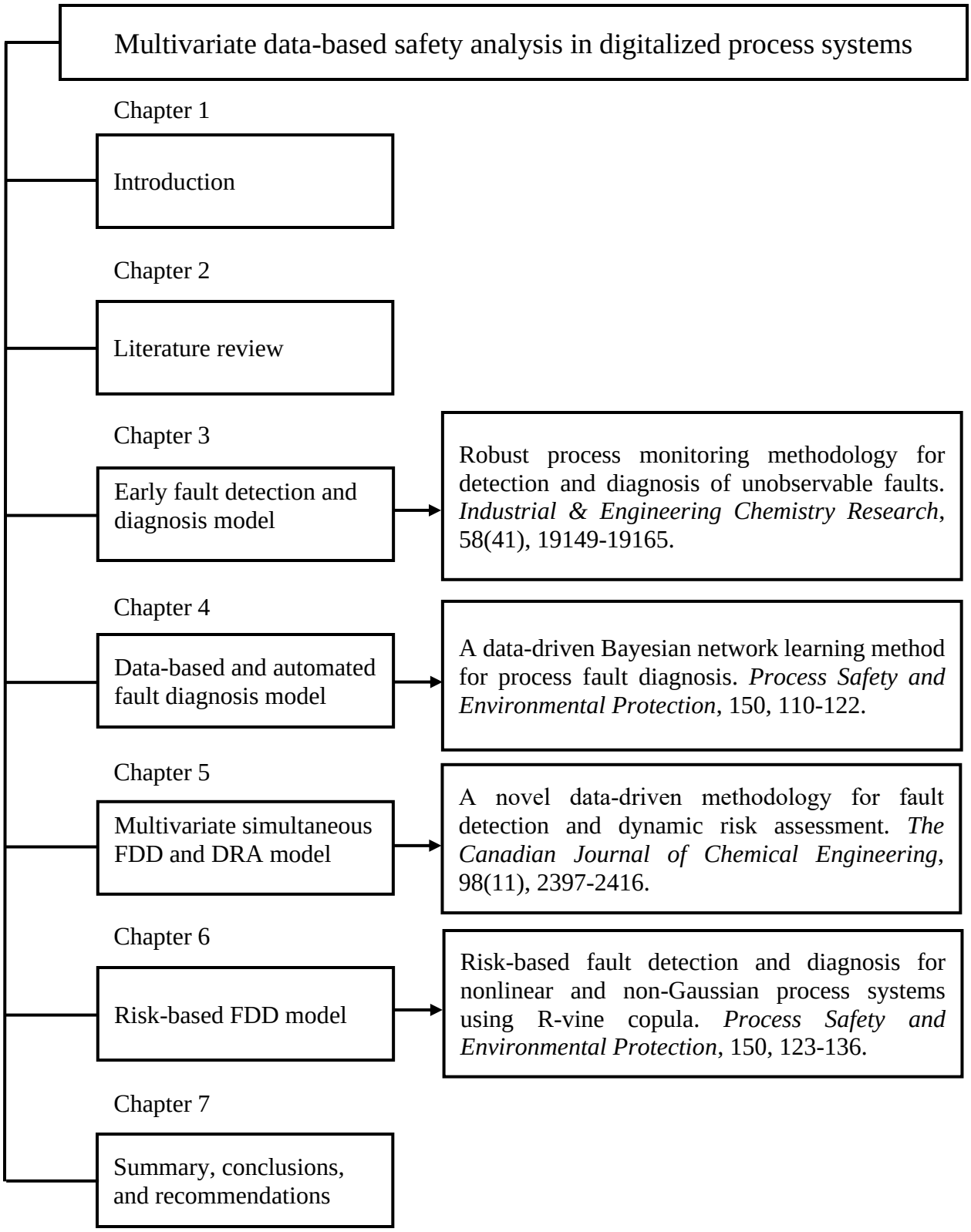

Figure 1.3: Thesis structure and related publications.

1.5. Co-authorship Statement

I am the primary author of this thesis and the four papers on which this thesis is based. With the help of the co-authors, Drs. Faisal Khan, Salim Ahmed, and Syed Imtiaz, I developed the conceptual understanding of the model requirement and its potential applications. I carried out the literature review. I have prepared the first draft of the manuscripts presented in this thesis, subsequently revised the manuscripts based on the co-authors' feedback. Dr. Faisal Khan helped in the development, testing, and improvement of the models. He also assisted in reviewing and revising the manuscripts. Drs. Salim Ahmed and Syed Imtiaz helped in reviewing, analyzing, and testing the concepts/models. They also reviewed and corrected the models and results and contributed to preparing, reviewing, and revising the manuscript.

Chapter 2: Literature Review

2.1. Multivariate Data-based FDD Tools

Data-based quantitative multivariate tools are being used in process FDD for almost three decades (Alauddin et al., 2018). These tools can be classified into two major categories: statistical process monitoring and machine learning tools (Venkatasubramanian et al., 2003c). Machine learning-based techniques such as the artificial neural network (ANN) and support vector machine (SVM) require in-depth information about normal and faulty data. The training time is also longer, and accurate performance is not guaranteed when facing an unknown fault type (Ge et al., 2013).

On the contrary, the multivariate statistical process monitoring (MSPM) tools such as the principal component analysis (PCA) and independent component analysis (ICA) only require normal data to develop the monitoring model. Any deviation from the normal operating region is considered a fault. Thus, the requirement for faulty data is avoided. It saves a considerable amount of time to develop the monitoring models. Also, these tools can provide reliable performance (Ge et al., 2013; Venkatasubramanian et al., 2003c).

Many review articles found the PCA, ICA, partial least squares (PLS), and their derivatives as the predominant members of multivariate statistical FDD family (Alauddin et al., 2018; Ge, 2017). The PCA was first invented by Pearson (1901). It was originally used for data compression. Later, it became popular in process industries after the works by Wise et al. (1988) and Kresta et al. (1991). It transforms a higher-dimensional data into a lower-dimensional feature space keeping the most significant information of original data.

The PCA uses a linear transformation to find a set of uncorrelated variables, which are called the PCs. Each PC is orthogonal to each other and linear combination of original variables. Singular value decomposition (SVD) is the most widely used technique to find PCs. This method decomposes the covariance or correlation matrix to find a set of vectors that has the same properties as the PCs.

Monitoring each PC is cumbersome. Usually, the first few PCs contain the most crucial variational information and are used to monitor the process. Still, the necessity of monitoring the process with one control chart is not met. To handle this issue, two statistics: the Hotelling's T^2 and squared prediction error (SPE), are used with the PCA to monitor the process with one consolidated control chart. The SPE gives a measurement of the distance between the sample space and residual space, while the T^2 indicates how far a sample lies from the centre of the feature space (Jackson, 2005). When an online sample violates the threshold of T^2 or SPE control chart, a fault is detected.

The selection of an appropriate number of PCs largely affects the monitoring performance. The SCREE (Cattell, 1966) and CPV (Malinowski and Howery, 1980) are the two most commonly used approaches (Valle et al., 1999). However, both these approaches are heavily user-perspective. The SCREE uses a graphical plot to select the required number of PCs. It starts searching from the first PC with the highest variation and stops when the PCs do not show a significant difference in variation. Although it is easier to use in lower-dimensional cases, it becomes ineffective when the data dimension is higher. On the contrary, the CPV uses a mathematical model. Still, it requires the information of how much variation one wants to capture while building the model. Although a thumb rule of 90% is suggested, it is found ineffective in many cases (Imtiaz et al., 2008).

One of the intrinsic limitations of PCA is the distribution assumption. It assumes process data to be following the Gaussian distribution that may not be a valid assumption since process data

contains both Gaussian and non-Gaussian features. The PLS suffers from the same limitation, as well.

To overcome the distribution assumption and capture non-Gaussian data, Kano et al. (2003) proposed an ICA-based process monitoring model. The ICA uses independent components (ICs) with the I^2, SPE, and I_e^2 statistics for FDD (Lee et al., 2004b). It could explain non-Gaussian data using higher-order statistics such as kurtosis and negentropy. However, the ICA cannot extract important ICs. Therefore, during ICA's inception in FDD, the number of ICs was set equal to the number of PCs obtained from PCA. Lee et al. (2006) proposed a modified ICA (MICA) approach to address the aforementioned issue. It included an additional pre-processing of the whitened score matrix that enabled the ICA to capture the most significant ICs like the PCA.

Data nonlinearity is another issue which the PCA and ICA cannot address since they use linear transformation. An auto-associative neural network-based nonlinear PCA (NLPCA) was proposed by Kramer (1991). However, training an NLPCA is time-consuming. In recent years, kernel-based methods have become popular to address data nonlinearity. Lee et al. (2004a) proposed a kernel PCA (KPCA)-based fault detection technique. The KPCA was found efficient in monitoring nonlinear processes. However, it cannot provide good performance when non-Gaussianity is predominant. Kernel ICA is utilized to capture both the nonlinearity and non-Gaussianity (Lee et al., 2007).

The kernel methods transform lower-dimensional data into a higher-dimensional feature space. Hence, they become computationally onerous. Also, selecting the appropriate kernel function and associated parameters requires trial and error. One of the major limitations of all the methods discussed above is their limited diagnosis capacity. Although these tools can generate multivariate

contribution plots that indicate where is the possible root cause of the fault, these diagnosis reports are often inaccurate (Gharahbagheri et al., 2017b; Yu et al., 2015b).

Recently, vine copula-based methods have been proposed by many researchers for nonlinear and non-Gaussian process monitoring. Nonlinear dependence is measured by Kendall's rank correlation coefficient, τ, and the empirical distribution is used to capture both the Gaussian and non-Gaussian data. Unlike the statistical techniques, no dimensionality reduction is required while developing the vine copula-based FDD tools. Instead, these methods seek to find the correlation structure among process variables and subsequently, copula density which is further utilized for calculating the joint probability density functions (JPDFs). Then density quantile analysis (DQA) on JPDFs is used to estimate the fault probability.

Ren et al. (2015) introduced the vine copula-based process monitoring scheme. The authors used the C-vine model for fault detection. The first few trees of a vine model usually contain the most critical dependence information, and significant computation time can be saved by discarding some of the high-dimensional conditional copulas. Based on this motivation, Wan and Li (2019) proposed a pruning C-vine copula-based FDD model. The authors found an improved detection rate in the Tennessee Eastman (TE) chemical process compared to the work by Ren et al. (2015).

One of the intrinsic limitations of the C-vine-based method is its inability to maximize the correlation structure due to the used decomposition technique. C-vine copula uses a star structure to describe the correlation pattern. A variable is selected as the root node, and other variables are connected to it. The D-vine is another multivariate vine modelling technique that uses a sequential decomposition technique. The C-vine and D-vine models have superiority when process variables are strongly and weakly dependent, respectively.

Cui and Li (2020) used a combination of C-vine and D-vine copulas to capture both the stronger and weaker correlations. The authors used the maximum information coefficient (MIC) (Reshef et al., 2014) to determine the stronger and weaker correlations. The combined C-D vine model provided better performance than each of these vine models alone. However, the D-vine copula also fails to maximize the correlation structure due to its sequential decomposition technique. The R-vine copula can aid in this context, as it does not have any predefined structure like the C-vine or D-vine copulas. The applications of the R-vine model can be found in the works by Zhou and Li (2018) and Jia and Li (2020).

The majority of these vine-based works mainly aim at fault detection. Ren et al. (2017) proposed a copula subspace division-based fault diagnosis technique. Two distinct contribution plots: margin deviation contribution (MDC) and dependence variation contribution (DVC), were used for diagnosis. However, like the statistical tools, these cannot secure accurate root cause diagnosis. Even though the current progress in fault detection is significant, a comparison of the performance of data-driven FDD tools such as the PCA, ICA, and their derivates on the benchmark TE chemical process suggests that these tools cannot successfully detect three faults: IDV 3, IDV 9, and IDV 15 (Yin et al., 2012). Therefore, many authors have described these faults as unobservable or challenging to detect. Interested readers are referred to the original article by Downs and Vogel (1993) for details of the TE chemical process and these faults' description. Even the recently developed copula-based tools are found ineffective in case of these faults.

Shams et al. (2011) proposed a cumulative sum (CUSUM) PCA-based monitoring model for these faults. The authors used the average detection delay to diagnose the fault type. The proposed method took several hundred hours to detect IDV 3 and IDV 9. Later, Du and Du (2018) used the ensemble empirical mode decomposition (EEMD), PCA, and CUSUM statistics to develop a better

monitoring model that could detect IDV 3 within 42 minutes. Nonetheless, detecting these faults early, like the other faults, is still considered a challenging task.

2.2. BN-based FDD Tools

The BN, a causal model, is becoming increasingly popular in FDD literature. The BN overcomes the limited diagnostic capacity of MSPM tools. It utilizes probabilistic reasoning for fault diagnosis. BN has received growing attention in FDD in the last fifteen years (Zerrouki et al., 2020). At the dawn of multivariate FDD, in the late 1980s and early 1990s, the use of rule-based expert systems was predominant for diagnosis (Kramer and Palowitch, 1987; Wilcox and Himmelblau, 1994). These tools suffered from uncertainty handling capacity and thus, showed poor performance while dealing with a new fault condition (Gao et al., 2015; Venkatasubramanian et al., 2003a).

To address this issue, Rojas-Guzman and Kramer (1993) proposed a BN-based probabilistic reasoning model and demonstrated the superiority of BN over the then rule-based methods. Process knowledge was used to develop the BN structure, and the Monte Carlo Simulation (MCS) was utilized for developing the CPTs. Ibargüengoytla et al. (1996) used BN to check the consistency of sensor data and the presence of possible faults. A single sensor fault detection and identification technique was proposed by Mehranbod et al. (2003). The authors considered three types of sensor faults: noise, bias, and drift in steady operating conditions. Later, a more sophisticated mechanism to address multiple faulty sensors in the transient operating condition was developed by Mehranbod et al. (2005). These works used the probability absolute difference (PAD) for fault detection. PAD was defined as the absolute difference between the normal state probability and updated probability. Then, rules-based methods were used to identify the fault types.

Verron et al. (2006) proposed a BN-based classifier for chemical process fault diagnosis. Since the classifier could not provide good performance while all the variables were used to train a fault class, crucial class variables were identified using mutual information (MI), and the diagnosis performance was found to be better. Such classifier-based fault diagnosis methods using BN can be found in (Verron et al., 2010b, 2010a, 2007). These works' major problem is the requirement of all the possible fault information that may not always be obtainable.

The conventional BNs are static. On the contrary, process operations are dynamic in nature. Being motivated by this fact, Yu and Rashid (2013) introduced a dynamic BN (DBN) for process monitoring. The abnormality likelihood index (ALI) was used for fault detection, and the dynamic Bayesian contribution index (DBCI) was utilized for fault diagnosis. Unlike the tools discussed in Section 2.1, the proposed method could provide insight into the fault propagation pathway.

Industrial data are often imperfect and missing. Zhang and Dong (2014) proposed a multiple time-slice DBN-based FDD model that could handle missing data. The authors reported that increasing the number of time-slices while constructing the DBN could significantly improve monitoring performance. The DBN-based method proposed by Yu and Rashid (2013) used an arbitrary threshold for fault detection. To address this issue, Amin et al. (2019b) proposed a dynamic Bayesian anomaly index (DBAI)-based thresholding technique in the context of DBN.

Although the DBN-based methods can provide better performance because they can detect and diagnose a fault and identify its propagation path, they suffer from early fault detection capacity when fault magnitude is lower. Many hybrid methods are found in FDD literature that have used the early fault detectability of PCA, ICA, and their derivatives and accurate root cause diagnosis capacity of a BN to ensure a fault is detected early, and the root cause is diagnosed accurately (Amin et al., 2018a, 2017; Gharahbagheri et al., 2017a; Mallick and Imtiaz, 2013; Yu et al.,

2015b). Thus, the limitations of data-based multivariate statistical process monitoring tools (limited diagnostic capacity) and DBN (delayed fault detection) are overcome, and a more reliable FDD tool is developed.

Mallick and Imtiaz (2013) combined PCA with BN. This hybrid method can provide better diagnostic performance than the conventional PCA. The BN was developed from process knowledge. As discussed earlier, PCA cannot capture the non-Gaussianity. Yu et al. (2015b) proposed an MICA-BN framework to overcome this issue. Though the qualitative parts were developed from prior knowledge, process data were utilized to estimate the quantitative parts. Wang et al. (2017) integrated the BN with semiparametric PCA for nonlinear and non-Gaussian fault diagnosis. These two works (Wang et al., 2017; Yu et al., 2015b) showed monitoring the inputs and outputs could be sufficient for root cause diagnosis. Gharahbagheri et al. (2017b) proposed a data-driven BN learning algorithm using Granger causality and transfer entropy. A continuous data discretization technique was used to estimate the prior and conditional probabilities. The KPCA-BN was used for nonlinear fault diagnosis.

The above mentioned BN-based hybrid methods consider a hard evidence-based updating mechanism for root cause diagnosis. Amin et al. (2018b) showed such updating technique could result in inaccurate diagnosis due to information loss and proposed a multiple likelihood evidence-based fault diagnosis method. Later, Galagedarage Don and Khan (2019) developed a hidden Markov model (HMM)-BN-based FDD model adopting the diagnostic methodology proposed by Amin et al. (2018b). For quantitative probability estimation, Amin et al. (2018b) and Galagedarage Don and Khan (2019) used the methodology proposed by Gharahbagheri et al. (2017b). However, discretizing continuous data may result in information loss. Moreover, except

for the work by Gharahbagheri et al. (2017b), the other works are not purely data-driven, as these frameworks use process knowledge to develop the BN structure.

2.3. Risk-based FDD Tools

Although risk is the measure of safety, the FDD tools mentioned in Sections 2.1 and 2.2 cannot estimate it. Also, the conventional risk assessment methods cannot monitor the process in a multivariate manner. To address these issues, Zadakbar et al. (2012) proposed a PCA-based multivariate fault detection and DRA technique. The use of PCA enabled to monitor all the process variables efficiently. Unlike the conventional T^2 and SPE statistics-based monitoring, this work used risk as the indicator of fault. The dynamic risk profile was developed from PCA scores. Later, the Kalman filter (Zadakbar et al., 2013) and particle filter (Zadakbar et al., 2015) were also utilized for simultaneous multivariate fault detection and risk assessment. The use of particle filter allowed to monitor and risk assessment of nonlinear and non-Gaussian process systems.

The major limitation of Zadakbar's works is the inability to show different failure paths, as these works used different severity indexes to calculate risk ignoring the effect of safety barriers' performance. Besides, these methods cannot provide any solution for root cause diagnosis. Yu et al. (2015b) proposed a risk-based FDD framework using the self-organizing map (SOM) that provided the solutions to the limitations faced by previously discussed risk-based FDD and DRA models. The use of an event tree provided a robust mechanism to visualize the failure paths. Additionally, the SOM can be applied to both nonlinear and non-Gaussian cases.

Operational risk assessment is often needed to predict dynamic operational loss. The above mentioned works used pre-defined severity indices to estimate the risk. However, loss itself shows dynamic behaviour. Suppose $\mu \pm \sigma$ is used to generate a warning about a process deviation. μ and σ represent mean and standard deviation, respectively. Consider a sample fall outside of $\mu+2\sigma$;

another sample is found outside of $\mu+3\sigma$. The warning will be generated in both cases. The earlier methods will assign the same severity index in both cases. However, the second sample should represent a higher loss since it is more spreader from the target or mean. Yu et al. (2016) used SOM and loss function to overcome this issue. The use of loss function enabled capturing dynamic loss characteristics.

Although all the methods discussed in Section 2.3 use multivariate methods to monitor the process, these frameworks develop the dynamic risk profile in a univariate manner. The variable with the highest contribution in PCA score or SOM dynamic loading is used to compute risk. However, this practice may lead to inaccurate risk estimation due to information loss.

2.4. Identified Knowledge Gaps

The following knowledge gaps are identified from the above literature review of different multivariate data-based FDD and DRA approaches:

i. The current research has made remarkable advancements in fault detection. Still, there exist challenges in early fault detection.
ii. Although the PCA and ICA are data-driven approaches, these require user-opinion to select the PCs or ICs based on percentage variation captured.
iii. The BNs can provide a better solution in fault diagnosis. However, most of the existing works rely on process knowledge for developing BN.
iv. The current literature lacks a technique that can estimate CPTs from continuous process data without discretizing them.
v. Granger causality and transfer entropy are the used tools to learn BN topology from process data. The application of other mutual information (MI) transfer-based methods such as the Kullback-Leibler divergence (KLD) has not yet been tested in this context.

vi. Works on simultaneous multivariate FDD and DRA are limited. Some of them cannot show how a fault can lead a process to failure. All the existing works use univariate fault probability to compute dynamic risk.

vii. Vine copula-based tools are promising in generating a multivariate probability index for each observation. However, these frameworks mostly suffer from diagnosis modules.

Chapter 3: Robust Process Monitoring Methodology for Detection and Diagnosis of Unobservable Faults

Preface

A version of this chapter has been published in the ***Industrial & Engineering Chemistry Research*** journal. I am the primary author, along with the co-authors, Drs. Faisal Khan, Salim Ahmed, and Syed Imtiaz. I developed the conceptual framework for the FDD model and carried out the literature review. I prepared the first draft of the manuscript and subsequently revised the manuscript based on the co-authors' and peer review feedback. Co-author Dr. Faisal Khan helped in the concept development and testing the model, reviewing, and revising the manuscript. Co-authors Drs. Syed Imtiaz and Salim Ahmed provided support in implementing the concept and testing the model. The co-authors provided fundamental assistance in validating, reviewing, and correcting the model and results. The co-authors also contributed to the review and revision of the manuscript.

Reference: Amin, M. T., Khan, F., Imtiaz, S., & Ahmed, S. (2019). Robust process monitoring methodology for detection and diagnosis of unobservable faults. Industrial & Engineering Chemistry Research, 58(41), 19149-19165. https://doi.org/10.1021/acs.iecr.9b03406

Abstract

This chapter presents a new integrated methodology for fault detection and diagnosis. The methodology is built using the multivariate exponentially weighted moving average principal component analysis (MEWMA-PCA) and the Bayesian network (BN). The fault detection is carried out using the MEWMA-PCA; diagnosis is completed utilizing the BN models. A novel supervisory learning-based methodology has been proposed to develop the BNs from historical fault symptoms. Although the algorithm has been extensively applied to the Tennessee Eastman (TE) chemical process, monitoring of three specific (difficult to observe) faults: IDV 3, IDV 9, and IDV 15 has been demonstrated in this article. Most of the existing data-based methods have faced the challenge of detecting these faults with a good detection rate (DR). Hence, these faults have been reported as either unobservable or strenuous to detect. The overall fault detection performance of the squared prediction error (SPE) statistics combined with the MEWMA-PCA was found to be better than the T^2-based monitoring model. Although the cumulative sum (CUSUM) PCA-based approaches have demonstrated successful detection and diagnosis of these specific faults, the comparative studies suggest that the proposed methodology can outperform the CUSUM PCA approach.

Keywords: *Process monitoring, fault detection, unobservable faults, MEWMA-PCA, Bayesian network.*

3.1. Introduction

Early detection of an abnormal event (e.g. process deviation or equipment malfunction) is required for safe and reliable process operations. Finding the root cause(s) of such undesired events is also crucial to restore the process within a normal operating mode (Mnassri et al., 2009). These two actions are combinedly known as fault detection and diagnosis (FDD). FDD is the core element of any process monitoring scheme (Chiang et al., 2001; Venkatasubramanian et al., 2003b). The existing FDD techniques can be segregated into three categories: model-based methods, knowledge-based methods, and data-based methods (Venkatasubramanian et al., 2003b, 2003a, 2003c). In the modern process industries, data-based methods are widely used compared to model-based methods, as the precise mathematical models required to build the model-based monitoring models for process plants are often harder to obtain. Furthermore, the availability of a large volume of data makes the data-based tools more suitable than the model-based counterparts (Chiang et al., 2001; Ge et al., 2013; Qin, 2009).

Data-based methods are mainly divided into two types: univariate tools and multivariate tools (Pei et al., 2008; Venkatasubramanian et al., 2003c). Both these families of data-driven models use historical process data collected in normal operating condition (NOC) to define the control limits (CLs) of acceptable process operations. The Shewhart chart, exponentially weighted moving average (EWMA) chart, and cumulative sum (CUSUM) chart are the widely used univariate monitoring tools (Montgomery and Runger, 2010; Shewhart, 1930). However, process monitoring using the univariate tools is arduous for operations with a large number of variables due to the use of a dedicated control chart for each variable. Moreover, these charts are not adaptable to a change in the operating conditions; this may result in a false detection or missed alarm (Kondaveeti et al., 2009). Multivariate statistical process monitoring (MSPM) tools reduced some complexities

associated with the univariate monitoring tools and became more popular for FDD in recent decades (Ge et al., 2013; He and Wang, 2018; Qin, 2003).

According to a bibliometric review by Alauddin et al. (2018), principal component analysis (PCA), partial least squares (PLS), independent component analysis (ICA), Gaussian mixture model (GMM), and their derivates are the most widely used MSPM tools in process industries. PCA projects a higher-dimensional historical process data to a lower-dimensional feature space, retaining the significant information of original variables (Bakshi, 1998; Garcia-Alvarez et al., 2012; Misra et al., 2002). Fault is generally detected with the aid of the T^2, the Q or the squared prediction error (SPE)-based control charts (Mnassri et al., 2009). By employing PCA, PLS was also developed (MacGregor et al., 1994; Wilson and Irwin, 2000). Both PCA and PLS assume a linear correlation among the process variables and a Gaussian distribution of data. These assumptions limit the performance of these approaches. Additionally, conventional PCA and PLS are static in nature. Dynamic versions of PCA and PLS were also proposed to capture the dynamic process nature (Chen and Liu, 2002; Ku et al., 1995).

ICA was proposed to relax the distribution assumption, as it is capable of representing features from a non-Gaussian distribution (Kano et al., 2003; Lee et al., 2004b). However, the ICA cannot rank the important independent components (ICs) like the PCA, and therefore, modified versions of ICA (MICA) were proposed to capture the significant ICs (Lee et al., 2006; Zhang and Zhang, 2010). The combined PCA-ICA approach was presented by Jiang et al. (2016) for fault diagnosis in non-Gaussian processes. In real industrial processes, data are often found to be following both non-Gaussian and Gaussian distributions. Hence, GMM was proposed to address this issue (Yu and Qin, 2008). However, nonlinear relationships among the process variables affect the performance of these tools significantly. Kernel-based tools were introduced to overcome this

problem. Kernel PCA (KPCA), kernel ICA (KICA), kernel PLS (KPLS), and kernel GMM (KGMM) are some of the attempts to handle process nonlinearity (Kim et al., 2005; Lee et al., 2007, 2004a; Yu, 2012; Zhang et al., 2010). Dynamic extensions of these tools are also available in the existing literature (Fan and Wang, 2014; Jia et al., 2010; Jia and Zhang, 2016). However, kernel-based methods transform the lower-dimensional data into a higher-dimensional feature space, making the computation onerous. To avoid this issue, nonlinear versions of conventional PCA have also been proposed (Yu et al., 2016a, 2016b).

Although the MSPM tools have advanced the pace of fault detection remarkably, accurate diagnosis of faults is still an existing challenge. The hybrid methods have been developed to provide robust diagnostic performance, as no individual method is found to be fulfilling each and every aspect of FDD, according to the exhaustive review by Venkatasubramanian et al. (2003c). The main aim of these hybrid methods is to overcome the limitations of an individual tool. Although the MSPM tools cannot guarantee accurate diagnosis consistently, these can generate multivariate contribution plots after successful fault detection that contain useful information and can be used for fault diagnosis (Alcala and Qin, 2010, 2009; Li et al., 2016; Mnassri et al., 2015). This lucrative aspect of the MSPM tools has paved the way for developing several hybrid tools by combining them with the knowledge-based tools such as sign digraph (SDG), possible cause and effect graph (PCEG), Granger causality, transfer entropy, and Bayesian network (BN). Vedam and Venkatasubramanian (1999) proposed a PCA-SDG based hybrid method where the SDG overcomes the limited diagnostic capacity of the PCA. Efficacy of the PCA combined with the Granger causality and the transfer entropy in root cause diagnosis of a Fluid Catalytic Cracking Unit (FCCU) was shown by Gharahbagheri et al. (2015). Li et al. (2016) combined the DPCA with

the Granger causality for efficient fault diagnosis. Many hybrid methods have been developed using the BN, as well (Amin et al., 2018b; Gharahbagheri et al., 2017b; Yu et al., 2015b).

The Tennessee Eastman (TE) chemical process was introduced by Downs and Vogel (1993) in 1993, and it is the most widely used process model for demonstration of FDD tools (Bathelt et al., 2015; Chiang et al., 2001; Ding et al., 2009). It is an open-loop unstable process that contains real industrial process data and requires to operate under control action. A total of four single-input and single-output (SISO) plant-wide control structures and their performance for the TE chemical process were displayed by Lyman and Georgakis (1995). The decentralized control strategy of this process was demonstrated by Ricker (1996). Recently, Bathelt et al. (2015) presented a revised TE process model in MATLAB that extends the flexibility of stochastic simulation. This revision is an updated version of Ricker (2005). The advantages of this simulator are described in the work by Capaci et al. (2018).

There are 15 known and 5 unknown faults that can be introduced into the TE chemical process. According to the Web of Science and Scopus databases, the total number of published documents on FDD using the TE chemical process are 866 and 1,001, respectively (searched on April 6, 2019). The TE chemical process has been utilized to validate several data-driven MSPM tools over the last three and a half decades. However, most of the tools failed to provide a good DR for three specific faults: IDV 3 (a step change in the D feed temperature), IDV 9 (a random variation in the D feed temperature), and IDV 15 (condenser cooling water valve stiction). These three faults have been described as either unobservable or difficult to detect by many authors (Krishnannair and Aldrich, 2017; Shams et al., 2011; Yin et al., 2012). Table 3.1 shows a list of some of the articles reporting a lower DR for these faults employing several MSPM tools. It can be seen that major FDD tools such as PCA, ICA, PLS, and kernel-based methods consistently fail to detect these three

faults early. The DR was found to be lower than the other fault cases by applying some recently developed advanced tools (Dong and Qin, 2018; Gajjar et al., 2018; Wan and Li, 2019; Yu et al., 2016b; Zhu et al., 2018b).

Table 3.1: A list of works that have reported lower detection rates for IDV 3, IDV 9, and IDV 15.

Article	Reported Methods
(Lee et al., 2007)	PCA, ICA, MICA, KICA
(Salahshoor and Kiasi, 2008)	ICA, DICA
(Cheng et al., 2010)	PCA, KPCA, AKPCA
(Hsu et al., 2010)	PCA, ICA, ICA-AO
(Vahed et al., 2010)	PCA, RBF, RBF-GA
(Zhang and Zhang, 2010)	ICA, Fast ICA, PSO-ICA
(Yin et al., 2011)	PLS, MPLS
(Yin et al., 2012)	PCA, DPCA, ICA, MICA, FDA, PLS, TPLS, MPLS, SAP
(Rato and Reis, 2013)	PCA, DPCA, DPCA-DR
(Yu et al., 2014)	PCA, SOM
(Yu et al., 2015c)	PCA, KPCA, KICA, SPA, MWKPCA, NLGBN
(Yu et al., 2015b)	PCA, ICA, G-Copula
(Yu et al., 2016b)	PCA, KPCA, KICA, IKICA, SPA, MWKPCA, SePCA (Spearman correlation), SePCA (Distance correlation),
(Zhu et al., 2018b)	Distributed parallel GMM
(Gajjar et al., 2018)	PCA, SPCA, RNPCA, KPCA, KICA, ASPCA
(Zhu et al., 2018a)	PCA, PPCA, BWPCA, Distributed BN
(Dong and Qin, 2018)	DPCA
(Wan and Li, 2019)	KPCA, ICA, VCDD, TVCDD, PVCDD

Shams et al. (2011) proposed a CUSUM PCA-based method to detect these three faults. The out-of-control average run length (ARL_{OC}) was used to diagnose the fault types. The ARL_{OC} is the minimum number of samples (expressed in unit time) required to detect a fault after its inception. This methodology took longer to detect these three faults. The ARL_{OC} was found 0.15 hrs for IDV 7, IDV 11, and IDV 19; however, how these faults can be isolated in the case of equal ARL_{OC} was not mentioned. Furthermore, for real data, no information is generally available about the fault

inception time; this can make the estimation of ARL_{OC} arduous. When simulated data is used, calculation of ARL_{OC} is straightforward, as it is known that the fault has been introduced at that particular sample. On the contrary, calculation of ARL_{OC} is not possible if the fault initiation time is unknown. Du and Du (2018) applied an ensemble empirical mode decomposition (EEMD) PCA and integrated CUSUM statistics to improve the DR. Several threshold limits were utilized to diagnose the fault type. Krishnannair and Aldrich (2017) proposed a nonlinear singular spectrum analysis based on the autoencoders and the dissimilarity matrices to detect these faults. However, no analysis on fault diagnosis was presented in their work.

CUSUM models are built considering a target mean shift. Although it provides robust performance over EWMA while process deviation matches the target deviation, it cannot guarantee the superiority if the observed deviation is extremely larger or smaller than the designed one (Hawkins and Wu, 2014). On the contrary, EWMA is found efficient in detecting a fault of a smaller magnitude (Han et al., 2010). When the level of deviation is within one standard deviation around the mean, EWMA outweighs CUSUM-based monitoring (De Vargas et al., 2004). The pre-processing stages of the CUSUM model need more effort compared to the EWMA model. In multivariate cases, many variables do not show any variation over time using the CUSUM technique, which results in another data processing step for these variables before applying PCA or similar approaches on the pre-processed matrix. Furthermore, deviations can be of any magnitude in real industrial processes. These make the application of EWMA models more suitable over the CUSUM-based approaches.

Multivariate exponentially weighted moving average (MEWMA) statistics is an extension of the conventional univariate EWMA (Lowry et al., 1992) that can efficiently detect small shifts (Aparisi and García-Díaz, 2007; Carson and Yeh, 2008; Prabhu and Runger, 2018). MEWMA-

PCA is a marriage between MEWMA and PCA. Process monitoring scheme integrating MEWMA with PCA was first proposed by Wold (1994). MEWMA was applied to the scores of PCA in this work. A more elaborated work was presented by Chen et al. (2001). The control limits of the T^2 and the SPE control charts were defined, and the MEWMA model was applied to the auto-scaled process data in their work. They mentioned that a process could be monitored with a lower number of principal components (PCs) using the MEWMA-PCA model. Lane et al. (2003) proposed an exponentially weighted PCA model for monitoring a film manufacturing process. Unlike the previous works, they used the MEWMA model to update the covariance matrix. Cheng et al. (2010) proposed an adaptive KPCA based monitoring tool applying the MEWMA model to the whitened components. Chouaib et al. (2015) proposed another adaptive KPCA model using the MEWMA model to update the gram matrix. Lee et al. (2003) presented two combinations of ICA with MEWMA. The first one applied the MEWMA model to the auto-scaled data (MEWMA-ICA), and the second one utilized the MEWMA to update the monitoring statistics (e.g. I^2 and SPE) (ICA-MEWMA). These works (with MEWMA) reported improved performance compared to the conventional tools such as the PCA, the ICA, and the KPCA.

The inability of several MSPM FDD tools to provide a quick detection and good DR for IDV 3, IDV 9, and IDV 15 of the TE chemical process is the main motivation behind this work. Even though the main aim of this article is to develop a tool that will detect and diagnose these faults early, the proposed method can provide the desired FDD performance for all the faults in the TE chemical process. The MEWMA has been integrated with the PCA to improve its fault detectability, and a BN is used to diagnose the fault type. The comparative studies with the previously published works based on CUSUM PCA (Du and Du, 2018; Shams et al., 2011) suggest that the proposed method is a more efficient FDD tool.

The rest of this chapter is organized as follows: Section 3.2 describes the methodology. A brief discussion on the TE chemical process along with the application of the proposed methodology is demonstrated in Section 3.3. Comparative performance evaluation with previous works is presented in Section 3.4. The advantages, limitations, and future work scopes are discussed in Section 3.5.

3.2. Proposed Methodology

This proposed integrated methodology (Figure 3.1) is comprised of MEWMA-PCA and BN. Henceforth, the integrated methodology is referred to as MEWMA-PCA-BN. MEWMA-PCA detects a fault and provides the primary diagnostic report in terms of multivariate contribution plots (e.g. T^2 and SPE). Although this diagnostic report is incomplete and points towards a group of variables as the probable causes of the detected fault, this information can be utilized to collect the fault signatures. A bank of MEWMA-PCA models for each fault type is trained to collect the fault signatures and used to train the BNs; these BNs are utilized to identify the fault type after fault detection. Even though several techniques have been described in Section 3.1 to build the MEWMA-PCA model, we have constructed the model in a different manner: first applying the MEWMA to the auto-scaled historical process data and then, performing the conventional PCA. The procedure is analogous to the method of constructing the MEWMA-ICA model described by Lee et al. (2003). This technique is found to be the simplest compared to the methods described in Section 3.1. Furthermore, it can serve the purpose of quicker detection and requires less computation.

The limited diagnostic capacity of the MEWMA-PCA is overcome by coupling it with the BN. Even though a BN has ample application in process safety and risk analysis (Bobbio et al., 2001; Hashemi et al., 2016), reliability and availability analysis (Amin et al., 2018c; Cai et al., 2012),

and dependability and maintainability modelling (Weber et al., 2012), still, it is at a premature stage in the field of FDD in spite of several documents published using it. It is a directed acyclic graph (DAG)-based tool that uses probabilistic reasoning to reach a certain conclusion from either certain or uncertain observations. The flexibility of modelling the BNs from both process knowledge and historical data has made it appealing to the researchers (Li et al., 2016). In-depth process knowledge can be displayed in graphical view using a BN (Wang et al., 2017).

BNs are constructed using nodes, arcs, prior, and conditional probabilities. In the BNs, process variables are shown as nodes, and arcs are used to define their causal relationships. An arch is directed to a child node (effect) from a parent node (cause). The strength of the relationships among the process variables is defined using conditional probabilities. Prior probability is the anecdotal belief about an event. Another robust property of a BN is that it can get updated at any state of any node upon receiving evidence and provide new probabilities in the nodes. This makes the BNs suitable for fault diagnosis, as the renewed probabilities can be compared with the prior probabilities for measuring the effect of an evidence to the variables. Bayes' theorem (Equation 3.1) is the prime-mover of the BNs.

$$P(Y/X) = \frac{P(X/Y) \times P(Y)}{P(X)} \tag{3.1}$$

where $P(Y)$ is the prior belief, and $P(X)$ is the probability of an observation or evidence. $P(X/Y)$ is the conditional probability of X given Y, and $P(Y/X)$ is the conditional probability of Y given X.

For a certain evidence of X, the Bayesian belief updating equation can be obtained from Equation 3.2 as:

$$P(Y/X) = P(X/Y) \times P(Y) \tag{3.2}$$

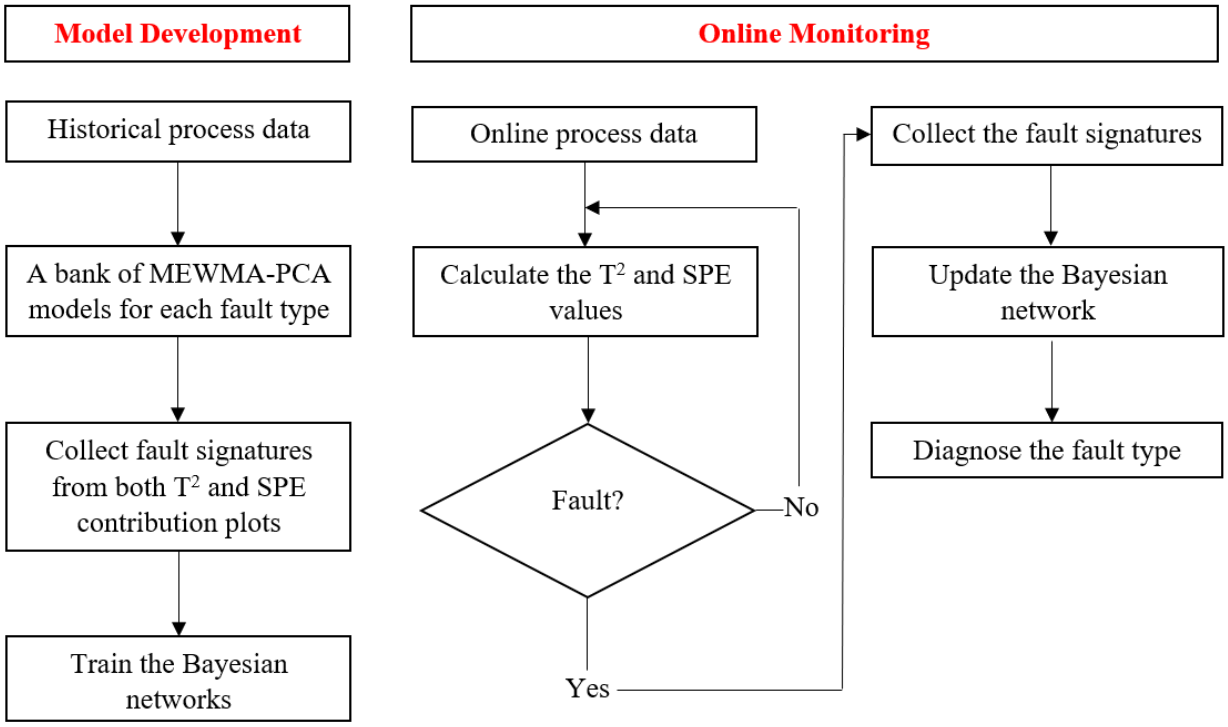

Figure 3.1: Flowchart of the proposed methodology.

The conventional approaches to build the BNs include constructing the causal network from prior knowledge and determining the prior and conditional probabilities from historical process data or the PCA residuals (Amin et al., 2019a, 2017; Gharahbagheri et al., 2017; Mallick and Imtiaz, 2013; Verron et al., 2010; Wang et al., 2017; Yu et al., 2015a; Yu and Rashid, 2013). Nevertheless, the BNs are constructed in a different manner in this work. Fault symptoms are expressed as a set of parent nodes, and fault types are shown as the child nodes. Fault signatures are inserted into the BNs in terms of conditional probabilities. The mathematical translation of conditional probabilities in the conditional probability table (CPT) of a fault node can be defined as expressed in Equation 3.3.

$$P(F) = \begin{cases} 1 & if\ \ x_j/x_1, x_2, \dots, x_{j-1} is\ faulty \\ 1 & if\ \ x_k/x_1, x_2, \dots, x_{k-1} is\ faulty \\ 0 & if\ \ x_k/x_1, x_2, \dots, x_{k-1} is\ not\ faulty \\ 0.50 & in\ all\ other\ cases \end{cases} \tag{3.3}$$

where j is the number of variables used to collect the fault signatures. k is the total number of variables associated with a fault node, and $j \leq k$.

The development procedure of a BN from multiple MEWMA-PCA models is shown in Figure 3.2.

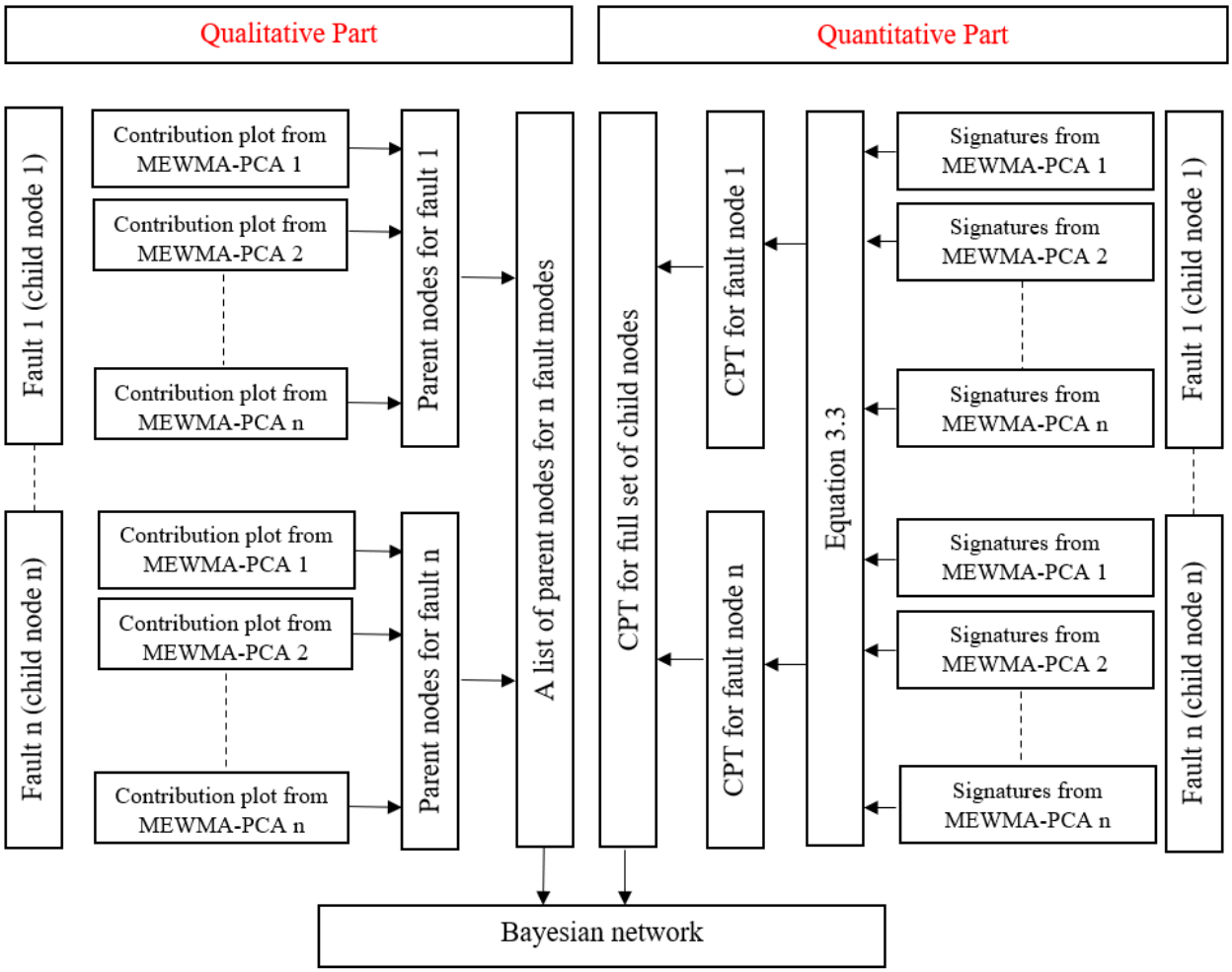

Figure 3.2: Flowchart of the BN development technique.

Suppose a process has two fault types: DN 1 and DN 2, and four variables: A, B, C, and D exhibit symptoms due to these faults. A, C, and D exhibit the fault symptoms associated with DN 1, and B and C are associated with DN 2. A BN can be constructed using the following steps:

Step 1 (determining the child nodes): There will be two child nodes, as there are two fault types in this process. The child nodes will represent DN 1 and DN 2.

Step 2 (determining the parent nodes): A total of four nodes will be assigned as the parent nodes. A, C, and D will be the parent nodes for DN 1, while B and C will serve as the parent nodes for DN 2.

Step 3 (assigning the arcs): Each pair of parent and child nodes (i.e. C and DN 1, C and DN 2) will be connected by an arc. A variable corresponding to a symptom can act as the parent node of multiple child nodes.

Step 4 (assigning the states): All nodes are considered with binary states: faulty (*F*) and normal (*NF*) for simplicity in diagnosis. A node can have more than two states.

Step 5 (assigning the CPTs): This BN will have two CPTs: one for DN 1 and another one for DN 2. Tables 3.2 and 3.3 show the CPTs for DN 1 and DN 2, respectively. The number of columns in a CPT will be 2^h. h is the number of parent nodes for a child node. Therefore, there will be 8 and 4 columns in the CPTs for DN 1 and DN 2, respectively. The first and last columns of Table 3.2 satisfy conditions 1 and 3, respectively, in Equation 3.3. Hence, $P(F)$ will be 1 in column 1, and $P(F)$ will be 0 in column 8. $P(F)$ is assigned in the other six columns (column 2-7) as 0.50 using condition 4 since all three variables associated with fault DN 1 are not in a faulty state for these six columns. On the contrary, $P(F)$ will be assigned as 1 and 0 for columns 1 and 4, respectively, in Table 3.3, using conditions 1 and 3 of Equation 3.3, respectively. Additionally, Column 1 also satisfies condition 2 of Equation 3.3 in this case. $P(F)$ will be 0.50 for columns 2 and 3, following condition 4. It is noteworthy to mention that condition 2 of Equation 3.3 is frequently used when a BN is trained with a large number of MEWMA-PCA models. Figure 3.3(A) shows the developed BN for the illustrative process.

Table 3.2: CPT for DN 1.

A		F				NF			
C		F		NF		F		NF	
D		F	NF	F	NF	F	NF	F	NF
DN 1	F	1	0.50	0.50	0.50	0.50	0.50	0.50	0
	NF	0	0.50	0.50	0.50	0.50	0.50	0.50	1

Table 3.3: CPT for DN 2.

B		F		NF	
C		F	NF	F	NF
DN 2	F	1	0.50	0.50	0
	NF	0	0.50	0.50	1

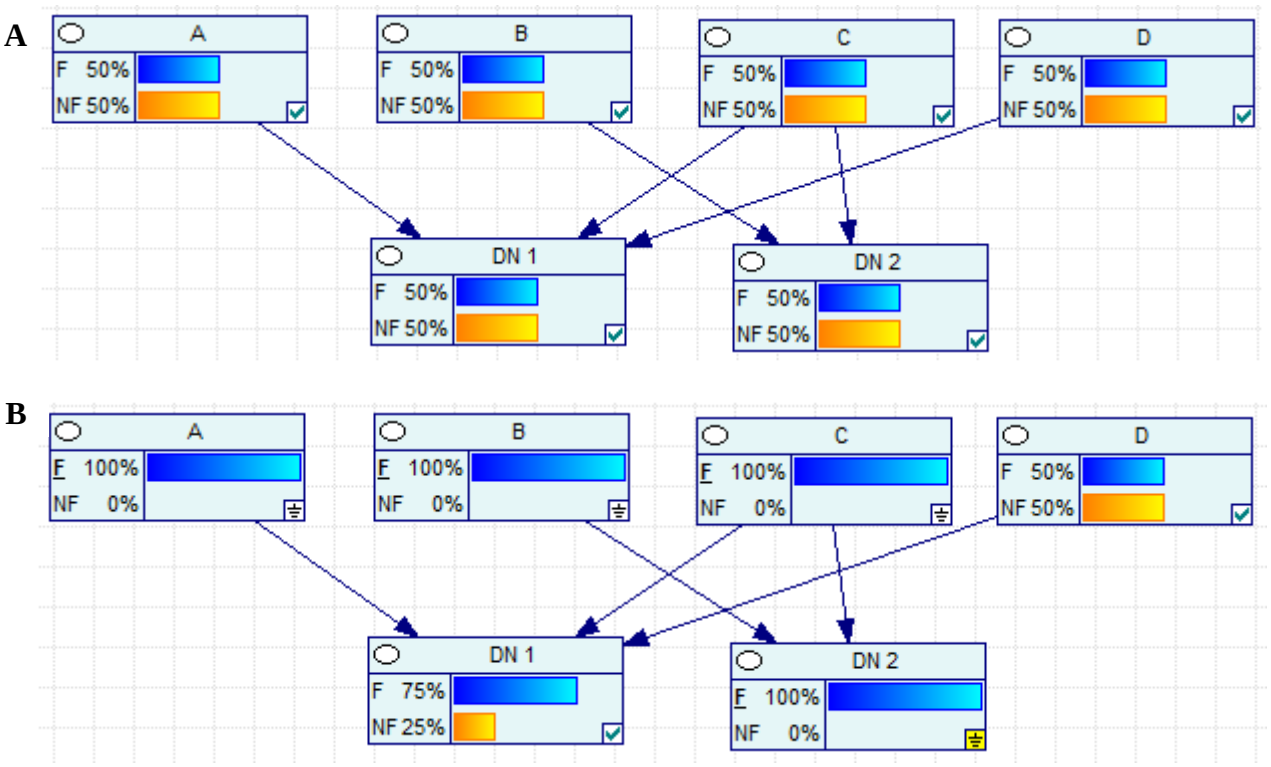

Figure 3.3: (A) Construction of a simple BN of four symptoms and two fault types (B) illustration of fault diagnosis scheme.

Now, if A, B, and C are identified as the probable causes of a fault by the multivariate contribution plot after successful detection, the BN will be updated with three hard evidence (i.e. $P(F)$ =100%) to the faulty state of A, B, and C (Figure 3.3(B)), and DN 2 will be diagnosed as the fault type since it has the closest similarity with the observed fault signatures.

It can be seen from Figure 3.1 that the proposed methodology works in two phases: model development and online monitoring. Model development is done in offline mode using the historical process data collected in both normal and faulty operating conditions, and real-time online samples are used to distinguish the faulty and non-faulty conditions of process operations. If fault is detected by the MEWMA-PCA, a contribution plot is generated, and the trained BN(s) is updated using the fault signatures to diagnose the fault type.

The model development phase consists of the following steps:

Step 1: The process system is fully studied, and the faults associated with the process is identified.

Step 2: This step is mainly concerned with the development of the MEWMA-PCA model using the historical process data and is comprised of the following sub-steps.

Sub-step 2a: Historical process data in NOC is collected and auto-scaled to zero mean and unit variance.

Sub-step 2b: The MEWMA model is developed using Equation 3.4.

$$Z_t = \lambda X_t + (1 - \lambda) Z_{t-1} \tag{3.4}$$

where λ is a tuning parameter. $X = [x_1, x_2, x_3, \ldots, x_m]$ is the auto-scaled data from previous sub-step. m is the number of process variables. The value of λ falls within 0 to 1 (i.e. $0 < \lambda \leq 1$). Selection of an optimal λ is crucial for the proper process monitoring. Hunter (1986) proposed a calculation method for λ based on the smallest sum of one step ahead prediction errors. Lee et al. (2003) found this procedure unsuitable. Montgomery (2007) suggested an interval from 0.05 to

0.25. Chen et al. (2001) proposed that λ value should be selected in such a way that it can capture the optimal process behaviour. In general, a lower λ value is used to detect smaller shifts. λ can be assigned by expert opinion, as well. In this study, we have selected the optimal λ value, following the strategy mentioned in (Chen et al., 2001).

Sub-step 2c: Principal component analysis is performed on the MEWMA model. PCA is the most widely used FDD tool, and details on PCA can be found in (Garcia-Alvarez et al., 2009; Jackson, 2005; Jackson and Mudholkar, 1979).

Sub-step 2d: Two statistics, the Hotelling's T^2 and the SPE are used in MEWMA-PCA based fault detection. The T^2 value is a measure of the distance between samples and focus of the feature space, while the SPE value indicates a measure of lack of mismatch of a sample from the residual space (Yu et al., 2015b). The T^2 value and contribution for a sample can be calculated using Equations 3.5 and 3.6, respectively.

$$T_i^2 = t_i t_i^T \tag{3.5}$$

$$t_i = x_i P_l \wedge_b^{-1/2} P_l^T \tag{3.6}$$

where t_i is the T^2 contribution of the i^{th} monitored sample. P_l is the loading, and $\wedge_b$ is a diagonal matrix that contains the first 'b' number of eigenvalues in descending order. b is selected using the cumulative percentage of variation (CPV) approach, as described in Garcia-Alvarez et al. (2009). The SPE value and contribution for a sample can be calculated using Equations 3.7 and 3.8, respectively.

$$SPE_i = e_i x_i^T \tag{3.7}$$

$$e_i = x_i(I - P_l P_l^T) \tag{3.8}$$

where e_i is the SPE contribution of the i^{th} monitored sample. I is an m by m identity matrix.

Sub-step 2e: The thresholds of T^2 and SPE statistics can be computed using Equations 3.9 and 3.10, respectively.

$$T^2_{threshold} = \frac{(n^2-1)b}{n(n-b)} \times F_\alpha(b, n-b) \tag{3.9}$$

where $F\alpha$ (b, n-b) is the probability obtained from the F distribution with (b, n-b) degrees of freedom with a 1-α level of confidence. n and b denote the number of trained samples and selected PCs, respectively.

$$Q_\alpha = \Theta_1 \left[\frac{h_o c_\alpha \sqrt{2\Theta_2}}{\Theta_1} + 1 + \frac{\Theta_2 h_o (h_o - 1)}{\Theta_1^2} \right]^{\frac{1}{h_o}} \tag{3.10}$$

where $\Theta_i = \sum_{j=b+1}^{m} \lambda_j^i$ and $h_o = 1 - \frac{2\Theta_1\Theta_3}{3\Theta_2^2}$

c_α is obtained from a normal distribution for α level of confidence (Jackson and Mudholkar, 1979).

Step 3: A bank of MEWMA-PCA models is trained for each fault type.

Step 4: Fault signatures are collected using the contribution plots from the trained MEWMA-PCA models, and these are used to train the BN. Fault information is inserted in terms of conditional probabilities in the BN using Equation 3.3. It is noteworthy to mention that the six topmost contributing variables have been considered as the fault signatures for each MEWMA-PCA model. Two distinct BN models are trained from the results of T^2 and SPE contribution plots, respectively. Each BN has a number of decision nodes equal to the number of identified faults in the studied process system.

The online monitoring is performed in the following steps:

Step 5: Online samples are auto-scaled using the same mean and standard deviation values obtained in sub-step 2a.

Step 6: Equation 3.4 is applied to the auto-scaled online data samples using the same λ value that has been used in sub-step 2b.

Step 7: T^2 and SPE values of all the online samples are calculated using Equations 3.5 and 3.7, respectively. If the threshold value of any of these control charts is violated, fault is detected.

Step 8: Following the successful detection of fault, corresponding contribution plot (i.e. T^2 or SPE) is generated.

Step 9: Top six contributing variables are identified and used to update the belief of the corresponding BN.

Step 10: The percentage change in the faulty state of fault nodes is computed, and the fault node that has the highest percentage increase in the faulty state is diagnosed as the occurred fault type

3.3. Application of the Methodology to the TE Chemical Process

The TE chemical process (shown in Figure 3.4) has five major units: a reactor, a product condenser, a vapour-liquid separator, a recycle compressor, and a product stripper. The process produces two products in irreversible and exothermic reactions. A total of three main gaseous feeds (A, D, and E) are fed into the reactor in the gaseous form, where catalyzed chemical reactions form liquid products. The product stream from the reactor enters the condenser as a vapour and gets condensed. However, all the compounds are not condensed, and these are passed through the vapour-liquid separator, where the condensed and non-condensed products are separated. The non-condensed product is returned to the reactor as an additional feed by using a centrifugal compressor, while the condensed product stream enters the stripper unit to be stripped. Then, the final products exit from the stripper and are pumped for further purification.

The TE chemical process consists of a total of 53 variables: 41 measured variables and 12 manipulated variables. Among the measured variables, 22 variables are continuous process

variables, and 19 variables are related to composition measurements. The location of IDV 3, IDV 9, and IDV 15 in the different locations of the TE process is shown in Figure 3.4, and it can be seen that IDV 3 and IDV 9 occur in stream 2, while IDV 15 appears in stream 13. Variable description of the TE chemical process can be found in (Downs and Vogel, 1993).

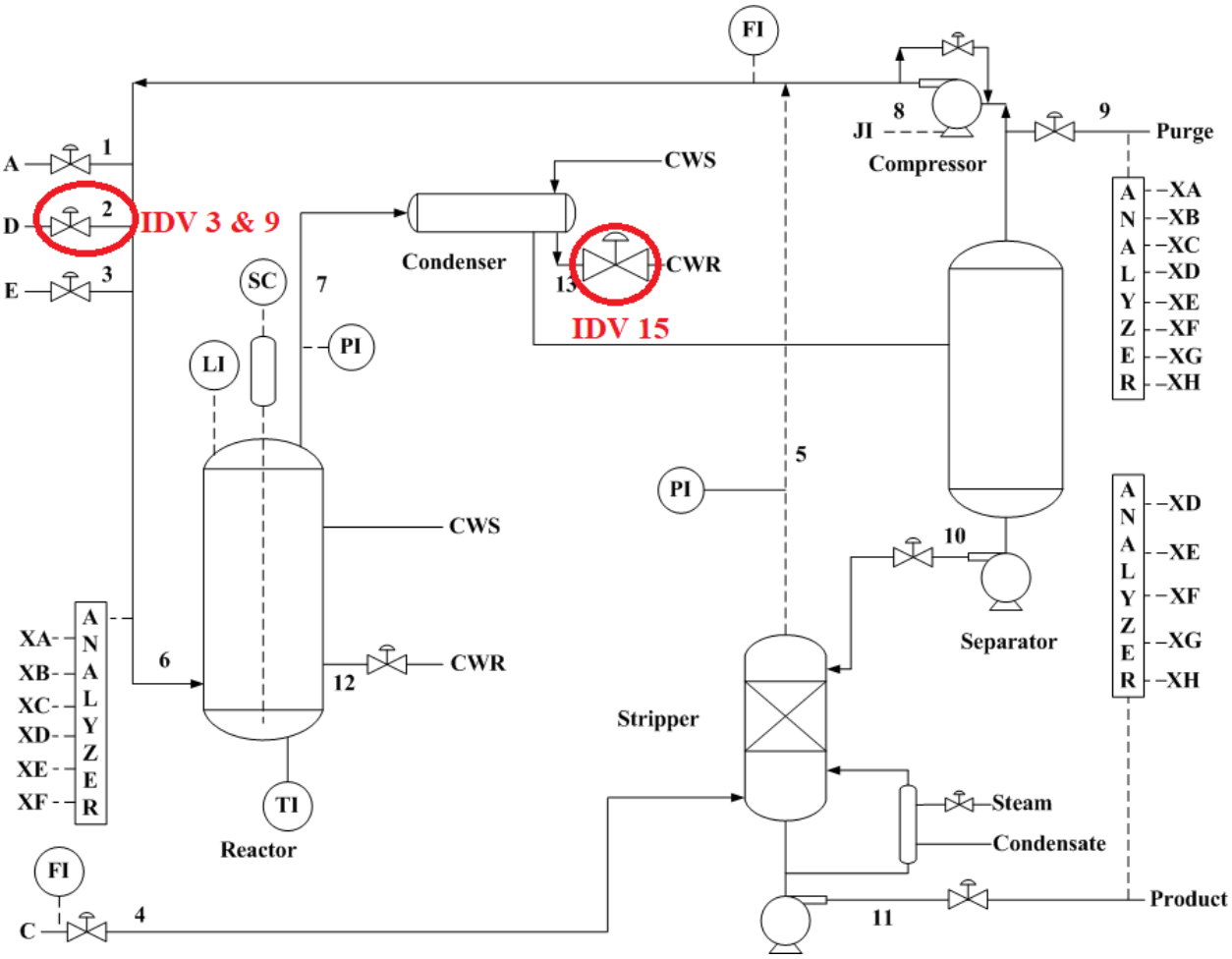

Figure 3.4: PFD of the Tennessee Eastman chemical process.

Chiang et al. (2000) presented a dataset for the TE chemical process. This dataset consists of 52 variables (except the agitation speed). The sampling time is 180 seconds, and a total of 960 test samples were generated for each fault case (48 hours of operation). After 8 hours (160 samples) of normal operation, fault starts for all 20 cases. Additionally, a training set of 960 samples is also presented that contains data from NOC. The results of PCA applied to this dataset for IDV 3, IDV

9, and IDV 15 are shown in Figure 3.5. The PCA model is built using the first 31 PCs that capture more than 90% variation. In Figure 3.5, the horizontal blue lines show the threshold limit of T^2 and SPE statistics, and the vertical green lines display the fault inception time. It can be seen that PCA provides a lower detection rate for all three cases. It should be noted that a level of confidence of 99% is used to calculate the thresholds of T^2 and SPE statistics.

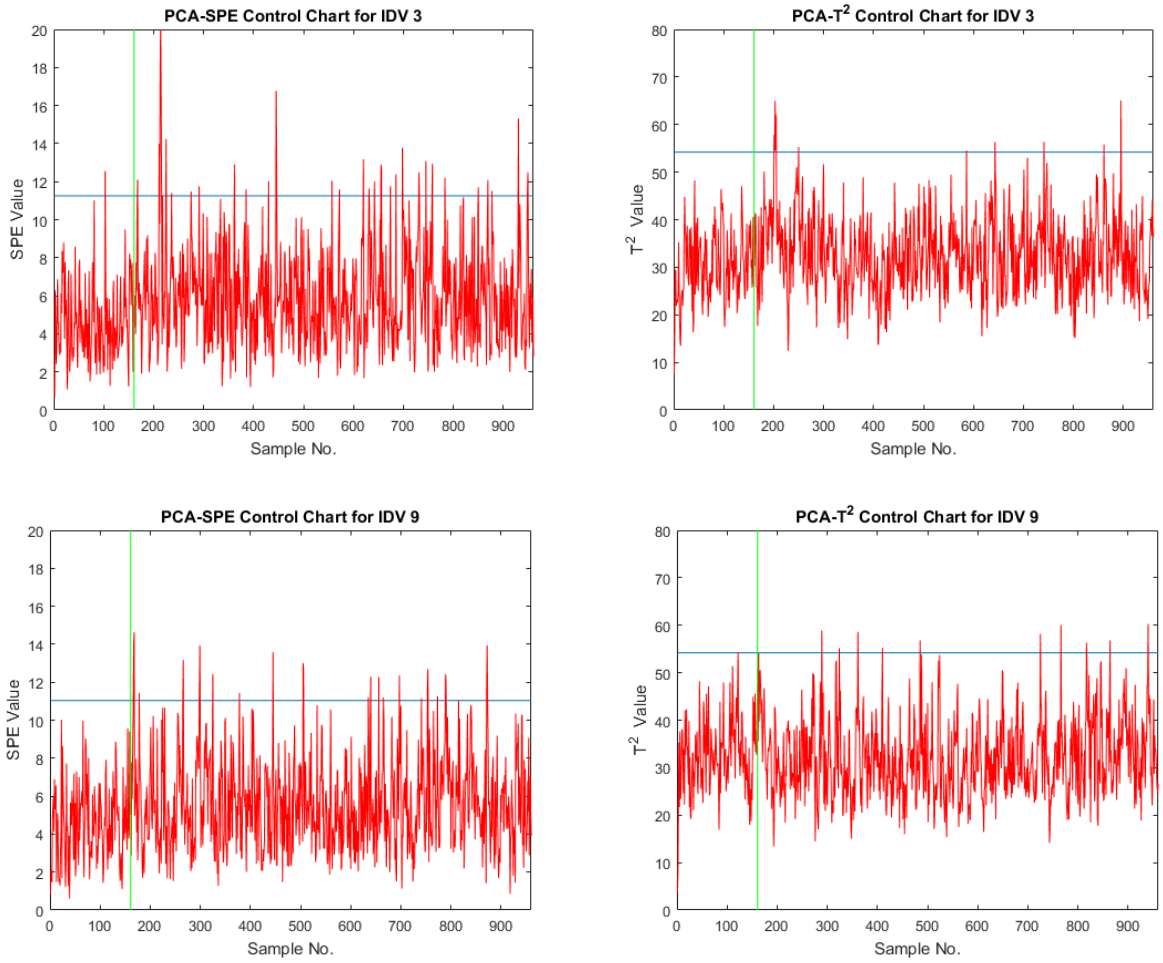

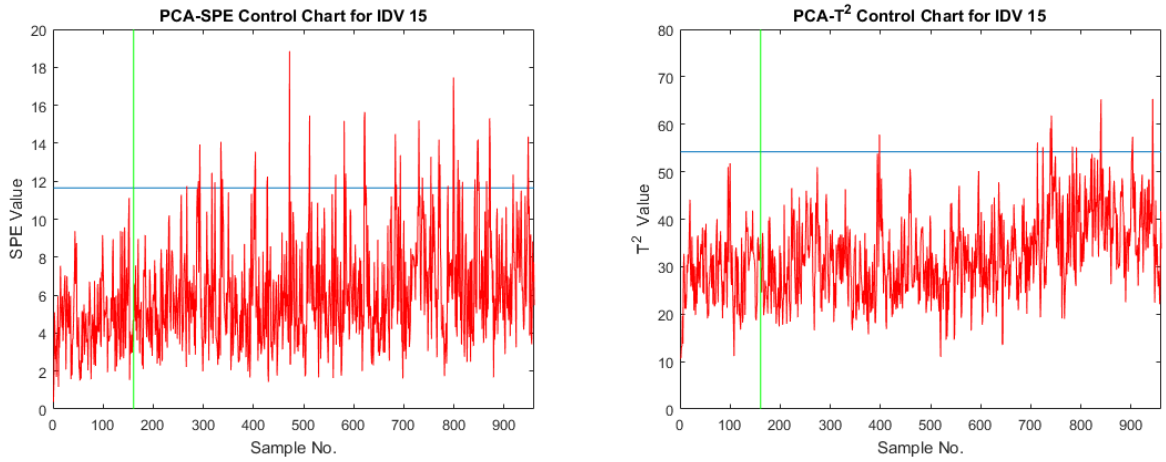

Figure 3.5: PCA based monitoring of IDV 3, IDV 9, and IDV 15.

A total of 160 samples (8 hours of normal process operation) in the NOC are used to build the MEWMA-PCA monitoring model. This regime has been considered to have a fair comparison with the work by Shams et al. (2011). These data are auto-scaled and transformed into the MEWMA model using Equation 3.4 with λ=0.03. By employing the CPV approach, it is found that the first 41 PCs can capture more than 99.99% variation and are selected to estimate the threshold limit of T^2 and SPE control charts, using Equations 3.9 and 3.10, respectively. Several MEWMA-PCA models have been trained to collect the fault signatures for each fault type where the fault was introduced after different periods of normal operation. Figure 3.6 shows the developed BN model for T^2 statistics. As the BNs are complicated and difficult to visualize due to the size of the structure, a truncated portion containing the fault nodes that show a significant increase after updating the BNs will be shown in the remainder of this chapter. However, percentage increase in the faulty state for all the fault nodes will be shown so that the diagnosis technique can lucidly be understood.

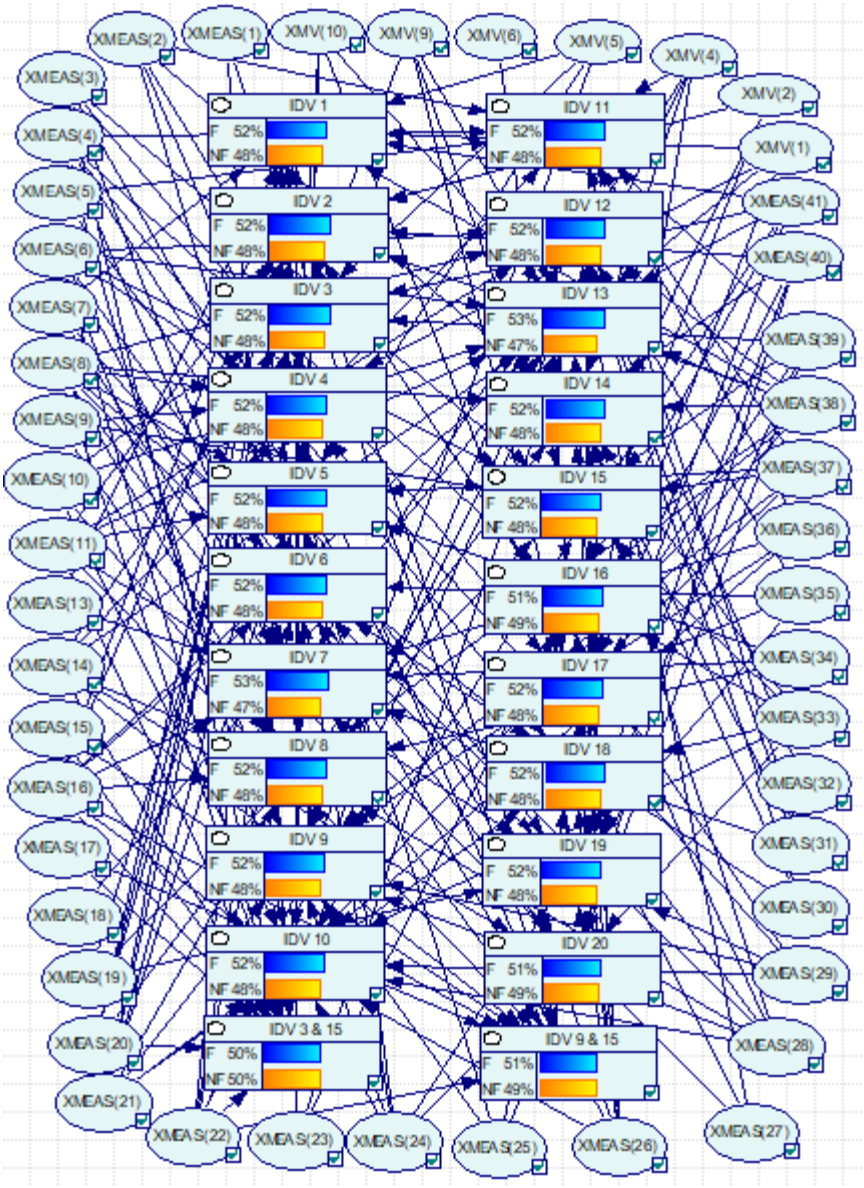

Figure 3.6: BN for T^2 control chart.

Fault starts from the 161st sample and continues for the rest of the 800 samples in all three cases. For IDV 3, SPE control chart detects the fault instantly (Figure 3.7(A)), while T^2 control chart takes a little longer and reports an abnormal situation at 162nd sample (Figure 3.7(B)). As this fault is detected earlier by the SPE control chart, SPE contribution plot is generated (Figure 3.7(C)), and it can be seen that XMV (9), XMEAS (21), XMEAS (18), XMEAS (11), XMEAS (16), and XMV (1) are the six variables that have the highest contributions to this fault. It is noteworthy to

mention that the 41 measured variables are sequentially placed first in the contribution plots as XMEAS (1) – XMEAS (41), followed by the 11 manipulated variables that are placed as XMV (1) – XMV (11).

The BN developed using the fault signatures collected from the SPE contribution plots is updated in the faulty state of the nodes that represent the above mentioned six top contributing variables. The updated BN in Figure 3.7(D) identifies IDV 3 as the diagnosed fault type accurately since it has an 86.29% increase in the faulty state, which is higher compared to the other fault nodes (Figure 3.7(E)). This diagnosis report also gives vital information about the part of the process from where the fault has emerged, as IDV 3 is a fault that appears in stream 2. It can guide the operators to restore the process quickly in normal operating mode by taking care of D feed temperature.

A

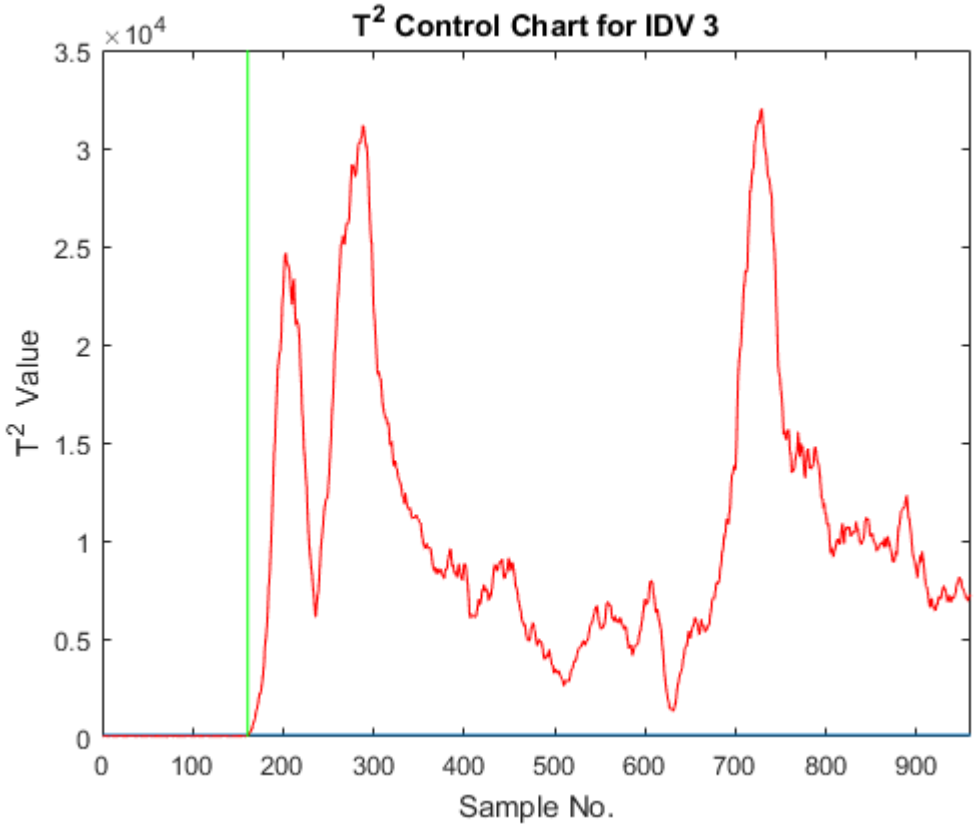

B

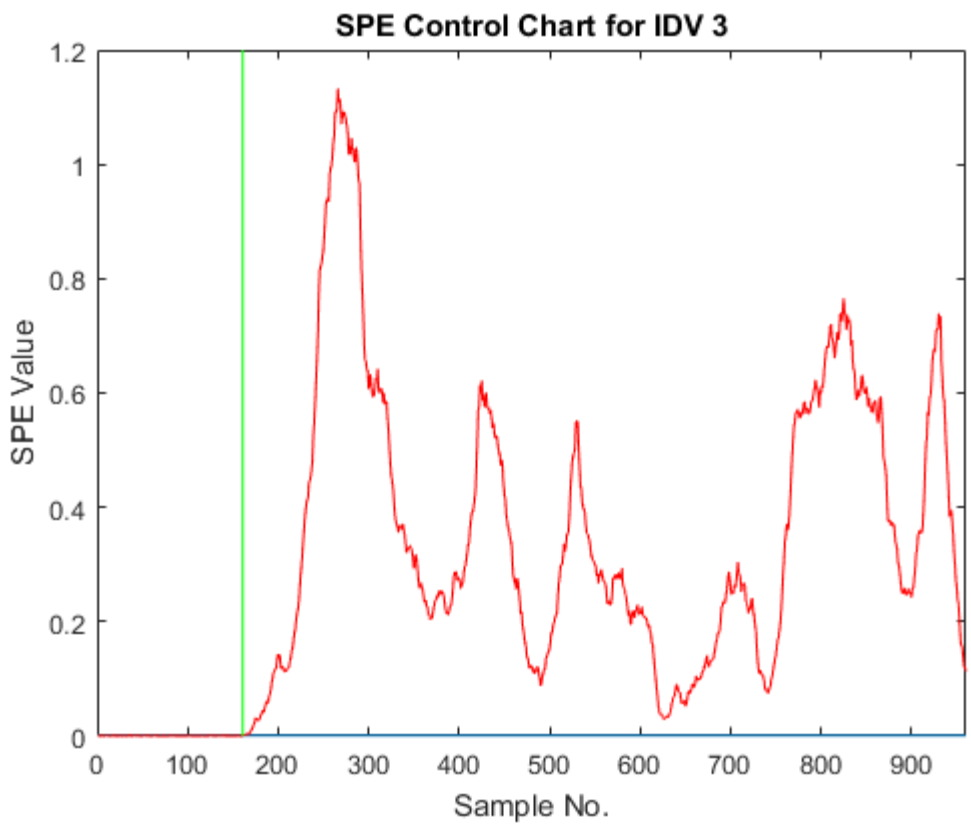
SPE Control Chart for IDV 3
SPE Value
Sample No.
0
0.2
0.4
0.6
0.8
1
1.2
0
100
200
300
400
500
600
700
800
900

C

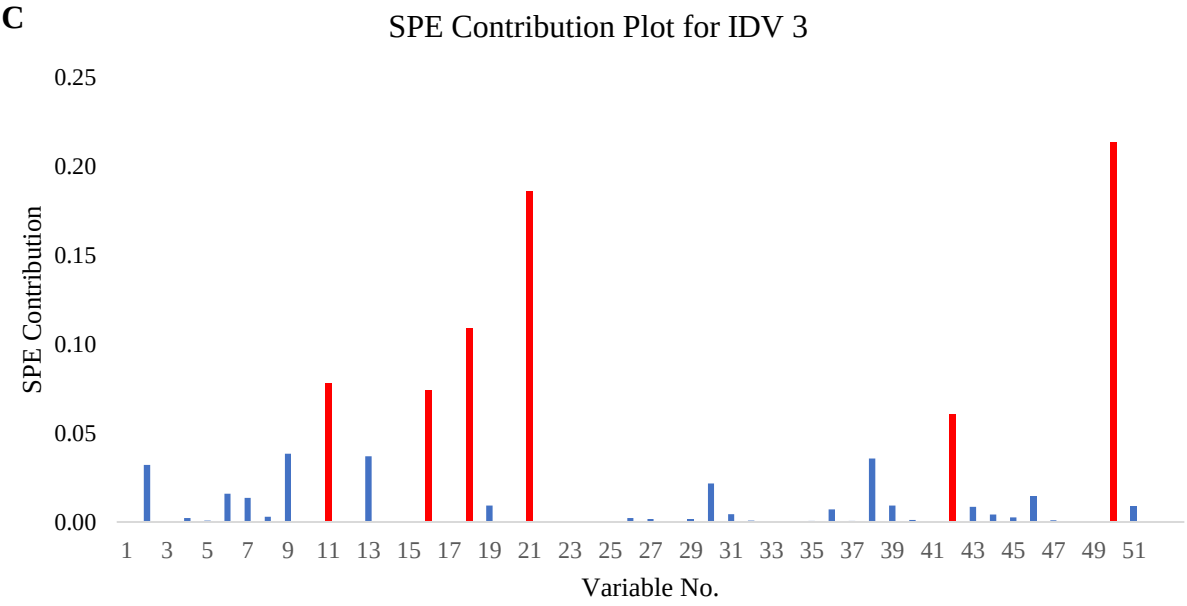
SPE Contribution Plot for IDV 3
SPE Contribution
Variable No.
0.00
0.05
0.10
0.15
0.20
0.25
1 3 5 7 9 11 13 15 17 19 21 23 25 27 29 31 33 35 37 39 41 43 45 47 49 51

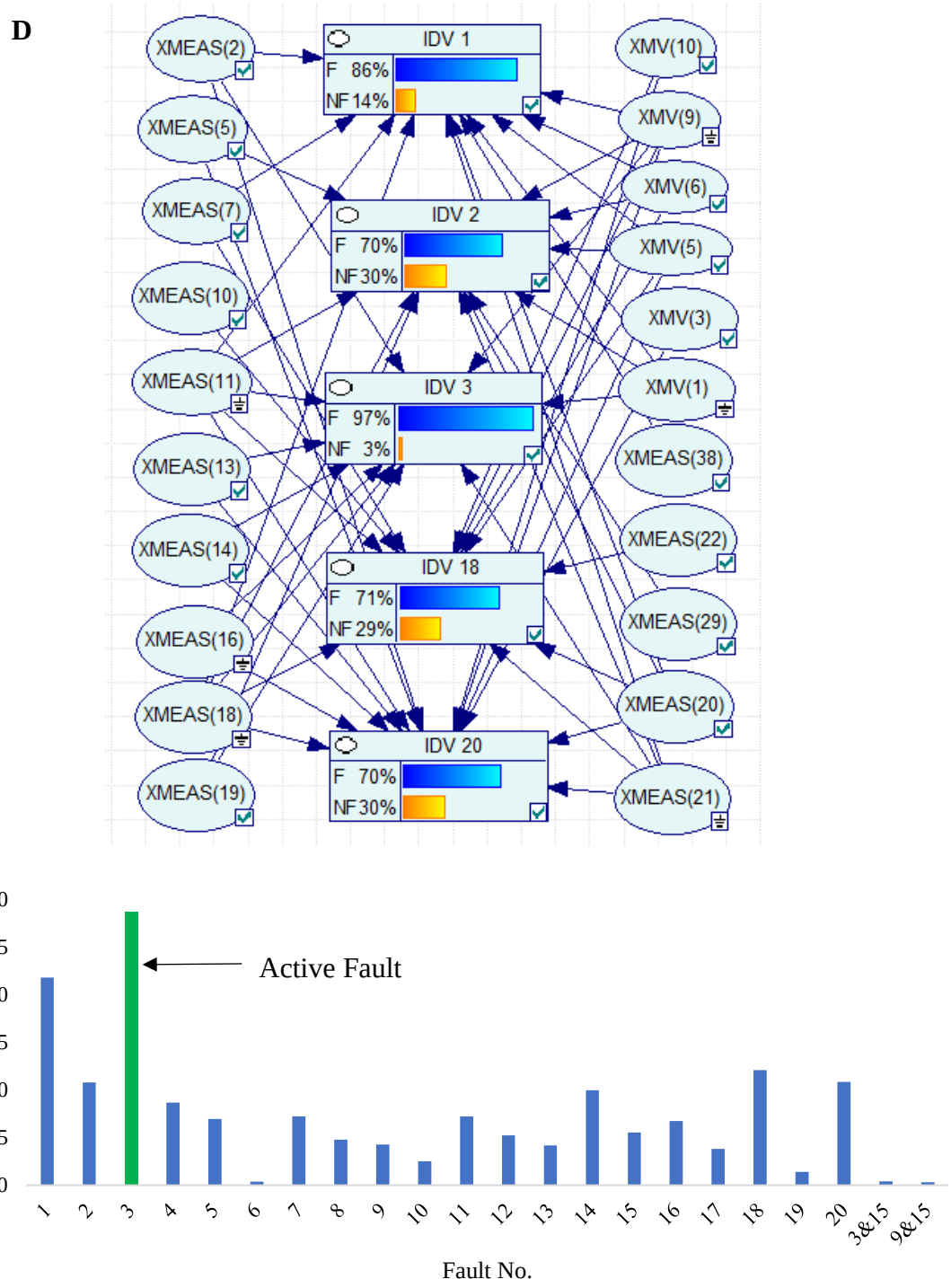

Figure 3.7: Fault detection and diagnosis by MEWMA-PCA-BN for IDV 3 (A) T^2 control chart, (B) SPE control chart (earlier detection), (C) SPE contribution plot, (D) updated SPE-based BN, and (E) fault diagnosis using percentage increase in the faulty state.

Although the location of IDV 9 is the same as that of IDV 3, the signal type (random variation) is different. Therefore, a little delay is observed to detect this fault by MEWMA-PCA. Both T^2 and SPE control charts detect this anomaly at 162nd sample (Figures 3.8(A) and 3.8(B)). After successful detection of fault, SPE contribution plot is generated (Figure 3.8(C)). XMV (5) and XMEAS (38) have the highest contributions, followed by the contributions of XMEAS (11), XMEAS (20), XMEAS (39), and XMV (1). The BN associated with the SPE statistics is utilized for fault diagnosis. The updated BN and percentage change in the faulty states of the fault nodes are shown in Figures 3.8(D) and 3.8(E), respectively, and it can be seen that IDV 7, IDV 9, IDV 10, IDV 13, and IDV 19 have significant increase in the faulty state after updating the BN with multiple evidence. However, IDV 9 has the highest percentage increase in the faulty state (70.02%) among all the fault nodes and can be diagnosed as the observed fault type.

A

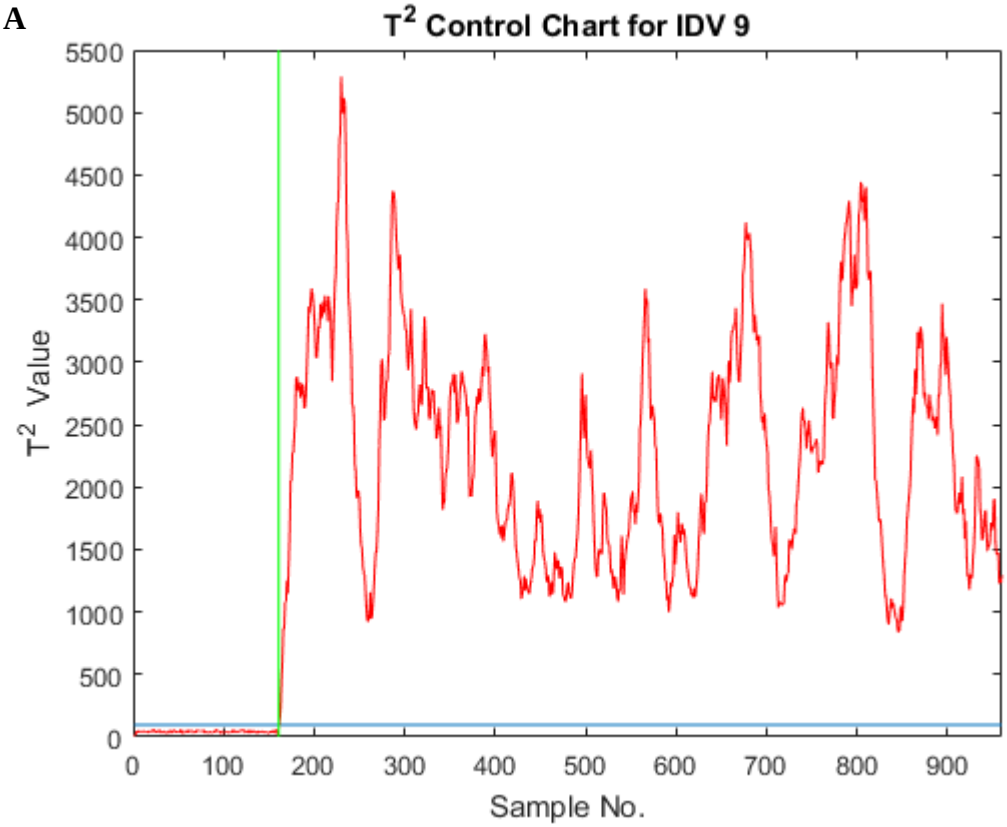

B

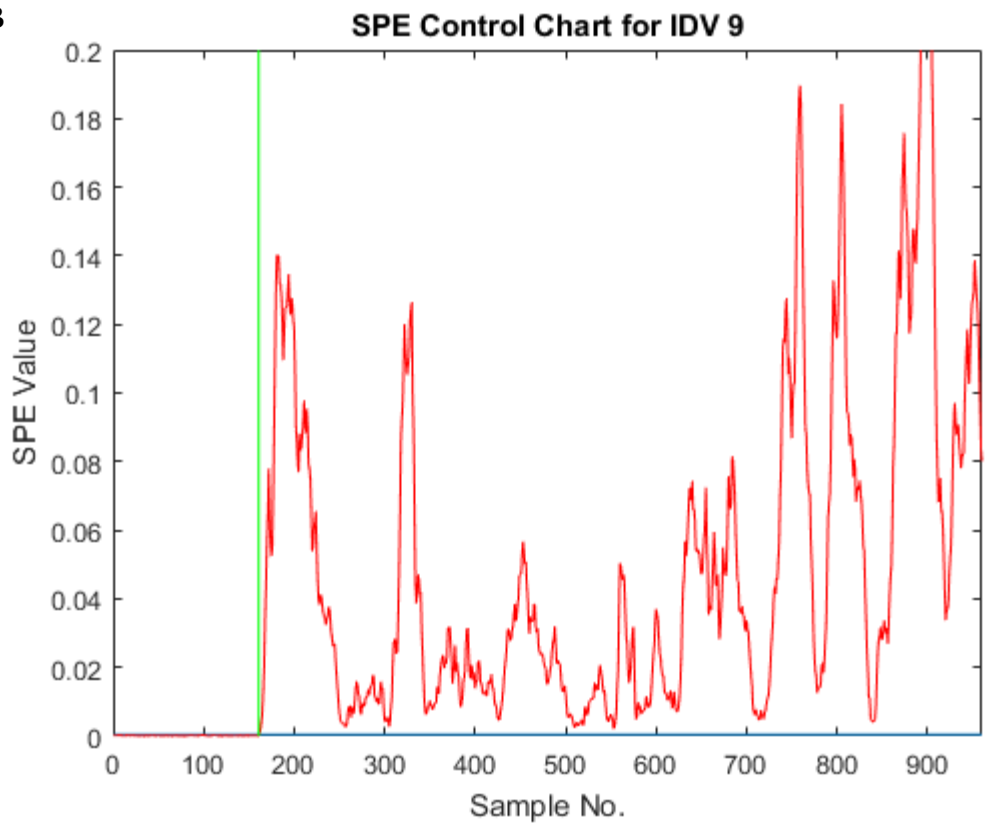
SPE Control Chart for IDV 9
SPE Value
Sample No.
0
0.02
0.04
0.06
0.08
0.1
0.12
0.14
0.16
0.18
0.2
0
100
200
300
400
500
600
700
800
900

C

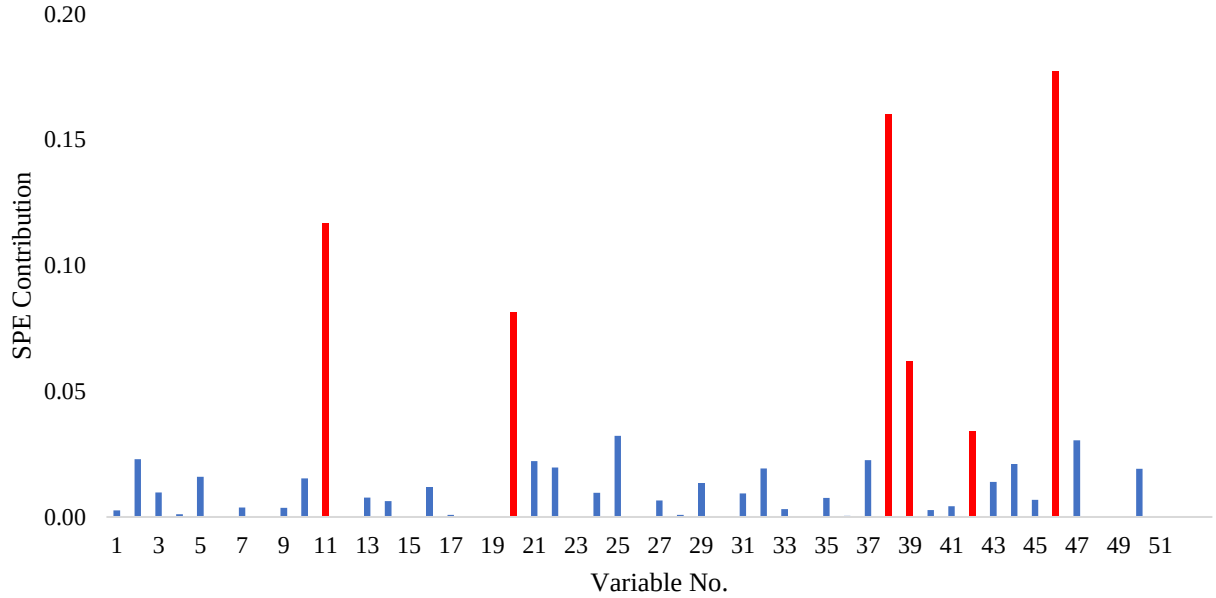
SPE Contribution Plot for IDV 9
SPE Contribution
Variable No.
0.00
0.05
0.10
0.15
0.20
1 3 5 7 9 11 13 15 17 19 21 23 25 27 29 31 33 35 37 39 41 43 45 47 49 51

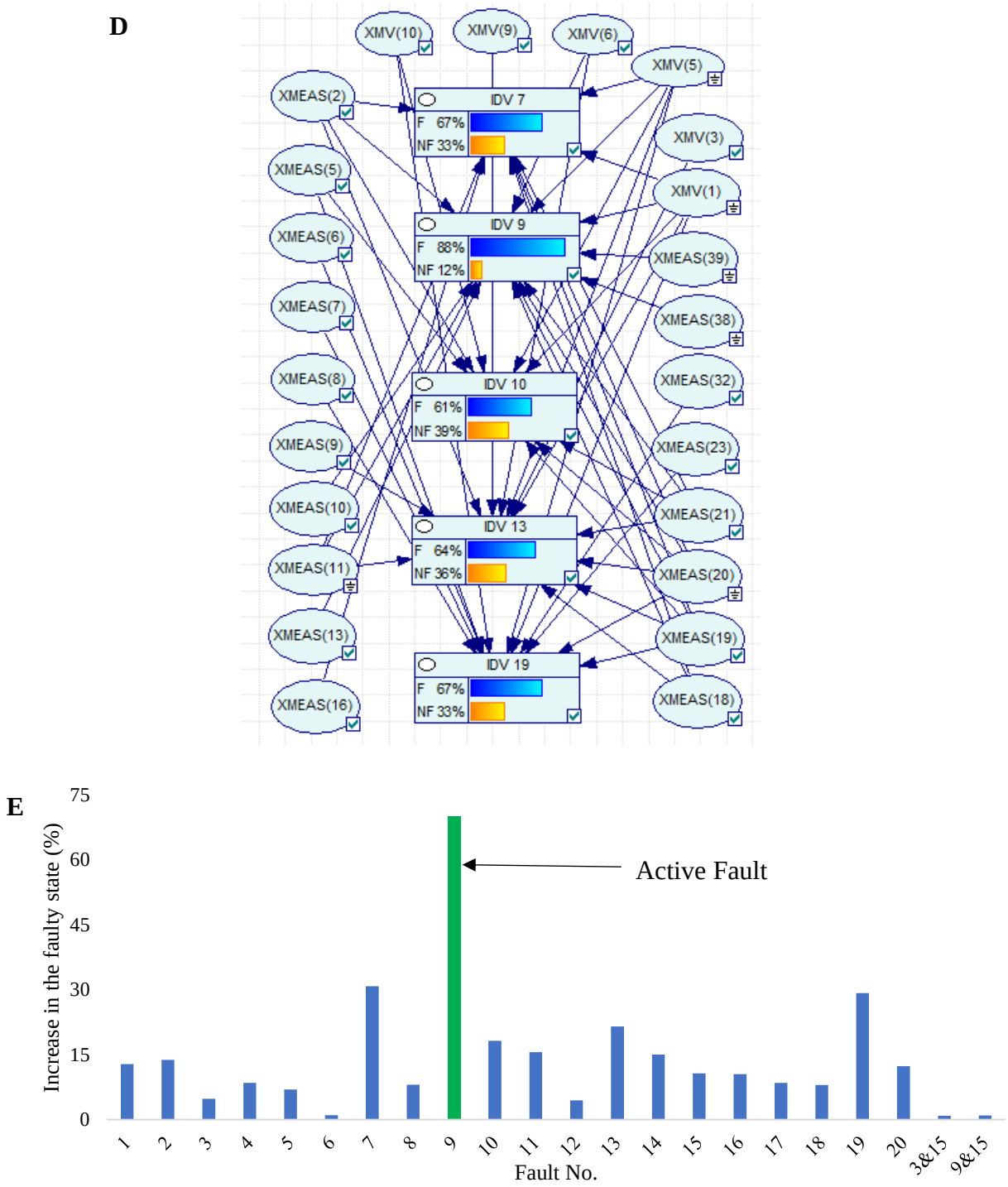

Figure 3.8: Fault detection and diagnosis by MEWMA-PCA-BN for IDV 9 (A) T^2 control chart, (B) SPE control chart, (C) SPE contribution plot, (D) updated SPE-based BN, and (E) fault diagnosis using percentage increase in the faulty state.

IDV 15 is the next fault that is activated after 8 hours of normal operation. Figures 3.9(A) and 3.9(B) show the T^2 and SPE control charts, respectively. Unlike the previous two cases, the T^2 control chart detects this fault earlier than the SPE control chart. Then, T^2 contribution plot is generated, as shown in Figure 3.9(C). XMEAS (33), XMV (2), XMEAS (19), XMEAS (37), XMV (9), and XMEAS (39) have the highest impact to this abnormal event, with a contribution of 15.78%, 6.08%, 5.79%, 3.98%, 3.68%, and 3.65%, respectively. As this fault is detected earlier by the T^2 control chart, the BN developed from the fault signatures collected from the T^2 contribution plots is selected to update, with the evidence received for the aforementioned six variables. The updated BN is shown in Figure 3.9(D), and it diagnoses IDV 15 as the observed fault type unequivocally since it is the only fault node that displays significant increase at the faulty state in the updated network (Figure 3.9(E)). In this case, the diagnosis report suggests that the fault has originated from stream 13, and condenser cooling valve stiction is the root cause of this process abnormality.

A

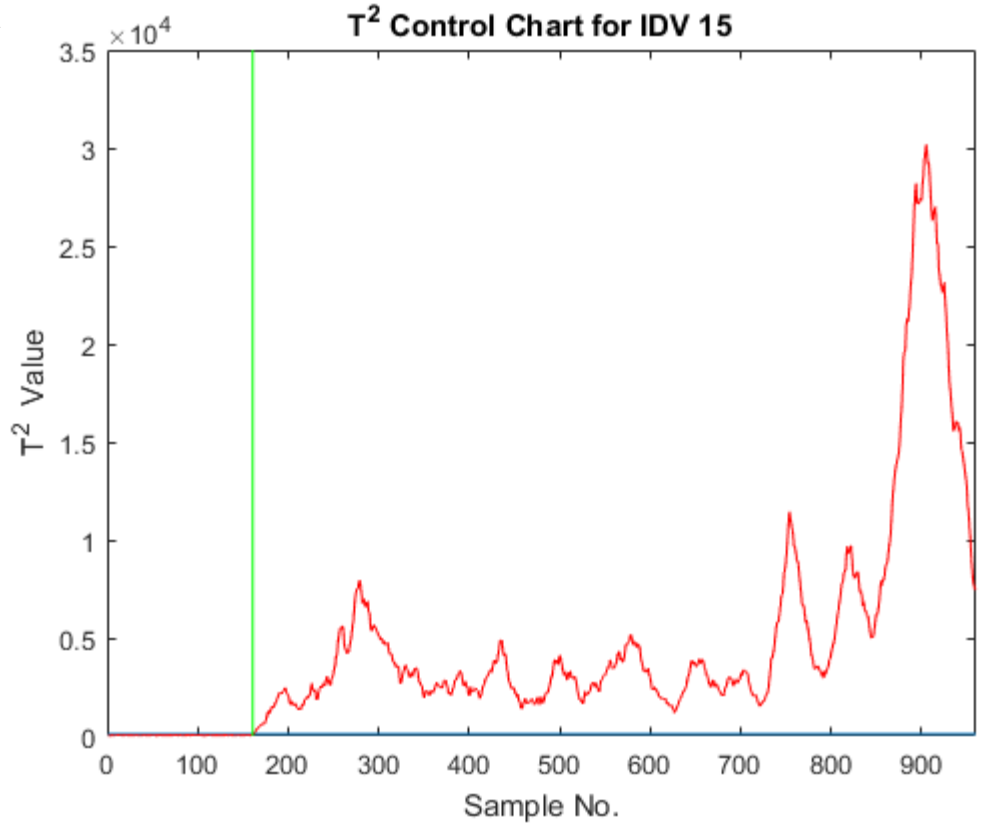
T² Control Chart for IDV 15
×10⁴
3.5
3
2.5
2
1.5
1
0.5
0
T² Value
0
100
200
300
400
500
600
700
800
900
Sample No.

B

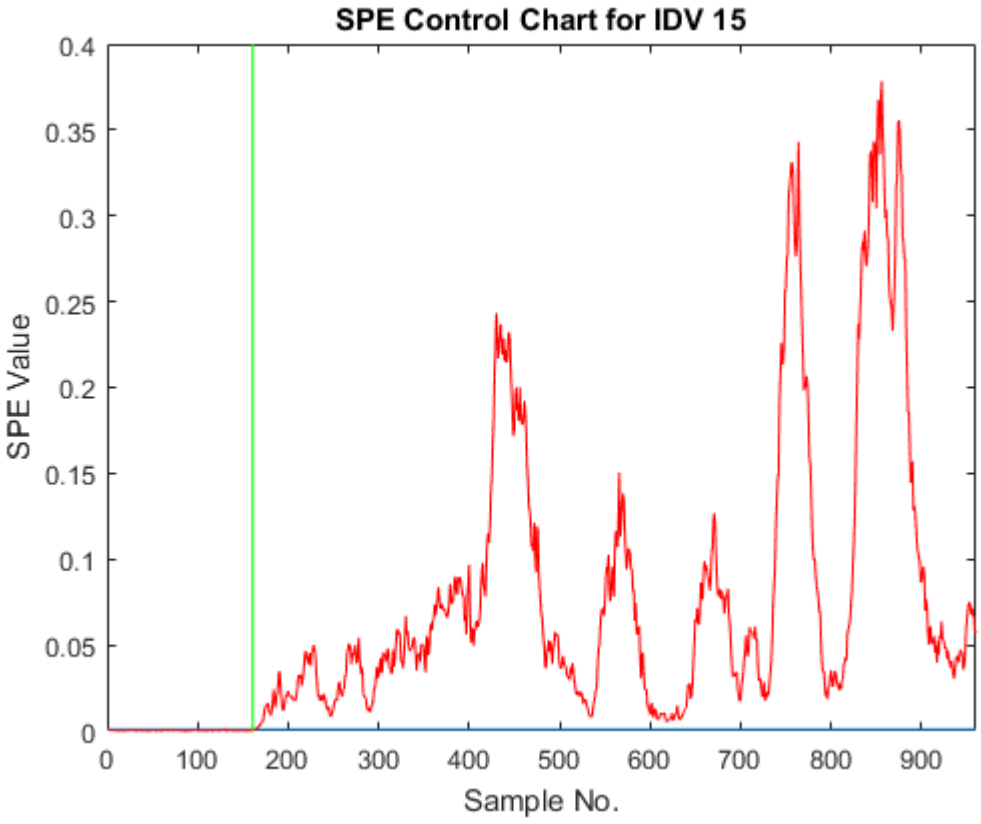
SPE Control Chart for IDV 15
0.4
0.35
0.3
0.25
0.2
0.15
0.1
0.05
0
SPE Value
0
100
200
300
400
500
600
700
800
900
Sample No.

C

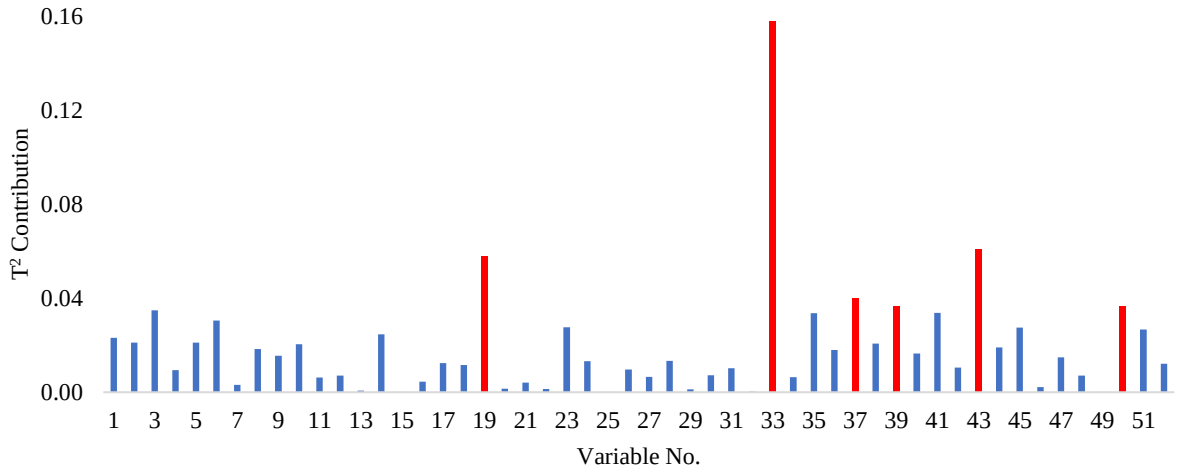
T² Contribution Plot for IDV 15
T² Contribution
0.16
0.12
0.08
0.04
0.00
1 3 5 7 9 11 13 15 17 19 21 23 25 27 29 31 33 35 37 39 41 43 45 47 49 51
Variable No.

D

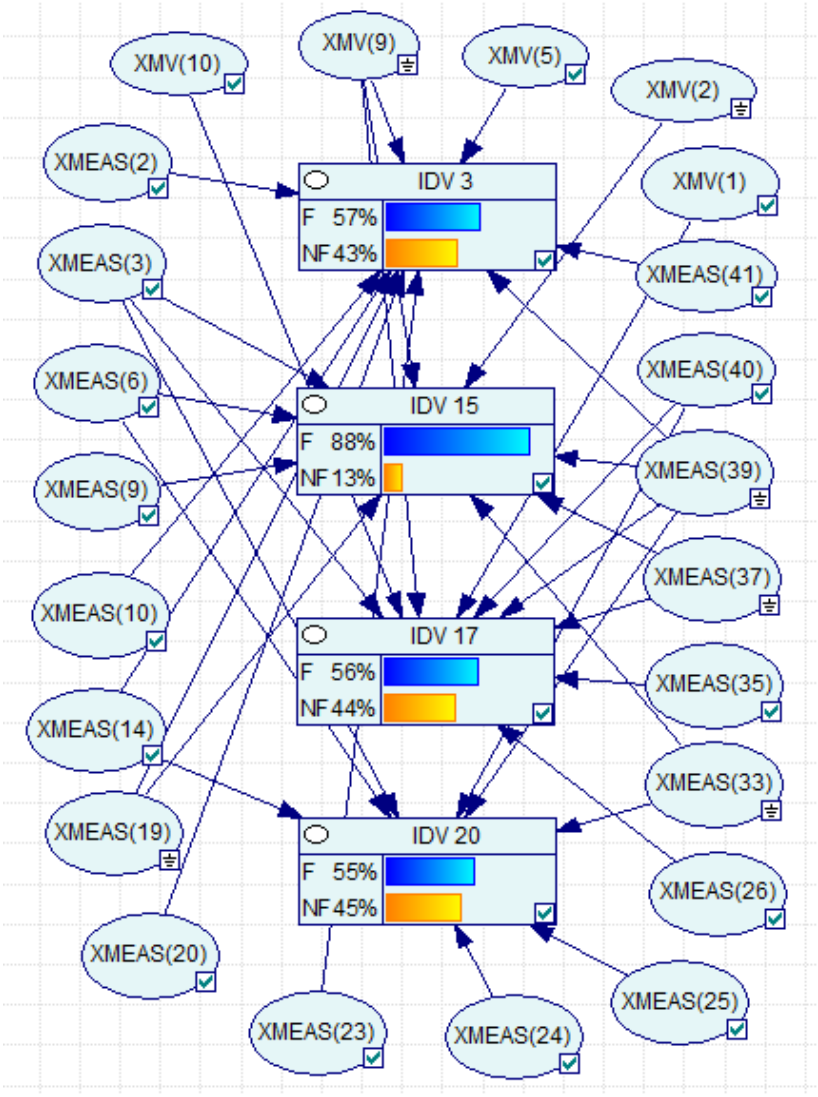
XMV(9)
XMV(10)
XMV(5)
XMV(2)
XMEAS(2)
IDV 3
F 57%
NF 43%
XMV(1)
XMEAS(3)
XMEAS(41)
XMEAS(6)
XMEAS(40)
IDV 15
F 88%
NF 13%
XMEAS(9)
XMEAS(39)
XMEAS(37)
XMEAS(10)
IDV 17
F 56%
NF 44%
XMEAS(35)
XMEAS(14)
XMEAS(33)
XMEAS(19)
IDV 20
F 55%
NF 45%
XMEAS(26)
XMEAS(20)
XMEAS(25)
XMEAS(23)
XMEAS(24)

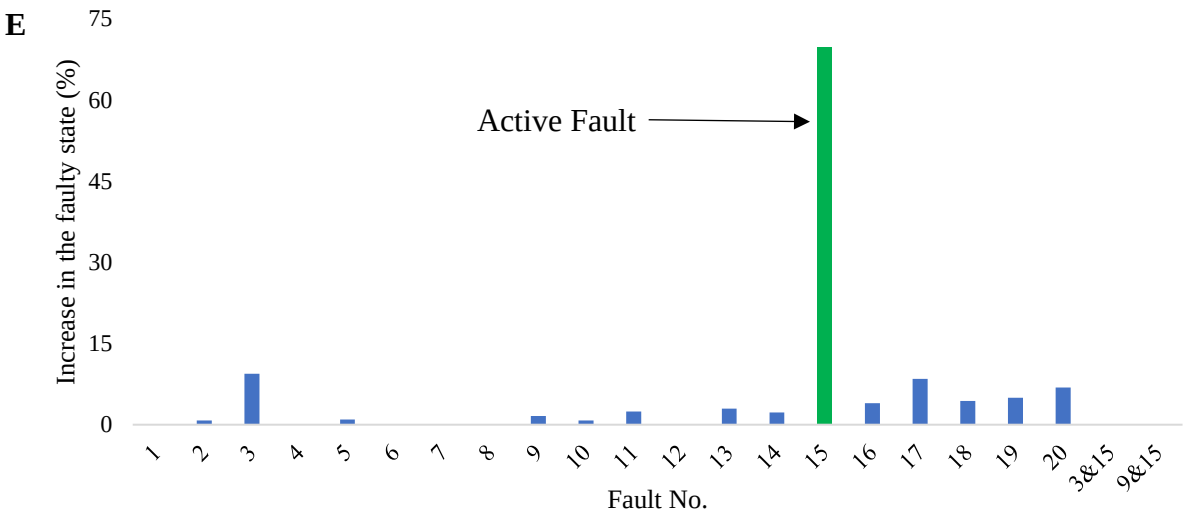

Figure 3.9: Fault detection and diagnosis by MEWMA-PCA-BN for IDV 15 (A) T^2 control chart (earlier detection), (B) SPE control chart, (C) T^2 contribution plot, (D) updated T^2-based BN, and (E) fault diagnosis using percentage increase in the faulty state.

This methodology has been applied to the concurrent action of two faults as well. In this tested fault scenario, both IDV 3 and IDV 15 start from the 161st sample, and a process abnormality is reported by the T^2 and SPE control charts at 166th and 162nd samples, respectively (Figures 3.10(A) and 3.10(B)). The T^2 and SPE values for the test samples become extremely higher than the other fault cases due to the simultaneous action of two faults. SPE contribution plot is generated since an alarm has been generated by the SPE control chart earlier than the T^2 control chart (Figure 3.10(C)). It can be observed that XMV (1) has the highest contribution, and the percentage contribution is much higher than the other variables. By norm, XMEAS (2), XMEAS (7), XMEAS (15), XMEAS (22), XMV (1), and XMV (11) are selected to update the BN. XMV (1) and XMV (11) are the manipulated variables that control the D feed temperature and condenser cooling water flowrate, respectively. Figure 3.10(D) shows the updated SPE-based BN. Updated fault probability for all the fault nodes have been recorded and compared with the values that have been obtained before updating the network. The percentage increase in the faulty state for all the fault nodes is

shown in Figure 3.10(E), and it can be seen that IDV 3 & 15 have simultaneously occurred to generate this abnormal situation. This diagnostic report suggests that the operators need to take required action in both streams 2 and 13, and D feed temperature and condenser cooling water valve are the specific places where they need to look at to restore the process in normal operating mode.

A

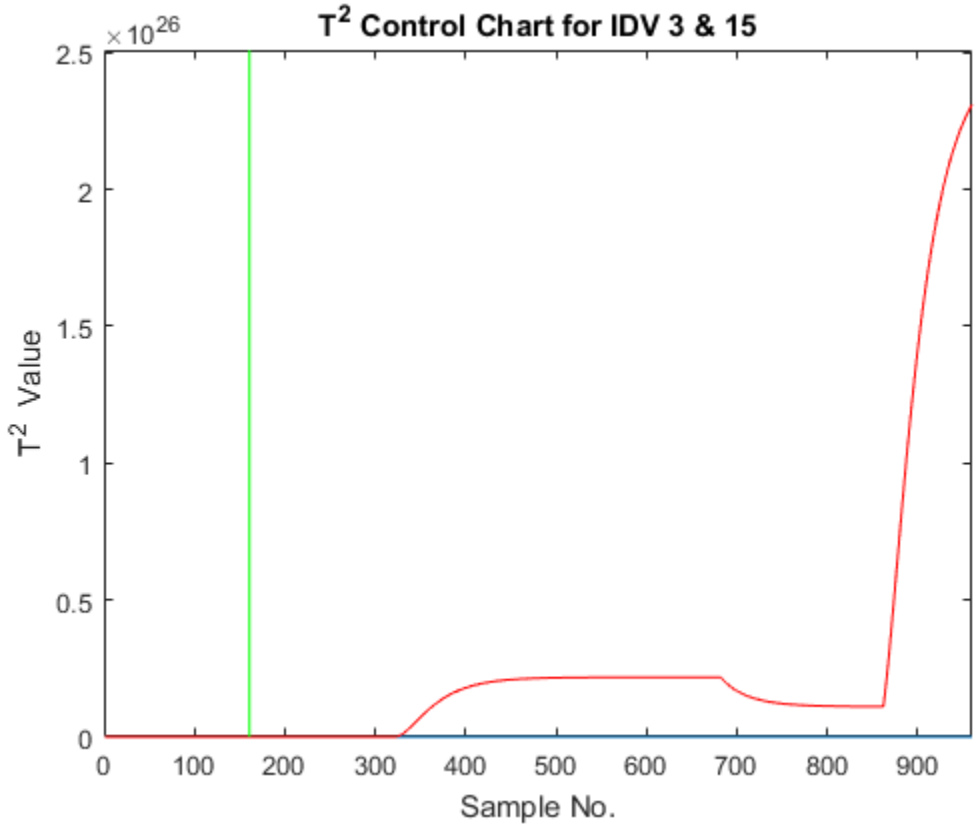

B

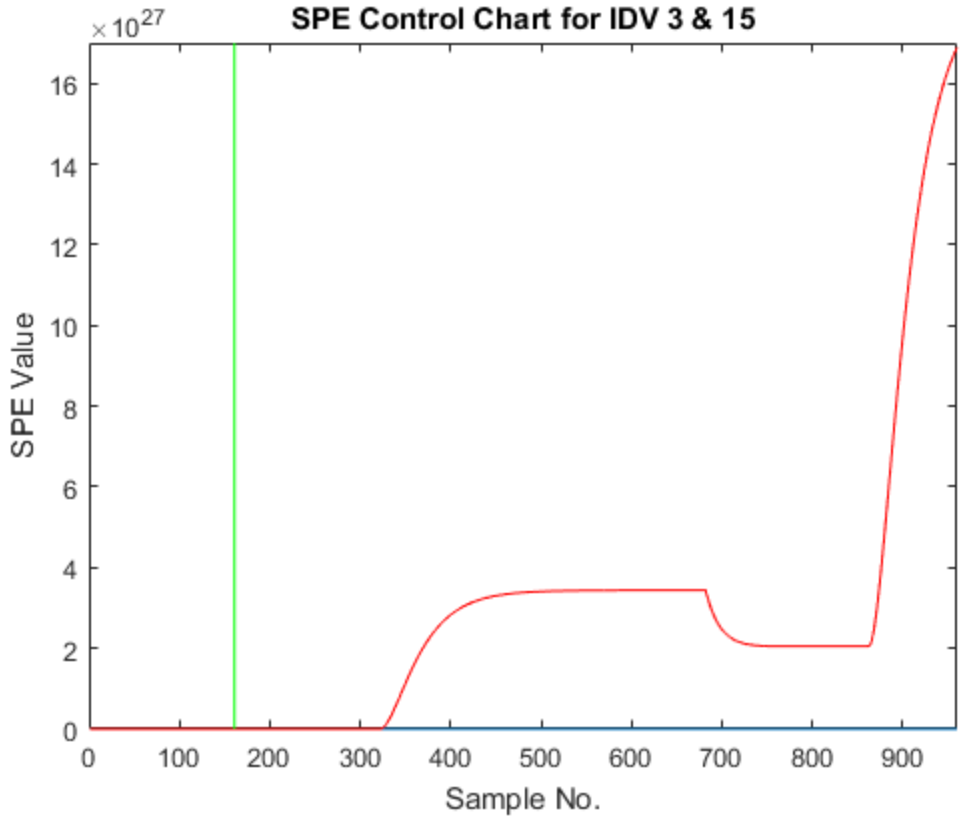
SPE Control Chart for IDV 3 & 15
×10^27
SPE Value
Sample No.
0
2
4
6
8
10
12
14
16
0
100
200
300
400
500
600
700
800
900

C

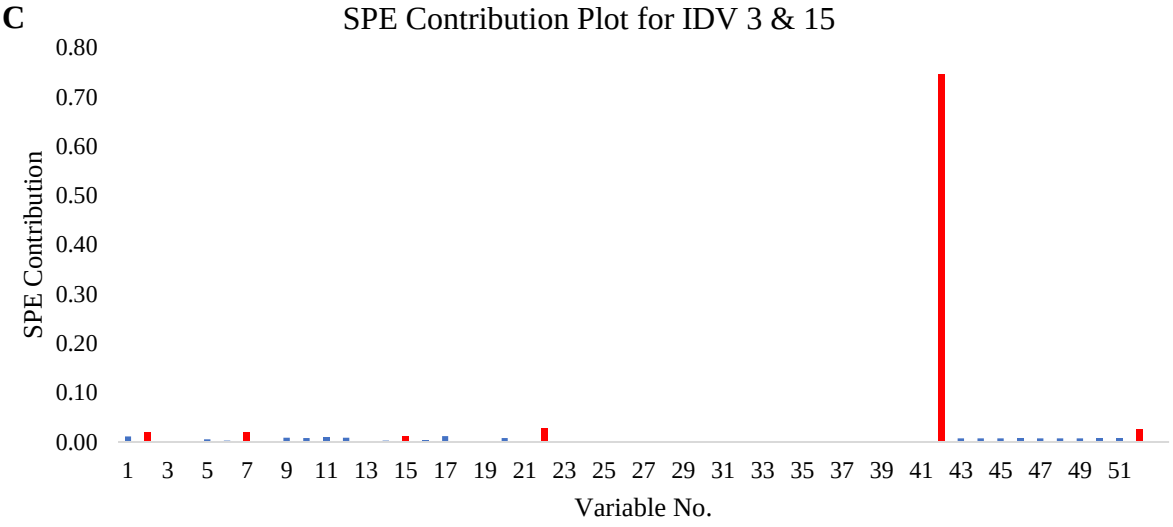
SPE Contribution Plot for IDV 3 & 15
SPE Contribution
Variable No.
0.00
0.10
0.20
0.30
0.40
0.50
0.60
0.70
0.80
1 3 5 7 9 11 13 15 17 19 21 23 25 27 29 31 33 35 37 39 41 43 45 47 49 51

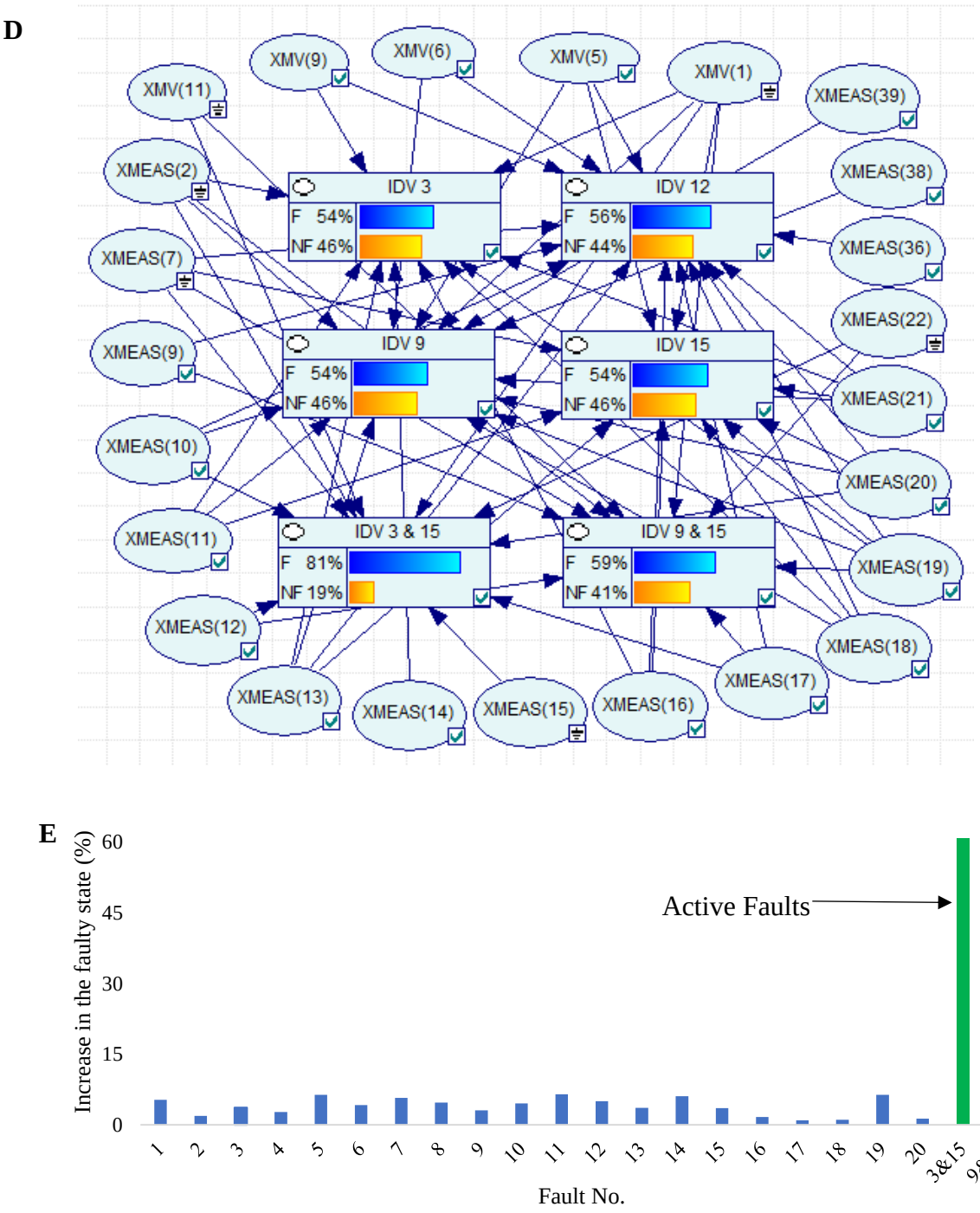

Figure 3.10: Fault detection and diagnosis by MEWMA-PCA-BN for IDV 3 & 15 (A) T^2 control chart, (B) SPE control chart (earlier detection), (C) SPE contribution plot, (D) updated SPE-based BN, and (E) fault diagnosis using percentage increase in the faulty state.

3.4. Results and Discussion

Performance of the MEWMA-PCA is compared with the previously published works on CUSUM PCA that reported the out-of-control average run length (ARL_{OC}), particularly for IDV 3, IDV 9, IDV 15, and IDV 3 & 15 of the TE chemical process. The comparison is shown in Table 3.4. It can be seen that the methodology proposed by Shams et al. (2011) takes the longest time to detect these faults. It takes 222.90 and 127.90 hours to detect IDV 3 and IDV 9, respectively. It gives a reasonable performance for IDV 15, where the ARL_{OC} is 0.60 hours for both T^2 and SPE control charts. The EEMD PCA CUSUM method proposed by Du and Du (2018) provides better performance than the previous CUSUM PCA-based method for all three fault cases, as it can be seen that the maximum time to detect the fault is 0.70 hours, and that has been observed for IDV 3.

On the contrary, the current MEWMA-PCA outweighs the performance of the previous two methods, as it detects IDV 3 and IDV 9 much faster than the EEMD CUSUM PCA. Although these two faults are detected earlier by the CUSUM PCA-SPE control chart, T^2-based control chart is a better choice with the combination of MEWMA-PCA. Nevertheless, IDV 15 is found to be detected earlier by the T^2 control chart using the proposed methodology, and the detection time is twelve-times and two-times faster than the methods proposed by Shams et al. (2011) and Du and Du (2018), respectively. For the simultaneous action of IDV 3 & 15, SPE control chart provides a much faster detection than T^2 control chart in integration with the MEWMA-PCA model. The proposed methodology also provides earlier detection than the other two previous works in this fault scenario. Even though the overall performance of SPE control chart is found to be superior in the exhaustive applications to the TE chemical process, it is essential to monitor the T^2 control chart, as evident from IDV 15.

Table 3.4: Comparison of out-of-control average run length (bold implies the best performance).

Work	CUSUM PCA (Shams et al., 2011)		EEMD PCA CUSUM (Du and Du, 2018)		Current	
Statistics	T^2	SPE	T^2	SPE	T^2	SPE
Fault ID	ARL_{oc} (hr)					
IDV 3	467.60	222.90	7.20	0.70	0.05	**0.04**
IDV 9	143.80	127.90	0.80	0.40	**0.05**	0.08
IDV 15	0.60	0.60	0.10	0.10	**0.05**	0.075
IDV 3 & 15	0.60	0.60	0.10	0.10	0.38	**0.05**

The proposed methodology is applied to the TE chemical process for the other 17 fault scenarios, and the comparative ARL_{OC}, average fault detection rate (FDR), and accurate diagnosis capacity between the current methodology and CUSUM PCA is shown in Table 3.5. It is worthy to mention that exhaustive application to the TE chemical process is not mentioned in (Du and Du, 2018) that enables including the results from (Shams et al., 2011) only in the comparison. It can be seen that the MEWMA-PCA model provides earlier detection in 19 cases, and the detection time is the same in IDV 8 for both derivatives of the conventional PCA. The difference in detection time between these two methods can rise to more than several hundred hours, as evident from IDV 3 and IDV 9. MEWMA-PCA-SPE is found to be providing a better performance in 9 fault scenarios, while this number is found to be 8 for MEWMA-PCA-T^2. IDV 7, IDV 11, and IDV 12 are the three fault cases where MEWMA-PCA-T^2 and MEWMA-PCA-SPE have the same average detection delay (DD). However, the maximum difference in detection time between the two statistics is observed as 6 minutes for any of the test cases. The proposed methodology detects IDV 1, IDV 2, IDV 4, IDV 5, IDV 6, IDV 7, and IDV 10 without any delay that is not observed for CUSUM PCA, as an associated detection delay is noticed by the CUSUM-based approach. The average FDR is also

found to be better by the MEWMA-PCA model. It gives a consistent average FDR irrespective of the fault type.

Table 3.5: Comparison of ARL_{OC}, average FDR, and accurate diagnosis capacity for all fault cases in the TE chemical process (bold implies the best performance).

Fault ID	Detection Performance						Accurate Diagnosis	
	CUSUM PCA-T^2	MEWMA-PCA		CUSUM PCA-T^2	MEWMA-PCA		CUSUM PCA with ARL_{oc} based diagnosis	MEWMA-PCA-BN
		T^2	SPE		T^2	SPE		
	ARLoc (hr)			Average FDR (%)				
IDV 1	0.05	0.05	**0.00**	99.88	99.88	**100**	No	**Yes**
IDV 2	1.05	0.05	**0.00**	97.38	99.88	**100**	No	**Yes**
IDV 3	467.60	0.05	**0.04**	36.98	99.88	**99.90**	**Yes**	**Yes**
IDV 4	13.70	**0.00**	0.04	65.75	**100**	99.90	**Yes**	**Yes**
IDV 5	0.10	**0.00**	0.06	99.75	**100**	99.85	No	**Yes**
IDV 6	0.50	0.05	**0.00**	98.75	99.88	**100**	**Yes**	**Yes**
IDV 7	0.15	**0.00**	**0.00**	99.63	**100**	**100**	No	**Yes**
IDV 8	**0.05**	**0.05**	0.08	**99.88**	**99.88**	99.80	No	**Yes**
IDV 9	143.80	**0.05**	0.08	80.62	**99.88**	99.80	**Yes**	**Yes**
IDV 10	11.65	0.15	**0.00**	70.88	99.63	**100**	**Yes**	**Yes**
IDV 11	0.15	**0.05**	**0.05**	99.63	**99.88**	**99.88**	No	**Yes**
IDV 12	1.05	**0.05**	**0.05**	97.38	**99.88**	**99.88**	No	**Yes**
IDV 13	3.70	**0.03**	0.06	90.75	**99.93**	99.85	**Yes**	**Yes**
IDV 14	0.25	**0.01**	0.05	99.38	**99.98**	99.88	**Yes**	**Yes**
IDV 15	0.60	**0.05**	0.08	98.50	**99.88**	99.80	**Yes**	**Yes**
IDV 16	49.75	0.05	**0.01**	93.30	99.88	**99.98**	**Yes**	**Yes**
IDV 17	0.10	0.04	**0.03**	99.75	99.90	**99.93**	No	**Yes**
IDV 18	2.60	**0.05**	0.11	93.50	**99.88**	99.73	**Yes**	**Yes**
IDV 19	0.15	0.05	**0.02**	99.63	99.88	**99.95**	No	**Yes**
IDV 20	4.90	0.06	**0.03**	87.75	99.85	**99.93**	**Yes**	**Yes**

Table 3.5 also gives a justification of using the BNs in fault diagnosis, as it can be found that several faults have the same ARLoc, and the DD-based fault diagnosis strategy demonstrated by Shams et al. (2011) becomes inefficient and misleading in IDV 1, IDV 2, IDV 5, IDV 7, IDV 8, IDV 11, IDV 12, IDV 17, and IDV 19. CUSUM PCA with a misdetection-based diagnosis strategy

can provide an accurate diagnosis in 11 (55%) cases, while this number is 20 (100%) for MEWMA-PCA-BN.

To understand the underlying reason behind MEWMA-PCA's better performance over CUSUM PCA, the filtering effect of these two statistics on XMEAS (1) is shown in Figure 3.11 as an example. The slack parameter of CUSUM was set to half of the standard deviation. It can be seen that the location CUSUM (LCS) can merely follow the original signal, and it is only sensitive to any variation that is significantly higher than the mean value. Although the standard CUSUM (SCS) can mimic the raw process data, it is observed to be fluctuating with a higher magnitude. On the contrary, pre-processed data from the MEWMA model takes a while to follow the original data due to a lower value of the tuning parameter, λ. However, once it starts following the signal, it can closely follow the mean of the original signal with a more smoothed form. Additionally, it captures the deviations in both the upper and lower sides of the mean. It implies that the MEWMA model provides a lesser noisy dataset retaining the dynamic variational property. This makes the feature extraction easier for PCA, as it can capture the significant deviations with a lower number of PCs and distinguish the faulty samples with a smaller magnitude more vigorously.

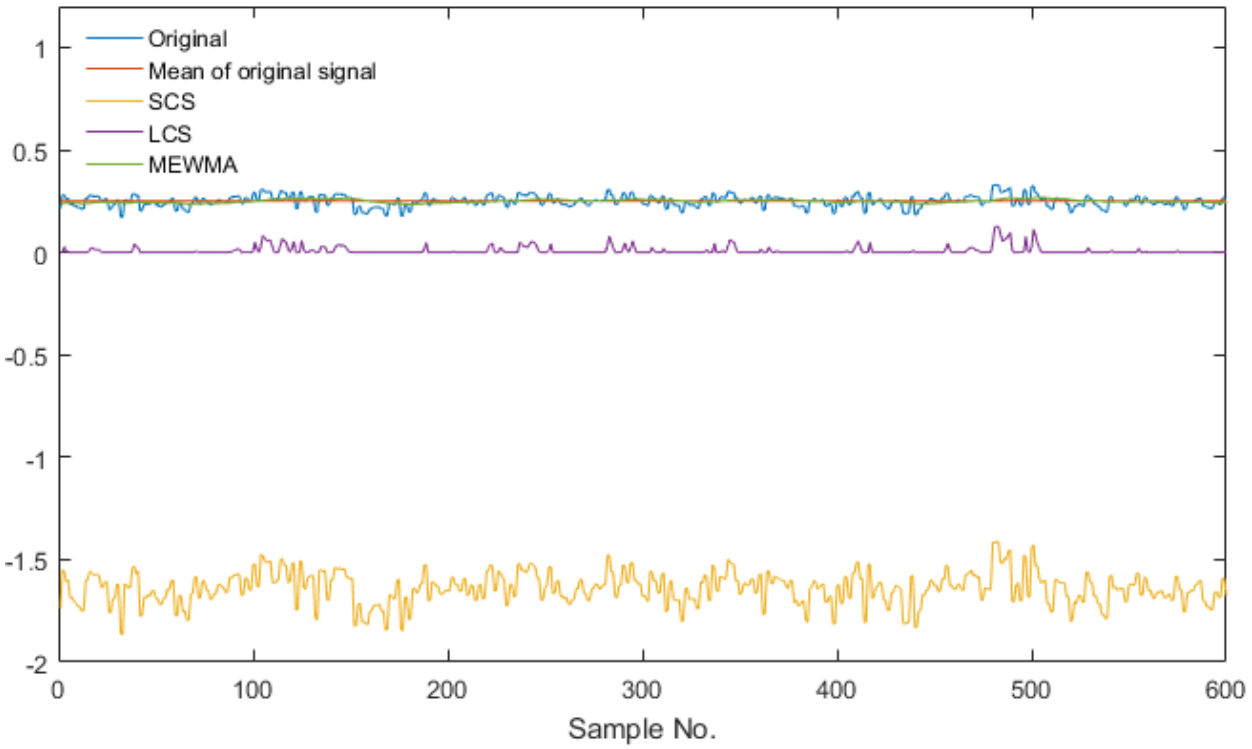

Figure 3.11: Effect of MEWMA and CUSUM on original data.

3.5. Conclusion

This chapter presents a robust FDD methodology, developed using the MEWMA-PCA and the BN models. Detection capacity of the conventional PCA is found to increase significantly by integrating it with the MEWMA model. Successful applications of the MEWMA-PCA model has been demonstrated for three specific faults: IDV 3, IDV 9, and IDV 15 of the benchmark TE process. These faults have been selected, as many advanced MSPM tools are found to be inefficient in detecting them. Simultaneous occurrence of two faults can also be detected and diagnosed by applying the MEWMA-PCA-BN model proposed in this article. The comprehensive applications to the other fault cases of the TE chemical process suggest that the proposed method can successfully be applied to different types of fault signals, and still, an early detection can be achieved.

Although CUSUM PCA-based FDD tools have demonstrated the capacity to detect and diagnose these faults efficiently, the newly proposed tool provides a better detection rate. It can detect the fault earlier than previously reported two CUSUM PCA-based approaches, as evident from Table 3.4. Furthermore, the computational cost of CUSUM PCA is essentially higher, as each sample consists of twice the volume of the original data matrix due to the simultaneous application of LCS and SCS. For example, CUSUM PCA needs to monitor a matrix that contains 104 columns for the demonstrated TE chemical process, while MEWMA-PCA monitors only 52 columns. However, MEWMA-PCA cannot diagnose the faults consistently, which is a drawback of this MSPM tool. Although a misdetection-based diagnosis technique is available in the existing literature, this method is found misleading, as many faults can have similar misdetection rates, and hence, a BN is used to diagnose the active fault type. It is found that the proposed MEWMA-PCA-BN model can detect the fault early and diagnose the fault type accurately.

This work demonstrates a simple, yet effective procedure to develop an MEWMA-PCA model. Unlike the traditional approaches, a novel technique to construct and train the BNs from the observed fault symptoms in a supervised learning method is also presented, which can be efficiently utilized by other MSPM tools to build the hybrid methods. Furthermore, the current work presents an FDD tool to overcome the limitations of several tools that face difficulty while detecting and diagnosing the unobservable process faults. The advantages of this hybrid method are: (i) early fault detection, (ii) higher detection rate, (iii) lower computational cost than CUSUM PCA, (iv) consistent accurate diagnosis, and (v) easier construction process.

Despite this work having demonstrated a robust methodology for FDD, identification of fault propagation pathway is another aspect of process monitoring that can be integrated to make the work more comprehensive. A separate BN constructed by following the conventional techniques

can be utilized to serve this purpose. Six topmost contributing variables are selected to train and update the BNs. Integrating the contribution of more variables will provide more confidence in fault diagnosis. As the number of faults increases, training of the BN models becomes complex and time-consuming. An automated training method can help in this context. This methodology assumed a stationary process application; recursively updated or moving window-based versions of the MEWMA-PCA could be utilized to capture the non-stationary conditions. The above will be promising venues to improve this work significantly.

Chapter 4: A Data-Driven Bayesian Network Learning Method for Process Fault Diagnosis

Preface

A version of this chapter has been published in the ***Process Safety and Environmental Protection*** journal. I am the primary author, along with the co-authors, Drs. Faisal Khan, Salim Ahmed, and Syed Imtiaz. I developed the conceptual framework for the FDD model and carried out the literature review. I prepared the first draft of the manuscript and subsequently revised the manuscript based on the co-authors' and peer review feedback. Co-author Dr. Faisal Khan helped in the concept development and testing the model, reviewing, and revising the manuscript. Co-authors Drs. Syed Imtiaz and Salim Ahmed provided support in implementing the concept and testing the model. The co-authors provided fundamental assistance in validating, reviewing, and correcting the model and results. The co-authors also contributed to the review and revision of the manuscript.

Reference: Amin, M. T., Khan, F., Ahmed, S., & Imtiaz, S. (2021). A data-driven Bayesian network learning method for process fault diagnosis. Process Safety and Environmental Protection, 150, 110-122. https://doi.org/10.1016/j.psep.2021.04.004

Abstract

This chapter presents a data-driven methodology for fault detection and diagnosis (FDD) by integrating the principal component analysis (PCA) and Bayesian network (BN). Though the integration of PCA-BN for FDD purposes has been studied in the past, the present work makes two contributions for process systems. First, the application of correlation dimension (CD) to select principal components (PCs) automatically. Second, the use of Kullback-Leibler divergence (KLD) and copula theory to develop a data-based BN learning technique. To avoid discretizing continuous high-dimensional process data and to capture nonlinear dependence, this methodology uses a combination of vine copula and Bayes' theorem. The data-driven integrated PCA-BN framework has been applied to two process systems. The performance of the proposed methodology is compared with the independent component analysis (ICA), kernel principal component analysis (KPCA), kernel independent component analysis (KICA), and their integrated frameworks with the BN. The comparative study suggests that the proposed framework provides superior performance.

Keywords: *Process monitoring*, *fault diagnosis*, *process safety*, *correlation dimension*, *vine copula*, *Bayesian network*.

4.1. Introduction

Fault detection and diagnosis (FDD) has the utmost importance in increasing the profitability of a process plant by ensuring safety, reliability, and product quality. By nature, process industries are a source of high-dimensional correlated data due to multivariate process operations and digitalization. The success of an FDD tool largely depends on an accurate analysis of these data for predicting the process state (i.e. faulty or normal) and decoding the underneath causal relationships and correlation structure among the process variables (Jia and Li, 2020; Zhou and Li, 2018). Data-based process FDD tools play a pivotal role in preventing a fault from propagating to an accident by providing an early indication of fault and information about the root cause. The multivariate statistical process monitoring (MSPM) tools are continually drawing researchers' attention due to their ease of implementation, reliable performance, and relatively lower historical data requirement compared to machine learning techniques (i.e. artificial neural network).

The principal component analysis (PCA) (Wise et al., 1988), partial least squares (PLS) (Kresta et al., 1991), independent component analysis (ICA) (Kano et al., 2003), and their derivatives are the major MSPM tools used in FDD. An appropriate number of principal component (PC) or independent component (IC) selection greatly affects the performance of these MSPM tools. The cumulative percentile variation (CPV) (Malinowski and Howery, 1980) and SCREE (Cattell, 1966) procedures are the two most common and reliable means in this context. Unlike PCA, the ICA cannot distinguish variations captured by the ICs, and therefore, the number of ICs is often set equal to the number of PCs from PCA. The modified ICA (MICA) is another alternative formulation of ICA to capture the significant process variations with the required ICs (Lee et al., 2006). Like PCA, the MICA utilizes CPV or SCREE approach to pick the significant ICs to build the monitoring model.

Due to SCREE's graphical nature, its output is prone to error when the dimension is higher. On the other hand, the CPV uses a simple mathematical formulation to estimate the required number of PCs. Usually, the first few PCs are selected based on the percentage variation that an MSPM designer wants to capture. Although the CPV uses a straightforward equation, it is a user-perspective approach, as different researchers have used a wide range of values (i.e. 65-99%) to construct the monitoring models, with a view to reducing false alarms, yet securing an early fault detectability.

The correlation dimension (CD) finds a set of linear or nonlinear axes that represents the multidimensional data in a reduced dimension retaining the vital information of original data (Grassberger and Procaccia, 1983). This exactly matches to the definition of PC or IC, and the existing techniques to measure the required number of PCs or ICs to build the FDD model can be improved and made automated by including it in model development (i.e. the CD is an assumption-free approach, and no user preference is required).

Along with early fault detectability, the MSPM tools can provide diagnostic information in terms of multivariate contribution plots. However, this diagnosis is often inaccurate and misleading due to the smearing effect (Westerhuis et al., 2000). The Bayesian networks (BNs) are becoming increasingly popular in FDD, especially in fault diagnosis. In addition to FDD, BNs are widely used in process safety and risk analysis (Adedigba et al., 2017; Amin et al., 2020; Barua et al., 2016; Ghosh et al., 2020; Guo et al., 2019; Ping et al., 2018; Rostamabadi et al., 2020; Yazdi and Kabir, 2017).

Rojas-Guzman and Kramer (1993) showed the suitability of a BN over the then rule-based expert systems in fault diagnosis. Process knowledge was utilized as the basic building block of the network. A BN-based single sensor fault detection and identification technique was proposed by

Mehranbod et al. (2003). The probability absolute difference was utilized for fault detection. Nonetheless, the authors did not address how continuous data were converted into probabilities that were further used to update the BN.

A combination of T^2 statistics and BN was proposed by Verron et al. (2010). The authors utilized the causal decomposition of T^2 statistics for fault diagnosis. However, the application to a hot forming process suggested that the proposed method could not ensure accurate diagnosis in all the studied cases. The conventional BN is static, and hence, it cannot capture the dynamic nature of process operations. To address this issue, Yu and Rashid (2013) proposed a dynamic BN (DBN)-based process monitoring model. The kernel distribution was utilized to learn the parameters, while the network topology was developed from prior knowledge and process flow diagram. The other applications of DBN in process monitoring can be found in the works by Zhang and Dong (2014) and Amin et al. (2019a). The major advantage of DBN-based methods is their capability to detect and diagnose a fault and identify its propagation pathway by a solitary tool. However, these cannot provide early detection in case of subtle faults.

Many integrated frameworks have been developed using the early fault detectability of the MSPM tools and accurate diagnosis capacity of a BN. A fault is first detected by an MSPM tool; then, diagnosis is completed by the BN using contribution plots. As a result, both the early fault detection and accurate diagnosis features are captured. Some of the hybrid methods adopting this philosophy are PCA-BN by Mallick and Imtiaz (2013), MICA-BN by Yu et al. (2015), KPCA-BN by Gharahbagheri et al. (2017), and PCA-BN with likelihood evidence by Amin et al. (2018). Strong prior knowledge of BN structure and conditional probability tables (CPTs) was the prerequisite for the first PCA-BN work. Yu et al. (2015) and Amin et al. (2018) utilized prior knowledge and data for learning structure and CPTs, respectively.

Developing BNs from process data is still an existing challenge. Yang et al. (2014) demonstrated the applications of Granger causality and transfer entropy for capturing causality and connectivity from process data. Later, Gharahbagheri et al. (2017) utilized these tools to build BNs from process data. Selecting the optimal lag for Granger causality requires significant effort. Besides, the outputs from transfer entropy are often error-prone in the context of process data (Yu and Rashid, 2013). One of the salient features of Gharahbagheri's work was the use of residuals for estimating priors and CPTs. However, continuous data were discretized at the cost of information loss. Zhu et al. (2019) proposed a multiblock transfer entropy (MBTE)-based BN learning technique for root cause diagnosis. The authors segregated the process into different sub-systems based on prior knowledge and subsequently, used the MBTE to find causal relations. This technique cannot be considered purely data-driven since prior knowledge is used to divide the entire process.

Meng et al. (2019) applied a family transfer entropy (FTE) technique to the alarm repository and proposed a score-based BN learning method. Process variables were classified based on alarm history. Suppose fault A causes a total of five variables exceeding the pre-defined thresholds. These variables are included in the developed BN for diagnosing fault A. The causal structure of these five variables is then determined using FTE. This procedure is carried out for each fault type. Wang et al. (2018) proposed a BN-based fault diagnosis methodology. Knowledge of faults and Pearson's correlation coefficient were used to develop the causal structure for each fault type, and the parameters were learnt using the expectation-maximization algorithm. Amin et al. (2019) combined the multivariate exponentially weighted moving average PCA (MEWMA-PCA) with the BN to detect and diagnose some faults in the Tennessee Eastman chemical process that have been described as unobservable or difficult to detect. The authors proposed a data-based BN structure learning algorithm that utilized historical fault signatures. However, in-depth fault

information is required to develop the BNs in the above mentioned works which may not be obtainable in many cases.

The Kullback-Leibler divergence (KLD) is an approach that is used in information theory to measure the distance between two probability distributions (Kullback and Leibler, 1951). Also, it can be utilized to determine the amount and direction of mutual information (MI) transfer between two variables. Several studies are conducted to use MI by KLD to learn BN topologies (Friedman et al., 2013; Wu et al., 2001). These works mainly consider discrete data. The KLD is a lag selection free technique, and its calculation is straightforward compared to Granger causality and transfer entropy. Therefore, it can be utilized to develop a BN topology learning method to overcome the limitations faced by Granger causality and transfer entropy. Besides, it will eliminate the necessity of process knowledge or detailed fault information to build the BN and enable developing a data-driven BN structure.

Copula functions provide the estimate of joint density among multi-dimensional variables without discretizing data. The correlation estimates provided by the copula functions in terms of Kendall's rank correlation coefficient and Spearman's rank correlation coefficient are often described as a measure of nonlinear dependence, as well. Although the conventional bivariate copulas can be used to model dependency between two variables, these cannot be utilized flexibly to measure the dependence in high-dimensional cases (Joe, 1996).

Elidan (2010) developed a technique to estimate the joint densities in a flexible manner using bivariate copulas and proposed a copula Bayesian network (CBN) model. It overcomes the limitation of traditional discrete BNs, as the use of copulas allowed to model continuous variables. Additionally, the CBN preserves the strengths of traditional BNs. Conditional independence among variables was assumed to estimate high-dimensional joint densities. However, this may not

be a valid assumption, especially in chemical systems, as process variables exhibit strong nonlinear dependence.

The vine copula models such as the R-vine, C-vine, and D-vine are pertinent in this context, as these can capture the joint dependence in high-dimensional cases using the bivariate copula decompositions. Furthermore, no conditional independence assumption is required. Although several process monitoring schemes are available in the existing literature that have utilized the vine copula models (Ren et al., 2015; Zhou and Li, 2018), none of them utilized the copula-based BN for fault diagnosis. The vine copula-based models can provide a good detection performance like the MSPM tools. However, the diagnostic task is not straightforward like the BN-based methods, as each pair of variables needs to be analyzed that may introduce a vast computational burden for large-scale processes. On the contrary, the BNs only need to be updated, and the percentage change in each node can be used for fault diagnosis. Therefore, a vine copula aided BN model can be utilized for fault diagnosis that ensures high-dimensional continuous process data are utilized in building the CPTs, avoiding a considerable amount of computational efforts.

The current research first examines the efficacy of CD-based PCA, ICA, KPCA, and KICA over the CPV-based counterparts. It then integrates the data-based BN structure with PCA-CD, as PCA-CD-BN is found to be the most effective method for FDD based on four fault cases studied in the continuous stirred tank heater (CSTH) and binary distillation column.

This work proposes a CD-based PC or IC selection technique since it can provide an unbiased measurement of required dimensions to reduce the original dataset. A data-driven BN learning technique is also proposed using the KLD and copula theory. Although bivariate copulas are easier to apply to estimate the joint density between two variables, process operations often contain

higher dimensional dependencies among variables where the bivariate copulas may not be suitable. Therefore, a combination of vine copula and Bayes' theorem is used to overcome this problem.

The remainder of this chapter is organized as follows: Section 4.2 describes the distinct steps of this methodology. Applications of the proposed framework to two process systems are displayed in Section 4.3. Detailed comparative performance analysis with the ICA, KICA, and KPCA-based methods are discussed in Section 4.4. The concluding remarks, advantages, limitations, and future work scopes are summarized in Section 4.5.

4.2. Proposed Methodology

The proposed methodology (Figure 4.1) is comprised of CD-based PCA and KLD and copula-based BN. Fault is first detected using the PCA, and subsequently, root cause is diagnosed by the BN, utilizing PCA contributions. The proposed methodology for FDD works in two phases. The first task is to develop the monitoring model by using the following nine steps.

Step 1: Historical normal and faulty data are collected. Normal process data is auto standardized to zero mean and unit variance.

Step 2: PCA is performed on data obtained from the previous step. The details of PCA algorithm can be found in the works by Kresta et al. (1991), Garcia-Alvarez et al. (2012), Adedigba et al. (2017), and How and Lam (2018), just to name a few. For estimating CD, this work uses the algorithm proposed by Grassberger and Procaccia (1983). It is computed based on the assumption that two points lie at a distance of r. The point correlation for $X \in \Re^{n \times m}$ can be calculated as:

$$C_u(r) = \frac{q}{n-1} \tag{4.1}$$

where q is the number of points x_v within the hypersphere radius, r of a reference point x_u.

The radial correlation function can be estimated by averaging the point correlation function, as shown in Equation 4.2.

$$C(r) = \frac{1}{n} \sum_{u=1}^{n} C_u(r) \tag{4.2}$$

The correlation sum for all the hypersphere radii can be computed as:

$$C(r) = \lim_{n\to\infty} \frac{2}{n\,(n-1)} \sum_{u=1}^{n} \sum_{v=u+1}^{n} H(r - |x_u - x_v|) \tag{4.3}$$

where *H* denotes the Heaviside function. $|x_u - x_v|$ is measured using the Euclidean distance. The distance between each pair of points are measured, and the points that give a value less than *r* are included in calculating the correlation sum.

If *r* becomes smaller, the correlation sum follows a power law (Equation 4.4).

$$\lim_{n\to\infty} \lim_{r\to 0} C(r) = r^{CD} \tag{4.4}$$

Finally, the CD can be obtained by taking the logarithm of both sides.

$$CD = \lim_{n\to\infty} \lim_{r\to 0} \frac{log\, C(r)}{log(r)} \tag{4.5}$$

CDs of the original data matrix (*X*) and score matrix (*T*) are estimated. The higher value between these two is rounded off to the next positive integer and used to select the number of required PCs to build the PCA monitoring model. The minimum distance is chosen as the absolute difference between the median and maximum values.

Step 3: Thresholds of T^2 and squared prediction error (SPE) statistics are calculated. A level of 99% confidence is used in the proposed approach.

Step 4: PCA residuals are collected. Gharahbagheri et al. (2017) used these residuals to estimate the CPTs after discretizing them. However, these are not readily usable to estimate CPTs using the copula functions. According to the theorem by Sklar (1959), data need to be transformed into

cumulative density functions (CDFs) to estimate the correlation measure. Therefore, the kernel density estimator (KDE) is used to estimate the probability density functions (PDFs) and CDFs. The kernel PDF, f_h and CDF, F_h for a random variable, x can be obtained using Equations 4.6 and 4.7, respectively (Bowman and Azzalini, 1997).

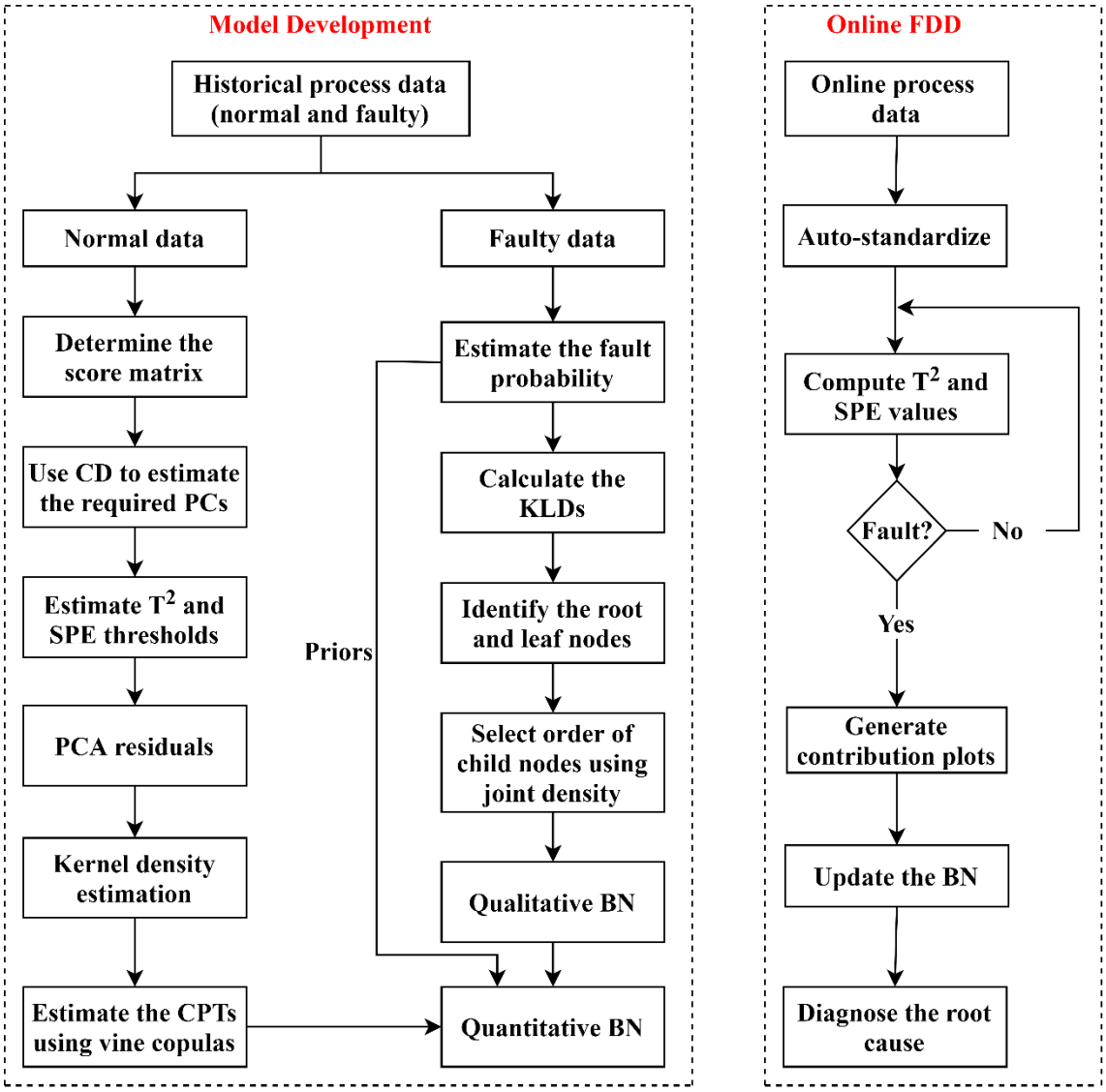

Figure 4.1: The proposed methodology for FDD.

$$f_h(x) = \frac{1}{nh}\sum_{i=1}^{n} K\left(\frac{x - x_i}{h}\right) \tag{4.6}$$

$$F_h(x) = \int_{-\infty}^{x} f_h(x)dx \tag{4.7}$$

where i = 1, 2, 3, …, n is the number of samples. h is the bandwidth, and K (·) is the kernel smoothing function. A Gaussian kernel is considered in this work.

The kernel bandwidth, h is calculated using the rule provided by Silverman (1986). For a sample size of n with σ standard deviation, h can be computed as shown in Equation 4.8.

$$h = \left(\frac{4\sigma^5}{3n}\right)^{\frac{1}{5}} \tag{4.8}$$

Step 5: Faulty data are used to build the topology of BN using the KLD. However, data need to be fitted in a probability distribution to estimate the KLD. The probability of fault for each variable from faulty dataset is estimated using the Gaussian cumulative distribution by Equation 4.9.

$$P(Fault) = \varphi\left(\frac{X \pm \mu}{\sigma}\right) \tag{4.9}$$

where X, μ, and σ are the arbitrary value, mean, and standard deviation, respectively.

A limiting zone needs to be defined for efficient fault probability estimation. The upper and lower thresholds for this zone are selected as μ+3σ and μ-3σ, respectively. The probability of fault is considered as 0.50 and 0 at μ±3σ and μ, respectively (Bao et al., 2011). μ and σ are calculated from the normal operational data of step 1. Although ±3σ gives a wider horizon, this work considers this limit due to the susceptibility of process data to random noise.

for x_{ij}>μ_j,

$$P(Fault) = \varphi\left(\frac{x_{ij} - (\mu_j + 3\sigma_j)}{\sigma_j}\right)$$

$$= \int_{-\infty}^{x_{ij}} \frac{1}{\sigma_j\sqrt{2\pi}} e^{-\frac{\{x_{ij}-(\mu_j+3\sigma_j)\}^2}{2\sigma_j^2}} dx \tag{4.10}$$

for $x_{ij}<\mu_j$,

$$P(Fault) = 1 - \varphi\left(\frac{x_{ij} - (\mu_j - 3\sigma_j)}{\sigma_j}\right)$$

$$= 1 - \int_{-\infty}^{x_{ij}} \frac{1}{\sigma_j\sqrt{2\pi}} e^{-\frac{\{x_{ij}-(\mu_j-3\sigma_j)\}^2}{2\sigma_j^2}} dx \tag{4.11}$$

where i =1, 2, …., n and j =1, 2, …., m.

Step 6: The KLD for each pair of variables is calculated from the probabilities obtained from the previous step and presented in a confusion matrix. The KLD between two random variables X_1 and X_2 can be computed as shown in Equation 4.12.

$$D_{KL}(X_1||X_2) = \sum_{i=1}^{n} P(X_1)\, ln\frac{P(X_1)}{P(X_2)} \tag{4.12}$$

where D_{KL} is the measure of Kullback–Leibler divergence, and P denotes probability.

It is noteworthy to mention that the average KLD is used to represent the confusion matrix after discarding lower values. A threshold of 0.60 is used in this context. An average measure is required to set up a general threshold level for different process operations. Suppose 1000 and 2000 faulty samples are collected from two process operations. It is expected that the second dataset will yield a higher total value of KLD; thus, it is difficult to set a common threshold. However, if the average value is used, it will give the measure of KLD per observation. Hence, the obtained KLD from Equation 4.12 is divided by the total number of faulty samples.

Step 7: The root and leaf nodes are identified from the confusion matrix. The variables that have zero values all through the corresponding columns are selected as the root node. This implies that information flows from these variables to others. On the other hand, the variables with zero values all through the corresponding rows are selected as the leaf nodes.

Step 8: The order of the intermediate nodes is selected using the best child searching strategy. Suppose a process has five variables (X_1-X_5). X_1 and X_2 are the root nodes, and the confusion matrix does not provide any concrete information about the leaf nodes. The joint densities of X_1 and X_3, X_1 and X_4, and X_1 and X_5 are estimated, and the variable among X_3, X_4, and X_5 gives the highest joint density with X_1 is selected as the best child node for X_1. The same procedure is recursively performed unless the qualitative network is constructed.

Step 9: The prior probability of root nodes is calculated by averaging the fault probability of corresponding variables from step 5. The CPTs are estimated using the copula functions. For pairwise cases, bivariate copulas are used. On the contrary, the D-vine copula model with Bayes' theorem is used in multivariate cases. The reason for selecting D-vine is that it does not require computation of the root node of the first tree. Also, it performs better in capturing weaker correlations (Cui and Li, 2020). A statistical software, R has been used to model the copulas. The 'CDVine' package by Brechmann and Schepsmeier (2013) in R provides the flexibility of modelling a wide range of copula types. Kendall's rank correlation coefficient, τ is used to describe the nonlinear dependence among the variables. The maximum value of τ by applying distinct copula types is used to compute the CPTs. As the range of τ varies from -1 to 1, an absolute value is considered when building the CPTs.

Once the joint density of multiple variables is computed using the D-vine copula, the CPTs can be estimated by dividing the probability of child variable(s). Consider a four-dimensional case. Using

D-vine copula, the joint density of four variables, $f(X_1, X_2, X_3, X_4)$, can be computed by Equation 4.13 as follows:

$$f(X_1, X_2, X_3, X_4) = f(X_1)f(X_2)f(X_3)f(X_4)C_{12}C_{23}C_{34}C_{1,3|2}\,C_{2,4|3}\,C_{1,4|2,3} \quad (4.13)$$

$f(X_1)$, $f(X_2)$, $f(X_3)$, and $f(X_4)$ can be computed from the residuals' kernel density, while D-vine will give the measure of required copula functions. Suppose $P(X_1|X_2, X_3, X_4)$ needs to be computed. We can compute $P(X_2, X_3, X_4|X_1)$ by Equation 4.14.

$$P(X_2, X_3, X_4|X_1) = \frac{f(X_1,X_2,X_3,X_4)}{f(X_1)} = \frac{P(X_1,X_2,X_3,X_4)}{P(X_1)} \quad (4.14)$$

Now, the Bayes' theorem can be utilized to calculate the required conditional probability as follows:

$$P(X_1|X_2, X_3, X_4) = \frac{P(X_2,X_3,X_4|X_1)P(X_1)}{P(X_2, X_3, X_4)} \quad (4.15)$$

In Equation 4.15, $P(X_2, X_3, X_4)$ can be computed by applying further D-vine decomposition on X_2, X_3, and X_4. In this way, the conditional probability of any combination can be obtained. It is noteworthy to mention that no discretization of data is required to define the quantitative parts following the described approach.

The online part consists of the following four simple steps.

Step 9: Online process data is auto standardized using the same mean and standard deviation obtained from step 1.

Step 10: The T^2 and SPE values for each observation are computed. If any T^2 or Q value exceeds the threshold obtained from step 3, fault is detected.

Step 11: Once fault is detected, diagnosis is completed using the methodology proposed by Amin et al. (2018); the authors viewed the contribution plots as a set of uncertain evidence and suggested to update the BN with multiple likelihood evidence for accurate root cause diagnosis. The average

contribution of the first ten faulty samples is utilized to generate the contribution plots. These contributions are rescaled on a scale of 0-80%.

Step 12: The variables that have more than 20% rescaled contribution are selected to update the BN, and the percentage change of each variable is calculated from the updated BN. Then, the variable that has the highest percentage in the faulty state is identified as the root cause if it is a root node; otherwise, the root cause is identified among its parent nodes based on their respective percentage increase in the faulty state.

4.3. Applications of the Proposed Methodology

4.3.1. Continuous Stirred Tank Heater (CSTH)

The continuous stirred tank heater (CSTH) is a common sub-unit in several process operations. It is used as a testing example in many studies (Tong et al., 2014; Yu and Qin, 2008). The considered CSTH model (Figure 4.2) was developed at the University of Alberta. It contains real disturbances data, and this process is highly nonlinear. A total of five variables: cold water valve demand, steam valve demand, level, temperature, and output water flowrate have been monitored in this study. All the measurements are collected on a scale of 4-20 mA. Detailed process description of the considered CSTH simulator can be found in the article by Thornhill et al. (2008). Two fault cases have been considered in this work. In both scenarios, fault starts after 1000 samples of normal operation. The fault description and their root cause are listed in Table 4.1.

Table 4.1: Fault description in the CSTH.

Fault scenario no.	Fault description	Root cause
A1	Steam valve stiction	Steam valve
A2	Step change in cold water valve	Cold water valve

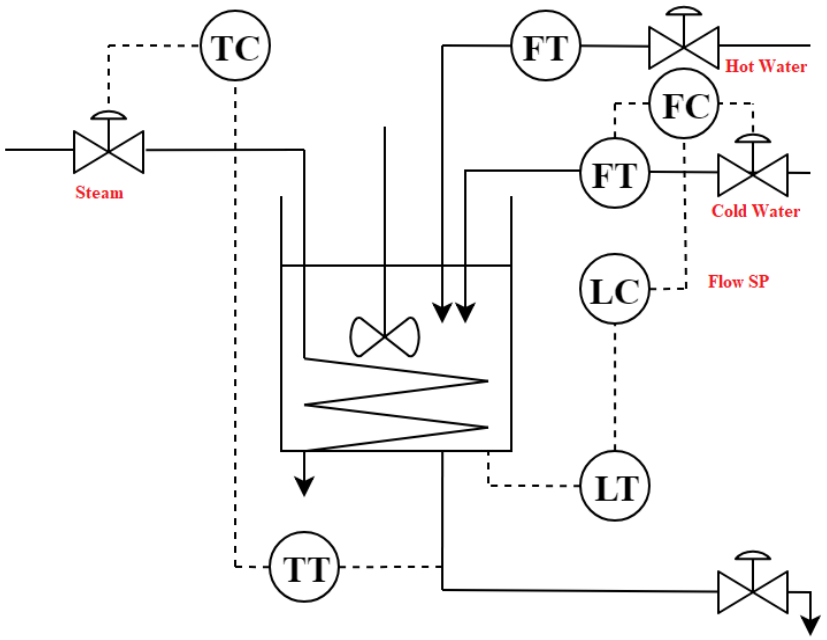

Figure 4.2: The continuous stirred tank heater (modified and redrawn from (Thornhill et al., 2008)).

First, a total of 1000 normal and 200 faulty samples are collected. The faulty samples are generated by providing random signals in the inputs to the system. It is noteworthy to mention that these faulty samples are different from the ones that are being used to examine the efficacy of proposed methodology. The normal samples are auto standardized to zero mean and unit variance. The singular value decomposition (SVD) is performed on the covariance matrix, and loadings and score matrices are calculated. Then, the CD is performed on the raw data and score matrix. CD(X) and CD(T) are calculated as 2.66 and 2.86, respectively; this implies that 3 PCs are required to build the PCA monitoring model. Once the number of PCs is determined, thresholds of T^2 and SPE statistics are calculated as 11.43 and 5.12, respectively, for a 99% confidence level.

The fault probabilities for the 200 faulty samples are estimated using Equations 4.10 and 4.11. The required mean and standard deviation are calculated from 1000 normal samples. The KLD for each

pair of variables is calculated using Equation 4.12 and divided by 200. A confusion matrix is constructed from the obtained results, as shown in Table 4.2.

Table 4.2: Confusion matrix for the CSTH.

Variables	Cold water valve demand	Steam valve demand	Level	Water flowrate	Temperature
Cold water valve demand	0	0	0.61	0	1.40
Steam valve demand	0	0	0.73	0.65	0
Level	0	0	0	0	1.11
Water flowrate	0	0	0	0	0.61
Temperature	0	0	0.63	0.61	0

It can be seen that the first two columns are filled with zeroes; hence, the corresponding variables: cold water valve demand and steam valve demand can be identified as the root nodes. However, no variable has only zeroes row-wise, and no leaf node is identified from the confusion matrix. Then, the joint probability density is estimated from the joint frequency distribution. The joint density of the cold water valve and level, cold water valve and temperature, and cold water valve and flowrate is calculated as 0.37, 0, and 0.31, respectively. Hence, level can be identified as the best child for the cold water valve demand. Similarly, temperature is identified as the child node of steam valve demand, as the joint probability of the steam valve demand and level, steam valve demand and flowrate, and steam valve demand and temperature is calculated as 0, 0.07, and 0.84, respectively. The optimality of level and temperature is checked and found that level has a higher joint density with the flowrate. However, the temperature is also affected by the level (from Table 4.2). Therefore, level is used as the parent nodes of both the temperature and flowrate. This completes the qualitative BN structure.

To determine the priors, the average fault probability of cold water valve demand and steam valve demand is calculated from 200 faulty samples. PCA residuals are used to estimate the CPTs, as the residuals contain more significant causal information (Gharahbagheri et al., 2017b). Bivariate copulas are used to estimate the dependency between single parent-child pairs (i.e. level and flowrate). Table 4.3 shows the justification of using residuals with KDE for building the CPTs. From process knowledge, it is obvious that there exists a strong dependency between the level and flowrate. However, the copula function fails to capture the true measure of dependence from raw data and residuals, as they often exceed the limit of 0 to 1. On the contrary, it provides a realistic value of τ when copula function is applied to the kernel CDFs that are obtained from PCA residuals.

Table 4.3: A comparison of Kendall's rank correlation coefficient for different data sources.

Pair	Cold water valve and level			Level and flowrate		
Data type	Raw data	Residual	Residual with KDE	Raw data	Residual	Residual with KDE
Kendall's rank correlation coefficient, τ	0.1647	0.1563	0.5492	0.0087	0.0215	0.8131

The D-vine copula is used to estimate the CPT of temperature, as it has two parent nodes: level and steam valve demand. It should be noted that binary states: faulty (*F*) and non-faulty (*NF*) have been considered in this work since the focus is to differentiate the abnormal condition from the normal one. Our aim is to estimate *P*(temperature=*F* | steam valve demand=*F*, level=*F*) in the first column of CPT. The marginal fault probabilities are estimated from the residuals. The maximum value among 1000 residual samples is considered as the marginal probability. It yields:

P(steam valve demand=*F*) = 0.9990, *P*(temperature=*F*) = 0.9993, and *P*(level=*F*) = 0.9995.

Then, D-vine copula is applied to steam valve demand, level, and temperature, and the copula parameters are obtained. The joint density of these three variables is calculated.

f(temperature=F, steam valve demand=F, level=F) = $0.9990 \times 0.9993 \times 0.9995 \times 0.9757 \times 0.9893 \times 0.9999 = 0.9631$

Therefore, P(steam valve demand=F, level=F | temperature=F) = $\frac{0.9631}{0.9993} = 0.9637$

Applying bivariate copula, P(steam valve demand=F, level=F) is found as 0.9971.

Finally, P(temperature=F | steam valve demand=F, level=F) = $\frac{0.9637 \times 0.9993}{0.9971} = 0.9658$

The other columns of the CPT are estimated using a similar procedure. Finally, the BN is inserted with all the priors and CPTs and ready to be used for fault diagnosis. Figure 4.3 shows the developed BN for CSTH, modelled in GeNIe 2.0.

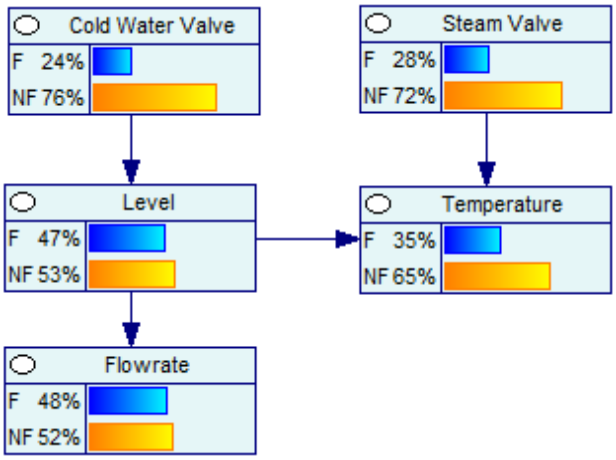

Figure 4.3: BN for the CSTH.

4.3.1.1. Fault Scenario A1 (Steam Valve Stiction)

Valve stiction is a frequently encountered operational problem in process industries and one of the main reasons for plant-wide oscillation and poor control loop performance. Therefore, an FDD scheme should be capable of tackling it. In this fault case, steam valve demand stiction occurs after 1000 samples. This scenario is generated by using a switch in the Simulink that provides a constant value from the 1001 sample. As a result of stiction, temperature upset occurs. The controller tries to maintain the setpoint; however, it fails as the steam valve remains in the same position. The T^2

control chart detects this fault much earlier than the SPE control chart (Figures 4.4(A) and 4.4(B)). As this fault is detected earlier by the T^2 control chart, corresponding contribution plot is generated (Figure 4.4(C)). The contribution plot suggests temperature as the root cause, which is inaccurate. The T^2 contributions are rescaled from 0-80% with respect to temperature's original contribution. In the contribution plot, the left-hand bar (green coloured) and right-hand bar (red coloured) represent the original and rescaled contributions, respectively. The rescaled contributions of cold water valve demand, steam valve demand, level, temperature, and flowrate become 2.38%, 6.68%, 1.23%, 80%, and 15.39%, respectively. Therefore, the BN is updated with the likelihood evidence of temperature, as it is the only variable that has more than 20% rescaled contribution.

Figures 4.4(D) and 4.4(E) show the updated BN and percentage change in the probability at the faulty state. Although all the variables show an increasing probability to be in the faulty state, temperature and steam valve demand have prominent increases. Temperature has the highest probability increase (95.51%). Since it is a child node, it is not considered as the root cause. It has two parent nodes: level and steam valve demand. Steam valve demand and level have 82.30%, 13.32% increase in the faulty state, respectively. Hence, level can be ignored, and steam valve demand can be accurately identified as the root cause.

A

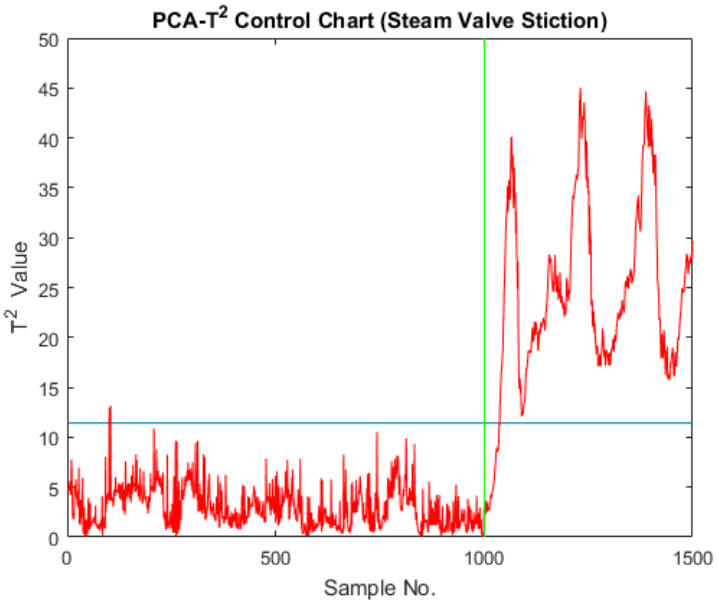
PCA-T2 Control Chart (Steam Valve Stiction)
T2 Value
Sample No.
0
5
10
15
20
25
30
35
40
45
50
0
500
1000
1500

B

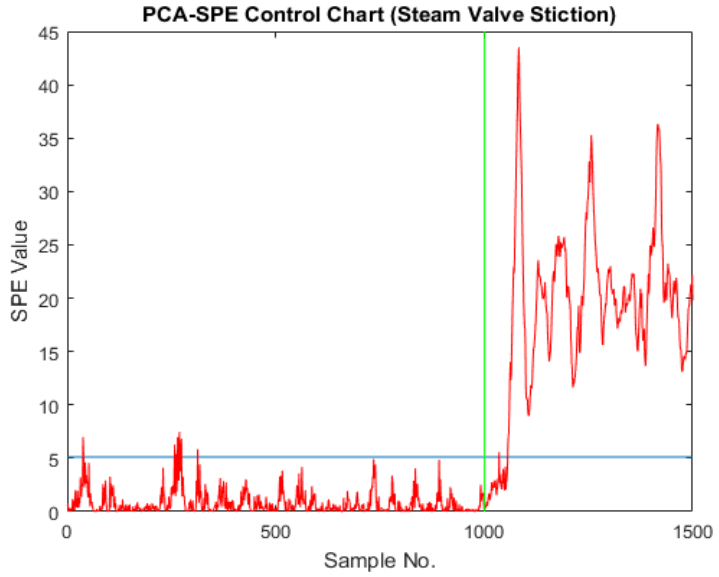
PCA-SPE Control Chart (Steam Valve Stiction)
SPE Value
Sample No.
0
5
10
15
20
25
30
35
40
45
0
500
1000
1500

C

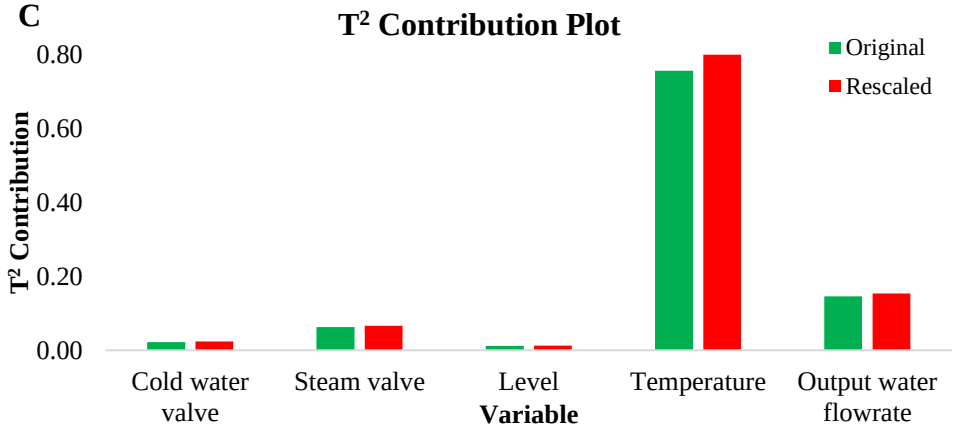
T2 Contribution Plot
Original
Rescaled
T2 Contribution
0.00
0.20
0.40
0.60
0.80
Cold water valve
Steam valve
Level
Temperature
Output water flowrate
Variable

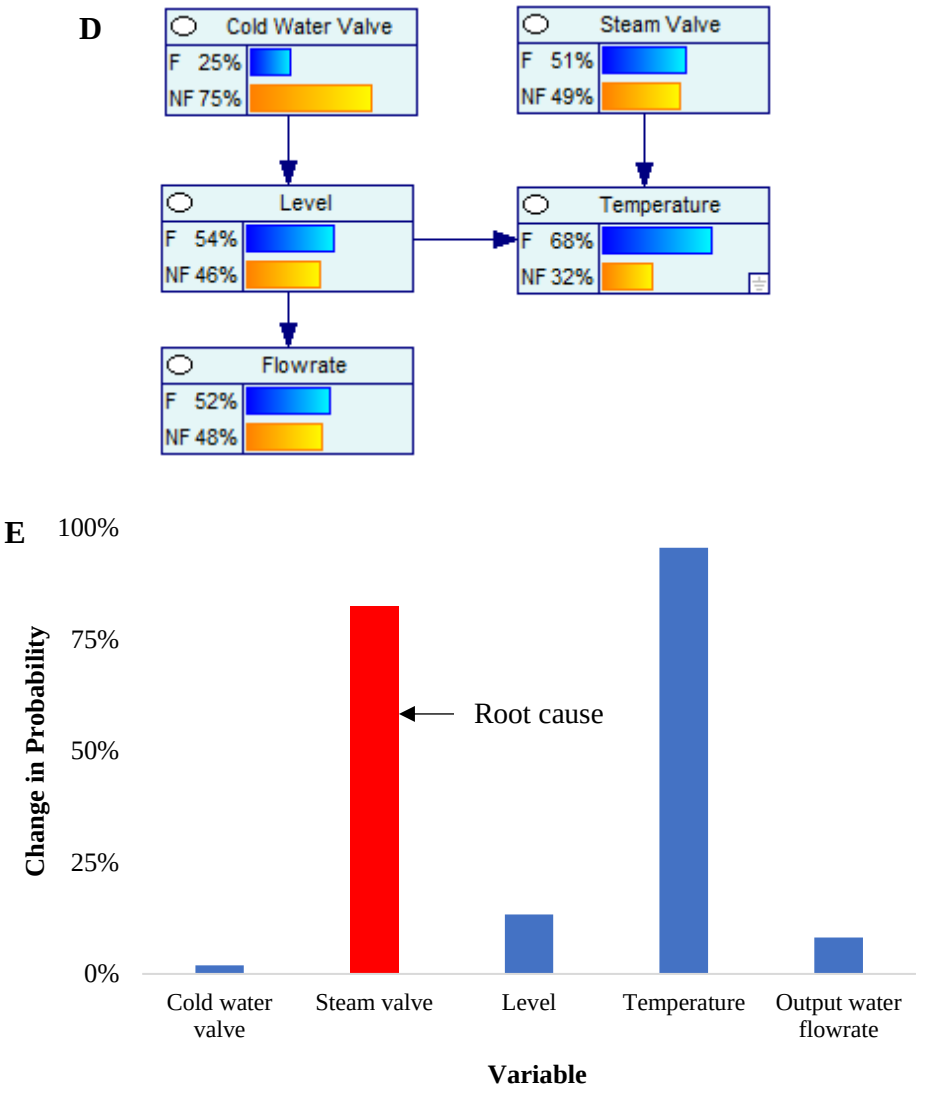

Figure 4.4: Monitoring results for steam valve stiction (A) PCA-T^2 control chart, (B) PCA-SPE control chart, (C) PCA-T^2 contribution plot, (D) updated BN, and (E) root cause diagnosis by percentage change in the faulty state.

4.3.1.2. Fault Scenario A2 (Step Change in Cold Water Valve)

This fault scenario has been generated by using a step type signal. Figures 4.5(A) and 4.5(B) show the PCA-T^2 and PCA-SPE control charts, respectively. Both these control charts can detect this fault immediately. However, after a brief period, the T^2 and SPE values return under the thresholds. This fault changes the level in the tank and output water flowrate. Cold water valve demand and

flowrate are operated in a closed-loop by a proportional-integral-derivative (PID) controller. Hence, the controller tries to compensate for the change in flowrate by altering the valve opening. As a result, the effect of this fault is mitigated.

PCA-T^2 contribution plot is generated (Figure 4.5(C)). All the contributions are rescaled, and cold water valve demand, flowrate, and temperature are the variables that are selected to update the BN. Figure 4.5(D) shows the updated BN. The updated probabilities are compared, and the percentage change in the faulty state is plotted in Figure 4.5(E). Any negative percentage change implies that the variable has an increasing probability in the non-faulty state. It can be seen that cold water valve demand has the highest increase in the faulty state (136.17%), and it is a root node. Therefore, it can be identified as the root cause of the fault.

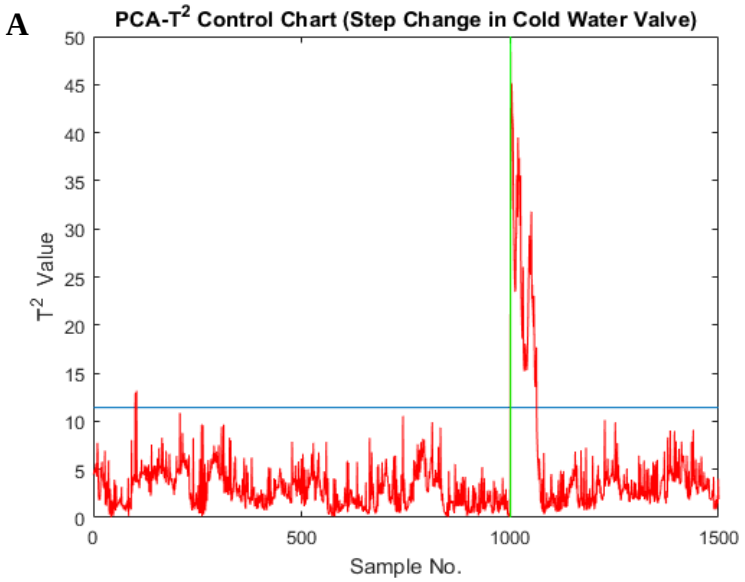

B

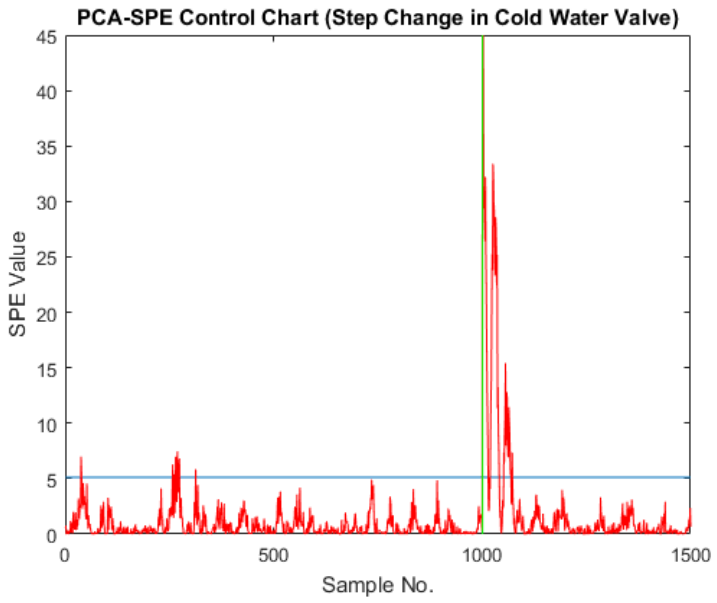
PCA-SPE Control Chart (Step Change in Cold Water Valve)
SPE Value
Sample No.
0
5
10
15
20
25
30
35
40
45
0
500
1000
1500

C

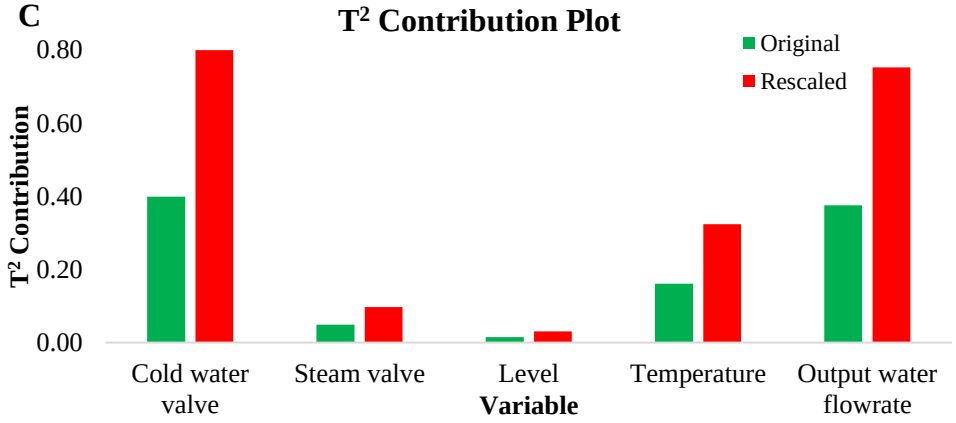
T² Contribution Plot
Original
Rescaled
T² Contribution
0.00
0.20
0.40
0.60
0.80
Cold water valve
Steam valve
Level
Temperature
Output water flowrate
Variable

D

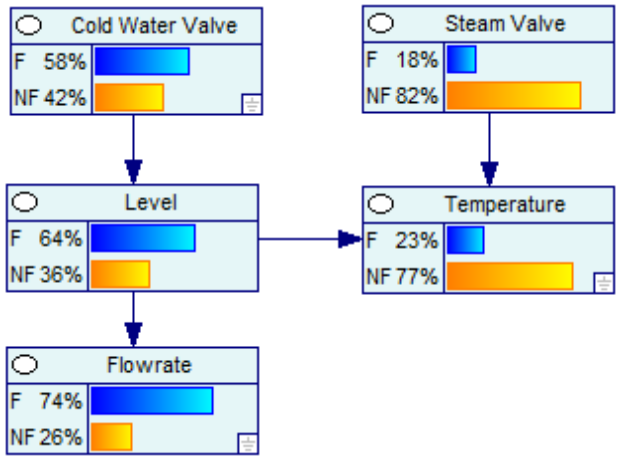
Cold Water Valve
F 58%
NF 42%
Steam Valve
F 18%
NF 82%
Level
F 64%
NF 36%
Temperature
F 23%
NF 77%
Flowrate
F 74%
NF 26%

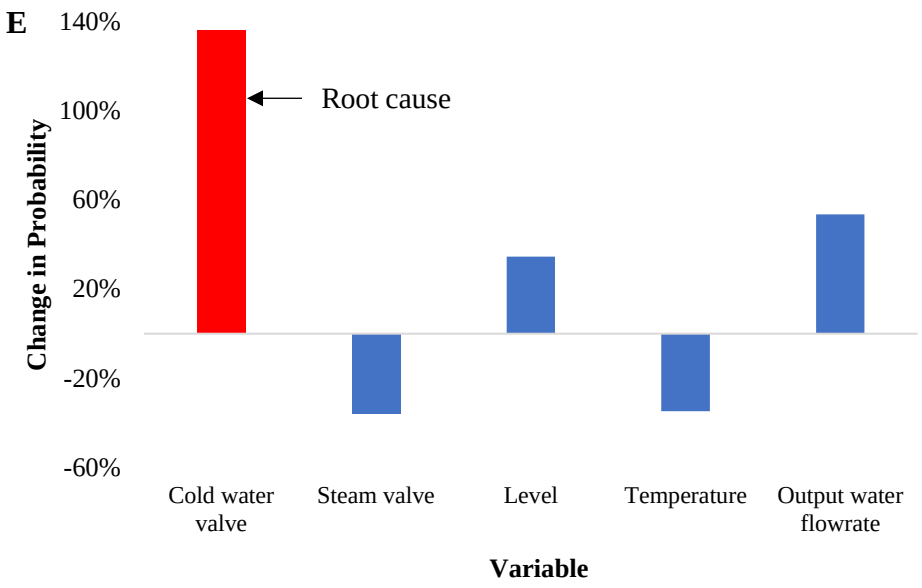

Figure 4.5: Monitoring results for step change in cold water valve demand (A) PCA-T^2 control chart, (B) PCA-SPE control chart, (C) PCA-T^2 contribution plot, (D) updated BN, and (E) root cause diagnosis by percentage change in the faulty state.

4.3.2. Binary Distillation Column

The distillation column is a common sub-system in process industries. Distillation is the process of separating a mixture of two or more components by heating the mixture to a temperature between their boiling and condensing points. In this study, a binary distillation column (Figure 4.6) is considered. It consists of 40 stages and separates a mixture of relative volatility of 1.5 into products of 96% purity. Three input variables: feed rate, feed composition, and reflux flowrate and two output variables: top composition and bottom composition have been monitored. The description of this process and relevant assumptions are available at (Skogestad, 1997). Two fault cases are considered for this process model. Table 4.4 shows the fault description and their root cause.

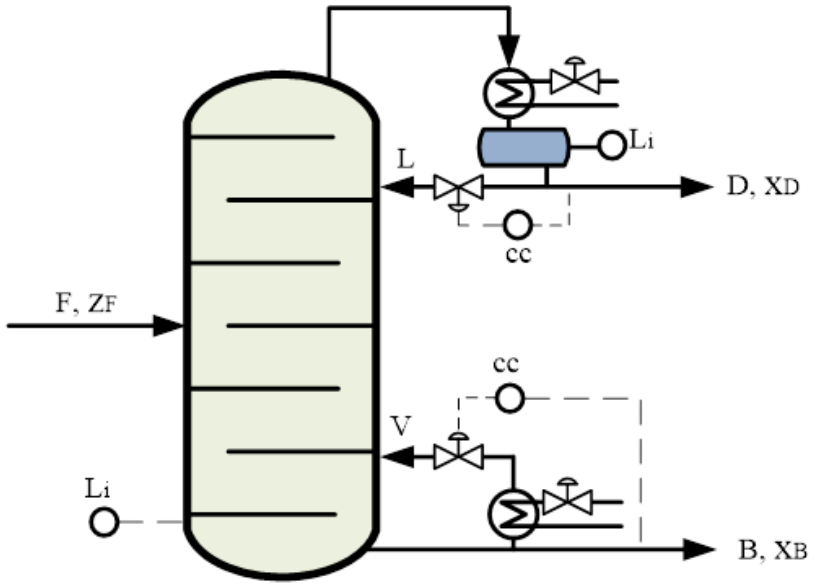

Figure 4.6: A binary distillation column (modified and redrawn from (Skogestad, 1997)).

Table 4.4: Fault description in the binary distillation column.

Fault scenario no.	Fault description	Root cause
B1	Random variation in reflux flowrate	Reflux flowrate
B2	Step change in feed rate	Feed rate

A total of 500 samples are collected, where the first 400 samples are collected in the normal operating condition, and the rest consist of faulty data. The non-faulty samples are used to build the PCA monitoring model. The samples are auto standardized to zero mean and unit variance. The SVD is performed, and the score matrix, T is computed using the standard PCA procedure. Correlation dimension analysis on X and T yields 1.79 and 1.45, respectively. Hence, the first 2 PCs are selected, and thresholds of T^2 and SPE are calculated as 9.34 and 0.05, respectively, with a level of 99% confidence. It should be noted that the CPV method also suggests the same number of PCs to build this FDD model.

The faulty samples are converted into probabilities using Equations 4.10 and 4.11. The KLDs for all possible pairs of variables are calculated using Equation 4.12 and divided by 100. The

respective confusion matrix (Table 4.5) is constructed from the average KLD. It is noteworthy to mention that the average KLD values lower than 0.60 has been assigned zero in the confusion matrix, considering lower than 0.60 as insignificant information flow.

Table 4.5: Confusion matrix for the binary distillation column.

Variables	Feed rate	Feed composition	Reflux flowrate	Top composition	Bottom composition
Feed rate	0	0	0	2.47	1.78
Feed composition	0	0	0	3.11	2.31
Reflux flowrate	0	0	0	3.11	2.31
Top composition	0	0	0	0	0
Bottom composition	0	0	0	0	0

The feed rate, feed composition, and reflux flowrate are found as the root nodes, as their respective columns contain only zeroes. On the contrary, top composition and bottom composition are the leaf nodes. Also, both these leaf nodes are receiving significant information from all the root nodes. Hence, six arcs are directed from feed rate, feed composition, and reflux flowrate towards top composition and bottom composition (three each). The priors are calculated from the faulty samples, and the CPTs are estimated using the D-vine copula and Bayes' theorem. Figure 4.7 shows the developed BN.

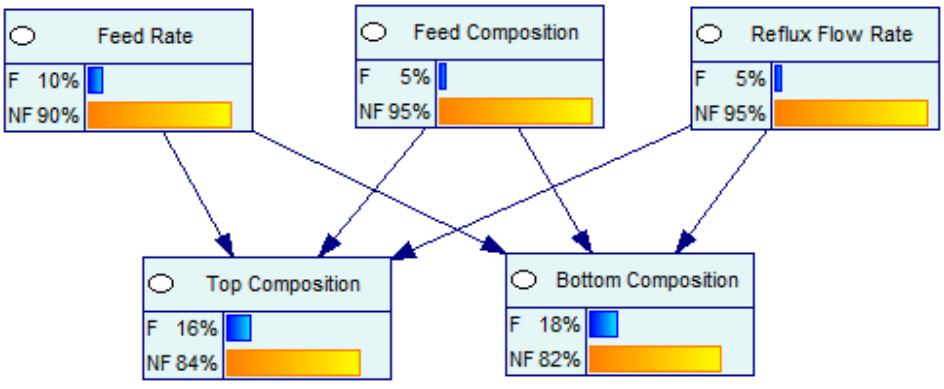

Figure 4.7: BN for the binary distillation column.

4.3.2.1. Fault Scenario B1 (Random Variation in Reflux Flowrate)

In a distillation column, the vapour from top of the column is condensed in a condenser and collected at a receiver in the bottom of the tower. A portion of this liquid is pumped back at the top of the tower; this is called the reflux flowrate, and it has a significant impact on the purity of the products (Skogestad and Morari, 1988). In this fault scenario, a random variation starts from the 401st sample that directly affects the top and bottom composition and results in products of undesired quality. The PCA-SPE control chart detects the fault immediately; however, the PCA-T^2 fails to detect the fault due to a lower magnitude of the random variation (Figures 4.8(A) and 4.8(B)).

The PCA-SPE contribution plot is generated using 401-410 samples. It shows that three variables: reflux flowrate, top composition, and bottom composition are highly affected by this fault. The bottom composition has the highest contribution (32.28%), and its contribution is used to rescale the other contributions, as shown in Figure 4.8(C). The BN is updated with three likelihood evidence of the variables stated above, as their rescaled contribution is higher than 20%.

The updated BN is shown in Figure 4.8(D). Then, the percentage change in the fault probability is calculated and displayed in Figure 4.8(E). It is noticed that all the variables show an increasing tendency to be in the faulty state because feed rate and feed composition are also the parent nodes of top composition and bottom composition, and any evidence in these leaf nodes have an effect on all the three root nodes. Among all the root nodes, reflux flowrate has the highest increase in the faulty state (336.81%) and is successfully diagnosed as the root cause of the observed anomaly.

A

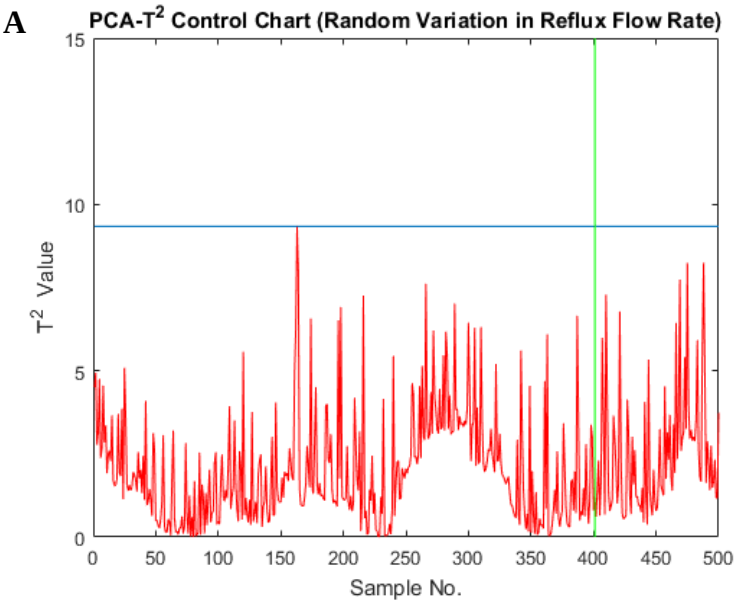
PCA-T2 Control Chart (Random Variation in Reflux Flow Rate)
T2 Value
Sample No.
0
5
10
15
0
50
100
150
200
250
300
350
400
450
500

B

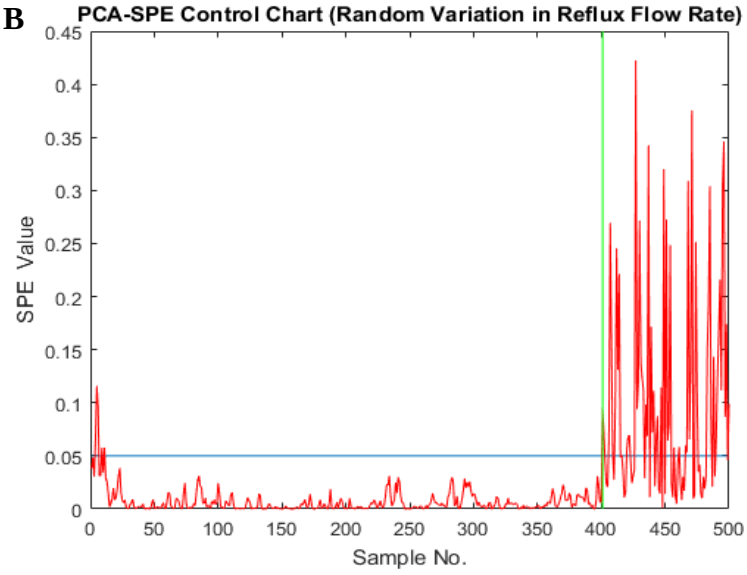
PCA-SPE Control Chart (Random Variation in Reflux Flow Rate)
SPE Value
Sample No.
0
0.05
0.1
0.15
0.2
0.25
0.3
0.35
0.4
0.45
0
50
100
150
200
250
300
350
400
450
500

C

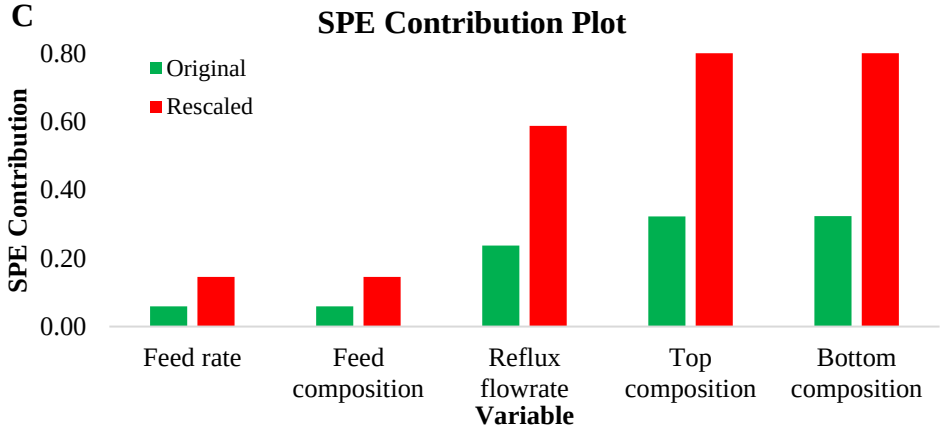
SPE Contribution Plot
SPE Contribution
Original
Rescaled
0.00
0.20
0.40
0.60
0.80
Feed rate
Feed composition
Reflux flowrate
Top composition
Bottom composition
Variable

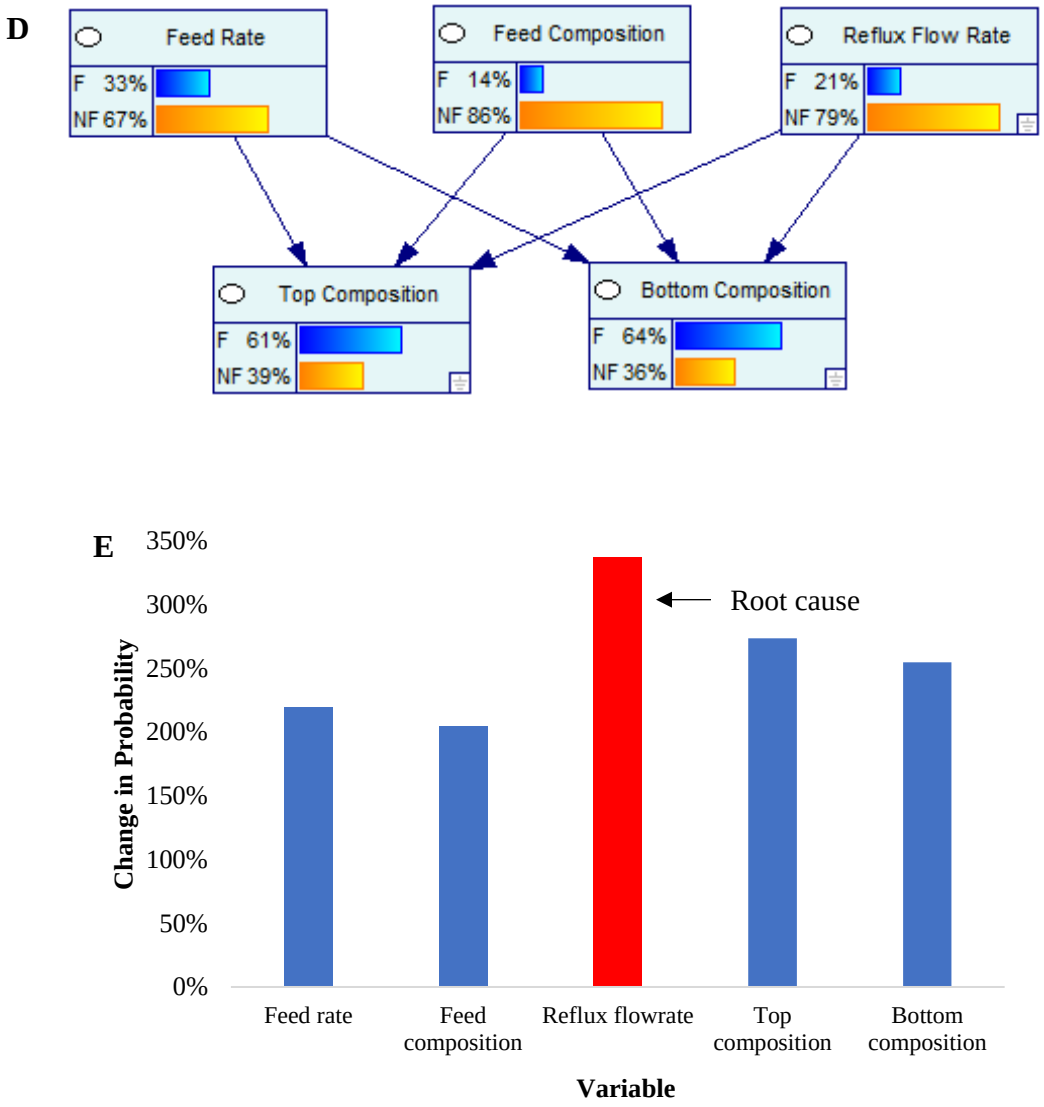

Figure 4.8: Monitoring results for random variation in reflux flowrate (A) PCA-T^2 control chart, (B) PCA-SPE control chart, (C) PCA-SPE contribution plot, (D) updated BN, and (E) root cause diagnosis by percentage change in the faulty state.

4.3.2.2. Fault Scenario B2 (Step Change in Feed Rate)

In this fault case, a step reduction occurs in the feed rate after 400 samples. Again, PCA-SPE detects the fault much earlier than PCA-T^2 (Figures 4.9(A) and 4.9(B)). Upon successful fault detection, the contribution plot is generated and rescaled (Figure 9(C)). Three variables: feed rate,

feed composition, and reflux flowrate have more than 20% rescaled contribution. Therefore, the BN is updated with the likelihood evidence of these variables.

Figures 4.9(D) and 4.9(E) show the updated BN and percentage change in the faulty state, respectively. It can be seen that feed rate, top composition, and bottom composition have an increasing proclivity towards the abnormal state, while the other two variables: reflux flowrate and feed composition have an increased probability to be in the normal state. This implies that these two variables are not the reason behind the fault. Feed rate has the highest increase in the faulty state (205.77%), and it is the only root node with an increasing tendency to be in a faulty state. Hence, it can be diagnosed as the root cause in this fault scenario.

A

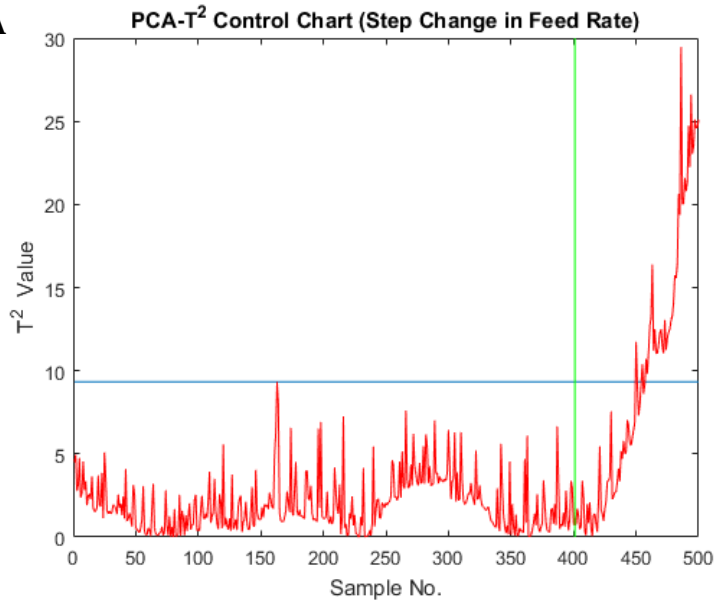

B

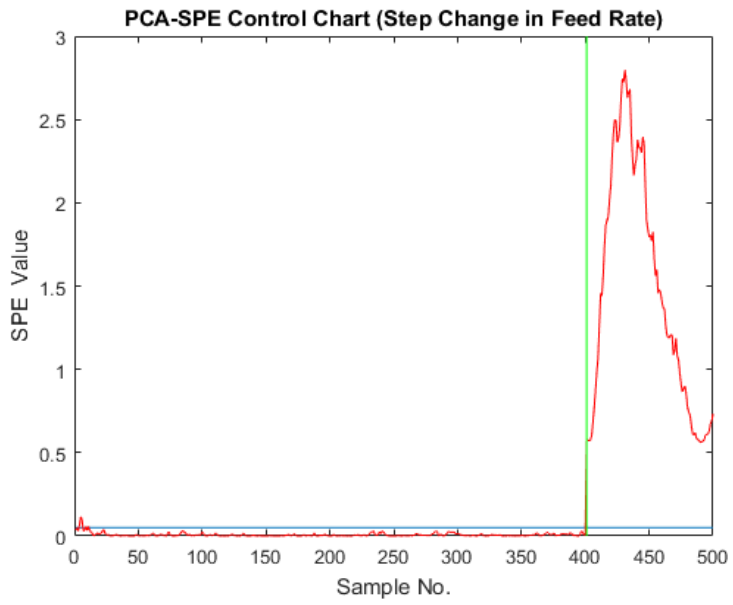
PCA-SPE Control Chart (Step Change in Feed Rate)
SPE Value
Sample No.
0
0.5
1
1.5
2
2.5
3
0
50
100
150
200
250
300
350
400
450
500

C

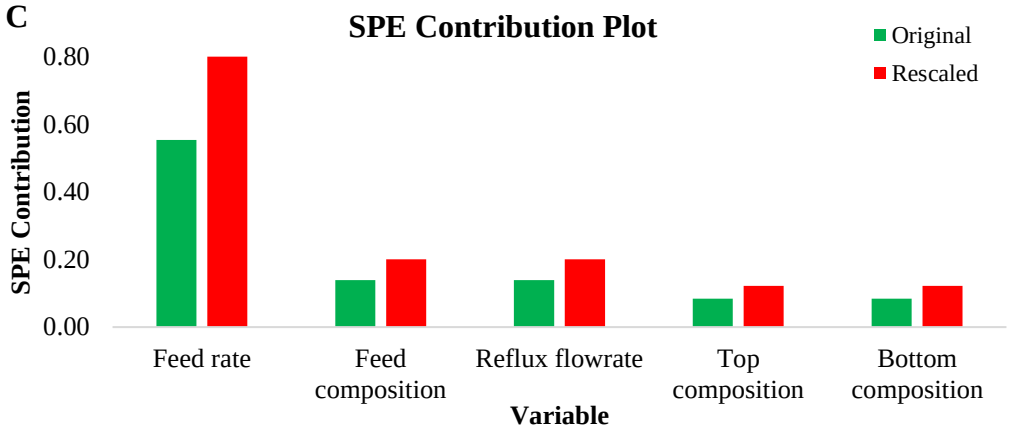
SPE Contribution Plot
Original
Rescaled
SPE Contribution
0.00
0.20
0.40
0.60
0.80
Feed rate
Feed composition
Reflux flowrate
Top composition
Bottom composition
Variable

D

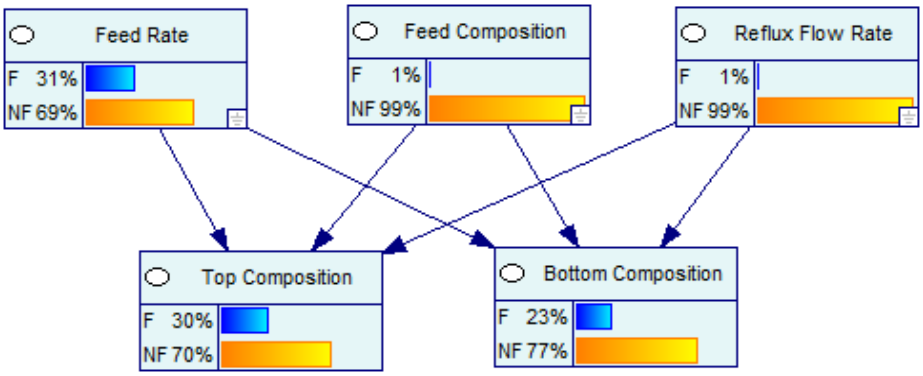
Feed Rate
F 31%
NF 69%
Feed Composition
F 1%
NF 99%
Reflux Flow Rate
F 1%
NF 99%
Top Composition
F 30%
NF 70%
Bottom Composition
F 23%
NF 77%

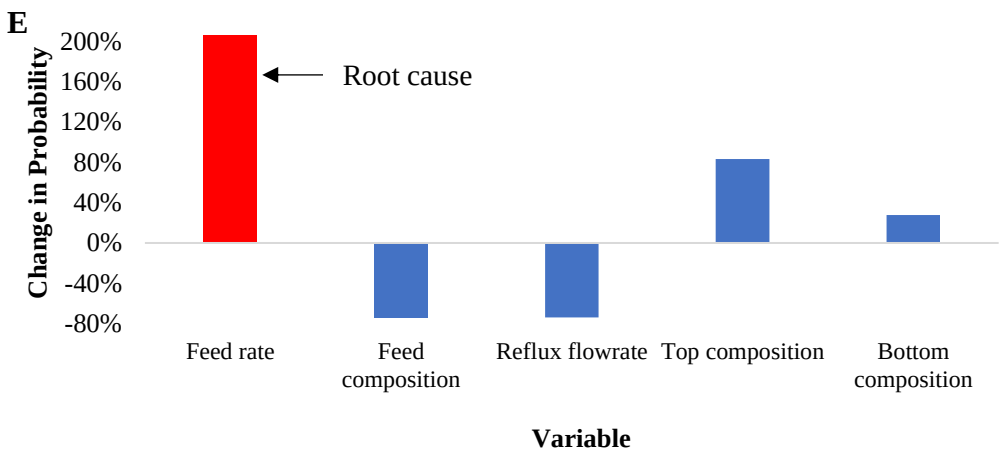

Figure 4.9: Monitoring results for step change in feed rate (A) PCA-T^2 control chart, (B) PCA-SPE control chart, (C) PCA-SPE contribution plot, (D) updated BN, and (E) root cause diagnosis by percentage change in the faulty state.

4.4. Results and Discussion

The performance of proposed CD-based PCA, KPCA, ICA, and KICA in terms of false alarm rate (FAR), detection rate (DR), and detection delay (DD) is compared with that of CPV-based PCA, KPCA, ICA, and KICA. Interested readers are referred to the works by Cho et al. (2005) and Lee et al. (2007) for details of KPCA and KICA algorithms, respectively. The comparison is displayed in Table 4.6. It should be noted that the CPV-based models are built using 4 and 2 PCs for the CSTH and binary distillation column, respectively; these PCs or ICs are required to capture more than 90% variation. Although the CPV method cannot be directly applied to the ICA and KICA, the same number of PCs obtained by the PCA and KPCA are utilized to build the CPV-based ICA and KICA models for a fair comparison. The SCREE procedure gives the same number of PCs or ICs as that of CPV and therefore, is not included in Table 4.6.

Table 4.6: Fault detection performance comparison of distinct tools (bold implies the best performance).

Fault ID	Performance criterion	PCA (CD)		PCA (CPV)		KPCA (CD)		KPCA (CPV)		ICA (CD)		ICA (CPV)		KICA (CD)		KICA (CPV)	
		T^2	SPE	T^2	SPE	T^2	SPE	T^2	SPE	I^2	SPE	I^2	SPE	I^2	SPE	I^2	SPE
A1	FAR (%)	**0.20**	1.20	0.30	0.80	**0.20**	1.20	0.30	1	0.80	0.90	0.90	0.80	0.90	1	1	1.10
	DR (%)	92.60	89	93	71.80	92.60	89	93	72.40	90.40	94.40	96.40	93.80	94.60	94.80	**96.80**	94.20
	DD (s)	37	56	35	**8**	37	56	35	**8**	**8**	25	**8**	32	**8**	25	**8**	32
A2	FAR (%)	**0.20**	1.20	0.30	1	**0.20**	1.20	0.30	1	0.80	0.90	0.90	0.80	0.90	1	1	1.10
	DR (%)	12.60	11.00	13.40	6.60	12.60	11.20	13.40	7.20	7.20	13.80	11.20	12.60	7.60	**14.00**	11.80	12.80
	DD (s)	**0**	**0**	**0**	**0**	**0**	**0**	**0**	**0**	**0**	**0**	**0**	**0**	**0**	**0**	**0**	**0**
B1	FAR (%)	**0**	2.50	**0**	2.50	**0**	0.50	**0**	0.50	1.25	1.50	1.25	1.50	1.25	1.75	1.25	1.75
	DR (%)	0	60	0	60	0	13	0	13	**100**	**100**	**100**	**100**	**100**	**100**	**100**	**100**
	DD (s)	NA	**0**	NA	**0**	NA	27	NA	27	**0**	**0**	**0**	**0**	**0**	**0**	**0**	**0**
B2	FAR (%)	**0**	2.50	**0**	2.50	**0**	0.50	**0**	0.50	1.25	1.50	1.25	1.50	1.25	1.75	1.25	1.75
	DR (%)	45	**100**	45	**100**	44	90	44	90	**100**	**100**	**100**	**100**	**100**	**100**	**100**	**100**
	DD (s)	55	**0**	55	**0**	59	7	59	7	**0**	**0**	**0**	**0**	**0**	**0**	**0**	**0**

Overall, the KICA and ICA provides better DRs; this implies that a strong non-Gaussian feature is predominant in the studied fault cases, which causes them to perform better. However, the FARs are also higher for KICA compared to the PCA, ICA, and KPCA. In terms of DD, the PCA and KPCA give a compatible performance as that of the ICA and KICA. This suggests that all these MSPM tools can detect the fault early. The PCA and KPCA provide almost the same performance. It is noteworthy to mention that the Gaussian type kernel function is used to build the KPCA and KICA models, as it is the most widely used kernel function in this context.

In general, the CD-based models provide lesser false alarms. However, the DRs are also slightly lower than the CPV-based models for PCA, ICA, KICA, and KPCA. One of the notable facts about the proposed CD-based method is the perseverance of early detection capacity; even the conventional PCA-CD can detect the fault as early as that of KICA in 3 out of 4 cases. As a result, an optimum monitoring performance can be obtained, which secures lower FAR and early anomaly detection. Besides, the automated manner of PC or IC selection provides a more reliable way of constructing the PCA or ICA-based MSPM tools and relaxes the necessity of incorporating user-perspective.

The root cause diagnosis capacity of CD-based PCA, KPCA, ICA, KICA, and their combination with the existing residual discretization-based BN and newly proposed data-driven KLD and copula-based BN are also studied, and the relative comparison is shown in Table 4.7. None of the standalone MSPM tools is capable of securing an accurate root cause diagnosis feature. The PCA, ICA, and KICA can diagnose the root cause in two cases, while this number is one for KPCA. Both the ICA and KICA provide a robust FDD performance in the distillation column. The time of fault detection is the same for the I^2 and SPE control charts for ICA and KICA, which may

create an ambiguity, as an accurate diagnosis is provided by the SPE and I^2 control charts for fault B1 and B2, respectively. From the real industrial perspective, it will be hard to isolate the acceptable results from a control chart in such cases since they provide the opposing diagnostic report concurrently, and none of them consistently provide accurate information.

Table 4.7: Root cause diagnosis performance comparison of distinct tools (bold implies the best performance).

Tool	Fault ID			
	A1	A2	B1	B2
PCA-CD	No	**Yes**	No	**Yes**
KPCA-CD	No	**Yes**	No	No
ICA-CD	No	No	**Yes**	**Yes**
KICA-CD	No	No	**Yes**	**Yes**
PCA-CD-BN (Discrete)	**Yes**	**Yes**	No	**Yes**
KPCA-CD-BN (Discrete)	**Yes**	**Yes**	No	No
ICA-CD-BN (Discrete)	No	No	**Yes**	**Yes**
KICA-CD-BN (Discrete)	No	No	**Yes**	**Yes**
PCA-CD-BN (Copula)	**Yes**	**Yes**	**Yes**	**Yes**
KPCA-CD-BN (Copula)	**Yes**	**Yes**	No	No
ICA-CD-BN (Copula)	No	**Yes**	No	**Yes**
KICA-CD-BN (Copula)	No	**Yes**	No	**Yes**

The adjunction of BN (both copula and data discretization-based) with the aforementioned FDD tools increases the diagnostic accuracy of the PCA and KPCA while the diagnostic performance still remains the same for the ICA and KICA. The data discretization-based BNs have been developed according to the work by Gharahbagheri et al. (2017). The residuals are discretized around one standard deviation. The samples that lie outside this limit are considered faulty, and subsequently, maximum likelihood estimation is used to estimate the CPTs. The PCA-BN with copula is found to be the best choice from diagnostic perspective, as it can diagnose the root cause in all four cases. When process data is discretized, a significant amount of information is lost. The

use of copula function allows to prevent this loss and therefore, helps the BNs to capture a better dependence measure.

The copula-based CPT modelling strategy from residuals provide distinct conditional probabilities for the studied MSPM tools. For illustration, the CPT estimation for level in the CSTH is considered. The τ of cold water valve and level is found as 0.5492, 0.1659, 0.1563, and 0.1374 from the PCA, KPCA, ICA, and KICA, respectively. Obviously, cold water valve demand greatly influences the level in the tank, and the PCA residuals provide more robust information about this causality. This is the underlying reason behind PCA-CD-BN's success over the other three integrated approaches.

4.5. Conclusion

A data-driven hybrid FDD tool is proposed here. This methodology is built using the early fault detectability of PCA and accurate root cause diagnosis capacity of BN. A unique PC selection criterion is demonstrated using the CD, which eradicates the necessity of inserting user-opinion during PCA model construction. A comparative study among the CD-based PCA, KPCA, ICA, and KICA confirms the efficacy of the CD-based PCA, as it can provide lesser false alarms without sacrificing the early fault detectability.

Unlike most of the exiting BN-based integrated methods, this work constructs the BN solely from process data. The KLD is utilized for BN topology learning, while the copula functions are utilized for parameter estimation. Although the vine copula models are found suitable for high-dimensional CPT modelling, these alone cannot provide the exact form of the conditional densities required to insert into the BN. The Bayes' theorem has been utilized to overcome this issue. A total of sixteen BNs have been developed from PCA, ICA, KICA, and KPCA residuals and integrated with the

CD-based MSPM tools. The PCA-CD-BN is found to be the best combination due to its accurate diagnostic property.

The main advantages of this hybrid method are: (i) free of expert judgment, (ii) purely data-driven, (iii) lesser false alarms, (iv) early fault detection, (v) consistently accurate root cause diagnosis, and (vi) no data discretization while building the CPTs. Furthermore, the data-driven nature will add its value in process digitalization, as the task of FDD can be done in an automated manner. Consequently, the process plants will operate efficiently in the entire life cycle due to early anomaly detection and accurate diagnosis that will save considerable maintenance costs and enhance asset integrity.

This methodology is built using conventional PCA, and it may not provide the optimal performance when dealing with extreme nonlinearity and non-Gaussianity. Even though a comparative study among the PCA-CD-BN, KPCA-CD-BN, ICA-CD-BN, and KICA-BN finds it as the most suitable method from both the detection and diagnostic perspectives, several other MSPM tools such as semi-parametric PCA and sparse PCA can be examined for their efficacy. The Grassberger-Procaccia algorithm has been utilized for estimating the CD. Many advanced versions of this algorithm are available in the existing literature that can be applied to estimate the number of PCs. These might significantly improve the methodology.

Chapter 5: A Novel Data-Driven Methodology for Fault Detection and Dynamic Risk Assessment

Preface

A version of this chapter has been published in ***The Canadian Journal of Chemical Engineering***. This work was featured as the **Trend in Chemical Engineering**. I am the primary author, along with the co-authors, Drs. Faisal Khan, Salim Ahmed, and Syed Imtiaz. I developed the conceptual framework for the FDD and DRA model and carried out the literature review. I prepared the first draft of the manuscript and subsequently revised the manuscript based on the co-authors' and peer review feedback. Co-author Dr. Faisal Khan helped in the concept development and testing the model, reviewing, and revising the manuscript. Co-authors Drs. Syed Imtiaz and Salim Ahmed provided support in implementing the concept and testing the model. The co-authors provided fundamental assistance in validating, reviewing, and correcting the model and results. The co-authors also contributed to the review and revision of the manuscript.

Reference: Amin, M. T., Khan, F., Ahmed, S., & Imtiaz, S. (2020). A novel data-driven methodology for fault detection and dynamic risk assessment. The Canadian Journal of Chemical Engineering, 98(11), 2397-2416. https://doi.org/10.1002/cjce.23760

Abstract

This chapter presents a novel methodology for dynamic risk assessment, integrating the multivariate data-based process monitoring and logical dynamic failure prediction model. This concept for dynamic risk assessment is comprised of the fault assessment and dynamic failure prognosis modules. A combination of the naïve Bayes classifier, Bayesian network, and event tree analysis is utilized to manifest the concept. The naïve Bayes classifier is used for fault detection and diagnosis; it also generates a multivariate probability for a fault class in each time-step, which is used for dynamic failure prognosis by different paths a fault can lead to a process to failure. The proposed framework has been applied to two process systems: a binary distillation column and the RT 580 experimental setup in four fault scenarios, and it is found the developed technique can effectively monitor the process and predict the failure.

Keywords: *Risk analysis, predictive safety, fault assessment, Bayesian network, failure prognosis*.

5.1. Introduction

Chemical plants are inherently large dimensional highly correlated systems with many process variables both in open loop and closed loop. In order to ensure safe and event free operation, these large sets of variables need to be monitored continuously. Dynamically calculated process risk is a good indicator of process state at any time. Hence, a process monitoring scheme, capable of capturing the complex relationships among the interacting process variables and showing continuous process risk estimate is required (Yu et al., 2015a).

The data-based multivariate statistical process monitoring (MSPM) tools such as the principal component analysis (PCA) (Bakshi, 1998), independent component analysis (ICA) (Lee et al., 2004b), partial least squares (PLS) (MacGregor et al., 1994), and Gaussian mixture model (GMM) (Yu and Qin, 2008) provide excellent solutions by monitoring in reduced dimension with fewer control charts. However, these tools suffer from a lack of accuracy in diagnosis capacity. A number of hybrid methods have been developed to provide robust solutions for fault detection and diagnosis (FDD) (Amin et al., 2019c, 2018b; Vedam and Venkatasubramanian, 1999; Yu et al., 2015b). Recent developments in data-based process monitoring can be found in (Jiang et al., 2019; Youqing Wang et al., 2018). One of the significant limitations of the above mentioned data-based methods is that these cannot qualitatively show how a fault can lead a process to several possible paths (i.e. safe, near-miss, mishap, incident, accident, and catastrophic accident).

Dynamic risk assessment (DRA) is a novel concept that has been getting attention by industry and as well as academia in recent years (Villa et al., 2015). An accurate quantitative estimation of possible failure paths is a prerequisite for DRA. A study on the evolution of DRA depicts that the Boolean logic gates-based fault tree analysis (FTA), logical failure modelling technique-based event tree analysis (ETA), and bow-tie (BT) are the most widely used tools in this context. A BT

can be considered as a marriage between FT and ET. An FT is placed on the left-hand side of the BT that gives the probability of a hazard, while the ET is placed on the right-hand side, which shows the possible consequences the hazard can exert, based on the sequential failure or success of the safety barriers. Khakzad et al. (2012) used the BT for DRA; failure probabilities of the safety barriers were updated periodically using the Bayes' theorem from the accident pre-cursor data. Islam et al. (2017) proposed a BT-based DRA methodology for drilling operations. Fault trees were used to determine the reliability of safety barriers.

The major drawbacks of the FTA are that it cannot model complex inter-dependency and represent uncertainty, while the ETA cannot show the non-sequential nature of an accident. A Bayesian network (BN) is an advanced probabilistic tool that can overcome the limitations of FTA and ETA (Adedigba et al., 2016a; Bobbio et al., 2001). A technique to map the BT to BN is demonstrated by Khakzad et al. (2013). Zarei et al. (2017) proposed a dynamic safety and risk analysis approach, utilizing the hazard and operability studies (HAZOP) and BN. An application to a flammable liquid storage system at a gas refinery was used for validation. A process safety and dynamic risk assessment tool, Process Unit Life Safety Evaluation (PULSE), was developed using BN by the ExxonMobil Research Qatar (EMRQ) and Mary Kay O'Connor Process Safety Center - Qatar (MKOPSC-Q) (Kanes et al., 2017). This tool can report the potential increases in risk levels by monitoring the pre-identified risk factors and process safety-related data.

One of the major limitations of the above mentioned DRA approaches is that these tools monitor the process in a univariate manner; this may result in delayed process anomaly detection. Zadakbar et al. (2012) proposed a risk-based fault detection and dynamic risk assessment scheme using the PCA. This method was able to detect a fault much earlier than the univariate tools. However, this work did not account for the failure path analysis. The Kalman filter (KF) was also used for

concurrent fault detection and dynamic risk assessment (Zadakbar et al., 2013). Despite the robust state estimation capacity of the KF, it is considered unsuitable for applying to large-scale industrial processes due to the necessity of a precise model for its secured performance. Also, building such a model is complex and time-consuming when the number of variables is high for process operations. Furthermore, both the PCA and KF cannot provide optimal performance when the process variables exhibit nonlinearity.

Yu et al. (2015a) proposed a methodology for fault detection and dynamic risk assessment using the self-organizing map (SOM) to overcome the limitations of (Zadakbar et al., 2012). The process risk profile was generated using each variable's dynamic loading, which may yield over-estimation of system risk. Besides, this work did not consider the human and organizational factors while displaying the failure paths. Integration of loss function with the SOM is also available in the existing literature (Yu et al., 2016). Although this work can estimate the operational risk, it did not include the failure prognosis module. Gabbar et al. (2014) developed a novel fault semantic network (FSN)-based fault propagation behaviour analysis tool. Gabbar and Boafo (2016) demonstrated another application of FSN in fault propagation pathway analysis in a nuclear power plant. An FSN-BN-based dynamic risk assessment and safety verification methodology is also available in the existing literature (Gabbar et al., 2015). However, these methods have mainly focused on modelling the fault propagation paths.

The major limitation of PCA and KF-based methods is that these methods do not show detailed analysis on fault diagnosis. Although the SOM-based methods demonstrate root cause analysis, they heavily rely on individual variable's risk profile to estimate the overall risk. Furthermore, these cannot provide a multivariate posterior probability for a fault class based on the extracted features. The current authors believe that a modern DRA tool should be able to monitor (i.e. FDD)

a process in a multivariate manner and display the detailed failure paths to explain how a fault can lead a process to failure. Figure 5.1 shows a novel conceptual framework for DRA. It can be seen that the proposed dynamic risk assessment framework consists of two parts: fault assessment (by the data-based tools) and failure path realization (by the logical failure modelling tools). Predictive dynamic failure analysis can be conducted by adopting such a mechanism, which can be further utilized for DRA by integrating the severity of the consequences. This concept assumes that the existing faults in a process are known, and the probabilities of the faulty states are generated at each time-slice. These probability values work as the input of the logical failure modelling tools showing different failure paths, depending on the performance of the safety barriers. The barrier failure probabilities can be estimated by employing the BNs.

The machine learning techniques such as the artificial neural network (ANN), support vector machine (SVM), and naïve Bayes classifier (NBC) can generate a posterior probability for each fault class, and the fault class that has the highest posterior can be identified as the observed fault (He et al., 2014; Koivo, 1994; Widodo and Yang, 2007). The posteriors can also be used as the input to the failure pathway model to predict the dynamic failure probability. Perhaps the ANN and SVM are the predominating members among the machine learning-based classifiers due to their higher classification accuracy. However, the innate limitations of these powerful tools include the fitting problem, complex training process, lengthy training time, and higher computation cost and memory requirements. On the contrary, the NBC is easier to construct and has a lower computational cost and memory requirements. Furthermore, the volume of required training data is also lower. Hence, extensive research is ongoing on how an NBC can be efficiently utilized to perform the diagnostic analysis (Domingos and Pazzani, 1997; He et al., 2014).

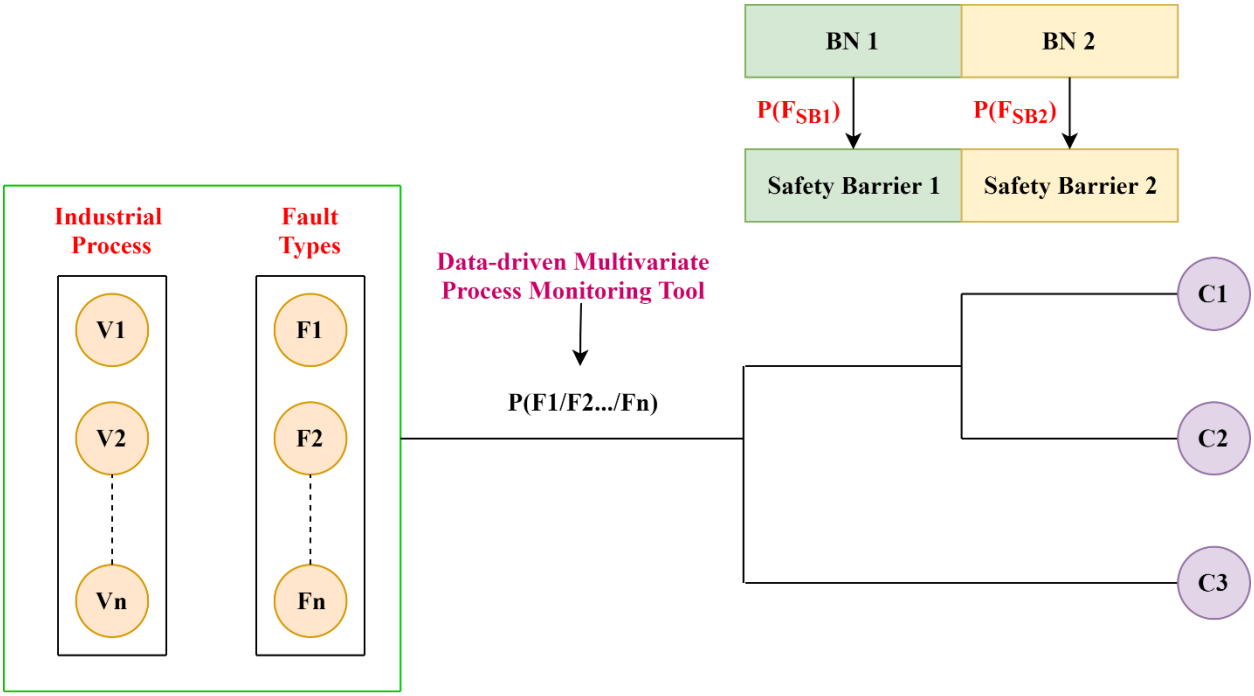

Figure 5.1: A conceptual illustration of the proposed dynamic risk assessment framework.

Muralidharan and Sugumaran (2012) integrated the wavelet analysis and NBC for fault diagnosis of a monoblock centrifugal pump. The features were extracted from the vibration signals using the wavelet analysis, and NBC was used to classify the various faulty conditions. Zhang et al. (2018) utilized a combination of the decision tree (DT), selective support vector machine (SSVM), and NBC for fault classification in the bearings. The DT was applied to extract the significant features, followed by the application of the SSVM to remove the redundant features. Finally, NBC was used to classify different faults. The effect of data pre-processing procedures such as the PCA, the ICA, and the class-conditional ICA (CC-ICA) on NBC is also available in the existing literature (Fan and Poh, 2007). The tree augmented network (TAN), an advanced version of the NBC, was applied to the fault diagnosis in the Tennessee Eastman (TE) chemical process; it provided a better performance over the Fisher discriminant analysis (FDA), proximal SVM (PSVM), and independent SVM (ISVM) (Verron et al., 2006b).

The primary motivation behind this work is to implement the concept of dynamic risk assessment by integrating the FDD and dynamic failure prognosis in a unified framework. Multivariate posterior probability generation capacity of the NBC has been utilized for FDD, and a logical failure modelling tool, ET has been used for failure prognosis. The failure probability of the safety barriers has been estimated using the BNs. Table 5.1 shows the comparison of the proposed methodology with the existing multivariate fault detection and DRA methodologies in terms of FDD, failure path analysis, and input probability to the failure prognosis model. It can be seen that the current method enables computing dynamic failure probability using the multivariate posterior probability for the observed process state, which cannot be obtained by any of the existing methods. The proposed methodology has been applied to a binary distillation column process simulator and an experimental setup situated in the Memorial University of Newfoundland, named the RT 580 (fault finding control-system). The results suggest the proposed tool can provide a better prediction of risk, associated with the different failure paths.

Table 5.1: A comparison of the multivariate fault detection and dynamic risk assessment methods.

Work	Fault detection?	Fault diagnosis?	Failure path analysis?	Input to the failure prognosis model
(Zadakbar et al., 2012)	Yes	No	No	Not applicable
(Zadakbar et al., 2013)	Yes	No	No	Not applicable
(Yu et al., 2015a)	Yes	Yes	Yes	Each variable's dynamic loading
(Yu et al., 2016)	Yes	Yes	No	Not applicable
Current	Yes	Yes	Yes	Multivariate posterior probability

The remainder of this chapter is organized as follows: Section 5.2 briefly discusses the NBC, BN, and ETA. Section 5.3 describes the methodology Applications of the proposed framework to two

process systems are demonstrated in Section 5.4. The contribution, advantages, limitations, and future work scopes are discussed in Section 5.5.

5.2. Preliminaries

5.2.1. Naive Bayes classifier (NBC)

The NBC is a supervised learning-based classifier that uses the Bayes' theorem (Equation 5.1) (Boullé, 2007).

$$P\left(\frac{f}{X}\right) = \frac{P\left(\frac{X}{f}\right)P(f)}{P(X)} \tag{5.1}$$

where f and X denote the fault class and feature vectors, respectively. If a process has i number of faults and j number of variables, $f = [f_1, f_2, f_3, \ldots, f_i]$ and $X = [X_1, X_2, X_3, \ldots, X_j]$, $P(X)$ and $P(f)$ are the prior probability of a feature and fault, respectively. $P(X/f)$ is the likelihood probability of a feature given that a fault has occurred, while $P(f/X)$ is the posterior probability of a fault, based on a set of features.

Equation 5.1 can be written as,

$$P(\frac{f}{X_1, X_2, \ldots, X_j}) = \frac{P(f)\ \prod_{n=1}^{j} P(\frac{X_n}{f})}{P(X_1)\,P(X_2)\ldots P(X_j)} \tag{5.2}$$

The denominator is constant for a given input. Hence, Equation 5.2 can be written as,

$$P(\frac{f}{X_1, X_2, \ldots, X_j}) \propto P(f)\prod\nolimits_{n=1}^{j} P(\frac{X_n}{f}) \tag{5.3}$$

The likelihoods of each observation can be computed using Equation 5.4 when the process data follow a Gaussian distribution.

$$P\left(\frac{X_j}{f_i}\right) = \frac{1}{\sqrt{2\pi\sigma_j^2}}\, exp\,\{-\frac{\left(y-\mu_j\right)^2}{2\sigma_j^2}\} \tag{5.4}$$

where y is a random observation. μ and σ denote the mean and standard deviation of a variable, respectively.

The posterior of each class is normalized by employing Equation 5.5.

$$P\left(\frac{f_i}{y}\right) = \frac{f_i}{\sum_{i=1}^{i=i} f_i} \tag{5.5}$$

In the application stage, Equations 5.3-5.5 are utilized to calculate the posterior of i number of fault classes. The fault class that has the highest normalized posterior is diagnosed as the observed fault class.

In essence, the NBC algorithm develops the classifier model in the following two steps:

Step 1: Class priors are estimated from the historical trained datasets.

Step 2: Process variables' mean and standard deviation are calculated for all classes.

When online samples come, the following three steps are utilized to classify the process state and diagnose the fault type.

Step 3: Likelihood probabilities, $P(X_j/f_i)$ are calculated using Equation 5.4.

Step 4: Posterior of each class, $P(f_i/X_j)$ is computed using Equation 5.3.

Step 5: Equation 5.5 is used to normalize the class posteriors. The class with the highest posterior is identified as the active class for an observation.

Let us consider a process system that has a total of two variables and three classes. Class 1, 2, and 3 imply the normal, fault 1, and fault 2, respectively. A total of 400 historical samples have been used to train the NBC model, where the number of samples from classes 1, 2, and 3 are 300, 50,

and 50, respectively. The mean and standard deviation of these variables from the trained samples are listed in Table 5.2.

Table 5.2: Mean and standard deviation of the variables for all classes.

Statistical Parameter	Variable		Class No.
	X1	X2	
Mean	40.001	33.311	Class 1
	200000.001	1.254	Class 2
	2.932	96.114	Class 3
Standard Deviation	0.112	0.307	Class 1
	0.002	4.028	Class 2
	10.318	14.063	Class 3

From the training dataset, P(Class 1) = 0.75, P(Class 2) = 0.125, and P(Class 3) = 0.125.

Let us consider a sample online observation, y = [9.62, 100]

$P(y=9.62/\text{Class 1})$ can be calculated using Equation 5.4 as follows,

$P(y=9.62/\text{Class 1}) = 1/(2*\pi*0.112^2)^{1/2} \exp\{-(9.62-40.001)^2/(2*0.112^2\} = 0$

Similarly, $P(y=9.62/\text{Class 2}) = 0$, $P(y=9.62/\text{Class 3}) = 0.031$, $P(y=100/\text{Class 1}) = 0$,

$P(y=100/\text{Class 2}) = 0$, and $P(y=100/\text{Class 3}) = 0.027$

$P(\text{Class 1}/y)$ can be calculated using Equation 5.3 as follows,

$P(\text{Class 1}/y) = P(y=9.62/\text{Class 1}) * P(y=100/\text{Class 1}) * P(\text{Class 1}) = 0*0*0.75 = 0$

Similarly, $P(\text{Class 2}/y)$ and $P(\text{Class 3}/y)$ can be obtained as 0 and $1.046*10^{-4}$, respectively.

Now, the normalized posterior probability for classes 1, 2, and 3 can be calculated as 0, 0, and 1, respectively, using Equation 5.5.

Since class 3 has the highest normalized posterior probability, the current process state based on the considered sample, y = [9.62, 100] can be distinguished as class 3.

5.2.2. Bayesian network (BN)

A BN is a directed acyclic graph (Heckerman et al., 1995). It is a powerful probabilistic tool that can be used to model complex interdependency among the process variables. A BN consists of both qualitative and quantitative parts (Neapolitan, 2004). There are four components in a BN: nodes, arcs, priors, and conditional probabilities. The nodes and arcs are the qualitative parts, while the priors and conditional probabilities are the quantitative parts of a BN. In the BNs, nodes are used to represent the process variables, and the arcs display the dependency among the variables. An arc is directed from a parent node to a child node (Bobbio et al., 2001). The priors express the anecdotal belief of the process variables, while the conditional probability shows the strength of the relationship between two connected variables. Each probability in a conditional probability table (CPT) is the state of a child node given that the state of its parent node(s). Both the data and knowledge uncertainty can be illustrated using the BN, which make it pertinent in the field of safety analysis.

5.2.3. Event Tree Analysis (ETA)

An ETA is a systematic method that is mostly used in the process industries for accident analysis. It is an inductive analysis technique that is utilized to reveal the event sequence given that the initiating event has occurred (Kalantarnia et al., 2009). It starts with a hazard or fault and ends with probable consequences. These consequences are called the end states. Safety barriers in an ET are placed chronologically. Therefore, it is termed as a sequential failure model (Adedigba et al., 2016a). An ETA clearly depicts how a fault can lead a process to failure by several paths, based on the success and failure of the functional or safety barriers. Although it is termed as a proactive risk analysis tool to identify and display a specific event sequence, it can be utilized for reactive

analysis as well, by using as a mean/tool for DRA. The occurrence probability of each path, $P(P_w)$ of an event tree can be calculated using Equation 5.6.

$$P(P_w) = \prod_{g \in SB_w} x_d^{\theta_{d,w}} (1 - x_d)^{1-\theta_{d,w}} \tag{5.6}$$

where *SB* denotes the safety or accident prevention barrier. *d* is the number of safety barriers available to prevent an accident, while *w* refers to the number of safety barriers associated with each path. *x* and θ are the failure probability of a barrier and severity level of the failure passes of safety barriers. $\theta_{d,w}$ takes a value of 0 when all the safety barriers work successfully. On the other hand, $\theta_{d,w}$ becomes 1 when all the safety barriers fail (Rathnayaka et al., 2011a).

5.3. Methodology

The proposed methodology (Figure 5.2) is comprised of the NBC, BN, and ETA. First, the current process state (i.e. faulty or normal) is assessed by the NBC. It generates the posterior probability for each class in each time-slice that is further utilized for fault diagnosis and predicting the process failure probability. The BN is used to estimate the failure probability of the safety barriers, and the ETA is used to model the failure paths. The quantitative dynamic failure analysis is conducted, utilizing the outputs from the NBC and BNs.

The model development stage is conducted in the offline mode, using the following six steps.

Step 1: Detail study on the faults associated with a process system is carried out. This can be done by the process simulator, as well as from expert judgment.

Step 2: Historical data for both the normal and identified fault conditions are collected. These data are labelled according to their class.

Step 3: The NBC is trained with the collected historical datasets. In this step, the prior probability of all the labelled classes is calculated. The mean and standard deviation of all the variables for all classes are also calculated to estimate the likelihoods.

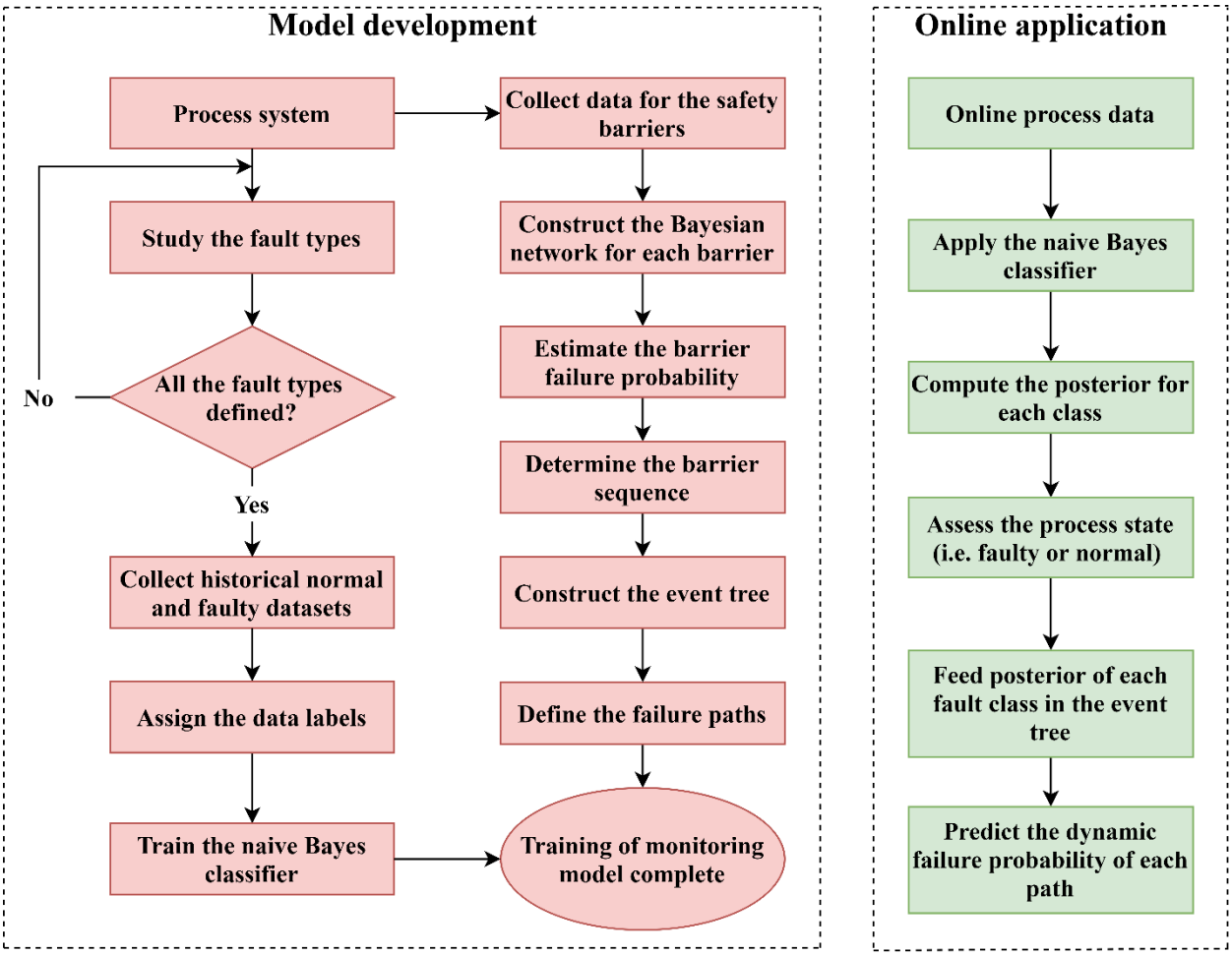

Figure 5.2: Flowchart of the proposed methodology.

Step 4: Safety barriers employed to prevent an accident for the studied process are identified, and failure data of the basic events for each safety barrier are gathered from the historical database, manufacturer-provided specifications, and expert opinion.

Step 5: The BNs for the safety barriers are constructed, and the failure probability of safety barriers are estimated. The principal advantage of using a BN in this context is that it can be updated based on the functionality of any element of a barrier. This enables the barriers to be designed with the

dynamic failure probabilities. A BN also considers the complex interdependency among the basic and intermediate events.

Step 6: The safety barriers' sequence is determined, and the ET is constructed. This gives the failure paths that a fault can exhibit. The end states are classified as the safe, near-miss, mishap, incident, accident, and catastrophe based on the potential of each path's impact on the plant, human health, and environment. Detail description of each end state with practical examples can be found in (Hashemi et al., 2014).

The online monitoring is done using the following three steps.

Step 7: Online process data is passed through the NBC. Equations 5.3-5.5 are used to determine the normalized posterior probability of each state. If the normal state has the highest posterior probability, the process is within the normal operating mode; otherwise, a fault is detected.

Step 8: Once a fault is detected, diagnosis is completed using the posterior distribution. The fault class that has the highest posterior probability is identified as the active fault type.

Step 9: The posterior probability of the diagnosed fault type is used as the initiating event's probability in the pathway realization model. This gives the predictive dynamic failure probability of each path in each sample due to the observed fault.

5.4. Applications of the Proposed Methodology

5.4.1. A Binary Distillation Column

A binary distillation column (Figure 5.3) is used to separate two distinct liquids by distillation. The distillation column model that has been utilized in this study consists of a total of 40 stages. It separates a mixture with a relative volatility of 1.5 into products of 96% purity. An equilibrium condition in all stages, a linearized liquid dynamic, no vapour holdup, and a total condensation

have been assumed. Besides, constant pressure and relative volatility have been considered while designing the distillation column unit (Skogestad, 1997). There are 82 states and 10 variables (6 inputs and 4 outputs) in the linearized dynamic model. Among these variables, three input variables: feed rate (F), feed composition (z_F), and boil up flowrate (V), and two output variables: top composition (x_D) and bottom composition (x_B) have been monitored in this study. Table 5.3 shows the considered fault types in the binary distillation column.

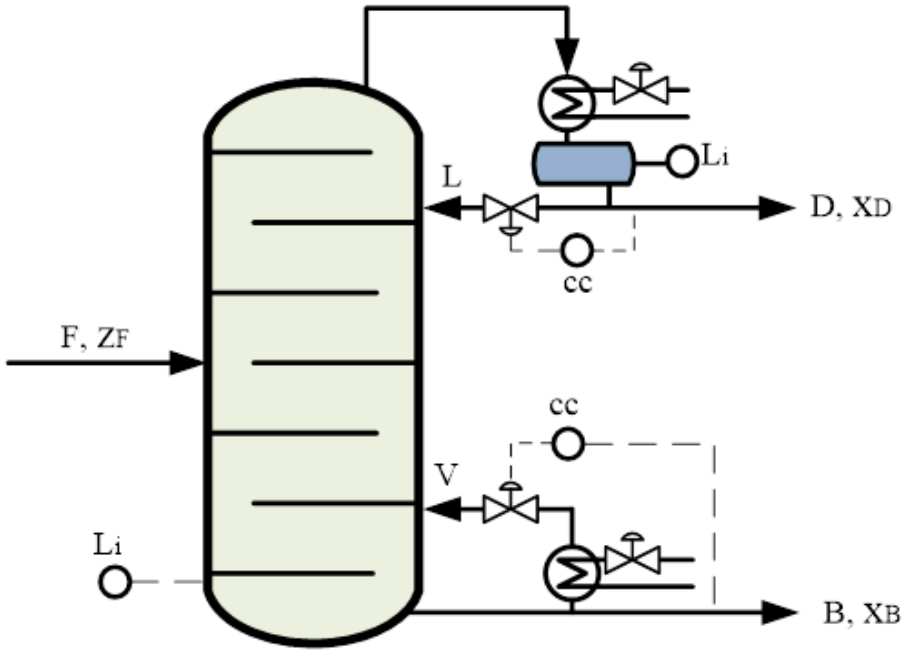

Figure 5.3: Schematic diagram of a binary distillation column (modified and redrawn from (Skogestad, 1997)).

Table 5.3: Fault descriptions in a binary distillation column.

Fault Scenario	Description
A1	10% sudden increase in feed rate
A2	Gradual increase in boil up flowrate

First, historical data for the normal operating zone, fault A1, and fault A2 are collected to train the NBC. Then, safety barriers are identified. The release prevention barrier (RPB), dispersion

prevention barrier (DPB), ignition prevention barrier (IPB), escalation prevention barrier (EPB), emergency management failure prevention barrier (EMFPB), human failure prevention barrier (HFPB), and organizational failure prevention barrier (OFPB) are adopted as the safety barriers, as these barriers are considered the major measures to prevent a fault being a failure. Detail description of these barriers is available in (Adedigba et al., 2016a; Rathnayaka et al., 2011a). The basic and intermediate events considered (Table 5.4) and their failure probabilities have been collected from (Adedigba et al., 2016a, 2016b; Amin et al., 2018c; Rathnayaka et al., 2011a).

Table 5.4: Event description and assigned probabilities for safety barriers.

Sl. No	Event description	Notation	Assigned probability
1	Operational error factors	ICE_1	Not applicable
2	Design error factors	ICE_2	Not applicable
3	Inspection error factors	ICE_3	Not applicable
4	Maintenance error factors	ICE_4	Not applicable
5	Physical barrier failure prevention factors	ICE_5	Not applicable
6	Natural factor	ICE_6	Not applicable
7	Process Upset	ICE_7	Not applicable
8	Operational error	ICE_8	Not applicable
9	Leak detection system failure	ICE_9	Not applicable
10	Monitoring Error	ICE_10	Not applicable
11	Improper maintenance procedure	ICE_11	Not applicable
12	Safety system barrier failure	ICE_12	Not applicable
13	Passive barrier failure	ICE_13	Not applicable
14	Isolation barrier failure	ICE_14	Not applicable
15	Ventilation system failure	ICE_15	Not applicable
16	Detection system failure	ICE_16	Not applicable
17	Automatic system failure	ICE_17	Not applicable
18	Manual system failure	ICE_18	Not applicable
19	Closing at point of inflow failure	ICE_19	Not applicable
20	Automatic emergency shutdown failure	ICE_20	Not applicable
21	Manual emergency shutdown failure	ICE_21	Not applicable
22	Emergency shutdown valve failure	ICE_22	Not applicable
23	Containment system failure	ICE_23	Not applicable
24	Inert system failure	ICE_24	Not applicable
25	Gas detection failure	ICE_25	Not applicable

26	Gas escalation mitigation failure	ICE_26	Not applicable
27	Emergency gas transfer system failure	ICE_27	Not applicable
28	Fire detection system failure	ICE_28	Not applicable
29	Automatic fire detection system failure	ICE_29	Not applicable
30	Manual fire detection system failure	ICE_30	Not applicable
31	Fire detection failure	ICE_31	Not applicable
32	Fire escalation barrier failure	ICE_32	Not applicable
33	Communication error factors	ICE_33	Not applicable
34	Management error factors	ICE_34	Not applicable
35	Knowledge error factors	ICE_35	Not applicable
36	Skill error factors	ICE_36	Not applicable
37	Hot work precaution barrier failure	ICE_37	Not applicable
38	Operator factors	ICE_38	Not applicable
39	Hot surface shielding barrier failure	ICE_39	Not applicable
40	Hot work failure factors	ICE_40	Not applicable
41	Inadvertent flame control system failure	ICE_41	Not applicable
42	Automatic inadvertent flame control system failure	ICE_42	Not applicable
43	Manual inadvertent flame control system failure	ICE_43	Not applicable
44	Unsuitable ambient temperature	BCE_1	2.50E-02
45	Difficulty in valve operation during start up	BCE_2	1.50E-02
46	Leaks in heat exchanger during start up	BCE_3	5.00E-02
47	Unknown disturbances	BCE_4	1.50E-03
48	Job carried without permission	BCE_5	1.00E-02
49	Inexperience	BCE_6	1.00E-02
50	External supervision failure	BCE_7	8.30E-02
51	Wrong procedure	BCE_8	5.00E-03
52	Insufficient instrument to measure process conditions	BCE_9	1.00E-03
53	High mechanical stress	BCE_10	1.00E-02
54	Poor quality of the construction materials	BCE_11	1.00E-02
55	Long delay in inspection interval	BCE_12	5.00E-02
56	Failure to detect a leak	BCE_13	5.00E-02
57	Failed to detect a minor release	BCE_14	5.00E-02
58	Inadequate training to the inspector for a detection	BCE_15	2.50E-02
59	Inadequate method required for a detection	BCE_16	9.00E-02
60	Material degradation monitoring failed	BCE_17	6.60E-02
61	Material degradation monitoring was not performed	BCE_18	5.00E-02
62	Physical barrier not available	BCE_19	1.00E-02
63	Higher external load	BCE_20	1.00E-02

64	Earthquake	BCE_21	5.00E-03
65	Harsh weather	BCE_22	4.50E-04
66	Long delay in response	BCE_23	1.00E-02
67	Emergency shutdown controller failure	BCE_24	2.50E-01
68	Emergency shutdown sensor failure	BCE_25	2.40E-02
69	Long delay in operator response	BCE_26	1.00E-02
70	Operator awareness failure	BCE_27	4.00E-02
71	Operator response failure	BCE_28	5.00E-02
72	Delayed operation	BCE_29	5.00E-02
73	Valve failed to close on demand	BCE_30	1.30E-01
74	Inert unavailable	BCE_31	5.00E-02
75	Inadequate inert	BCE_32	8.00E-02
76	Drainage not available	BCE_33	1.00E-03
77	Inadequate performance of the passive barrier	BCE_34	1.00E-03
78	Gas detection sensor failure	BCE_35	1.28E-01
79	Gas detection controller failure	BCE_36	1.00E-03
80	Gas detection alarm failure	BCE_37	2.00E-02
81	Detector malfunction	BCE_38	2.20E-04
82	Manual detection or minor release failure	BCE_39	5.00E-02
83	Manual inspection not performed	BCE_40	5.00E-02
84	Inadequate ventilation	BCE_41	6.70E-02
85	Forced dilution failure	BCE_42	4.00E-02
86	Manual closing at release point failure	BCE_43	2.50E-02
87	Inflow valve inaccessible	BCE_44	5.00E-02
88	Inadequate blowdown	BCE_45	1.00E-03
89	Inadequate scrubbers	BCE_46	8.00E-03
90	Fire detection sensor failure	BCE_47	8.00E-02
91	Fire detection controller failure	BCE_48	1.00E-03
92	Fire alarm failure	BCE_49	2.10E-02
93	Inadequate detector coverage	BCE_50	2.00E-01
94	Operator unaware of fire	BCE_51	5.00E-02
95	Operator unable to activate manual alarm	BCE_52	1.00E-03
96	Manual alarm button failure	BCE_53	1.11E-03
97	Sprinkler not available	BCE_54	1.00E-02
98	Sprinkler insufficient	BCE_55	4.00E-02
99	Sprinkler failure	BCE_56	4.50E-02
100	Inadequate firefighting equipment	BCE_57	2.00E-02
101	Site not aware of fire	BCE_58	1.10E-03
102	Alarm not audible	BCE_59	4.30E-03

103	Route not clear to follow	BCE_60	1.00E-04
104	Insufficient instrument to reach operators	BCE_61	2.00E-05
105	Poor management practice	BCE_62	2.50E-02
106	Insufficient funding behind safety	BCE_63	3.00E-04
107	Poor safety culture	BCE_64	1.00E-03
108	Insufficient evacuation resources	BCE_65	1.40E-02
109	Insufficient knowledge of emergency situation	BCE_66	5.00E-03
110	Inadequate safety drill	BCE_67	2.90E-03
111	Lack of operational skill	BCE_68	2.50E-04
112	Lack of awareness	BCE_69	1.80E-04
113	Failure to follow work permit	BCE_70	4.00E-02
114	Wrong work permit	BCE_71	4.50E-02
115	Operation without work permit	BCE_72	1.00E-02
116	Shielding unavailable	BCE_73	6.70E-03
117	Shielding failure	BCE_74	1.00E-02
118	Hot work permission not issued	BCE_75	3.30E-02
119	Improper guidelines	BCE_76	6.70E-02
120	Risk assessment was not performed	BCE_77	1.00E-01
121	Insulation failure	BCE_78	1.00E-02
122	Flame detector failure	BCE_79	5.60E-02
123	Flame detector unavailable	BCE_80	5.00E-02
124	Insufficient flame detectors	BCE_81	7.00E-02
125	Manually undetected	BCE_82	5.00E-02

The BNs for these safety barriers are shown in Figures 5.4-5.10. The safety barrier failure probabilities estimated through the BNs are listed in Table 5.5. The next step is to develop the logical failure paths. These failure paths have been identified using the ETA (Figure 5.11). It should be noted that S and F mean success and failure of a safety barrier, respectively. It can be seen that a fault can lead a process to 24 types of consequences, based on the performance of the safety barriers. C14, C16, C17, C19, and C21 are the paths that may lead a fault to an accident, while C18, C20, C22, C23, and C24 are the paths that represent the catastrophic accident.

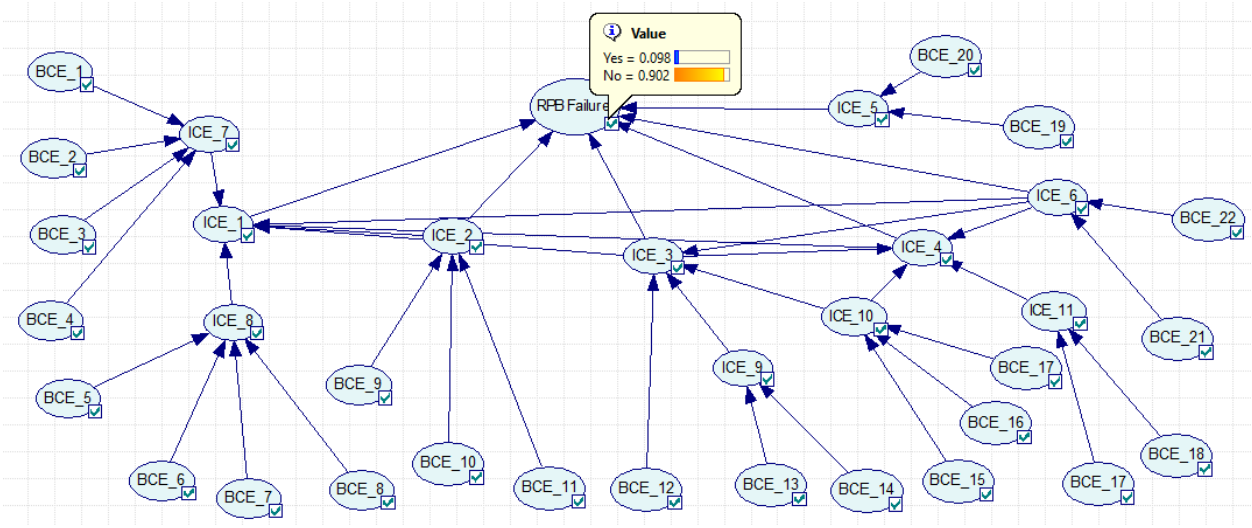

Figure 5.4: BN for the RPB.

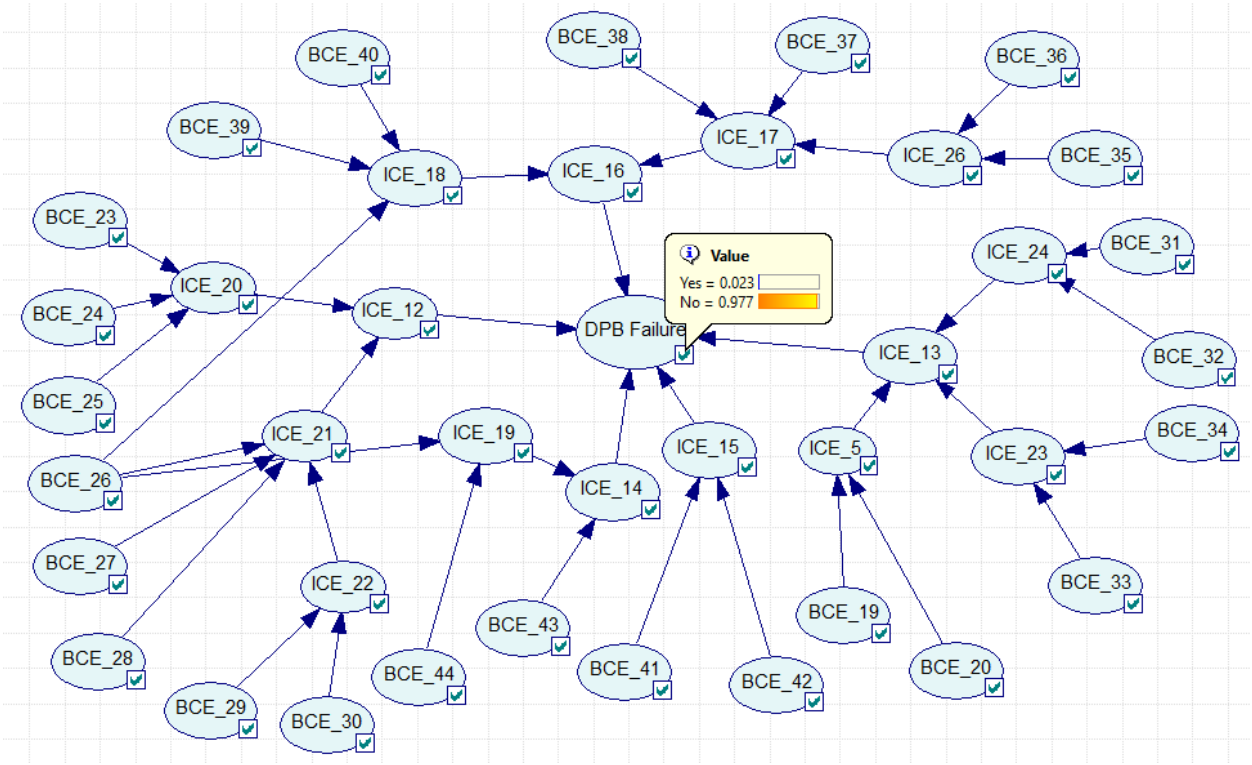

Figure 5.5: BN for the DPB.

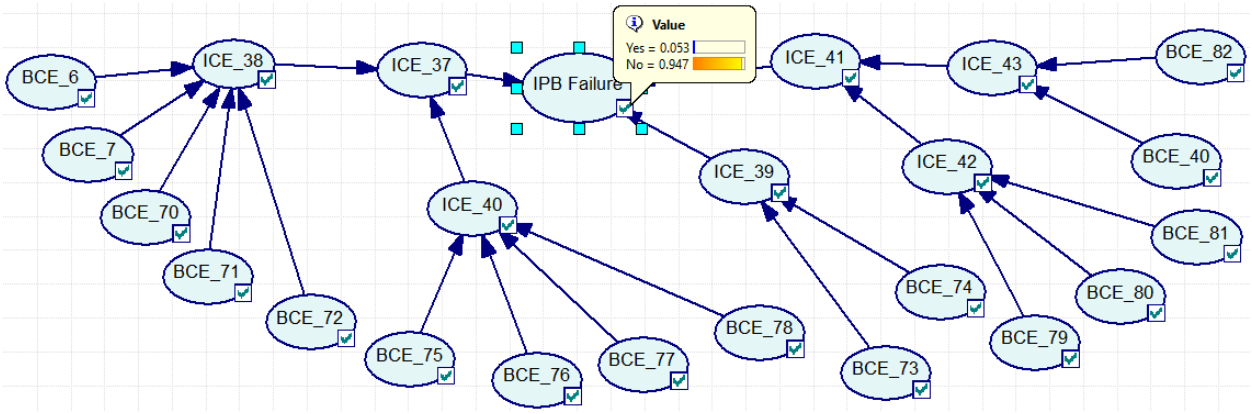

Figure 5.6: BN for the IPB.

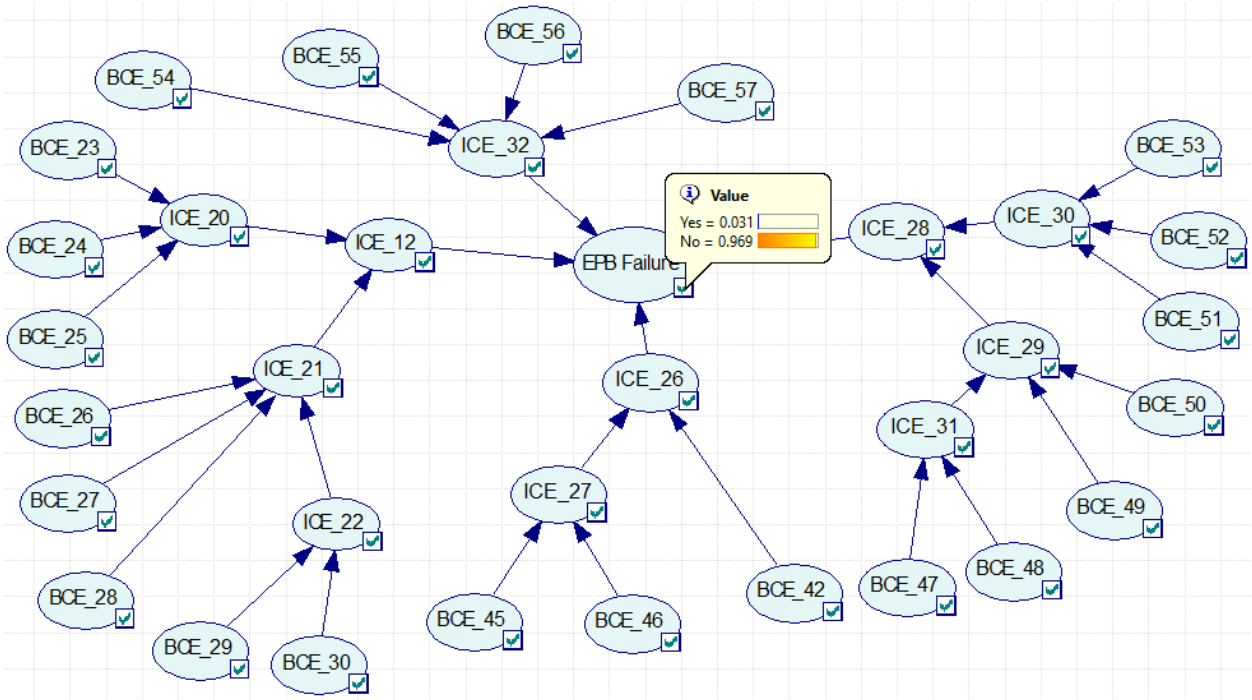

Figure 5.7: BN for the EPB.

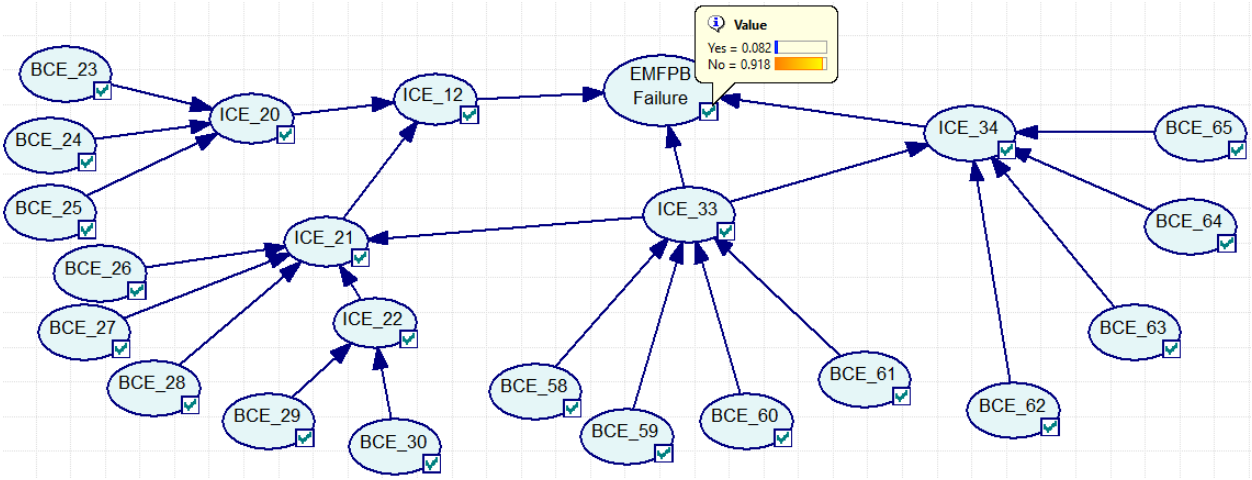

Figure 5.8: BN for the EMFPB.

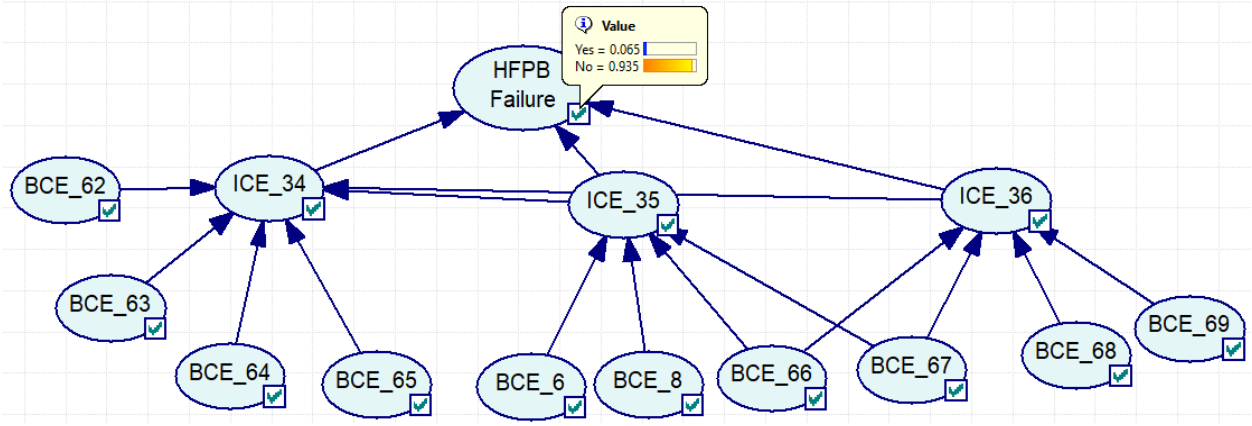

Figure 5.9: BN for the HFPB.

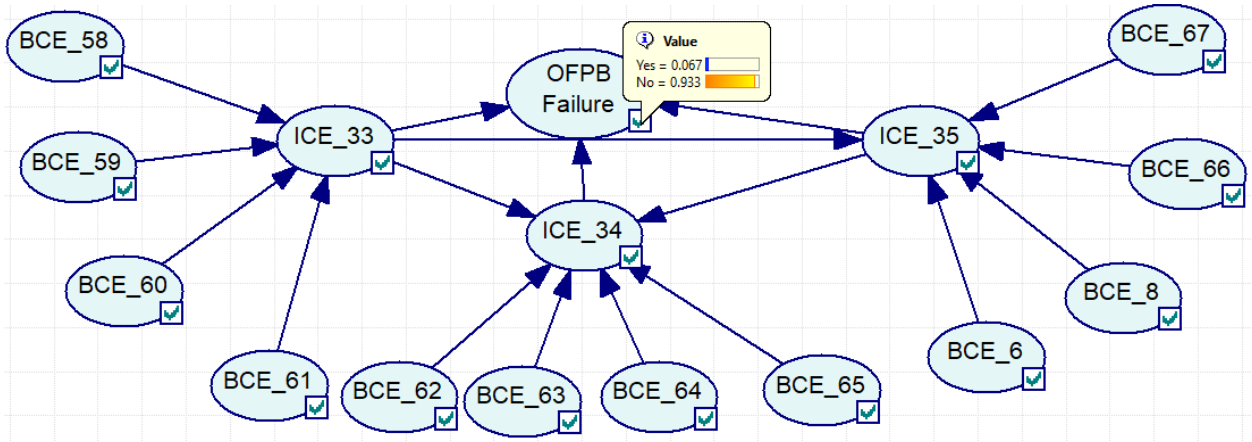

Figure 5.10: BN for the OFPB.

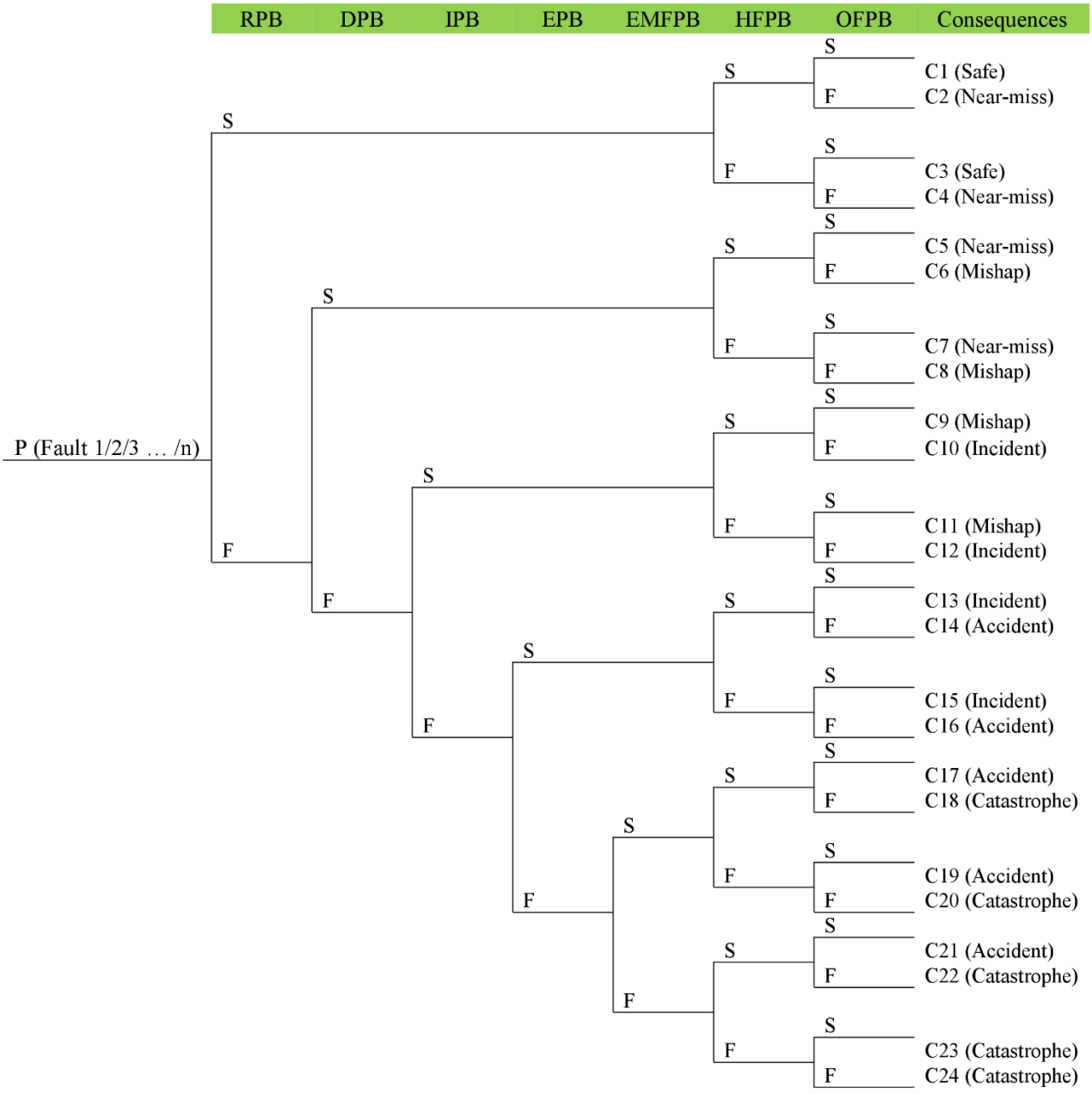

Figure 5.11: Pathway realization of a fault to failure.

Table 5.5: Failure probability of the safety barriers.

Sl. No	Name of the barrier	Notation	Failure probability
1	Release prevention barrier	RPB	0.0979
2	Dispersion prevention barrier	DPB	0.0227
3	Ignition prevention barrier	IPB	0.0530
4	Escalation prevention barrier	EPB	0.0306
5	Emergency management failure prevention barrier	EMFPB	0.0824
6	Human failure prevention barrier	HFPB	0.0646
7	Organizational failure prevention barrier	OFPB	0.0668

The results of process monitoring by the NBC in a distillation column are shown in Figure 5.12 for two fault cases, mentioned in Table 5.3. In both cases, the fault has been initiated from the 401^{st} sample. The NBC can accurately classify the normal condition for all the test samples. It takes only 1 sample to detect the fault A1. As this fault causes an increase in input feed rate, it affects the top and bottom compositions. Although the posterior probability of fault A1 shows some jittering from 402-450 samples, it remains close to 1 for the remaining test samples. On the contrary, the NBC can detect the fault A2 at the 406^{th} sample, as the posterior probability takes a value of 0.9947. A gradual increase in boil up flowrate may increase the vapour flowrate, which eventually may end up with increased pressure in the distillation column and off graded product.

The posteriors are fed into the failure pathway realization model in each time-slice; this gives the dynamic failure probability of a process system due to a fault. Although the pathway analysis model gives 24 possible outcomes, the catastrophic accident analysis consequences are presented in Figure 5.13. Figure 5.13(A) shows the prognosis results when fault A1 is activated after the 400^{th} sample. It can be seen that the probability of a catastrophic accident remains significantly lower when the process is in a normal state; however, it gets a sharp jump as soon as the fault is detected and reaches a level of 10^{-7} from 10^{-12}, which is a significant rise. In case of the dynamic failure profile due to fault A2 (Figure 5.13(B)), a sudden rise is reasonably observed at the 406^{th}

sample, which stays remarkably higher since the fault goes uncorrected. The probability also reaches a level of 10^{-7}; it indicates that the process needs to be undergone corrective actions to minimize the risk.

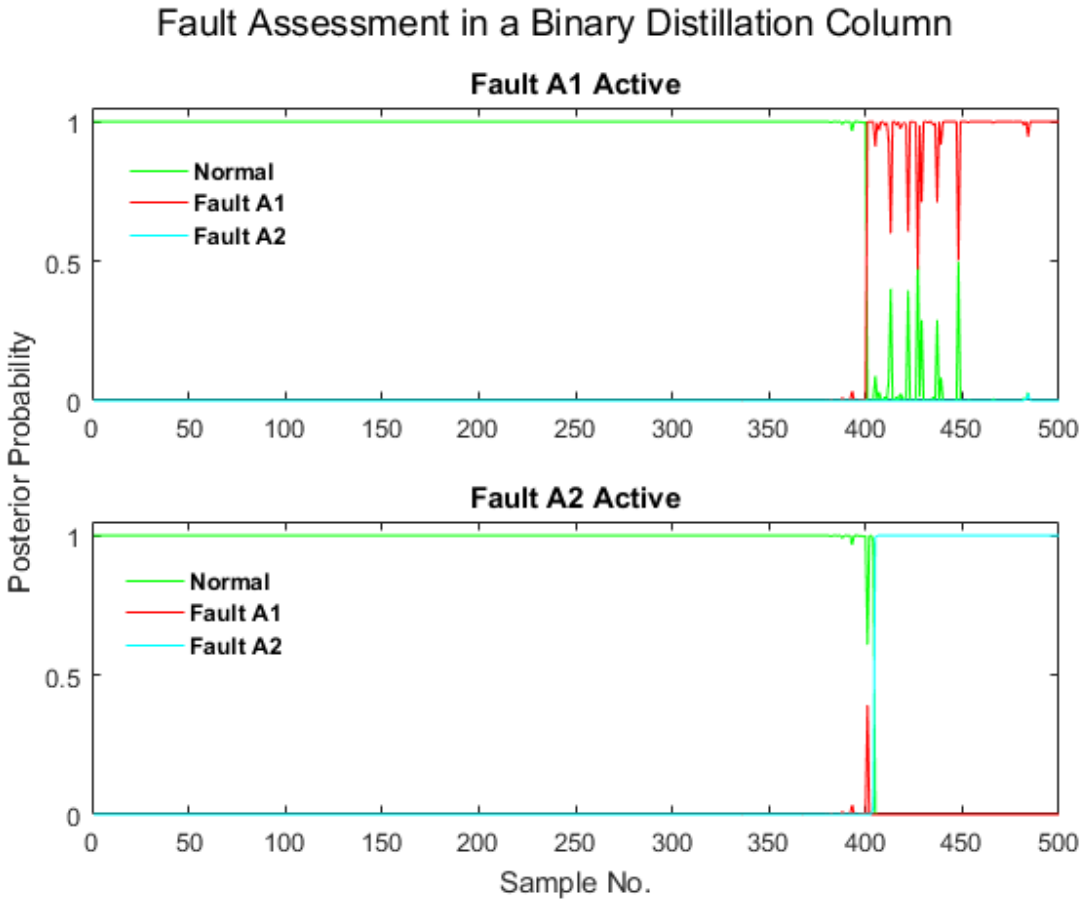

Figure 5.12: Fault assessment in a binary distillation column using an NBC.

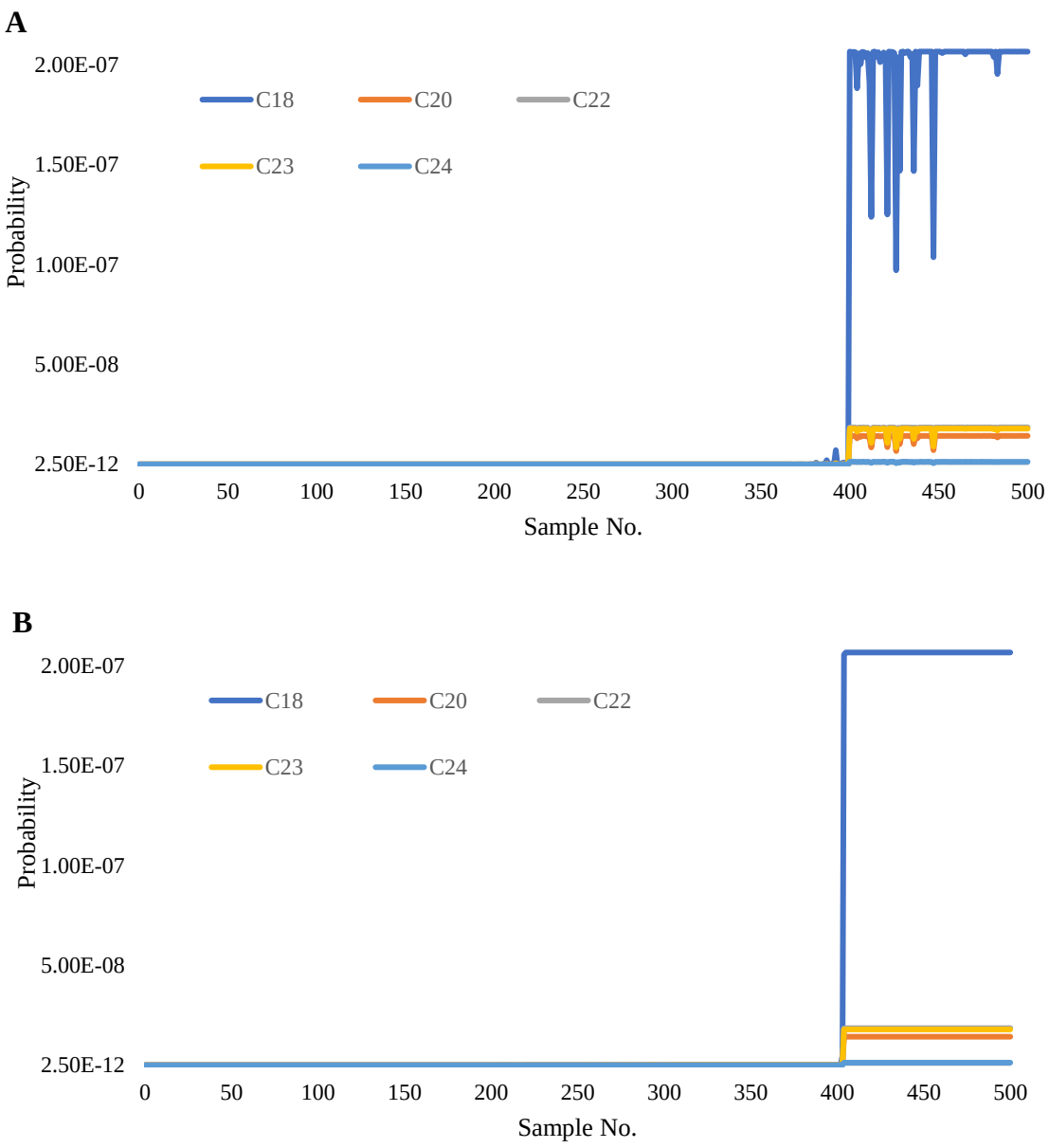

Figure 5.13: Prognosis of catastrophic accidents for (A) fault A1 and (B) fault A2.

5.4.2. The RT 580 Experimental Setup

The RT 580 fault-finding control system (Figure 5.14) has three circuits to control three commonly used process variables: level, flowrate, and temperature. A circuit consisting of a pump (P1), collecting tank (B1), and process tank (B2) is used for control of level and flowrate. There are four temperature sensors (TIR 01, TIR 02, TIR 03, and TIR 04) to measure the temperature of different

places in this circuit. There are three other sensors as well to measure the level, pressure, and flowrate. A pneumatic control valve, V7 works as an actuator. Additionally, the outlet of the tank has a valve that is used to generate disturbances that help to generate noisy data.

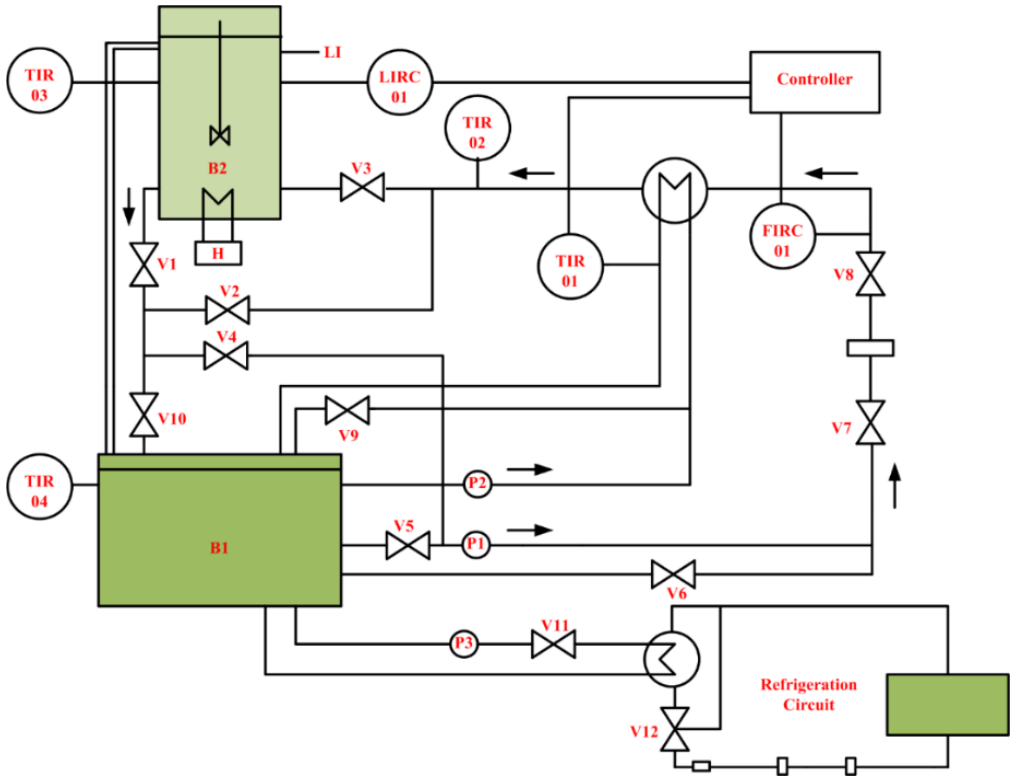

Figure 5.14: Schematic diagram of the RT 580 experimental setup (modified from (Ghosh et al., 2019)).

The temperature is controlled by two circuits. A refrigeration system cools the water in the collecting tank. A pump, P3 circulates the water via a heat exchanger (cooling circuit). A heater, H heats the water in the process tank. Another pump, P2 also circulates the warm water via the heat exchanger. In the heat exchanger, the water in the cooling circuit is heated. The controlled variable is the water temperature in the cooling circuit after heating in the heat exchanger. The actuator is the pneumatic control valve that adjusts the flowrate of the warm water.

This setup enables introducing the faults by pressing the fault switches. Two faults have been considered in this study, as shown in Table 5.6.

Table 5.6: Fault descriptions in the RT 580 experimental setup.

Fault Scenario	Description
B1	The wire to the pressure sensor of the process tank is broken
B2	V7 malfunction

The NBC is first trained with historical normal and faulty datasets. To have a good control performance, all the experiments were conducted considering the proportional-action range, integral-action time, and derivative-action time as 42, 11 s, and 0 s, respectively (Ghosh et al., 2019). The failure pathway realization model, displayed in Figure 5.11, is also used here. However, it is noteworthy to mention that the qualitative structure and quantitative outcomes of each path may vary for different process systems.

Both the test scenarios consist of 350 samples, and fault has been introduced from the 264^{th} sample using the fault switches for the specific fault types. Figure 5.15 shows the fault assessment results. It can be seen that the posterior probabilities for fault B1 and B2 remain close to zero till 263 samples. However, as soon as the faults are introduced, the posterior probability of the normal state comes down near to zero; it indicates that the process is in a faulty operating condition. Then, the posterior probability of each class is used to diagnose the fault type. When fault B1 is activated at the 264^{th} sample (fault scenario B1), the posterior of the corresponding fault class takes a value of near 1; hence, it can be concluded that fault B1 is the abnormality that has affected the process. Similarly, fault B2 is diagnosed as the observed abnormal phenomenon in the case of fault scenario B2. Finally, the generated posterior probability by the NBC, along with the safety barrier failure probabilities, is provided in the pathway realization model to predict the dynamic failure probabilities.

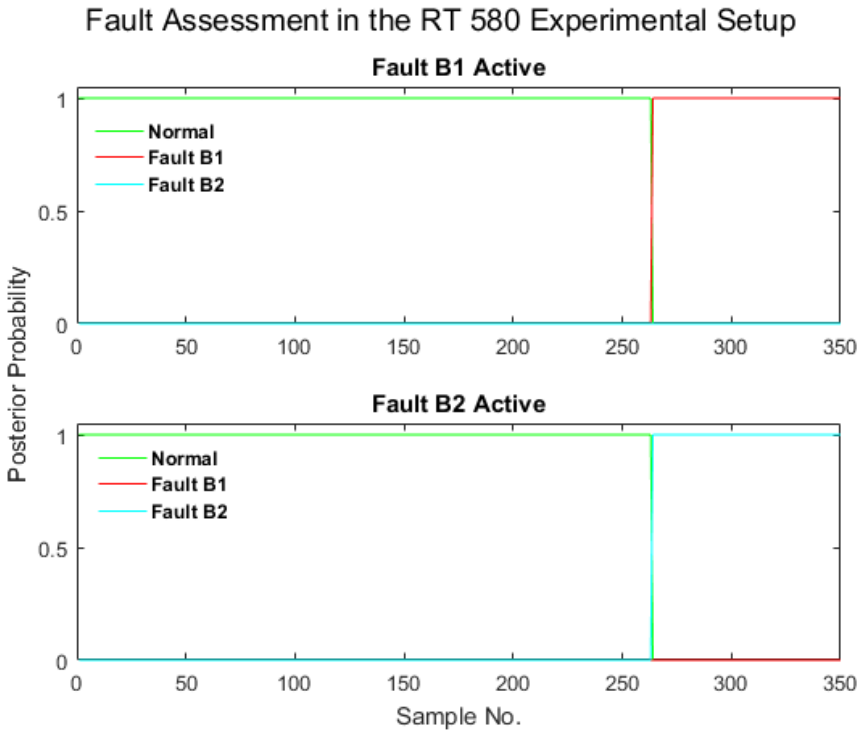

Figure 5.15: Fault assessment in the RT 580 experimental setup using an NBC.

The dynamic probabilities of catastrophic accident causation paths are shown in Figure 5.16. It is observed that the probability of catastrophic accidents rises to a level of 10^{-7} once the fault is detected, in case of the fault B1 (Figure 5.16(A)). As the sensor that takes the pressure reading in the process tank was working perfectly, the failure probability in the normal operating region remains close to zero. When fault B1 is activated, the controller takes the control action based on the observed value in the process tank, which is set at a significantly higher number. Hence, the flowrate is reduced, which eventually leads the tank to a dry-out condition.

On the contrary, the magnitude of catastrophic accidents gets an increase to an order of 10^{-19} from the initial level, when fault B2 is detected (Figure 5.16(B)). In the RT 580 setup, V7 works as an actuator which has a significant impact on the water flowrate and level in the process tank. As this valve starts malfunctioning in fault scenario B2, the flowrate in the level control circuit gets upset, which also affects the level in the process tank. As a consequence, the tank becomes empty (Figure

5.17) at the 279th sample. However, the proposed methodology can predict a higher failure risk quantitatively at the 264th sample by using the prognostic analysis.

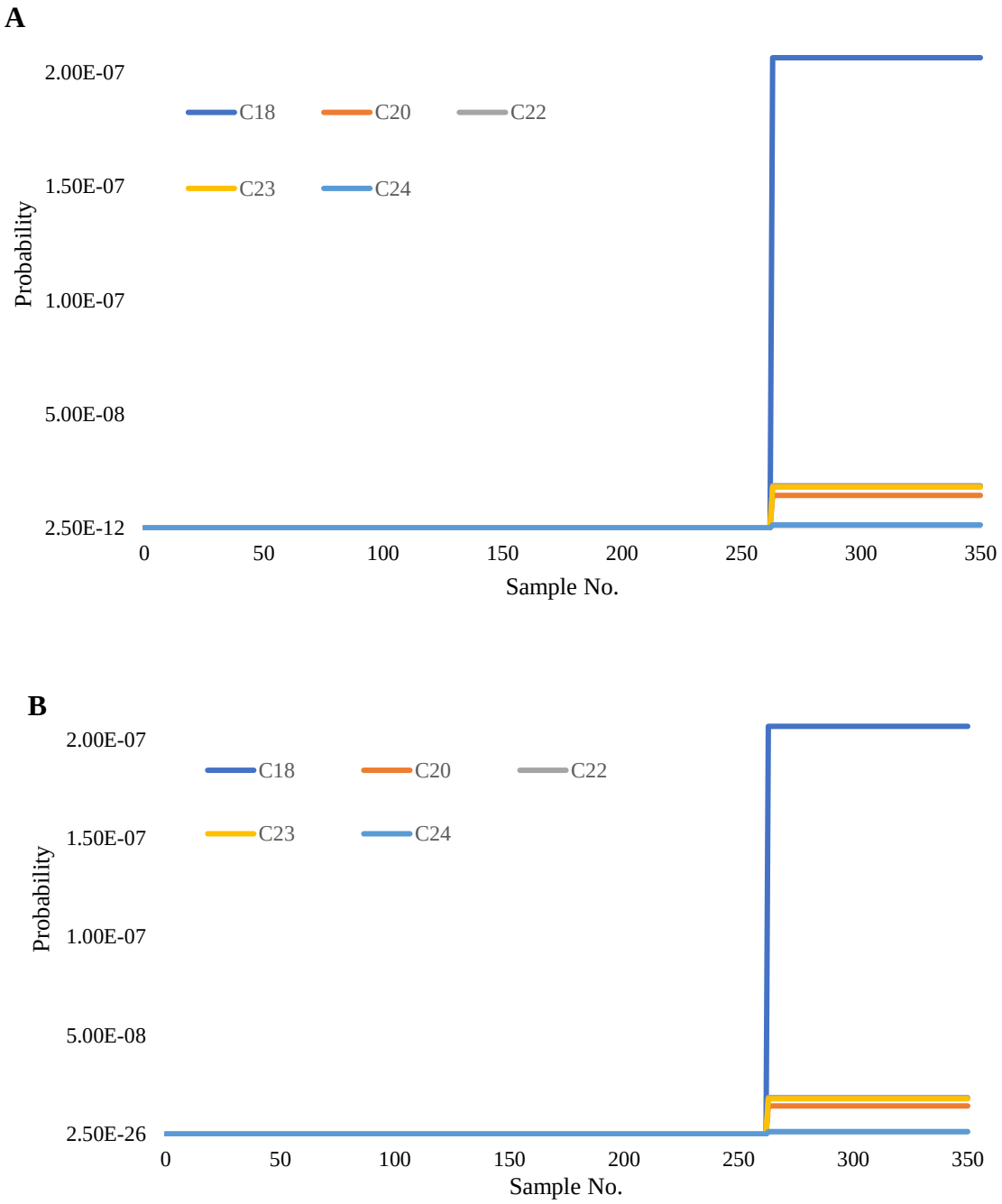

Figure 5.16: Prognosis of catastrophic accidents for (A) fault B1 and (B) fault B2.

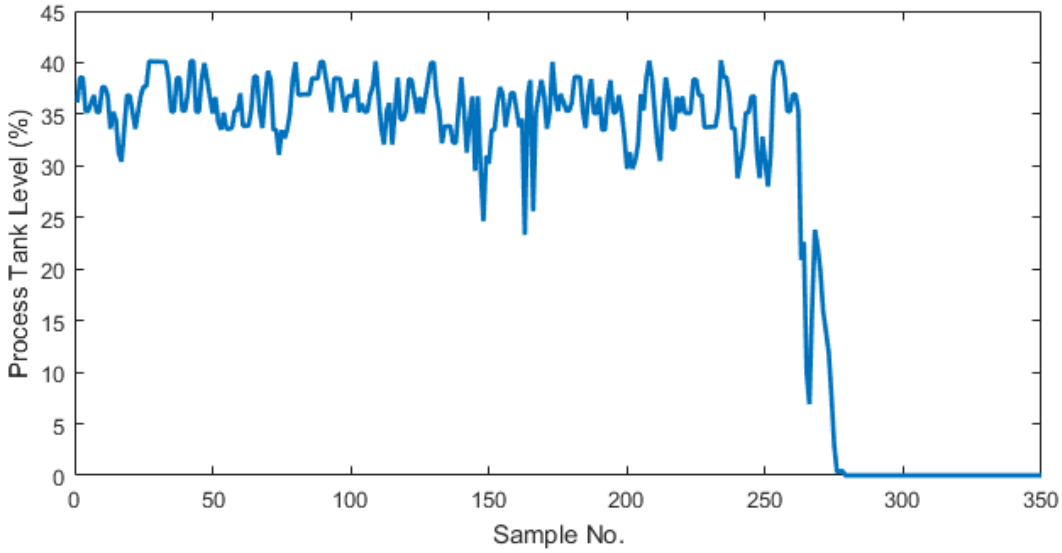

Figure 5.17: Water level in the process tank (%) for fault scenario B2.

5.5. Conclusion

This study demonstrates an NBC, BN, and ETA-based fault assessment and failure prognosis technique. Unlike the existing methods for DRA discussed in Section 5.1, the proposed methodology generates a multivariate probabilistic index to assess the process health, which is further utilized to predict the dynamic failure probability of a process system, based on the sequential success and failure of the applied safety barriers to prevent an unwanted event. The robust capacity of the BN to model complex relationships among the failure causation factors has been utilized to estimate the performance of the safety barriers. A total of two process systems: a binary distillation column and an experimental setup, the RT 580 fault-finding control system have been utilized to display the effective application of the developed framework.

The major contribution of this work is that it introduces a novel data-driven methodology for dynamic risk assessment, which includes monitoring the process by using a data-based multivariate process monitoring tool and predicting the dynamic failure frequency by utilizing a logical failure model. The proposed concept will contribute significantly to designing the next-

generation DRA tools and act as a pivotal concept in the predictive safety analysis. The developed NBC-BN-ETA-based framework is easier to construct, yet, it can provide robust performance.

Although the PCA, the KF, and the SOM-based frameworks have been successfully used for simultaneous fault detection and dynamic risk assessment, these methods have not either provided any solution to fault diagnosis or relied on individual variable's fault probability from the dynamic loadings for generating the overall system risk profile. Furthermore, the PCA and KF-based methods do not display any analysis on how a fault can turn into a failure. On the contrary, the proposed method can detect the fault and accurately diagnose the active fault type, which is a desired feature of an FDD tool. Besides, it can predict the real-time failure risk, utilizing the posterior probability of a fault class that has been generated in a multivariate manner. Hence, it eliminates the necessity to calculate the probability of a fault for each variable to estimate the process system risk.

The NBC assumes that all the features are conditionally independent of each other, which may not be the case in many industrial applications. This can affect the classification accuracy. The advanced versions of the NBC, such as the TAN and semi-naïve Bayesian classifier (SNBC) can aid in this context. A sequential logical failure model, the ETA has been utilized for failure prognosis. However, a fault can lead a process to failure by adopting a non-sequential path. A BN can be used to capture the non-sequential failure paths. The copula functions can also be added to the BNs to handle the nonlinear dependence among the barrier failure causation factors. Finally, the loss functions can be used to quantify the severity of the consequences and predict the dynamic process risk in a financial term. These will be promising venues to improve the present work significantly.

Chapter 6: Risk-based Fault Detection and Diagnosis for nonlinear and non-Gaussian Process Systems using R-vine Copula

Preface

A version of this chapter has been published in the ***Process Safety and Environmental Protection*** journal. I am the primary author, along with the co-authors, Drs. Faisal Khan, Salim Ahmed, and Syed Imtiaz. I developed the conceptual framework for this risk-based FDD model and carried out the literature review. I prepared the first draft of the manuscript and subsequently revised the manuscript based on the co-authors' and peer review feedback. Co-author Dr. Faisal Khan helped in the concept development and testing the model, reviewing, and revising the manuscript. Co-authors Drs. Syed Imtiaz and Salim Ahmed provided support in implementing the concept and testing the model. The co-authors provided fundamental assistance in validating, reviewing, and correcting the model and results. The co-authors also contributed to the review and revision of the manuscript.

Reference: Amin, M. T., Khan, F., Ahmed, S., & Imtiaz, S. (2021). Risk-based fault detection and diagnosis for nonlinear and non-Gaussian process systems using R-vine copula. Process Safety and Environmental Protection, 150, 123-136. https://doi.org/10.1016/j.psep.2021.04.010

Abstract

This chapter presents a risk-based fault detection and diagnosis methodology for nonlinear and non-Gaussian process systems using the R-vine copula and the event tree. The R-vine model provides a multivariate probability that is used in the event tree to generate a dynamic risk profile. An abnormal situation is detected from the monitored risk profile; subsequently, root cause(s) diagnosis is carried out. A fault diagnosis module is also proposed using the density quantiles, developed from marginal probabilities. The performance of this methodology is benchmarked using the Tennessee Eastman chemical process. The proposed risk-based framework has also been applied to an experimental setup and a real industrial isomer separator unit. The diagnosis module is found sensitive to both single and simultaneous faults. The results confirm that the proposed methodology provides better performance than the conventional principal component analysis and transfer entropy-based fault diagnosis techniques using the advantage of marginal density quantile analysis.

Keywords: *Process safety, risk assessment, process monitoring, fault diagnosis, R-vine copula*.

6.1. Introduction

Fault detection and diagnosis (FDD) has paramount significance in ensuring process safety. In the process industries, data-based multivariate FDD tools such as the principal component analysis (PCA), independent component analysis (ICA), and their derivatives found widespread use due to their ease with implementation and reliable performance (Kresta et al., 1991; Lee et al., 2007, 2004b; Wise et al., 1988). PCA provides the best performance when process data follow the Gaussian distribution. On the contrary, ICA is efficient in capturing non-Gaussian features. However, both these tools are not optimal for nonlinear datasets. Therefore, kernel-based derivatives of PCA and ICA are often used to handle nonlinearity (Lee et al., 2007, 2004a).

Even though these tools can provide early fault detection, their root cause diagnosis is not precise (Li et al., 2016; Vedam and Venkatasubramanian, 1999). Also, these multivariate FDD tools do not provide any indication of associated risk of the fault, which is highly desirable from safety analysis perspective. More recently, a risk-based multivariate fault detection methodology has been proposed by Zadakbar et al. (2012). The major advantage of this concept is the ability to calculate and visualize dynamic risk profile from continuous process data along with early fault detection. The PCA was used to monitor the process, and the risk profile was developed from the principal components (PCs). This method uses a dedicated control chart for each PC. Therefore, it requires monitoring several control charts depending on the number of selected PCs to build the PCA model. Additionally, it does not provide any solution for fault diagnosis.

In order to improve diagnosis of fault, Yu et al. (2015) proposed a self-organizing map (SOM)-based fault detection and dynamic risk assessment (DRA) framework. The event tree was used to display the failure paths, and the fault probability from the loading matrix was used to update the event tree. The SOM is applicable to both nonlinear and non-Gaussian datasets. It utilized the

Gaussian cumulative density functions (CDFs) for fault probability estimation. The diagnosis report was developed from each variable's dynamic loading, which may be inaccurate since the symptoms often show earlier responses compared to the root cause.

Amin et al. (2020) proposed a methodology that used the naïve Bayes classifier (NBC) and event tree for FDD and DRA, respectively. The event tree describes pathways that show how a fault propagates to an accident. The probability of occurrence of each pathway is highly significant to safety practitioners to minimize risk. The use of NBC enabled development of the risk profile in a multivariate manner; thus, it could eliminate the use of several control charts as in the PCA-based method. Nonetheless, the NBC is a supervised learning technique, and it requires an extensive amount of data and detailed information about available faults in a process. It may not provide a robust performance to unknown fault types.

The vine copula-based methods can provide a viable solution to generate multivariate probability in an unsupervised manner by using density quantile analysis (DQA). The nonlinear and non-Gaussian dependence structure can be captured utilizing the copula functions. Ren et al. (2015) proposed a novel C-vine copula-based process monitoring model. However, the C-vine model cannot maximize the correlation structure due to its innate decomposition technique (i.e. C-vine copula uses a star structure). The R-vine model can provide a better description of the correlation structure, as it can be of any form (i.e. star and linear) (Zhou and Li, 2018). Most vine-based methods perform the DQA on the joint probability density functions (JPDFs) for fault detection. Nevertheless, the DQA can also be performed on the marginal densities to accurately identify the variables that have deviated from the normal operating regime, and this analysis can be used for fault diagnosis.

The current work proposes an unsupervised FDD method using the R-vine copula model. The developed framework has been applied to the Tennessee Eastman (TE) chemical process and an experimental tank heater system at Memorial University. It has also been tested on a dataset collected from an isomer separator unit of a petroleum refinery. The results suggest that the proposed method can outperform the existing fault diagnosis techniques such as the PCA and transfer entropy. The contributions of this work are:

I. An unsupervised risk-based FDD technique for nonlinear and non-Gaussian processes using R-vine copula.
II. A DQA-based method applied to marginal distributions for fault diagnosis.
III. Diagnosing process faults from observed risk profile.

The remainder of this chapter is organized as follows: Section 6.2 briefly discusses the R-vine copula. Section 6.3 describes the different modules of this framework. Applications of the proposed framework to three process systems are presented in Section 6.4. Finally, Section 6.5 contains the concluding remarks, limitations, and future work scopes.

6.2. R-vine Copula

Copula functions are widely utilized to estimate the correlation among variables. These can also be used to measure the joint probability density function (JPDF) and are comprised of a marginal distribution function and a uniform distribution (Sklar, 1959). Let us consider a random vector $X = [x_1, x_2, \ldots, x_m]$ that contains m number of random variables. According to Sklar's theorem, there exists a copula function, C, such that,

$$F(x_1, x_2, \ldots, x_m) = C(F_1(x_1), F_2(x_2), \ldots, F_m(x_m)) \tag{6.1}$$

where F is the joint cumulative density function of X, and $F_i(x_i)$ is the marginal CDF of any random variable that can be estimated, as stated in Equation 6.2.

$$F_i(x_i) = \int_0^{x_i} f_i(t)dt \tag{6.2}$$

where $f_i(x_i)$ is the marginal probability density function (PDF) of x_i, and i = 1, 2, 3, …, m is the number of random variables.

The JPDF consists of two distinct spaces: univariate marginal probability density space and copula density region. The mathematical formulation of JPDF is shown in Equation 6.3.

$$f(x_1, x_2, \dots, x_m) = c(F_1(x_1), F_2(x_2), \dots, F_m(x_m)) \prod_{i=1}^{m} f_i(x_i) \tag{6.3}$$

where f is the joint probability density function of X, and c is the copula probability density function; it is defined as shown in Equation 6.4 (Wan and Li, 2019):

$$c(F_1(x_1), F_2(x_2), \dots, F_m(x_m)) = \frac{\partial^m C(F_1(x_1), F_2(x_2), \dots, F_m(x_m))}{\partial F_1(x_1), \partial F_2(x_2), \dots, \partial m(x_m)} \tag{6.4}$$

The PDFs and CDFs can be estimated from the appropriate probability distribution. Utilizing CDFs, the copula type and associated parameters are obtained. The Akaike information criterion (AIC) (Akaike, 1974) and the Bayesian information criterion (BIC) (Schwarz, 1978) are used to find the best-suited model among a set of candidate models (i.e. distribution or bivariate copula function). The AIC and BIC values can be computed by Equations 6.5 and 6.6, respectively.

$$AIC = 2K - 2\,ln(L) \tag{6.5}$$

where K and L are the number of parameters and the maximum value of the likelihood function, respectively.

$$BIC = Kln(n) - 2\,ln(L) \tag{6.6}$$

where n is the number of data points in a given sample space for a candidate model.

The application of bivariate copulas becomes remarkably difficult when data dimension is significantly higher. To address this issue, Joe (1996) proposed a vine copula model that could capture correlation among high dimensional data while preserving their tail correlation, asymmetry, and conditional correlation. It decomposes a multivariate copula into several bivariate copulas. An m dimensional vine copula consists of $m-1$ trees and $\frac{m(m-1)}{2}$ edges.

The vine model introduced by Joe (1996) used a sequential decomposition technique, which is familiarly known as the D-vine copula. Later, several vine models were proposed. Among them, the C-vine and R-vine models are noteworthy in the context of process monitoring (Ren et al., 2015; Zhou and Li, 2018). The C-vine model utilizes a star structure, while the R-vine is independent of any particular structure. Figure 6.1 shows an illustrative example of these three vine models for a four-dimensional case. There are four nodes, and any two nodes are connected by an edge, *E* (e.g. 1,2 for connecting node 1 and node 2). The C-vine model uses a root node (i.e. the node that shares edges with all other nodes), and the D-vine model places the nodes sequentially. On the other hand, the R-vine utilizes both the star and sequential structures and therefore, provides a better estimate of the correlation structure.

The JPDF of an R-vine model can be computed as follows.

$$f(x_1, x_2, \dots, x_m) = \prod_{i=1}^{m} f_i x_i \times C(F_1(x_1), F_2(x_2), \dots, F_m(x_m), \theta) \tag{6.7}$$

where θ denotes the parameters of the copula functions.

C is defined by Equation 6.8.

$$\begin{aligned} &C\big(F_1(x_1), F_2(x_2), \dots, F_m(x_m)\big) = \\ &\prod_{i=1}^{m-1} \prod_{e \in E_i} C_{j(e),k(e)|\, D(e)}\big(F\big(x_{j(e)}\big|x_{D(e)}\big), F\big(x_{k(e)}\big|x_{D(e)}\big), \theta_{D(e)}\big) \end{aligned} \tag{6.8}$$

where $E = [E_1, E_2, \ldots, E_{m-1}]$ are the edges. The bivariate copula density, $C_{j(e),k(e)|D(e)}$ is associated with each edge. $j(e)$ and $k(e)$ are the nodes under conditional set $D(e)$.

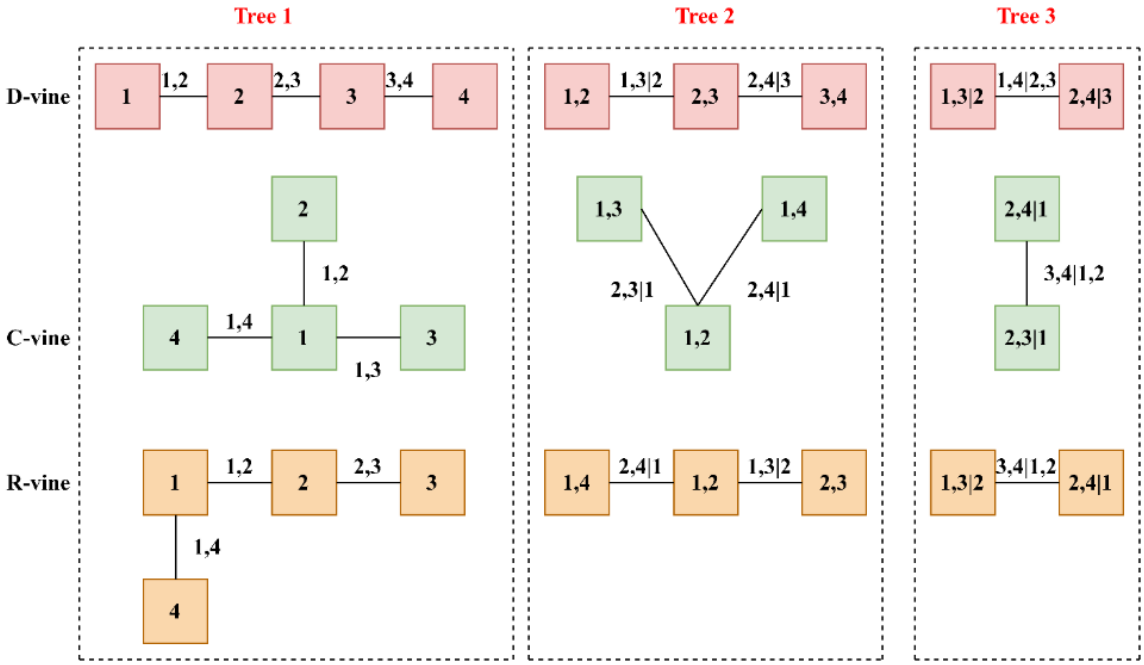

Figure 6.1: An illustrative example of four-dimensional D, C, and R-vine models.

As the R-vine has no specific structure like the C and D-vines, it is an arduous task to determine an accurate structure. Kendall's nonlinear rank correlation coefficient, τ is utilized for this purpose (Kendall, 1938). The first tree is selected in such a way that maximizes $\hat{\imath}$ in Equation 6.9 (Zhou and Li, 2018). The parameters and τ values of binary copulas are selected based on the BIC values. The copula family that yields the minimum BIC value is used to model the considered pair-wise relation (Cui and Li, 2020; Ren et al., 2015). Interested readers are referred to (Aas, 2016; Aas et al., 2009; Brechmann et al., 2012; Brechmann and Joe, 2015) for details on theoretical foundations and model development of R-vine copula.

$$\hat{\imath} = \underset{i}{argmax} \sum_{j=1}^{m} |\tau_{i,j}| \tag{6.9}$$

6.3. Proposed Methodology

The proposed risk-based FDD model is shown in Figure 6.2. The method utilizes the R-vine copula to describe the dependence structure and compute the JPDFs, which are further used to estimate fault probability. The dynamic failure prognosis module is developed using the event tree, as it can show how a fault can turn into an accident. The fault diagnosis module is built from univariate density quantiles. Once the observed failure value gets a sharp jump, a warning is generated, and root cause(s) is diagnosed using density quantiles. The proposed framework is mainly comprised of the data pre-processing, R-vine construction, fault probability estimator, failure probability estimator, multiple fault diagnosis, and online monitoring modules. The first five modules are used to develop the risk-based monitoring model (Figure 6.3) that consists of the fault probability and failure probability estimators. Details of each step are described in the following subsections.

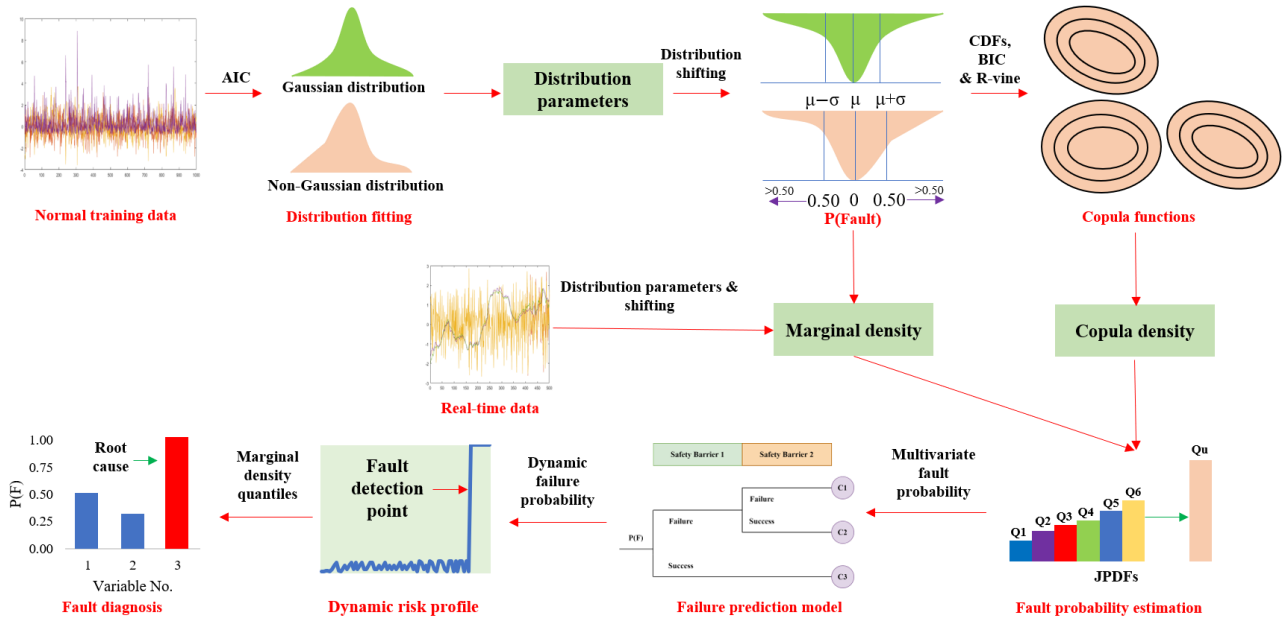

Figure 6.2: Conceptual framework of the proposed risk-based FDD framework.

6.3.1. Data Pre-processing

Normal operational data is collected, and process variables are fitted to a candidate distribution. This work considers the beta, exponential, gamma, generalized extreme value, log-normal, Gaussian, Rayleigh, t-location scale, and Weibull distributions to find the best distribution that fits process data. Once the suitable distribution is identified for a variable, corresponding distribution parameters are also estimated. We used AIC to find the distribution and optimal parameters. Then, the PDFs and CDFs are calculated for each variable.

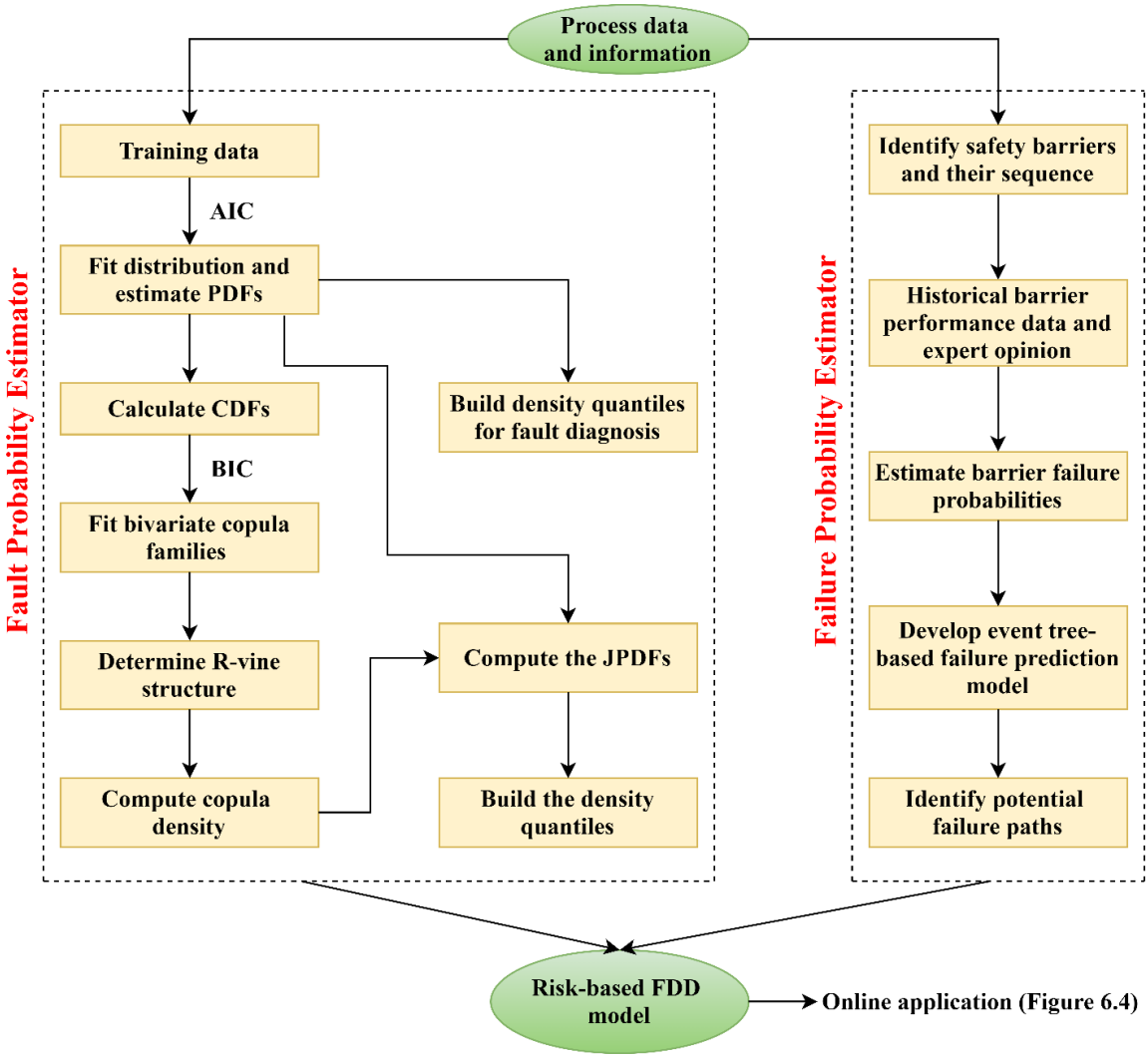

Figure 6.3: Proposed risk-based FDD model development phases.

Next, the PDFs and CDFs are shifted using Equation 6.10.

$$P(Fault) = \varphi\left(\frac{X \pm k\mu}{\sigma}\right) \tag{6.10}$$

where X, μ, k, and σ are the arbitrary sample, mean, multiplier, and standard deviation (SD), respectively. This mean shifting is important for risk calculation. Suppose a sample lies on the mean for a normal distribution; the PDF will be the highest compared to the other samples. However, this observation should exhibit the lowest fault probability, as process operations usually exhibit a higher likelihood to be in the normal state when data closely follow the mean. The probability of an abnormality is assumed 0 and 0.50 at mean and one SD, respectively. The choice of k depends on allowable deviations of process variables before generating warnings. Usually, a value of k between 0 and 3 is chosen. In this study, a value of 1 is used for k.

Consider a variable follows the Gaussian distribution with μ=10 and σ=1. The PDF and CDF can be estimated using Equations 6.11 and 6.12, respectively.

$$f(x) = \frac{1}{\sqrt{2\pi\sigma^2}} e^{-\frac{(x-\mu)^2}{2\sigma^2}} \tag{6.11}$$

$$F(x) = \int_{-\infty}^{x} \frac{1}{\sqrt{2\pi\sigma^2}} e^{-\frac{(x-\mu)^2}{2\sigma^2}} dx \tag{6.12}$$

Suppose a sample yields a value of 10.10 (greater than the mean value). According to Equations 6.11 and 6.12, the PDF and CDF for this sample will be 0.40 and 0.54, respectively.

From Equation 6.10, the shifted PDF and CDF equations for this variable can be written as:

$$f(x) = \frac{1}{\sqrt{2\pi\sigma^2}} e^{-\frac{(x-(\mu+\sigma))^2}{2\sigma^2}} \tag{6.13}$$

$$F(x) = \int_{-\infty}^{x} \frac{1}{\sqrt{2\pi\sigma^2}} e^{-\frac{(x-(\mu+\sigma))^2}{2\sigma^2}} dx \tag{6.14}$$

Then, the revised PDF and CDF will be 0.27 and 0.18, respectively. Clearly, the distribution shifting strategy provides a more realistic probability of fault.

6.3.2. R-vine Construction

The CDFs are used to estimate copula parameters. This work considers six bivariate copula types: Gaussian, t, Clayton, Gumbel, Frank, and Joe copula. The use of these copulas ensures that the asymmetric and tail dependence are captured.

The BIC is used to select the most suitable copula. Equation 6.6 can be re-written as:

$$BIC = Kln(n) - 2\sum_{i=1}^{n} ln(x1_i, x2_i|\theta) \tag{6.15}$$

where K = 2 for the t-copula (i.e. it is the only two parameter copula among the considered six bivariate copulas) and 1 for the other five copula families.

After selecting the appropriate copula family of each bivariate copula in the first tree, Kendall's τ is calculated; subsequently, the R-vine structure is determined. Although τ ranges from -1 to 1, this work uses an absolute value (i.e. $0 \leq \tau \leq 1$). Consider a process with four variables (x_1-x_4). Table 6.1 shows the approximated τ values. The pair of x_2 and x_3 exhibits the strongest correlation (0.95), followed by x_1 and x_2 (0.90). Therefore, x_2 can be placed in between x_1 and x_3. x_4 is the remaining variable that needs to be connected with any of the other variables. The fourth row or column of Table 6.1 depicts that x_4 gives a higher τ value when coupled with x_1 (0.85) than x_2 (0.80) and x_3 (0.50). Finally, x_4 can be adjoined with x_1 to maximize the correlation structure and complete the first tree. The R-vine model in Figure 6.1 displays the structure, as described earlier.

Table 6.1: Kendall's τ values for illustrative four variable process.

Variable	x_1	x_2	x_3	x_4
x_1	/	0.90	0.80	0.85
x_2	0.90	/	0.95	0.80
x_3	0.80	0.95	/	0.50
x_4	0.85	0.80	0.50	/

6.3.3. Multivariate Density Quantile Development

The JPDF of each sample is calculated by multiplying the marginal and copula densities. However, these probabilities are not readily usable for risk assessment since a process industry is a source of numerous variables which may yield a lower and impractical value of fault probability. Let us consider a process with 4 variables. For JPDF, there will be 4 marginal probabilities and $\frac{4\times3}{2}$ = 6 probabilities from the vine model. For simplification, let us assume all these probabilities have a value of 0.10. Therefore, JPDF will be 10^{-10}. For small processes, this probability value may make sense. For larger processes (say 20 variables), the fault probability from JPDF will be close to 10^{-200}, which is impractical and vague. Ren et al. (2015) proposed a DQA technique to address this issue. The DQA uses a set of discrete intervals to fit a probability distribution. The fault probability of a sample can be computed using Equation 6.16.

$$P(Fault)_i = \frac{JPDF_i}{Q(high)_u} * P(Fault)_{Q_u} \tag{6.16}$$

where i = 1, 2, 3, …, n is the sample number. Q and u represent the quantile and quantile number, respectively. $Q(\text{high})_u$ is the highest value in u^{th} quantile, and $P(\text{Fault})_{Q_u}$is the maximum fault probability corresponding to u^{th} quantile.

Suppose the obtained JPDFs are divided into 100 quantiles (u =100). This implies the first and last quantiles refer to a maximum fault probability of 0.01 and 1, respectively. Consider a sample that

has a JPDF 9.81×10^{-201}. The third quantile is ranged from 9.71×10^{-201} to 9.95×10^{-201}. Therefore, According to Equation 6.16, the probability of fault for this sample can be calculated as follows.

$$P(\text{Fault}) = \frac{9.81\times10^{-201}}{9.95\times10^{-201}} \times 0.03 = 0.0296$$

If any sample does not fit any of the hundred known quantiles, P(Fault) is 1, considering this sample to be out of normal operating zone.

6.3.4. Failure Probability Estimator

A process is usually equipped with a series of physical and non-physical protection systems to prevent a fault from leading to a failure. These are called safety barriers. The dynamic risk profile is greatly affected by the performance of these barriers, and an accurate sequence identification is required to assess the paths that a fault can propagate.

Although several safety barriers may be present in a process system, this work considers four commonly used safety barriers: control system (CS), alarm system (AS), emergency management failure prevention barrier (EMFPB), and human failure prevention barrier (HFPB). The failure probability of each barrier can be estimated from the historical database and subject matter specialists' opinions. One of the simplest ways to calculate barrier failure probability is dividing the failures on demand by the total number of occasions when the barrier was required to perform. However, this database may not always be available. This issue can be handled by using expert opinions and manufacture provided failure rate.

The ET is used to predict the online failure probability. It is a popular technique in logical accident analysis. Interested readers are referred to the works by Kalantarnia et al. (2009) and Rathnayaka et al. (2011b) for illustration of potential applications of event tree in the context of process accident analysis. Fault probability is continuously fed into the ET model, which shows the consequences as safe, near-miss, mishap, incident, accident, and catastrophe based on the potential

of each path's impact on the plant, personnel, and the environment. Suppose a minor deviation is suppressed by the control system; this will lead to a safe state, and no loss is expected. On the other hand, failure of all the barriers will lead to a catastrophic accident that will result in significant asset, business, and reputation loss, environmental impact, injuries, and fatalities.

6.3.5. Fault Diagnosis Module

The fault diagnosis module is built using the same concept described in Section 6.3.3. Each variable's marginal density is divided into density quantiles, and root cause(s) is diagnosed when dynamic risk profile reveals a sharp change. The variable(s) that has unit fault probability from the univariate DQA is selected as the root cause(s). Suppose two variables: A and B have a normal marginal density range of 0.20-0.40 and 0.30-0.50, respectively. A fault has occurred due to variable A, and the observed marginal densities are 0.45 and 0.50 for A and B, respectively. Clearly, the DQA will be able to diagnose A as the root cause, as it violates its normal operating region. If the marginal densities are utilized without the DQA, variable B will be mistakenly diagnosed as the root cause.

6.3.6. Online Monitoring

The online application part of this methodology (Figure 6.4) monitors dynamic risk and generates a warning when needed. First, the online samples are projected to the marginal density space using the distribution parameters obtained in the data pre-processing stage. The JPDF of each observation is calculated using copula parameters from the R-vine construction module. These JPDFs are passed through the density quantiles to estimate the fault probabilities which are continuously fed into the failure prediction model, and the dynamic risk profile is continuously monitored. If any sharp change is observed, a warning is generated. Finally, the fault diagnosis

module is utilized to identify the root cause(s). To capture the dynamic process behaviour and mean shifting data, the distribution parameters are recursively updated after each fifty samples if no fault is detected. Subsequently, the copula densities and density quantiles are also updated with the new distribution parameters.

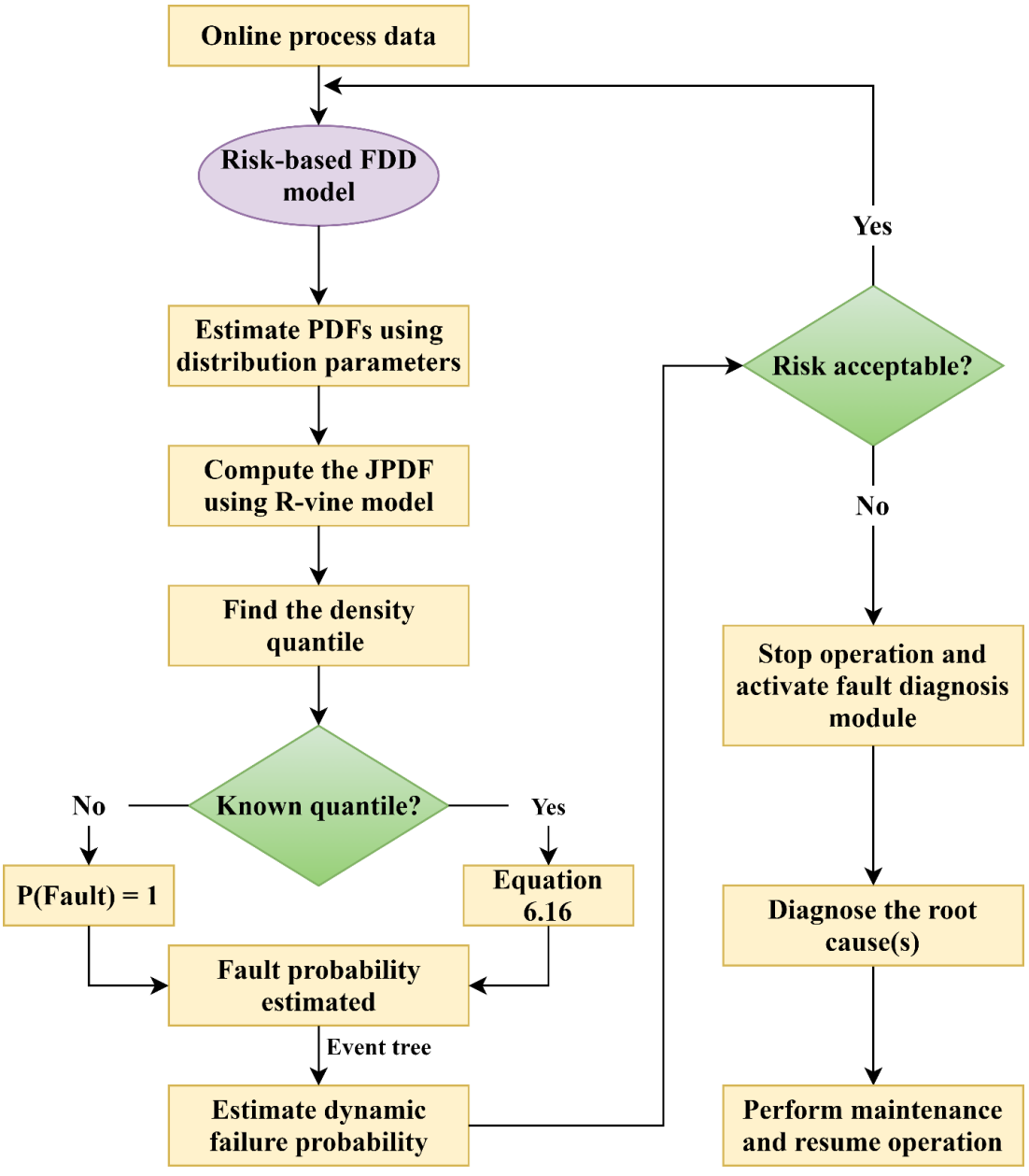

Figure 6.4: Online process monitoring using the proposed risk-based FDD model.

6.4. Applications of the Proposed Methodology

6.4.1. Benchmarking using the Tennessee Eastman (TE) Chemical Process

The TE chemical process (Figure 6.5) is the most widely used benchmark model for examining the efficacy of an FDD tool. There are 41 measured and 12 manipulated variables. A total of 22 variables (denoted by XMEAS (1), XMEAS (2), …, and XMEAS (22)) are continuous process variables which have been considered in this study (see Table 6.2). This work uses eleven fault cases to test the developed framework where the first nine scenarios contain single faults, and in the other two cases, two different faults simultaneously occurred at two different variables. These test cases have been generated using the simulator developed by Professor Daniel Rivera and his colleague, Marty Braun from Arizona State University. This simulator can be downloaded from https://7starm.asu.edu/node/33 (last checked on March 13, 2021). The concurrent fault conditions have been selected to demonstrate the proposed methods ability to diagnose simultaneous faults. In this section, the efficiency of developed method for detection and diagnosis of simultaneous step change in A/C feed ratio keeping B composition constant in stream 4 and A feed loss in stream 1 is discussed. The root causes for these faults are XMEAS (4) and XMEAS (1), respectively. A detailed process description can be found in the work by Downs and Vogel (1993).

A total of 1000 normal samples with a sampling time of 1 second are used to develop the R-vine-based fault probability estimator. The suitable distributions for the 22 monitored variables are selected by minimizing AIC, and subsequently, the distribution parameters are estimated. The PDFs and CDFs are estimated using these parameters and Equation 6.10. The CDFs are used to estimate copula parameters. The BIC is utilized for finding the most appropriate copula family. Then, the first tree of the R-vine model is selected in a way that maximizes the correlation structure. The binary copulas and associated parameters in other 20 trees are determined based on

BIC, as well. The parameters are used to compute Kendall's τ for all 231 binary copulas; this completes the R-vine construction module.

Table 6.2: Description of monitored variables in the TE chemical process (Downs and Vogel, 1993).

Variable No	Description	Unit
XMEAS (1)	A feed (stream 1)	kscmh
XMEAS (2)	D feed (stream 2)	kg/hr
XMEAS (3)	E feed (stream 3)	kg/hr
XMEAS (4)	A and C feed (stream 4)	kscmh
XMEAS (5)	Recycle flow (stream 8)	kscmh
XMEAS (6)	Reactor feed rate (stream 6)	kscmh
XMEAS (7)	Reactor pressure	kPa gauge
XMEAS (8)	Reactor level	%
XMEAS (9)	Reactor temperature	ºC
XMEAS (10)	Purge rate (stream 9)	kscmh
XMEAS (11)	Product separator temperature	ºC
XMEAS (12)	Product separator level	%
XMEAS (13)	Product separator pressure	kPa gauge
XMEAS (14)	Product separator underflow (stream 10)	m^3/hr
XMEAS (15)	Stripper level	%
XMEAS (16)	Stripper pressure	kPa gauge
XMEAS (17)	Stripper underflow (stream 11)	m^3/hr
XMEAS (18)	Stripper temperature	ºC
XMEAS (19)	Stripper steam flow	kg/hr
XMEAS (20)	Compressor work	kW
XMEAS (21)	Reactor cooling water outlet temperature	ºC
XMEAS (22)	Condenser cooling water outlet temperature	ºC

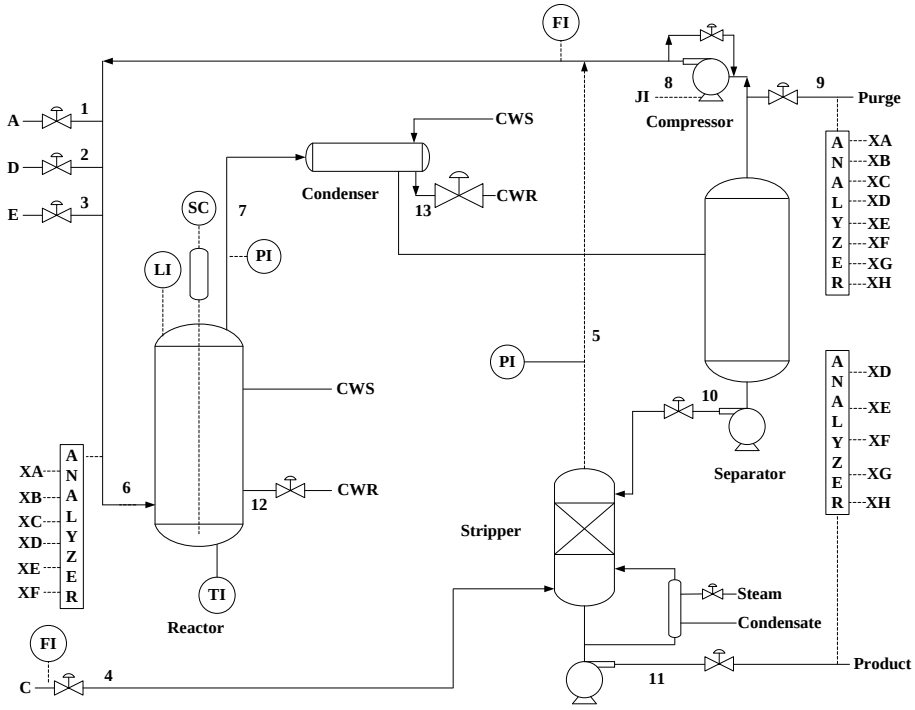

Figure 6.5: A schematic diagram of the TE chemical process (modified and redrawn from (Downs and Vogel, 1993)).

The marginal PDFs are multiplied by the copula densities to estimate the JPDFs. These JPDFs are segregated into 100 quantiles to build the fault probability estimator. Also, each univariate PDF is divided into 100 density quantiles for root cause diagnosis. The next task is to develop the failure prognosis module. As mentioned earlier, the event tree for failure prognosis is built considering the CS, AS, EMFPB, and HFPB. The failure probability of these barriers (Table 6.3) is collected from the existing literature. Figure 6.3 shows the event tree-based failure prediction model. A total of eight consequences are identified based on success (S) and failure (F) of the safety barriers. The controller can compensate for the smaller deviations. However, it may fail to maintain the setpoint if the deviation is higher. Then, the warning system will be activated to give an indication of an unwanted operating region and alert operator. If the alarm generated by the process monitoring

scheme is taken care of by the responsible personnel, a near-miss situation is observed. All the failure paths are designed using such logic.

Table 6.3: Failure probability of safety barriers (Amin et al., 2020; Yu et al., 2015a).

Sl. no	Name of the barrier	Notation	Failure probability
1	Control system	CS	0.01
2	Alarm system	AS	0.05
3	Emergency management failure prevention barrier	EMFPB	0.0824
4	Human failure prevention barrier	HFPB	0.0646

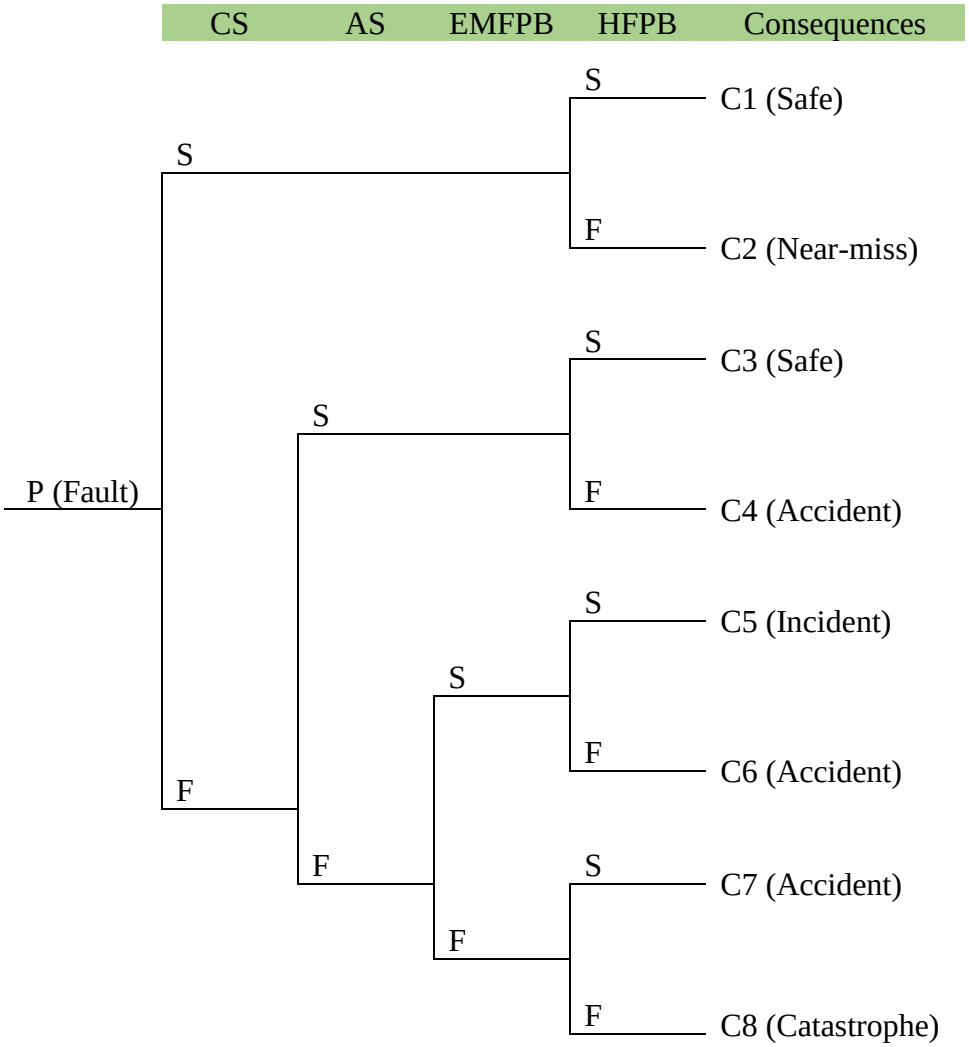

Figure 6.6: The failure prediction model for the TE chemical process.

The proposed method is validated using 500 test samples (1001-1500 sample in Figure 6.7), where faults start from the 1101st sample. The PDFs are estimated using the distribution parameters from data pre-processing module. The JPDFs are calculated by multiplying the online PDFs and copula densities. The fault probability is estimated by passing the JPDFs through the density quantiles built from multivariate joint distribution earlier. These probabilities are fed into the failure prediction model.

Although the event tree can lead a process to eight different paths, this article shows the prognosis result through the path, C8, as it represents the catastrophic failure probability. The fault and failure probabilities are shown in Figures 6.7(A) and 6.7(B), respectively. It can be seen that only one sharp rise in risk profile is observed in the first 1100 samples. While building density quantiles, the highest value among the JPDFs takes a fault probability of 1. This is the reason why this false alarm is generated.

These faults are detected at the 1103rd sample, as a sharp rise in risk profile is noticed through path C8. The fault probability for each variable is determined using individual density quantiles (Figure 6.7(C)). Both XMEAS (1) and XMEAS (4) are found to have a probability of fault equal to 1 at the 1103rd sample. This implies both these are the reasons behind the generated warning, and the operator(s) can do troubleshooting in streams 1 and 4 for restoring the process in normal operating condition.

A

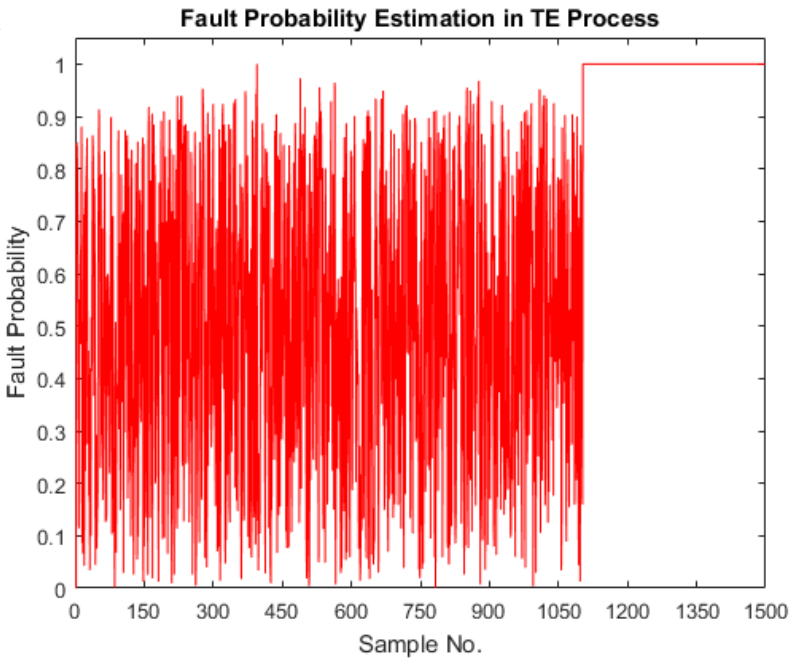
Fault Probability Estimation in TE Process
Fault Probability
Sample No.
0
0.1
0.2
0.3
0.4
0.5
0.6
0.7
0.8
0.9
1
0
150
300
450
600
750
900
1050
1200
1350
1500

B

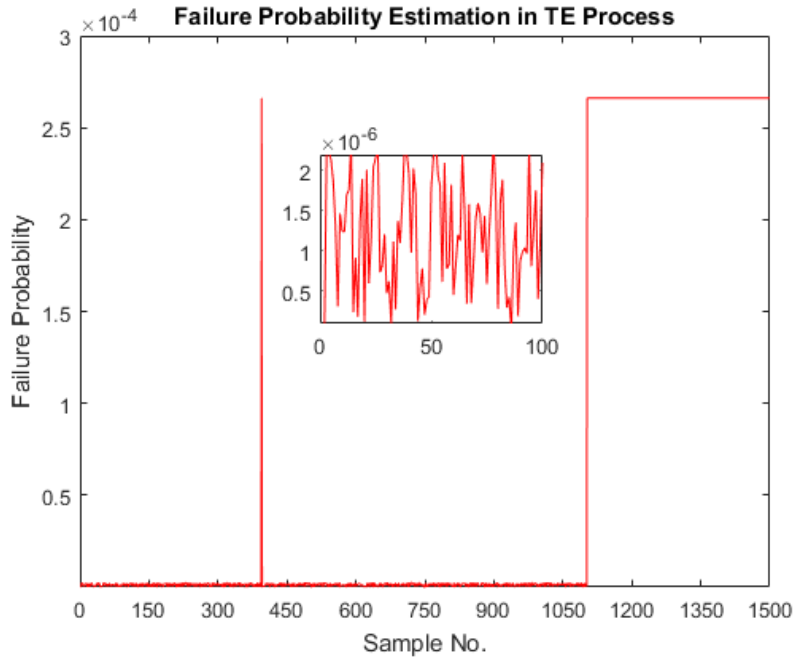
Failure Probability Estimation in TE Process
×10^-4
Failure Probability
Sample No.
×10^-6
0
0.5
1
1.5
2
2.5
3
0
150
300
450
600
750
900
1050
1200
1350
1500
0
50
100

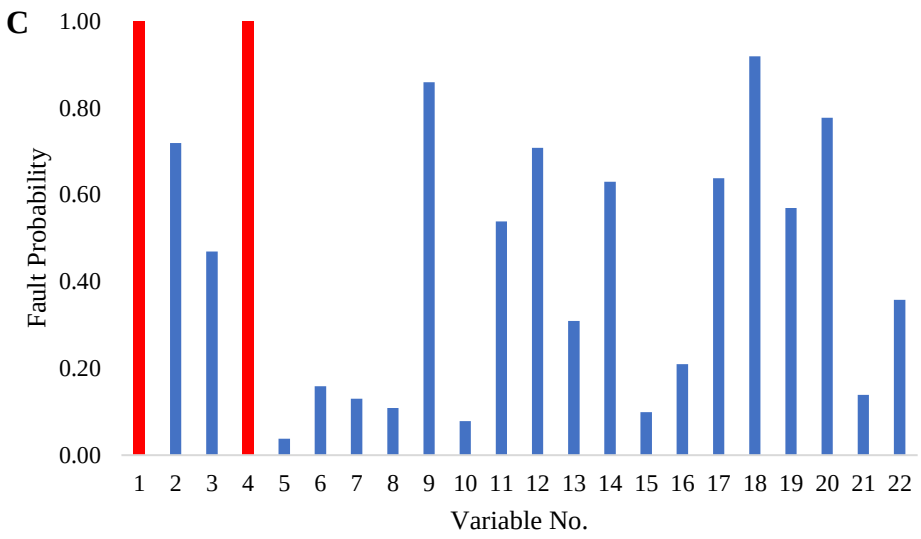

Figure 6.7: Monitoring results in the TE process for simultaneous A feed loss and step change in A/C feed ratio (A) fault probability estimation, (B) failure prognosis through C8, and (C) fault diagnosis.

The diagnosis capacity of PCA and transfer entropy is also examined in this dataset. PCA-SPE and PCA-T^2 can detect this fault at the 1102nd and 1103rd samples, respectively. Although PCA-SPE can detect this fault earlier, it does not provide significant information about the root causes (Figure 6.8(A)). PCA-T^2 provides a better diagnosis report, as it can diagnose the root cause of A feed loss. Nevertheless, it cannot provide any information about the presence of an abnormality in XMEAS (4) (Figure 6.8(B)). Since the proposed method can detect the fault at the 1103rd sample, the first 1103 sample is used to construct the transfer entropy-based causal map (Gharahbagheri et al., 2017a); thus, a fair comparison is ensured. Figure 6.8(C) shows the developed causal map, and it suggests XMEAS (2) and XMEAS (13) as the root causes, which is completely inaccurate. The diagnostic performance comparison in all 11 fault cases is presented in Table 6.4, which shows better accuracy by the proposed method compared to the PCA and transfer entropy.

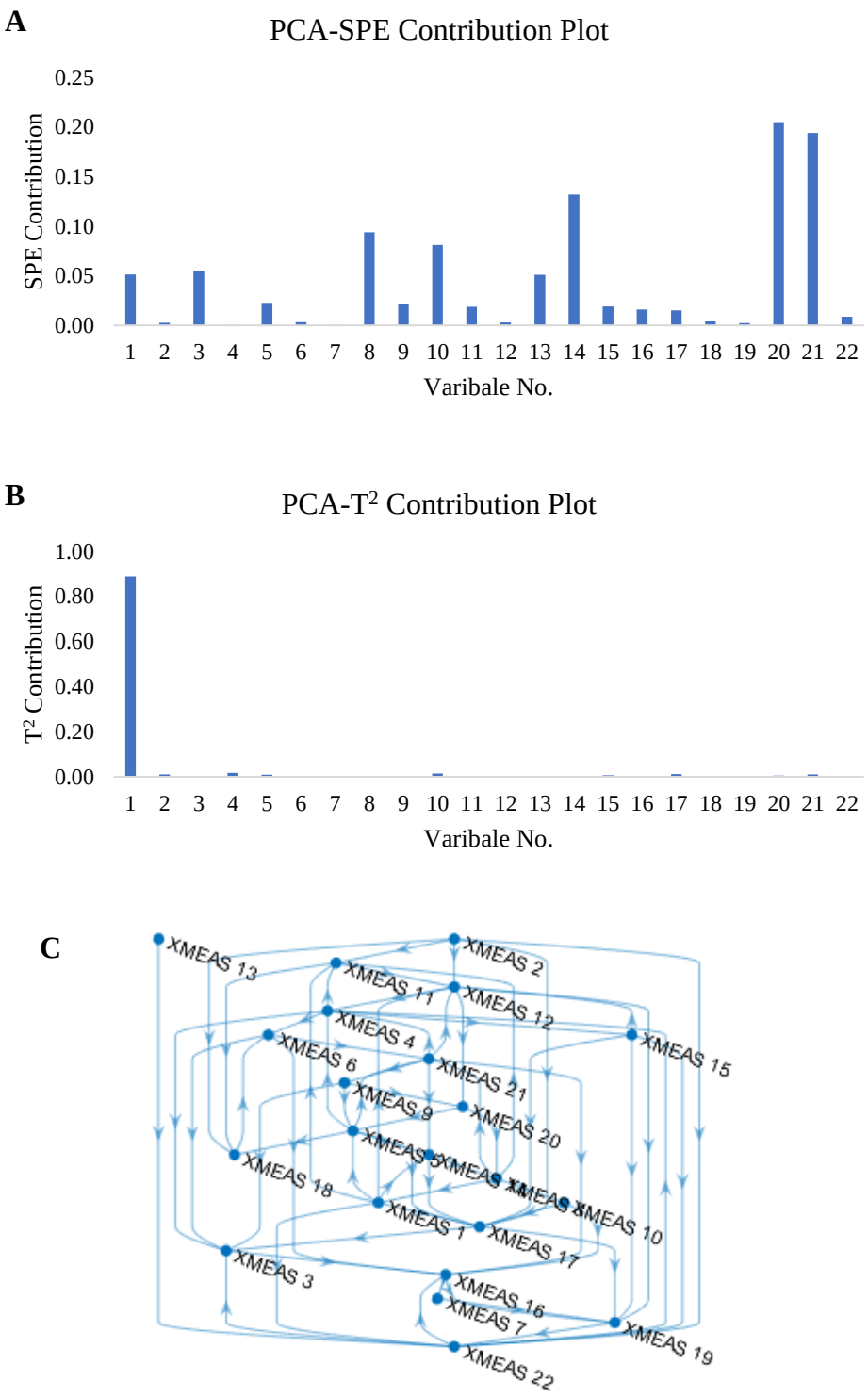

Figure 6.8: Root causes diagnosis of simultaneous A feed loss and step change in A/C feed ratio by (A) PCA-SPE contribution plot, (B) PCA-T^2 contribution plot, and (C) transfer entropy.

Table 6.4: Diagnostic performance comparison of proposed method, PCA, and transfer entropy.

Fault ID	Fault description	Accurate diagnosis			
		PCA		Transfer entropy	Proposed method
		T^2	SPE		
A1	A feed loss	**Yes**	No	No	**Yes**
A2	Step change in A/C feed ratio	**Yes**	No	No	**Yes**
A3	D feed loss	**Yes**	**Yes**	**Yes**	**Yes**
A4	E feed loss	**Yes**	No	No	**Yes**
A5	Random variation in purge rate	No	No	No	**Yes**
A6	Random variation in reactor cooling water flow	No	No	No	**Yes**
A7	Gradual increase in separator pot liquid flow	No	No	No	**Yes**
A8	Gradual increase in stripper liquid product flow	No	No	No	**Yes**
A9	Stripper steam valve stiction	**Yes**	No	No	**Yes**
A10	Simultaneous A feed loss and step change in A/C feed ratio	No	No	No	**Yes**
A11	Simultaneous D and E feed loss	No	No	No	**Yes**

6.4.2. The RT 580 Experimental Setup

The RT 580 fault-finding control system is an experimental setup, situated at the Memorial University for testing control and fault detection algorithms. In the RT 580 setup, several real-time fault conditions can be introduced by using different switches. Figure 6.9 shows the schematic diagram of RT 580. It consists of three circuits to control the level, flowrate, and temperature. The pump (P1), collecting tank (B1), and process tank (B2) are controlled by a circuit, while the other two circuits are used to control the temperature. A total of four temperature sensors are used to measure the temperature of the liquid flowing through different parts of this system. There is a pressure sensor to measure the water column height in the process tank. A magnetic induction flow sensor is installed at the entry to the process tank to measure the flowrate. A pneumatic control valve (V7) serves as the actuator. Detail process description can be found in the work by Ghosh et al. (2019).

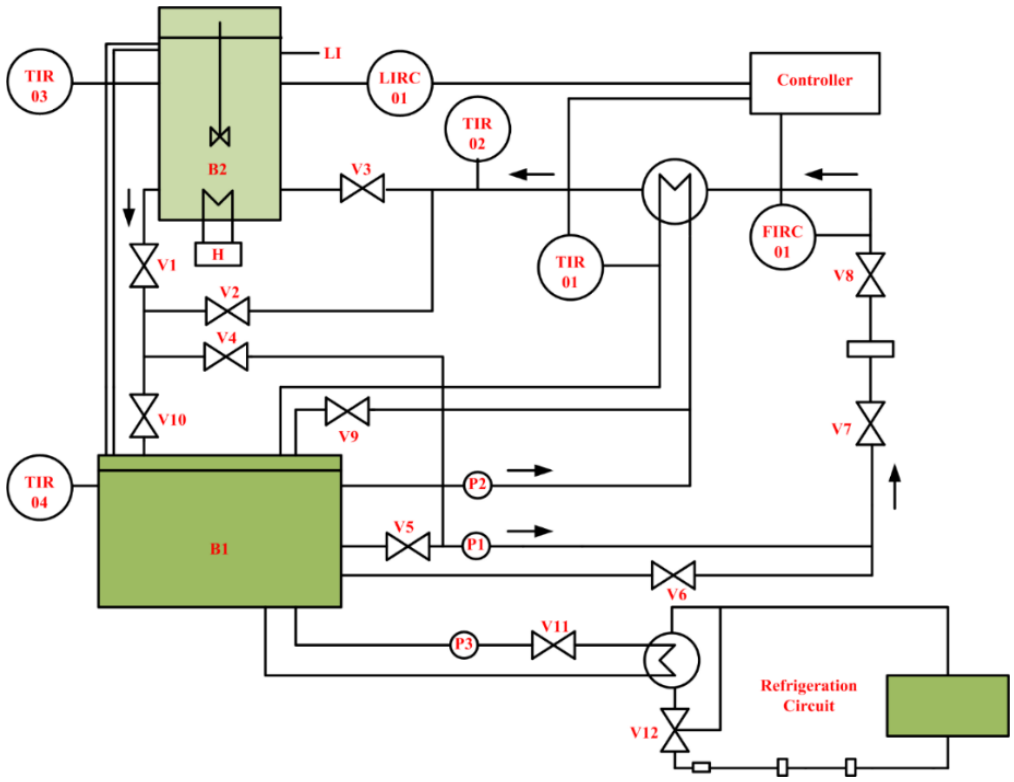

Figure 6.9: Schematic diagram of the RT 580 experimental setup (modified from (Ghosh et al., 2019)).

A total of seven variables are monitored in this study, as shown in Table 6.5. This case study consists of 300 samples where faulty condition is generated at 251st sample by simultaneously altering V7 and introducing a sensor fault to the sensor that measures the level in process tank, B2. There is no continuous measurement for V7; however, it directly affects the manipulated variable, Y1. Therefore, both the X1 and Y1 are the monitorable root causes in this fault scenario. The first 200 samples are used to build the R-vine model. The rest of the samples is utilized to examine the efficacy of the proposed method.

At first, the candidate distributions are used to fit process variables based on AIC values. The distribution that gives the lowest AIC value is selected to model the corresponding variable. Y1, T2, and T4 can be fitted with the generalized extreme value distribution, and the Weibull distribution is found to be suitable for T1, T3, and F. The other variable, X1 follows the normal

distribution. Once the candidate distribution is identified, associated parameters are estimated. A total of three parameters: the location, shape, and scale parameters are required to model the generalized extreme value distribution. On the contrary, the Weibull distribution needs the scale and shape parameters. These parameters can be used to calculate the mean and standard deviation of distinct process variables. Then the PDFs and CDFs are computed after shifting the fault probability, as demonstrated in Equation 6.10.

Table 6.5: Monitored variables in the RT 580 setup.

Variable		Unit
ID	Description	
X1	Actual process tank level	%
Y1	Manipulated variable	N/A
T1	Heat exchanger outlet temperature	ºC
T2	Process tank inlet temperature	ºC
T3	Process tank temperature	ºC
T4	Collecting tank temperature	ºC
F	Flow	L/h

The bivariate copula families and their associated parameters are estimated from the CDFs using BIC. The Kendall's rank correlation coefficient, τ for different copulas are calculated. The R-vine structure is defined, and τ for all the binary copulas are computed from respective copula parameters. The correlation coefficients for the entire R-vine structure are calculated and multiplied with the PDFs obtained earlier. This will give the JPDFs from the 200 samples, which are further utilized to build the density quantiles. The multivariate JPDFs are divided into 100 quantiles. A total of seven density quantiles are also built from the marginal PDFs of monitored variables for fault diagnosis. The failure prognosis module shown in Figure 6.6 is utilized in this case study, as well.

During the testing period, all the samples are projected to the PDF space using the distribution parameters obtained from 200 normal samples and Equation 6.10. The JPDFs are computed after multiplying these PDFs with the copula densities from 21 binary copulas from the R-vine model. Then, the fault probability is estimated by passing each JPDF through the developed density quantiles (Figure 6.10(A)). The fault probabilities are continuously fed into the failure prognosis module to realize any potential risk of failure. The catastrophic failure probability through path C8 is shown in Figure 6.10(B). Since no fault is detected from 201^{st} to 250^{th} samples, the distribution and copula parameters are updated using the first 250 samples. The density quantiles are also updated using the revised parameters. The failure risk experiences a sharp jump from the 251^{st} sample as soon as the faults are activated, and a warning is generated.

The fault probability of all variables at the 251^{st} sample is estimated using the univariate density quantiles and shown in Figure 6.10(C). Both X1 and Y1 have a unit failure probability which implies the maintenance needs to be done on these variables to take the process back to the normal operating zone. Figure 6.10(D) shows the risk profile through C8 that has been developed from the univariate analysis (from X1) and without considering the joint dependence structure. Although the univariate risk-based FDD module can timely detect the fault, it provides an improper estimation of risk, which results in higher false alarms than the R-vine-based model.

A

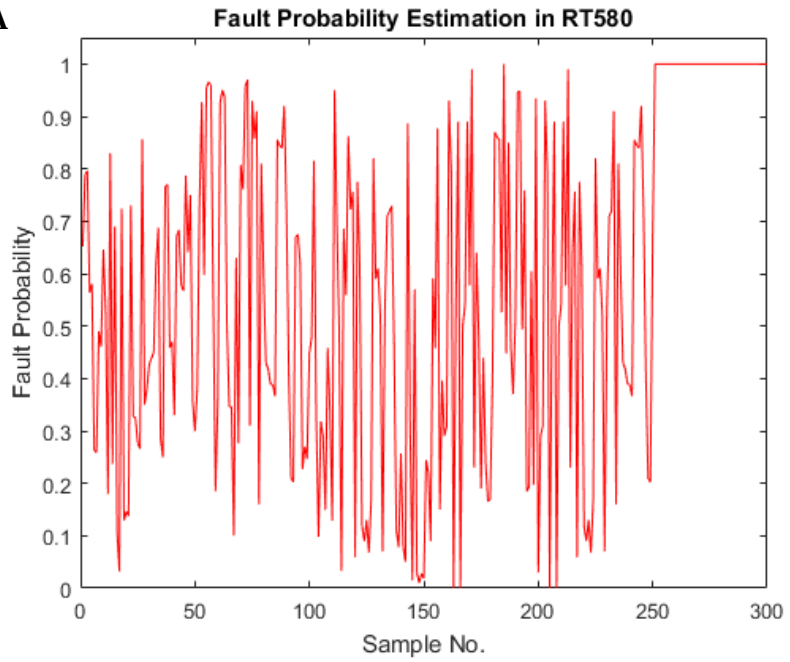
Fault Probability Estimation in RT580
Fault Probability
Sample No.
0
0.1
0.2
0.3
0.4
0.5
0.6
0.7
0.8
0.9
1
0
50
100
150
200
250
300

B

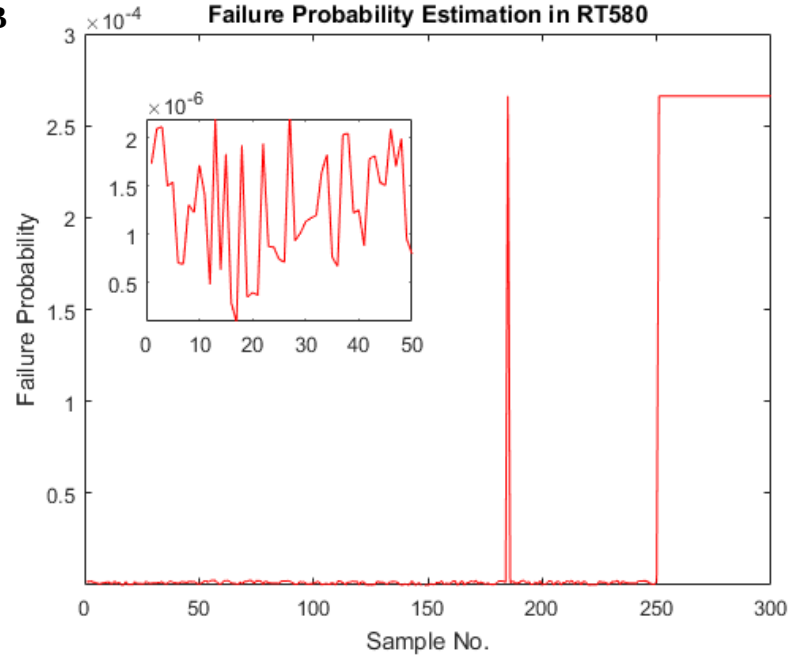
Failure Probability Estimation in RT580
×10^-4
Failure Probability
Sample No.
0
0.5
1
1.5
2
2.5
3
0
50
100
150
200
250
300
×10^-6
0.5
1
1.5
2
0
10
20
30
40
50

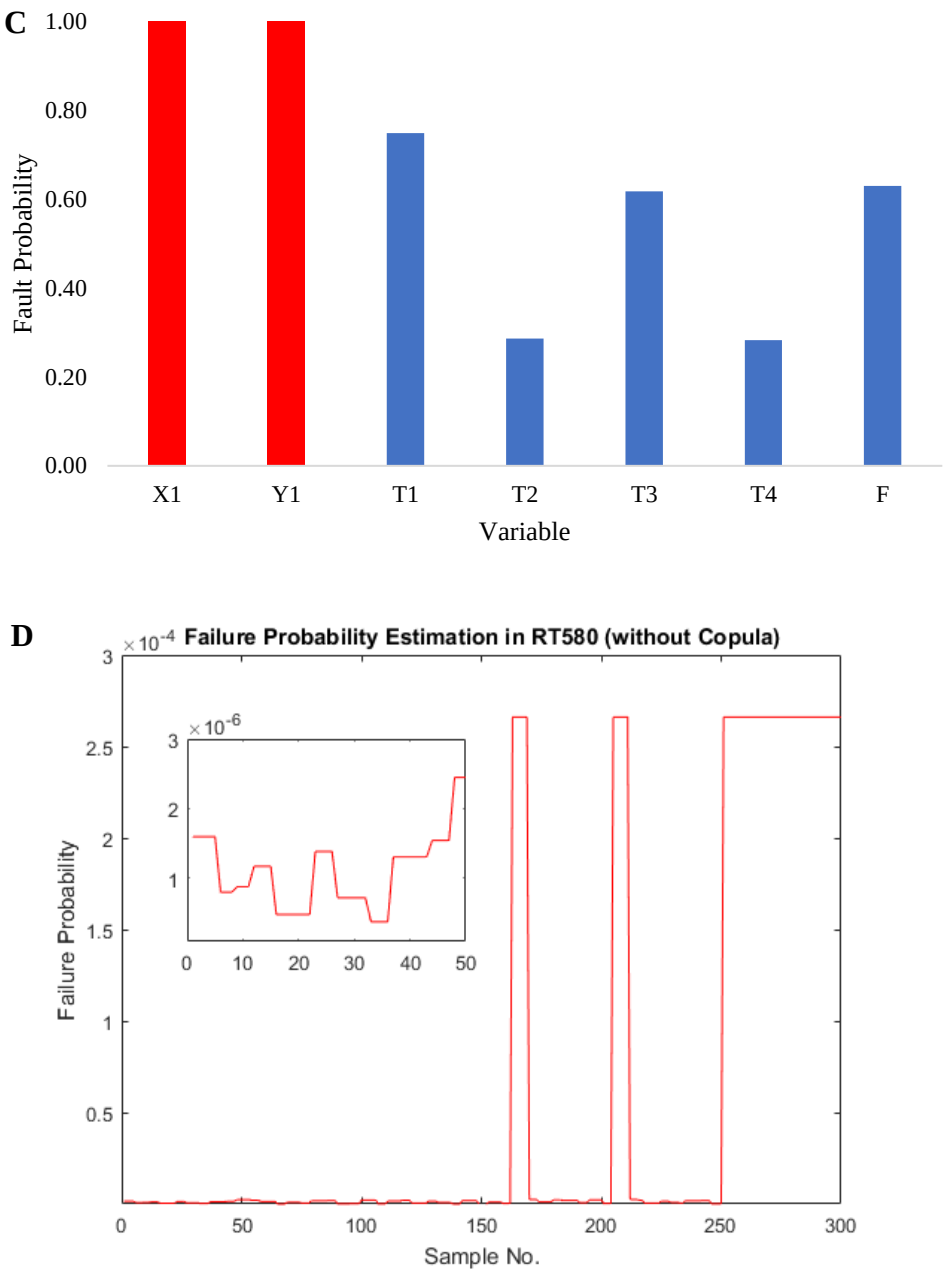

Figure 6.10: Monitoring results in the RT 580 fault finding setup (A) fault probability estimation, (B) failure prognosis through C8, (C) fault diagnosis, and (D) failure prognosis through C8 without considering joint dependence.

6.4.3. The Industrial Isomer Separator Unit

This case study contains a real industrial dataset from an isomer separator unit. This industry is one of the biggest petroleum refineries in Canada. The separator unit considered here is used to separate oil, water, and gas. The unit operates at 2400 psig and 100-110ºF. It is comprised of a horizontal low-pressure separator (LPS), vertical high-pressure separator (HPS), and wash water tank (WT) (Figure 6.11). The HPS works as the first stage separator. However, it cannot provide the desired product composition. Hence, the LPS is utilized for further separation.

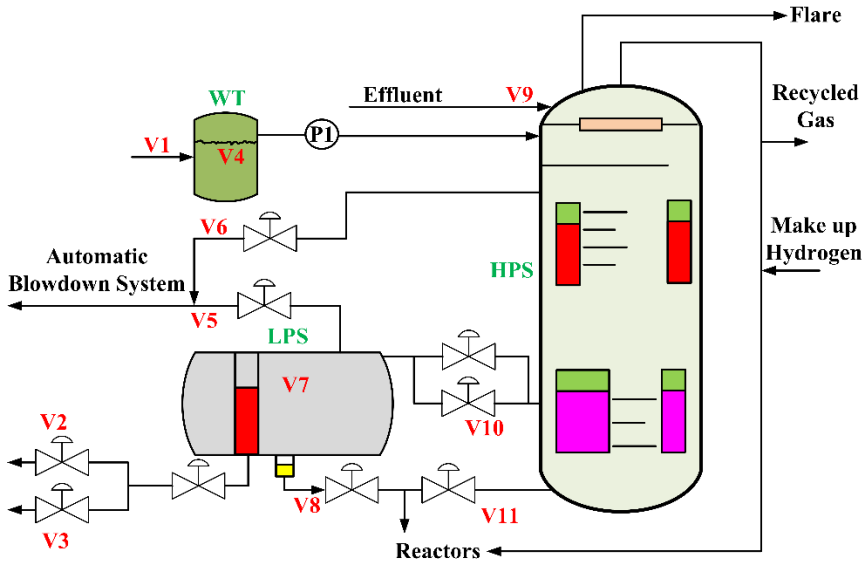

Figure 6.11: Schematic diagram of the isomer separator unit.

Effluent from the condenser enters into the HPS. As the effluent vapours are condensed, ammonium and hydrosulphide are formed due to the presence of ammonia and hydrogen sulphide. The wash water is injected into the WT at a flowrate of V1. It is then pumped into the HPS to dissolve ammonia salts. The water carries the dissolved salts out of the system, as it leaves the bottom of the HPS. The water is transferred to the sour water stripper for the removal of ammonia and hydrogen sulphide. The gas also exits from the HPS while the oils leave the LPS (V2 and V3). This unit is equipped with advanced safety systems such as the cascaded controller, alarm system,

flare system, emergency shutdown device, and automatic blowdown system. However, no multivariate risk monitoring system is equipped there.

The refinery suffered from an unwanted event that caused significant financial losses. This case study consists of data from the stated consequence. A total of 1200 samples are collected where the abnormal event was first detected in the refinery at the 1152nd sample. The sampling time is 1 minute. The first 700 samples are used to build the FDD model. A total of 11 monitored variables are found in this unit. The variable description and fitted distributions are listed in Table 6.6.

Table 6.6: Variable description and fitted distributions in the separator unit.

Variable		Unit	Fitted distribution
ID	Description		
V1	Flow to wash water tank	GPM	Generalized extreme value
V2	Feed 1 to debutanizer	BPD	Generalized extreme value
V3	Feed 2 to debutanizer	BPD	Generalized extreme value
V4	Wash water tank level	%	Gaussian
V5	LPS pressure	PSIG	Gaussian
V6	HPS trim pressure	PSIG	Generalized extreme value
V7	LPS level	%	Generalized extreme value
V8	LPS waterbooth interface level	%	t-location scale
V9	Effluent temperature	^{o}F	t-location scale
V10	HPS level	%	Generalized extreme value
V11	LPS water interface	%	t-location scale

The PDF and CDF are calculated for each variable using the distribution parameters and Equation 6.10. The CDFs are used to estimate the R-vine structure. Since the separator unit has 11 variables, the R-vine model has 55 binary copulas in 10 trees. The τ value for each copula function is estimated using BIC, and subsequently, the JPDFs for these 700 samples are calculated using the estimated PDFs. Then, the density quantiles are estimated from these JPDFs. The same failure prognosis module shown in Figure 6.6 is used in this case, as well. The reasons are twofold: firstly, the developed logical failure analysis model can capture the major safety devices equipped in the

refinery, and secondly, the refinery does not wish to expose their complete safety features due to confidential reasons.

The test region starts from the 701^{st} sample. Figure 6.12(A) shows the fault probability estimation results. Figure 6.12(B) shows the failure prognosis results. The failure risk remains significantly lower for the first 813 minutes of operation. Then, a sharp rise is observed in risk profile at the 814^{th} sample that lasts for 12 minutes, as V4 shows a slight deviation from its normal operating region due to a fluctuation in V1. The controller takes quick action and returns the process within normal condition. Many fluctuations are observed between the 1055^{th} to 1096^{th} samples. At the 1120^{th} sample, the risk value gets a rise from an order of 10^{-8} to 10^{-4} and never comes back during the remaining test samples. This fault eventually affected both V2 and V3.

Consequently, the other units in the refinery were affected, and notable financial damage happened. The refinery got an alarm only at the 1152^{nd} minute, as none of the variables exceeded the setpoint, and no multivariate monitoring technique was employed there. Figure 6.12(C) shows the fault diagnosis result from the 814^{th} sample, and it is observed that the proposed marginal DQA-based fault diagnosis module can accurately diagnose the flowrate to wash water tank (V1) and level in the wash water tank (V4) as the faulty variables that required troubleshooting. Since the proposed diagnostic module is sensitive to probability deviation, it could diagnose the root causes immediately after fault detection.

A

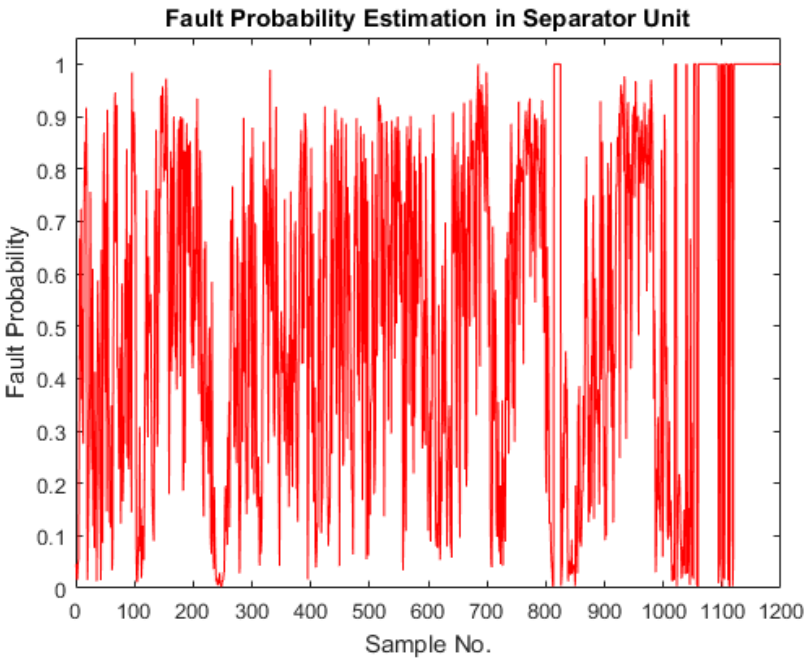
Fault Probability Estimation in Separator Unit
Fault Probability
Sample No.
0
0.1
0.2
0.3
0.4
0.5
0.6
0.7
0.8
0.9
1
0
100
200
300
400
500
600
700
800
900
1000
1100
1200

B

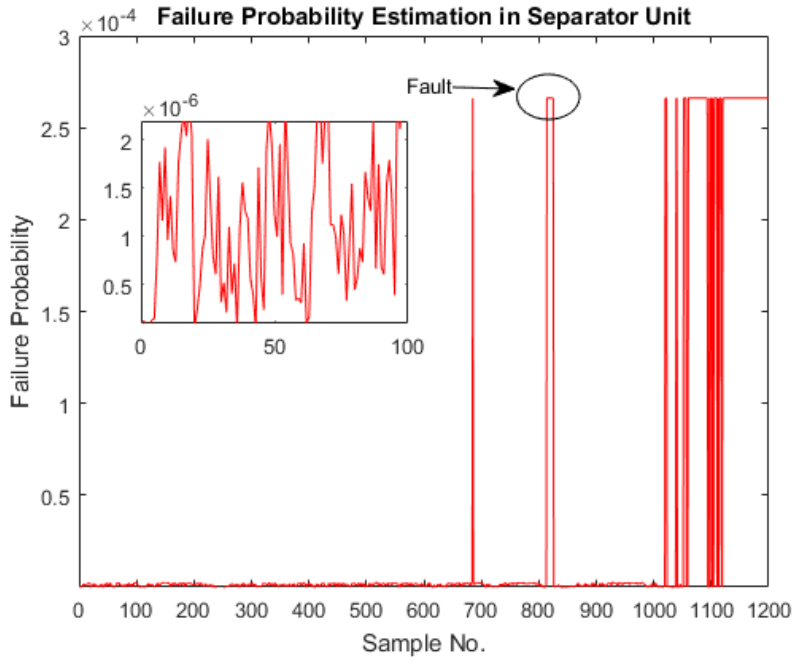
Failure Probability Estimation in Separator Unit
×10^-4
Failure Probability
Sample No.
Fault
×10^-6
0
0.5
1
1.5
2
2.5
3
0
50
100
0
100
200
300
400
500
600
700
800
900
1000
1100
1200

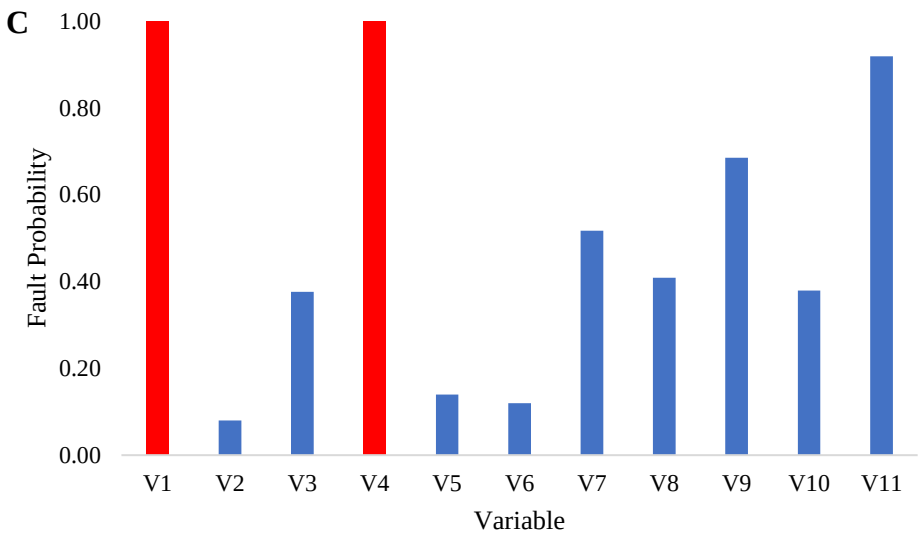

Figure 6.12: Monitoring results in the industrial separator unit (A) fault probability estimation, (B) failure prognosis through C8, and (C) fault diagnosis.

6.5. Conclusion

This work proposes a new risk-based FDD methodology using R-vine copula and ETA. The R-vine model is used for fault probability generation, and the ET is continuously updated by the fault probability obtained from the R-vine-based fault probability estimator. The outputs of ET are utilized for failure prediction. The use of the R-vine model relaxes the necessity to build an arduous supervised learning-based multivariate fault probability estimator.

Findings from the application to an experimental setup highlight the necessity of capturing the dependence structure in risk assessment (see Figure 6.10). Ignoring the joint dependence may lead to an improper risk assessment and subsequently, an unsatisfactory performance of the FDD tools. This article proposes a fault diagnosis module based on the density quantiles of marginal PDFs. The developed diagnosis technique is sensitive to simultaneous faults when two faults originate from two different variables and affect the process significantly. A comparison of the diagnostic performance of the proposed approach with that using PCA and transfer entropy on the benchmark

TE chemical process for eleven fault cases suggests that the proposed framework provides more meaningful information about the root cause(s).

Few areas can be considered to further advance the current work. The event tree is a sequential failure modelling tool that considers binary states of a safety barrier (i.e. success and failure). The safety barriers can have multiple states. The failure can also be non-sequential; therefore, the Bayesian network or the Petri net can be used as the failure prognosis model to overcome these issues. This will also enable to update failure probabilities of safety barriers and provide a robust failure prognosis mechanism. This work has considered simultaneously acting two faults from different sources. It will be interesting to examine the efficacy of the proposed method when more than two faults act concurrently in a process system.

Chapter 7: Summary, Conclusions, and Future Work Scopes

7.1. Summary

The use of multivariate data to solve many existing problems (i.e. early fault detection, automated PC selection, causal model development, and multivariate DRA), related to process safety analysis, is the main contribution of this work. Considering the strengths and limitations of different FDD and DRA methods, the current knowledge gaps and challenges to developing an efficient and practical safety assessment approach are identified. PCA, MEWMA-PCA, NBC, BN, ETA, and copulas are used to address the identified challenges. The efficacy of the proposed methods for FDD and DRA is compared with the existing methods. The results suggest that the developed frameworks provide better solutions.

The first two technical chapters are devoted to providing solutions to FDD. Instead of relying on process knowledge or operator experience, a common practice in process industries, this thesis uses available process data for fault diagnosis. The BNs, used for root cause identification, are developed from fault symptoms and continuous process data. An automated PC selection technique is also proposed. In a practical industrial scenario, the developed methods will reduce opeartors' burden and increase operational efficiency.

The latter technical chapters focus on integrated FDD and DRA since FDD alone is insufficient for safety analysis. Multivariate fault probability has been used to generate dynamic risk profiles. In this context, the risk-based abnormal situation management framework is capable of monitoring a nonlinear and non-Gaussian process. Also, it does not require prior fault information. These works will provide a paradigm shift in multivariate data-driven dynamic risk analysis.

The use of copula theory is another salient feature of this thesis. A novel technique to estimate CPTs using bivariate and vine copulas is proposed to handle continuous process data. Moreover, an R-vine copula-based multivariate fault probability estimator has been used for DRA. The R-vine model enables capturing high-dimensional correlation structures. The PCA-based method was highly appreciated by an oil and gas industry in Newfoundland, and they showed interest to implement the framework for FDD. The aforementioned developed methods are applied to a wide range of process systems. The datasets used for model testing and validation have been obtained from simulation, experiment, and industry.

7.2. Conclusions

There have been efforts for early fault detection, automated fault diagnosis, and dynamic risk assessment considering their importance on process safety analysis. A real-time dynamic risk assessment tool provides industries with a means to measure dynamic safety. Given the ever-increasing multi-dimensional and complex nature of digitalized process systems, it is expected that safety analysis tools will utilize the benefits of multivariate data and perform better than the conventional approaches. From these perspectives, this thesis provides a viable basis for dynamic multivariate safety analysis. The specific conclusions are listed below.

7.2.1. Development of an Early Fault Detection and Diagnosis Model

Early fault detection and diagnosis is always crucial as it gives a lead time from a safety perspective to take the process back to the normal operating condition. The developed MEWMA-PCA provides a better tool for early fault detection. Additionally, it can detect three specific faults (IDV 3, IDV 9, and IDV 15) of the benchmark TE chemical process. These three faults have been described as arduous to detect by many authors. However, MEWMA-PCA's diagnosis

performance is not better than PCA. Therefore, a BN has been integrated to overcome the limitation of MEWMA-PCA. The combined MEWMA-PCA-BN framework is found to be providing an excellent solution to fault detection and diagnosis utilizing the benefit of MEWMA-PCA's early detection and BN's robust diagnosis capabilities.

7.2.2. Development of a Data-Driven and Automated Fault Diagnosis Tool

Accurate root cause diagnosis is inevitable for digitalized process systems. Due to close loop control and complex correlation among process variables, a single fault may generate many simultaneous warnings. This makes diagnosing the actual root cause extremely difficult. Conventionally, operators' experience is used to solve this problem. In this thesis, a data-driven and automated fault diagnosis module based on PCA and BN is used to reduce operators workload. PCA is the first stage fault diagnosis tool. As it cannot provide accurate diagnosis in all cases, a BN is used as the second stage diagnosis tool. In terms of data-based automation, the PCs are selected using the correlation dimension analysis that does not require human interference for PC selection. A new BN topology learning method has been developed from continuous process data. The quantitative parts of the BN (prior and conditional probabilities) are estimated using bivariate and vine copulas. The copula functions are found efficient in capturing the degree of dependence among process variables. Application of KDE on PCA residuals aids copula functions significantly in this context.

7.2.3. Development of a Framework for Simultaneous FDD and DRA

From a safety analysis perspective, along with FDD, a continuous dynamic risk estimate is required. However, the conventional process monitoring models heavily focus on FDD. Although there is progress on multivariate FDD and DRA, most of these works lack a diagnostic feature.

Also, these tools estimate the dynamic risk profiles from univariate fault probabilities. As a result, an inaccurate risk level may be estimated because the univariate fault probability does not account for the combined contribution of all the process variables to a fault. This research has provided a solution to these problems. The NBC has been used for FDD and multivariate fault probability estimation that is further used by the ET for failure prediction. This work provides new insight into multivariate dynamic safety assessment and will help to develop next-generation process monitoring schemes.

7.2.4. Development of a Risk-Based Abnormal Situation Management Framework

In this thesis, a risk-based abnormal situation management framework has been proposed using the R-vine copula and ETA. The R-vine model has the advantage over other tools such as the SOM, PCA, KF, and PF in elucidating accurate correlation structure among the process variables. Also, it can generate a multivariate fault probability without prior fault information that can be utilized for dynamic risk assessment. To effectively manage an abnormal situation, it is essential to identify the faulty variables. A DQA-based fault diagnosis module is proposed in this context; it diagnoses the root cause(s) once an unacceptable deviation is observed in the dynamic risk profile. An application to a Canadian refinery suggests that the developed risk-based framework could save its significant financial loss due to abnormal situations.

7.3. Future Work Scopes

This PhD thesis attempts to introduce new concepts and overcome the limitations of existing techniques in the fields of FDD and DRA in the context of process industries. This study, however, can be further improved by adopting the following recommendations.

7.3.1. Tuning Parameter Selection for MEWMA-PCA

One of the crucial parameters for MEWMA-PCA's successful performance is the tuning parameter, λ. In this thesis, an optimization technique proposed by Chen et al. (2001) is used to select an optimal λ. This method requires a lot of trial and error. Further research is required on how an optimal λ can be selected in a computational friendly way. The genetic algorithm and particle swarm optimization can be explored in this context.

7.3.2. Automated PC Selection for MEWMA-PCA

Since the MEWMA-PCA model requires user input regarding an expected variance to be captured, the PC selection is semi-automated. The CD-based PC selection technique can also be applied to the MEWMA-PCA model to eliminate this semi-automated feature.

7.3.3. Application of Advanced Machine Learning Algorithms in DRA

The naïve Bayes classifier may not be suitable for large-scale process systems. Advanced machine learning algorithms such as the deep neural network and ensemble methods (i.e. bagging, boosting, and stacking) can be used to predict multivariate fault probability. Nonetheless, these tools should only be considered when in-depth fault information is available.

7.3.4. Sensor Fault Detection Module

None of the developed methods has considered sensor fault detection module before passing the data to the rest of the algorithms. A bank of Kalman filters or rule-based methods can be used in this regard. This will help to isolate the sensor faults early and distinguish them from process and actuators faults.

7.3.5. Multimodal Process Handling

This thesis has considered a single operational mode for process operations. However, in reality, a process system may be operated in multiple modes. Suppose process variables' setpoints can be different depending on the product requirements. In such cases, the developed frameworks may not provide satisfactory performance. Hence, further research is required to develop dynamic safety analysis frameworks for multimodal process operations.

7.3.6. R-vine Copula-based BN Topology Learning

This research has proposed two techniques for BN topology learning. These are suitable for process fault diagnosis. The R-vine model can also be used for examining another possible topology learning invention. Such an example can be found in the work by Jia and Li (2020).

7.3.7. Dynamic Loss Modelling

The developed risk assessment methodologies have considered loss as a static component. However, this may result in inaccurate risk estimation. Estimating dynamic losses using loss functions may provide a viable solution to this problem.

7.3.8. Integration of Intentional and Natural Threats

The developed frameworks have considered that a failure can only happen due to random process variation. Cyber-attacks and physical intrusions can cause process failure in highly digitalized process systems. Also, although rare, natural disasters such as lightning, flood, tsunami, hurricane, and earthquake can lead to partial or complete process failure. Therefore, the more holistic nature of process accidents, including all the mentioned threats above, needs to be considered while advancing the current work.

7.3.9. Imperfect Data Treatment

This thesis has considered datasets with perfect quality. No outlier or missing data has been considered during the model development phase. However, industrial datasets are not always of perfect quality, and a commendable time is lost in data cleaning. If a model is built with outliers, it will be less sensitive to fault detection. Also, offline and real-time datasets may contain missing data. Therefore, further research is required to integrate imperfect data treatment techniques with the developed frameworks for a robust solution to FDD and DRA. The works by Imtiaz and Shah (2008) and Zhang and Dong (2014) can be helpful in this context.

References

Aas, K., 2016. Pair-copula constructions for financial applications: A review. Econometrics 4, 43. https://doi.org/10.3390/econometrics4040043

Aas, K., Czado, C., Frigessi, A., Bakken, H., 2009. Pair-copula constructions of multiple dependence. Insur. Math. Econ. 44, 182–198. https://doi.org/10.1016/j.insmatheco.2007.02.001

Adedigba, S.A., Khan, F., Yang, M., 2017. Dynamic failure analysis of process systems using principal component analysis and Bayesian network. Ind. Eng. Chem. Res. 56, 2094–2106. https://doi.org/10.1021/acs.iecr.6b03356

Adedigba, S.A., Khan, F., Yang, M., 2016a. Dynamic safety analysis of process systems using nonlinear and non-sequential accident model. Chem. Eng. Res. Des. 111, 169–183. https://doi.org/10.1016/j.cherd.2016.04.013

Adedigba, S.A., Khan, F., Yang, M., 2016b. Process accident model considering dependency among contributory factors. Process Saf. Environ. Prot. 102, 633–647. https://doi.org/10.1016/j.psep.2016.05.004

Akaike, H., 1974. A new look at the statistical model identification. IEEE Trans. Automat. Contr. 19, 716–723. https://doi.org/10.1109/TAC.1974.1100705

Alauddin, M., Khan, F., Imtiaz, S., Ahmed, S., 2018. A bibliometric review and analysis of data-driven fault detection and diagnosis methods for process systems. Ind. Eng. Chem. Res. 57, 10719–10735. https://doi.org/10.1021/acs.iecr.8b00936

Alcala, C.F., Qin, S.J., 2010. Reconstruction-based contribution for process monitoring with kernel principal component analysis. Ind. Eng. Chem. Res. 49, 7849–7857. https://doi.org/10.1021/ie9018947

Alcala, C.F., Qin, S.J., 2009. Reconstruction-based contribution for process monitoring. Automatica 45, 1593–1600. https://doi.org/10.1016/j.automatica.2009.02.027

Amin, M.T., Imtiaz, S., Khan, F., 2018a. Process system fault detection and diagnosis using a hybrid technique. Chem. Eng. Sci. 189. https://doi.org/10.1016/j.ces.2018.05.045

Amin, M.T., Imtiaz, S., Khan, F., 2018b. Process system fault detection and diagnosis using a hybrid technique. Chem. Eng. Sci. 189, 191–211. https://doi.org/10.1016/j.ces.2018.05.045

Amin, M.T., Imtiaz, S., Khan, F., 2017. Process fault detection and root cause diagnosis using a hybrid technique, in: Fifth International Conference on Chemical Engineering (ICChE 2017). pp. 461–489. https://doi.org/http://icche-buet.com/index.php/icche/icche2017/paper/viewFile/104/68

Amin, M.T., Khan, F., Ahmed, S., Imtiaz, S., 2020. A novel data-driven methodology for fault detection and dynamic risk assessment. Can. J. Chem. Eng. 1–20. https://doi.org/https://doi.org/10.1002/cjce.23760

Amin, M.T., Khan, F., Amyotte, P., 2019a. A bibliometric review of process safety and risk analysis. Process Saf. Environ. Prot. 126, 366–381. https://doi.org/10.1016/j.psep.2019.04.015

Amin, M.T., Khan, F., Imtiaz, S., 2019b. Fault detection and pathway analysis using a dynamic Bayesian network. Chem. Eng. Sci. 195, 777–790. https://doi.org/https://doi.org/10.1016/j.ces.2018.10.024

Amin, M.T., Khan, F., Imtiaz, S., 2018c. Dynamic availability assessment of safety critical systems using a dynamic Bayesian network. Reliab. Eng. Syst. Saf. 178, 108–117. https://doi.org/10.1016/j.ress.2018.05.017

Amin, M.T., Khan, F., Imtiaz, S.A., Ahmed, S., 2019c. Robust process monitoring methodology

for detection and diagnosis of unobservable faults. Ind. Eng. Chem. Res. 58, 19149−19165. https://doi.org/https://doi.org/10.1021/acs.iecr.9b03406

Amruthnath, N., Gupta, T., 2018. A research study on unsupervised machine learning algorithms for early fault detection in predictive maintenance, in: 2018 5th International Conference on Industrial Engineering and Applications, ICIEA 2018. pp. 355–361. https://doi.org/10.1109/IEA.2018.8387124

Aparisi, F., García-Díaz, J.C., 2007. Design and optimization of EWMA control charts for in-control, indifference, and out-of-control regions. Comput. Oper. Res. 34, 2096–2108. https://doi.org/10.1016/j.cor.2005.08.003

Bakshi, B.R., 1998. Multiscale PCA with application to multivariate statistical process monitoring. AIChE J. 44, 1596–1610. https://doi.org/10.1002/aic.690440712

Bao, H., Khan, F., Iqbal, T., Chang, Y., 2011. Risk-based fault diagnosis and safety management for process systems. Process Saf. Prog. 30, 6–17. https://doi.org/https://doi.org/10.1002/prs.10421

Barua, S., Gao, X., Pasman, H., Mannan, M.S., 2016. Bayesian network based dynamic operational risk assessment. J. Loss Prev. Process Ind. 41, 399–410. https://doi.org/10.1016/j.jlp.2015.11.024

Bathelt, A., Ricker, N.L., Jelali, M., 2015. Revision of the Tennessee Eastman process model. IFAC-PapersOnLine 48, 309–314. https://doi.org/https://doi.org/10.1016/j.ifacol.2015.08.199

Bobbio, A., Portinale, L., Minichino, M., Ciancamerla, E., 2001. Improving the analysis of dependable systems by mapping fault trees into Bayesian networks. Reliab. Eng. Syst. Saf. 71, 249–260. https://doi.org/https://doi.org/10.1016/S0951-8320(00)00077-6

Boullé, M., 2007. Compression-based averaging of selective naive Bayes classifiers. J. Mach. Learn. Res. 8, 1659–1685.

Bowman, A.W., Azzalini, A., 1997. Applied smoothing techniques for data analysis: the kernel approach with S-Plus illustrations. OUP Oxford.

Brechmann, E.C., Czado, C., Aas, K., 2012. Truncated regular vines in high dimensions with application to financial data. Can. J. Stat. 40, 68–85. https://doi.org/10.1002/cjs.10141

Brechmann, E.C., Joe, H., 2015. Truncation of vine copulas using fit indices. J. Multivar. Anal. 138, 19–33. https://doi.org/10.1016/j.jmva.2015.02.012

Brechmann, E.C., Schepsmeier, U., 2013. Modeling dependence with C- and D-vine copulas: The R package CDVine. J. Stat. Softw. 52, 1–27. https://doi.org/10.18637/jss.v052.i03

Cai, B., Liu, Y., Liu, Z., Tian, X., Dong, X., Yu, S., 2012. Using Bayesian networks in reliability evaluation for subsea blowout preventer control system. Reliab. Eng. Syst. Saf. 108, 32–41. https://doi.org/10.1016/j.ress.2012.07.006

Capaci, F., Vanhatalo, E., Kulahci, M., Bergquist, B., 2018. The revised Tennessee Eastman process simulator as testbed for SPC and DoE methods. Qual. Eng. 1–18. https://doi.org/10.1080/08982112.2018.1461905

Carson, P.K., Yeh, A.B., 2008. Exponentially weighted moving average (EWMA) control charts for monitoring an analytical process. Ind. Eng. Chem. Res. 47, 405–411. https://doi.org/10.1021/ie070589b

Cattell, R.B., 1966. The scree test for the number of factors. Multivariate Behav. Res. 1, 245–276. https://doi.org/10.1207/s15327906mbr0102_10

Chen, J., Liao, C.-M., Lin, F.R.J., Lu, M.-J., 2001. Principle component analysis based control charts with memory effect for process monitoring. Ind. Eng. Chem. Res. 40, 1516–1527.

https://doi.org/10.1021/ie000407c

Chen, J., Liu, K.C., 2002. On-line batch process monitoring using dynamic PCA and dynamic PLS models. Chem. Eng. Sci. 57, 63–75. https://doi.org/10.1016/S0009-2509(01)00366-9

Cheng, C.Y., Hsu, C.C., Chen, M.C., 2010. Adaptive kernel principal component analysis (KPCA) for monitoring small disturbances of nonlinear processes. Ind. Eng. Chem. Res. 49, 2254–2262. https://doi.org/10.1021/ie900521b

Chiang, L., Russell, E.L., Braatz, R.D., 2001. Fault detection and diagnosis in industrial systems. Springer-Verlag London.

Chiang, L., Russell, E.L. El, Braatz, R.R.D., 2000. Fault diagnosis in chemical processes using Fisher discriminant analysis, discriminant partial least squares, and principal component analysis. Chemom. Intell. … 50, 243–252. https://doi.org/10.1016/S0169-7439(99)00061-1

Cho, J.-H., Lee, J.-M., Wook Choi, S., Lee, D., Lee, I.-B., 2005. Fault identification for process monitoring using kernel principal component analysis. Chem. Eng. Sci. 60, 279–288. https://doi.org/10.1016/j.ces.2004.08.007

Chouaib, C., Mohamed-Faouzi, H., Messaoud, D., 2015. New adaptive kernel principal component analysis for nonlinear dynamic process monitoring. Appl. Math. Inf. Sci. 9, 1833–1845.

Cui, Q., Li, S., 2020. Process monitoring method based on correlation variable classification and vine copula. Can. J. Chem. Eng. 1–18. https://doi.org/https://doi.org/10.1002/cjce.23702

De Vargas, V.D.C.C., Lopes, L.F.D., Souza, A.M., 2004. Comparative study of the performance of the CuSum and EWMA control charts. Comput. Ind. Eng. 46, 707–724. https://doi.org/10.1016/j.cie.2004.05.025

Ding, S.X., Zhang, P., Naik, A., Ding, E.L., Huang, B., 2009. Subspace method aided data-driven design of fault detection and isolation systems. J. Process Control 19, 1496–1510.

https://doi.org/10.1016/j.jprocont.2009.07.005

Domingos, P., Pazzani, M., 1997. On the optimality of the simple Bayesian classifier under zero-one loss. Mach. Learn. 29, 103–130.

Dong, Y., Qin, S.J., 2018. A novel dynamic PCA algorithm for dynamic data modeling and process monitoring. J. Process Control 67, 1–11. https://doi.org/10.1016/j.jprocont.2017.05.002

Downs, J.J., Vogel, E.F., 1993. A plant-wide industrial process control problem. Comput. Chem. Eng. 17, 245–255. https://doi.org/10.1016/0098-1354(93)80018-I

Du, Y., Du, D., 2018. Fault detection and diagnosis using empirical mode decomposition based principal component analysis. Comput. Chem. Eng. 115, 1–21. https://doi.org/https://doi.org/10.1016/j.compchemeng.2018.03.022

Elidan, G., 2010. Copula bayesian networks, in: Advances in Neural Information Processing Systems. pp. 559–567.

Fan, J., Wang, Y., 2014. Fault detection and diagnosis of non-linear non-Gaussian dynamic processes using kernel dynamic independent component analysis. Inf. Sci. (Ny). 259, 369–379. https://doi.org/10.1016/j.ins.2013.06.021

Fan, L., Poh, K.L., 2007. A comparative study of PCA, ICA and class-conditional ICA for naïve bayes classifier, in: Lecture Notes in Computer Science (Including Subseries Lecture Notes in Artificial Intelligence and Lecture Notes in Bioinformatics). pp. 16–22.

Fortune, 2021. Global 500 [WWW Document]. https://doi.org/https://fortune.com/fortune500/

Friedman, N., Nachman, I., Pe’er, D., 2013. Learning Bayesian network structure from massive datasets: The" sparse candidate" algorithm. arXiv Prepr. arXiv1301.6696 206–215.

Gabbar, H.A., Boafo, E.K., 2016. FSN-based cosimulation for fault propagation analysis in nuclear power plants. Process Saf. Prog. 35, 53–60. https://doi.org/10.1002/prs.11725

Gabbar, H.A., Hussain, S., Hosseini, A.H., 2014. Simulation-based fault propagation analysis - Application on hydrogen production plant. Process Saf. Environ. Prot. 92, 723–731. https://doi.org/10.1016/j.psep.2013.12.006

Gabbar, H.A., Isham, M., Hussain, S., Zhang, L., 2015. BBN-based reasoning approach for safety verification using FSN. J. Chem. Eng. Japan 48, 684–689. https://doi.org/10.1252/jcej.14we298

Gajjar, S., Kulahci, M., Palazoglu, A., 2018. Real-time fault detection and diagnosis using sparse principal component analysis. J. Process Control 67, 112–128. https://doi.org/10.1016/j.jprocont.2017.03.005

Galagedarage Don, M., Khan, F., 2019. Dynamic process fault detection and diagnosis based on a combined approach of hidden Markov and Bayesian network model. Chem. Eng. Sci. 201, 82–96. https://doi.org/10.1016/j.ces.2019.01.060

Gao, Z., Cecati, C., Ding, S.X., 2015. A survey of fault diagnosis and fault-tolerant techniques-part II: Fault diagnosis with knowledge-based and hybrid/active approaches. IEEE Trans. Ind. Electron. 62, 3768–3774. https://doi.org/10.1109/TIE.2015.2419013

Garcia-Alvarez, D., Fuente, M.J., Sainz, G.I., 2012. Fault detection and isolation in transient states using principal component analysis. J. Process Control 22, 551–563. https://doi.org/10.1016/j.jprocont.2012.01.007

Garcia-Alvarez, D., Fuente, M.J., Vega, P., Sainz, G., 2009. Fault detection and diagnosis using multivariate statistical techniques in a wastewater treatment plant. IFAC Proc. Vol. 42, 952–957. https://doi.org/https://doi.org/10.3182/20090712-4-TR-2008.00156

Ge, Z., 2017. Review on data-driven modeling and monitoring for plant-wide industrial processes. Chemom. Intell. Lab. Syst. 171, 16–25. https://doi.org/10.1016/j.chemolab.2017.09.021

Ge, Z., Song, Z., Gao, F., 2013. Review of recent research on data-based process monitoring. Ind. Eng. Chem. Res. 52, 3543–3562. https://doi.org/https://doi.org/10.1021/ie302069q

Gharahbagheri, H., Imtiaz, S., Khan, F., 2017a. Combination of KPCA and causality analysis for root cause diagnosis of industrial process fault. Can. J. Chem. Eng. https://doi.org/10.1002/cjce.22852

Gharahbagheri, H., Imtiaz, S., Khan, F., Ahmed, S., 2015. Causality analysis for root cause diagnosis in Fluid Catalytic Cracking unit. IFAC-PapersOnLine. https://doi.org/10.1016/j.ifacol.2015.09.631

Gharahbagheri, H., Imtiaz, S.A., Khan, F., 2017b. Root cause diagnosis of process fault using KPCA and Bayesian network. Ind. Eng. Chem. Res. 56, 2054–2070. https://doi.org/10.1021/acs.iecr.6b01916

Ghosh, A., Ahmed, S., Khan, F., 2019. Modeling and testing of temporal dependency in the failure of a process system. Ind. Eng. Chem. Res. 58, 8162−8171. https://doi.org/10.1021/acs.iecr.8b06300

Ghosh, A., Ahmed, S., Khan, F., Rusli, R., 2020. Process safety assessment considering multivariate non-linear dependence among process variables. Process Saf. Environ. Prot. 135, 70–80. https://doi.org/https://doi.org/10.1016/j.psep.2019.12.006

Grassberger, P., Procaccia, I., 1983. Measuring the strangeness of strange attractors. Phys. D Nonlinear Phenom. 9, 189–208. https://doi.org/10.1016/0167-2789(83)90298-1

Guo, C., Khan, F., Imtiaz, S., 2019. Copula-based Bayesian network model for process system risk assessment. Process Saf. Environ. Prot. 123, 317–326. https://doi.org/10.1016/j.psep.2019.01.022

Han, S.W., Tsui, K.L., Ariyajuny, B., Kim, S.B., 2010. A comparison of CUSUM, EWMA, and

temporal scan statistics for detection of increases in poisson rates. Qual. Reliab. Eng. Int. 26, 279–289. https://doi.org/10.1002/qre.1056

Hashemi, S.J., Ahmed, S., Khan, F.I., 2014. Risk-based operational performance analysis using loss functions. Chem. Eng. Sci. 116, 99–108. https://doi.org/10.1016/j.ces.2014.04.042

Hashemi, S.J., Khan, F., Ahmed, S., 2016. Multivariate probabilistic safety analysis of process facilities using the Copula Bayesian Network model. Comput. Chem. Eng. 93, 128–142. https://doi.org/10.1016/j.compchemeng.2016.06.011

Hawkins, D.M., Wu, Q., 2014. The CUSUM and the EWMA head-to-head. Qual. Eng. 26, 215–222. https://doi.org/10.1080/08982112.2013.817014

He, Q.P., Wang, J., 2018. Statistical process monitoring as a big data analytics tool for smart manufacturing. J. Process Control 67, 35–43. https://doi.org/10.1016/j.jprocont.2017.06.012

He, Y.L., Wang, R., Kwong, S., Wang, X.Z., 2014. Bayesian classifiers based on probability density estimation and their applications to simultaneous fault diagnosis. Inf. Sci. (Ny). 259, 252–268. https://doi.org/10.1016/j.ins.2013.09.003

Heckerman, D., Geiger, D., Chickering, D.M., 1995. Learning Bayesian networks: The combination of knowledge and statistical data. Mach. Learn. 20, 197–243.

How, B. shen, Lam, H.L., 2018. Sustainability evaluation for biomass supply chain synthesis: novel principal component analysis (PCA) aided optimisation approach. J. Clean. Prod. 189, 941–961. https://doi.org/10.1016/j.jclepro.2018.03.104

Hsu, C.C., Chen, L.S., Liu, C.H., 2010. A process monitoring scheme based on independent component analysis and adjusted outliers. Int. J. Prod. Res. 48, 1727–1743. https://doi.org/10.1080/00207540802552683

Hunter, J.S., 1986. The exponentially weighted moving average. J. Qual. Technol. 18, 203–210.

https://doi.org/https://doi.org/10.1080/00224065.1986.11979014

Ibargüengoytla, P.H., Sucar, L.E., Vadera, S., 1996. A probabilistic model for sensor validation, in: Proceedings of the Twelfth International Conference on Uncertainty in Artificial Intelligence, UAI'96. Morgan Kaufmann Publishers Inc., San Francisco, CA, USA, pp. 332–339.

Imtiaz, S.A., Shah, S.L., 2008. Treatment of missing values in process data analysis. Can. J. Chem. Eng. 86, 838–858. https://doi.org/10.1002/cjce.20099

Imtiaz, S.A., Shah, S.L., Patwardhan, R., Palizban, H.A., Ruppenstein, J., 2008. Detection, diagnosis and root Cause analysis of sheet-break in a pulp and paper mill with cconomic impact analysis. Can. J. Chem. Eng. 85, 512–525. https://doi.org/10.1002/cjce.5450850413

Isermann, R., 2005. Fault-diagnosis systems: an introduction from fault detection to fault tolerance. Springer Science & Business Media.

Islam, R., Khan, F., Venkatesan, R., 2017. Real time risk analysis of kick detection: Testing and validation. Reliab. Eng. Syst. Saf. 161, 25–37. https://doi.org/10.1016/j.ress.2016.12.014

Jackson, J.E., 2005. A user's guide to principal components. John Wiley & Sons.

Jackson, J.E., Mudholkar, G.S., 1979. Control procedures for residuals associated with principal component analysis. Technometrics 21, 341–349. https://doi.org/10.1080/00401706.1979.10489779

Jia, M., Chu, F., Wang, F., Wang, W., 2010. On-line batch process monitoring using batch dynamic kernel principal component analysis. Chemom. Intell. Lab. Syst. 101, 110–122. https://doi.org/10.1016/j.chemolab.2010.02.004

Jia, Q., Li, S., 2020. Process monitoring and fault diagnosis based on a regular vine and Bayesian network. Ind. Eng. Chem. Res. 59, 12144–12155. https://doi.org/10.1021/acs.iecr.0c01474

Jia, Q., Zhang, Y., 2016. Quality-related fault detection approach based on dynamic kernel partial least squares. Chem. Eng. Res. Des. 106, 242–252. https://doi.org/10.1016/j.cherd.2015.12.015

Jiang, Q., Yan, X., Huang, B., 2019. Review and perspectives of data-driven distributed monitoring for industrial plant-wide processes. Ind. Eng. Chem. Res. 58, 12899–12912. https://doi.org/10.1021/acs.iecr.9b02391

Jiang, Q., Yan, X., Li, J., 2016. PCA-ICA integrated with Bayesian method for non-Gaussian fault diagnosis. Ind. Eng. Chem. Res. 55, 4979–4986. https://doi.org/10.1021/acs.iecr.5b04023

Joe, H., 1996. Families of m-variate distributions with given margins and m (m-1)/2 bivariate dependence parameters. Lect. Notes-Monograph Ser. 28, 120–141.

Kalantarnia, M., Khan, F., Hawboldt, K., 2009. Dynamic risk assessment using failure assessment and Bayesian theory. J. Loss Prev. Process Ind. 22, 600–606. https://doi.org/10.1016/j.jlp.2009.04.006

Kanes, R., Ramirez Marengo, M.C., Abdel-Moati, H., Cranefield, J., Véchot, L., 2017. Developing a framework for dynamic risk assessment using Bayesian networks and reliability data. J. Loss Prev. Process Ind. 50, 142–153. https://doi.org/10.1016/j.jlp.2017.09.011

Kano, M., Tanaka, S., Hasebe, S., Hashimoto, I., Ohno, H., 2003. Monitoring independent components for fault detection. AIChE J. 49, 969–976. https://doi.org/10.1002/aic.690490414

Kendall, M.G., 1938. A new measure of rank correlation. Biometrika 30, 81–93. https://doi.org/10.2307/2332226

Khakzad, N., Khan, F., Amyotte, P., 2013. Dynamic safety analysis of process systems by mapping bow-tie into Bayesian network. Process Saf. Environ. Prot. 91, 46–53.

https://doi.org/10.1016/j.psep.2012.01.005

Khakzad, N., Khan, F., Amyotte, P., 2012. Dynamic risk analysis using bow-tie approach. Reliab. Eng. Syst. Saf. 104, 36–44. https://doi.org/10.1016/j.ress.2012.04.003

Khan, F., Amyotte, P., Adedigba, S., 2021. Process safety concerns in process system digitalization. Educ. Chem. Eng. 34, 33–46. https://doi.org/10.1016/j.ece.2020.11.002

Khan, F., Thodi, P., Imtiaz, S., Abbassi, R., 2016. Real-time monitoring and management of offshore process system integrity. Curr. Opin. Chem. Eng. 14, 61–71. https://doi.org/https://doi.org/10.1016/j.coche.2016.08.015

Khan, F.I., Abbasi, S.A., 1999. Major accidents in process industries and an analysis of causes and consequences. J. Loss Prev. Process Ind. 12, 361–378. https://doi.org/10.1016/S0950-4230(98)00062-X

Khan, F.I., Amyotte, P.R., Amin, M.T., 2020. Advanced methods of risk assessment and management: An overview. pp. 1–34. https://doi.org/10.1016/bs.mcps.2020.03.002

Kim, K., Lee, J.M., Lee, I.B., 2005. A novel multivariate regression approach based on kernel partial least squares with orthogonal signal correction. Chemom. Intell. Lab. Syst. 79, 22–30. https://doi.org/10.1016/j.chemolab.2005.03.003

Koivo, H.N., 1994. Artificial neural networks in fault diagnosis and control. Control Eng. Pract. 2, 89–101. https://doi.org/https://doi.org/10.1016/0967-0661(94)90577-0

Kondaveeti, S.R., Shah, S.L., Izadi, I., 2009. Application of multivariate statistics for efficient alarm generation. IFAC Proc. Vol. 42, 657–662. https://doi.org/10.3182/20090630-4-ES-2003.0383

Kramer, M.A., 1991. Nonlinear principal component analysis using autoassociative neural networks. AIChE J. 37, 233–243.

Kramer, M.A., Palowitch, B.L., 1987. A rule-based approach to fault diagnosis using the signed directed graph. AIChE J. 33, 1067–1078.

Kresta, J. V., Macgregor, J.F., Marlin, T.E., 1991. Multivariate statistical monitoring of process operating performance. Can. J. Chem. Eng. 69, 35–47. https://doi.org/10.1258/phleb.2011.010101

Krishnannair, S., Aldrich, C., 2017. Fault detection in the Tennessee Eastman benchmark process with nonlinear singular spectrum analysis. IFAC-PapersOnLine 50, 8005–8010. https://doi.org/10.1016/j.ifacol.2017.08.1223

Ku, W., Storer, R.H., Georgakis, C., 1995. Disturbance detection and isolation by dynamic principal component analysis. Chemom. Intell. Lab. Syst. 30, 179–196. https://doi.org/https://doi.org/10.1016/0169-7439(95)00076-3

Kullback, S., Leibler, R.A., 1951. On information and sufficiency. Ann. Math. Stat. 22, 79–86. https://doi.org/10.1214/aoms/1177729694

Lane, S., Martin, E.B., Morris, A.J., Gower, P., 2003. Application of exponentially weighted principal component analysis for the monitoring of a polymer film manufacturing process. Trans. Inst. Meas. Control 25, 17–35. https://doi.org/10.1191/0142331203tm071oa

Lee, J.-M., Qin, S.J., Lee, I.-B., 2007. Fault detection of non-ninear processes using kernel independent component analysis. Can. J. Chem. Eng. 85, 526–536. https://doi.org/10.1002/cjce.5450850414

Lee, J.-M., Qin, S.J., Lee, I.-B., 2006. Fault detection and diagnosis based on modified independent component analysis. AIChE J. 52, 3501–3514. https://doi.org/10.1002/aic.10978

Lee, J.-M., Yoo, C., Choi, S.W., Vanrolleghem, P.A., Lee, I.-B., 2004a. Nonlinear process monitoring using kernel principal component analysis. Chem. Eng. Sci. 59, 223–234.

https://doi.org/10.1016/j.ces.2003.09.012

Lee, J.-M., Yoo, C., Lee, I.-B., 2004b. Statistical process monitoring with independent component analysis. J. Process Control 14, 467–485. https://doi.org/10.1016/j.jprocont.2003.09.004

Lee, J.M., Yoo, C., Lee, I.B., 2003. Statistical process monitoring with multivariate exponentially weighted moving average and independent component analysis. J. Chem. Eng. Japan 36, 563–577. https://doi.org/10.1252/jcej.36.563

Li, G., Qin, S.J., Yuan, T., 2016. Data-driven root cause diagnosis of faults in process industries. Chemom. Intell. Lab. Syst. 159, 1–11. https://doi.org/10.1016/j.chemolab.2016.09.006

Liu, J., 2012. Fault diagnosis using contribution plots without smearing effect on non-faulty variables. J. Process Control 22, 1609–1623. https://doi.org/10.1016/j.jprocont.2012.06.016

Lowry, C.A., Woodall, W.H., Champ, C.W., Rigdon, S.E., 1992. A multivariate exponentially weighted moving average control chart. Technometrics 34, 46–53. https://doi.org/10.1080/00401706.1992.10485232

Lyman, P.R., Georgakis, C., 1995. Plant-wide control of the Tennessee Eastman problem. Comput. Chem. Eng. 19, 321–331. https://doi.org/10.1016/0098-1354(94)00057-U

MacGregor, J.F., Jaeckle, C., Kiparissides, C., Koutoudi, M., 1994. Process monitoring and diagnosis by multiblock PLS methods. AIChE J. 40, 826–838. https://doi.org/10.1002/aic.690400509

Malinowski, E.R., Howery, D.G., 1980. Factor analysis in chemistry. Wiley New York, New York.

Mallick, M.R., Imtiaz, S.A., 2013. A hybrid method for process fault detection and diagnosis. IFAC Proc. Vol. 46, 827–832. https://doi.org/https://doi.org/10.3182/20131218-3-IN-2045.00099

Mannan, M.S., Reyes-Valdes, O., Jain, P., Tamim, N., Ahammad, M., 2016. The evolution of

process safety: current status and future direction. Annu. Rev. Chem. Biomol. Eng. 7, 135–162. https://doi.org/10.1146/annurev-chembioeng-080615-033640

Mehranbod, N., Soroush, M., Panjapornpon, C., 2005. A method of sensor fault detection and identification. J. Process Control 15, 321–339.

Mehranbod, N., Soroush, M., Piovoso, M., Ogunnaike, B.A., 2003. Probabilistic model for sensor fault detection and identification. AIChE J. 49, 1787–1802.

Meng, Q.Q., Zhu, Q.X., Gao, H.H., He, Y.L., Xu, Y., 2019. A novel scoring function based on family transfer entropy for Bayesian networks learning and its application to industrial alarm systems. J. Process Control. https://doi.org/10.1016/j.jprocont.2019.01.013

Miller, P., Swanson, R., Heckler, C., 1998. Contribution plots: a missing link in multivariate quality control. Int. J. Appl. Math. Comput. Sci. 8, 775–792.

Misra, M., Yue, H.H., Qin, S.J., Ling, C., 2002. Multivariate process monitoring and fault diagnosis by multi-scale PCA. Comput. Chem. Eng. 26, 1281–1293. https://doi.org/10.1016/S0098-1354(02)00093-5

Mnassri, B., El Adel, E.M., Ananou, B., Ouladsine, M., 2009. Fault detection and diagnosis based on PCA and a new contribution plots. IFAC Proc. Vol. 42, 834–839. https://doi.org/10.3182/20090630-4-ES-2003.0117

Mnassri, B., El Adel, E.M., Ouladsine, M., 2015. Reconstruction-based contribution approaches for improved fault diagnosis using principal component analysis. J. Process Control 33, 60–76. https://doi.org/10.1016/j.jprocont.2015.06.004

Montgomery, D.C., 2007. Introduction to statistical quality control, 5th Editio. ed. John Wiley & Sons.

Montgomery, D.C., Runger, G.C., 2010. Applied statistics and probability for engineers. John

Wiley & Sons.

Moshgbar, M., Hammond, S., 2010. Advanced process control. Qual. Assur. J. 13, 62–66. https://doi.org/https://doi.org/10.1002/qaj.472

Muralidharan, V., Sugumaran, V., 2012. A comparative study of Naïve Bayes classifier and Bayes net classifier for fault diagnosis of monoblock centrifugal pump using wavelet analysis. Appl. Soft Comput. J. 12, 2023–2029. https://doi.org/10.1016/j.asoc.2012.03.021

Neapolitan, R.E., 2004. Learning bayesian networks. Pearson Prentice Hall Upper Saddle River, NJ.

Neogi, D., Schlags, C.E., 1998. Multivariate statistical analysis of an emulsion batch process. Ind. Eng. Chem. Res. 37, 3971–3979. https://doi.org/10.1021/ie980243o

Pandey, Y.N., Rastogi, A., Kainkaryam, S., Bhattacharya, S., Saputelli, L., 2020. Machine Learning in the Oil and Gas Industry. Apress. https://doi.org/10.1007/978-1-4842-6094-4

Pearson, K., 1901. LIII. On lines and planes of closest fit to systems of points in space. London, Edinburgh, Dublin Philos. Mag. J. Sci. 2, 559–572. https://doi.org/10.1080/14786440109462720

Pei, X., Yamashita, Y., Yoshida, M., Matsumoto, S., 2008. Fault detection in chemical processes using discriminant analysis and control chart. J. Chem. Eng. Japan 41, 25–31. https://doi.org/10.1252/jcej.07WE088

Ping, P., Wang, K., Kong, D., Chen, G., 2018. Estimating probability of success of escape, evacuation, and rescue (EER) on the offshore platform by integrating Bayesian Network and Fuzzy AHP. J. Loss Prev. Process Ind. 54, 57–68. https://doi.org/10.1016/j.jlp.2018.02.007

Prabhu, S.S., Runger, G.C., 2018. Designing a Multivariate EWMA Control Chart. J. Qual. Technol. 29, 8–15. https://doi.org/10.1080/00224065.1997.11979720

Qin, S.J., 2009. Data-driven fault detection and diagnosis for complex industrial processes. IFAC Proc. Vol. 42, 1115–1125.

Qin, S.J., 2003. Statistical process monitoring: basics and beyond. J. Chemom. 17, 480–502. https://doi.org/10.1002/cem.800

Rathnayaka, S., Khan, F., Amyotte, P., 2011a. SHIPP methodology: Predictive accident modeling approach. Part II. Validation with case study. Process Saf. Environ. Prot. 89, 75–88. https://doi.org/10.1016/j.exger.2014.09.014

Rathnayaka, S., Khan, F., Amyotte, P., 2011b. SHIPP methodology: Predictive accident modeling approach. Part I: Methodology and model description. Process Saf. Environ. Prot. 89, 151–164. https://doi.org/10.1016/j.psep.2011.01.002

Rato, T.J., Reis, M.S., 2013. Fault detection in the Tennessee Eastman benchmark process using dynamic principal components analysis based on decorrelated residuals (DPCA-DR). Chemom. Intell. Lab. Syst. 125, 101–108. https://doi.org/10.1016/j.chemolab.2013.04.002

Reis, M.S., Kenett, R., 2018. Assessing the value of information of data-centric activities in the chemical processing industry 4.0. AIChE J. 64, 3868–3881. https://doi.org/10.1002/aic.16203

Ren, X., Tian, Y., Li, S., 2015. Vine copula-based dependence description for multivariate multimode process monitoring. Ind. Eng. Chem. Res. 54, 10001–10019. https://doi.org/10.1021/acs.iecr.5b01267

Ren, X., Zhu, K., Cai, T., Li, S., 2017. Fault detection and diagnosis for nonlinear and non-Gaussian processes based on copula subspace division. Ind. Eng. Chem. Res. 56, 11545–11564. https://doi.org/10.1021/acs.iecr.7b02419

Reshef, Y.A., Reshef, D.N., Sabeti, P.C., Mitzenmacher, M., 2014. Theoretical foundations of equitability and the maximal information coefficient. arXiv Prepr. arXiv1408.4908.

Ricker, N.L., 2005. Tennessee Eastman Challenge Archive. https://doi.org/http://depts.washington.edu/con-trol/LARRY/TE/download.html

Ricker, N.L., 1996. Decentralized control of the Tennessee Eastman Challenge Process. J. Process Control 6, 205–221. https://doi.org/10.1016/0959-1524(96)00031-5

Rojas-Guzman, C., Kramer, M.A., 1993. Comparison of belief networks and rule-based expert systems for fault diagnosis of chemical processes. Eng. Appl. Artif. Intell. 6, 191–202. https://doi.org/10.1016/0952-1976(93)90062-3

Rostamabadi, A., Jahangiri, M., Zarei, E., Kamalinia, M., Alimohammadlou, M., 2020. A novel fuzzy Bayesian network approach for safety analysis of process systems; an application of HFACS and SHIPP methodology. J. Clean. Prod. 244, 118761. https://doi.org/10.1016/j.jclepro.2019.118761

Salahshoor, K., Kiasi, F., 2008. Online statistical monitoring and fault classification of the Tennessee Eastman challenge process based on dynamic independent component analysis and support vector machine. IFAC Proc. Vol. 41, 7405–7412. https://doi.org/https://doi.org/10.3182/20080706-5-KR-1001.01252

Schwarz, G., 1978. Estimating the dimension of a model. Ann. Stat. 6, 461–464. https://doi.org/10.1214/aos/1176344136

Shams, M.A. Bin, Budman, H.M., Duever, T.A., 2011. Fault detection, identification and diagnosis using CUSUM based PCA. Chem. Eng. Sci. 66, 4488–4498. https://doi.org/https://doi.org/10.1016/j.ces.2011.05.028

Shewhart, W.A., 1930. Economic quality control of manufactured product. Bell Labs Tech. J. 9, 364–389.

Silverman, B.W., 1986. Density estimation for statistics and data analysis. Chapman and

Hall/CRC, New York. https://doi.org/10.1007/978-1-4899-3324-9

Sklar, A., 1959. Fonctions de reprtition an dimensions et leursmarges. Publ. l'Institut Stat. l'Universit´e Paris 8, 229–231.

Skogestad, S., 1997. Dynamics and control of distillation columns: A tutorial introduction. Chem. Eng. Res. Des. 75, 539–562. https://doi.org/https://doi.org/10.1205/026387697524092

Skogestad, S., Morari, M., 1988. LV-Control of a high-purity distillation column. Chem. Eng. Sci. 43, 33–48. https://doi.org/10.1016/0009-2509(88)87124-0

Talebberrouane, M., Khan, F., Lounis, Z., 2016. Availability analysis of safety critical systems using advanced fault tree and stochastic Petri net formalisms. J. Loss Prev. Process Ind. 44, 193–203. https://doi.org/10.1016/j.jlp.2016.09.007

Thornhill, N.F., Patwardhan, S.C., Shah, S.L., 2008. A continuous stirred tank heater simulation model with applications. J. Process Control 18, 347–360. https://doi.org/10.1016/j.jprocont.2007.07.006

Tong, C., El-Farra, N.H., Palazoglu, A., Yan, X., 2014. Fault detection and isolation in hybrid process systems using a combined data-driven and observer-design methodology. AIChE J. 60, 2805–2814. https://doi.org/10.1002/aic.14475

Vahed, S.H., Mokhtare, M., Nozari, H.A., Shoorehdeli, M.A., Simani, S., 2010. Fault detection and isolation of Tennessee Eastman process, in: Proceedings of the 8th ACD 2010 European Workshop on Advanced Control and Diagnosis. Ferrara, Italy, pp. 362–367.

Valle, S., Li, W., Qin, S.J., 1999. Selection of the number of principal components: The variance of the reconstruction error criterion with a comparison to other methods. Ind. Eng. Chem. Res. 38, 4389–4401. https://doi.org/10.1021/ie990110i

Vathoopan, M., Johny, M., Zoitl, A., Knoll, A., 2018. Modular fault ascription and corrective

maintenance using a digital twin. pp. 1041–1046. https://doi.org/10.1016/j.ifacol.2018.08.470

Vedam, H., Venkatasubramanian, V., 1999. PCA-SDG based process monitoring and fault diagnosis. Control Eng. Pract. 7, 903–917. https://doi.org/https://doi.org/10.1016/S0967-0661(99)00040-4

Venkatasubramanian, V., Rengaswamy, R., Kavuri, S.N., 2003a. A review of process fault detection and diagnosis part II: Qualitative models and search strategies. Comput. Chem. Eng. https://doi.org/10.1016/S0098-1354(02)00161-8

Venkatasubramanian, V., Rengaswamy, R., Yin, K., Kavuri, S.N., 2003b. A review of process fault detection and diagnosis, Part I Quantitative model-based methods. Comput. Chem. Eng. 27, 293–311. https://doi.org/10.1016/S0098-1354(02)00160-6

Venkatasubramanian, V., Rengaswamy, R., Yin, K., Kavuri, S.N., 2003c. A review of process fault detection and diagnosis Part III: Process history based methods. Comput. Chem. Eng. https://doi.org/10.1016/S0098-1354(02)00160-6

Verron, S., Li, J., Tiplica, T., 2010a. Fault detection and isolation of faults in a multivariate process with Bayesian network. J. Process Control 20, 902–911. https://doi.org/https://doi.org/10.1016/j.jprocont.2010.06.001

Verron, S., Tiplica, T., Kobi, A., 2010b. Fault diagnosis of industrial systems by conditional Gaussian network including a distance rejection criterion. Eng. Appl. Artif. Intell. 23, 1229–1235. https://doi.org/https://doi.org/10.1016/j.engappai.2010.05.002

Verron, S., Tiplica, T., Kobi, A., 2007. Procedure based on mutual information and bayesian networks for the fault diagnosis of industrial systems, in: 2007 American Control Conference. IEEE, New York City, pp. 420–425.

Verron, S., Tiplica, T., Kobi, A., 2006a. Bayesian networks and mutual information for fault diagnosis of industrial systems, in: Workshop on Advanced Control and Diagnosis (ACD'06). Nancy.

Verron, S., Tiplica, T., Kobi, A., 2006b. Fault diagnosis with bayesian networks: Application to the tennessee eastman process, in: 2006 IEEE International Conference on Industrial Technology. IEEE, pp. 98–103.

Villa, V., Paltrinieri, N., Cozzani, V., 2015. Overview on dynamic approaches to risk management in process facilities. Chem. Eng. Trans. 43, 2597–2502. https://doi.org/10.3303/CET1543417

Wan, J., Li, S., 2019. Modeling and application of industrial process fault detection based on pruning vine copula. Chemom. Intell. Lab. Syst. 184, 1–13. https://doi.org/10.1016/j.chemolab.2018.11.005

Wang, Y., Liu, Y., Khan, F., Imtiaz, S., 2017. Semiparametric PCA and bayesian network based process fault diagnosis technique. Can. J. Chem. Eng. 95, 1800–1816. https://doi.org/https://doi.org/10.1002/cjce.22829

Wang, Youqing, Si, Y., Huang, B., Lou, Z., 2018. Survey on the theoretical research and engineering applications of multivariate statistics process monitoring algorithms: 2008–2017. Can. J. Chem. Eng. 96, 2073–2085. https://doi.org/10.1002/cjce.23249

Wang, Yalin, Yang, H., Yuan, X., Cao, Y., 2018. An improved Bayesian network method for fault diagnosis. IFAC-PapersOnLine 51, 341–346. https://doi.org/10.1016/j.ifacol.2018.09.443

Weber, P., Medina-Oliva, G., Simon, C., Iung, B., 2012. Overview on Bayesian networks applications for dependability, risk analysis and maintenance areas. Eng. Appl. Artif. Intell. 25, 671–682. https://doi.org/10.1016/j.engappai.2010.06.002

Westerhuis, J.A., Gurden, S.P., Smilde, A.K., 2000. Generalized contribution plots in multivariate

statistical process monitoring. Chemom. Intell. Lab. Syst. 51, 95–114. https://doi.org/https://doi.org/10.1016/S0169-7439(00)00062-9

Widodo, A., Yang, B.S., 2007. Support vector machine in machine condition monitoring and fault diagnosis. Mech. Syst. Signal Process. 21, 2560–2574. https://doi.org/10.1016/j.ymssp.2006.12.007

Wilcox, N.A., Himmelblau, D.M., 1994. The possible cause and effect graphs (PCEG) model for fault diagnosis—I. Methodology. Comput. Chem. Eng. 18, 103–116.

Wilson, D.J.H., Irwin, G.W., 2000. PLS modelling and fault detection on the Tennessee Eastman benchmark. Int. J. Syst. Sci. 31, 1449–1457. https://doi.org/10.1080/00207720050197820

Wise, B.M., Veltkamp, D.J., Davis, B., Ricker, N.L., Kowalski, B.R., 1988. Principal component analysis for monitoring the West Valley liquid fed ceramic melter. Waste Manag. 88, 811–818.

Wold, S., 1994. Exponentially weighted moving principal components analysis and projections to latent structures. Chemom. Intell. Lab. Syst. 23, 149–161. https://doi.org/10.1016/0169-7439(93)E0075-F

Wu, X., Lucas, P., Kerr, S., Dijkhuizen, R., 2001. Learning Bayesian-network topologies in realistic medical domains, in: Lecture Notes in Computer Science (Including Subseries Lecture Notes in Artificial Intelligence and Lecture Notes in Bioinformatics). Springer, Berlin, Heidelberg, pp. 1–4. https://doi.org/10.1007/3-540-45497-7_46

Yang, F., Duan, P., Shah, S.L., Chen, T., 2014. Capturing connectivity and causality in complex industrial processes, in: SpringerBriefs in Applied Sciences and Technology. Springer-Verlag, New York, pp. 41–65. https://doi.org/10.1007/978-3-319-05380-6

Yazdi, M., Kabir, S., 2017. A fuzzy Bayesian network approach for risk analysis in process

industries. Process Saf. Environ. Prot. https://doi.org/10.1016/j.psep.2017.08.015

Yin, S., Ding, S.X., Haghani, A., Hao, H., Zhang, P., 2012. A comparison study of basic data-driven fault diagnosis and process monitoring methods on the benchmark Tennessee Eastman process. J. Process Control 22, 1567–1581.

Yin, S., Ding, S.X., Zhang, P., Hagahni, A., Naik, A., 2011. Study on modifications of PLS approach for process monitoring. IFAC Proc. Vol. 44, 12389–12394. https://doi.org/10.3182/20110828-6-IT-1002.02876

Yu, H., Khan, F., Garaniya, V., 2016. Risk-based process system monitoring using self-organizing map integrated with loss functions. Can. J. Chem. Eng. 94, 1295–1307. https://doi.org/10.1002/cjce.22480

Yu, Hongyang, Khan, F., Garaniya, V., 2016a. A sparse PCA for nonlinear fault diagnosis and robust feature discovery of industrial processes. AIChE J. 62, 1494–1513. https://doi.org/10.1002/aic.15136

Yu, Hongyang, Khan, F., Garaniya, V., 2016b. An alternative formulation of PCA for process monitoring using distance correlation. Ind. Eng. Chem. Res. 55, 656–669. https://doi.org/10.1021/acs.iecr.5b03397

Yu, H., Khan, F., Garaniya, V., 2015a. Risk-based fault detection using self-organizing map. Reliab. Eng. Syst. Saf. 139, 82–96. https://doi.org/10.1016/j.ress.2015.02.011

Yu, H., Khan, F., Garaniya, V., 2015b. Modified independent component analysis and Bayesian network-based two-stage fault diagnosis of process operations. Ind. Eng. Chem. Res. 54, 2724–2742. https://doi.org/10.1021/ie503530v

Yu, H., Khan, F., Garaniya, V., 2015c. Nonlinear Gaussian belief network based fault diagnosis for industrial processes. J. Process Control 35, 178–200.

https://doi.org/10.1016/j.jprocont.2015.09.004

Yu, H., Khan, F., Garaniya, V., Ahmad, A., 2014. Self-organizing map based fault diagnosis technique for non-gaussian processes. Ind. Eng. Chem. Res. 53, 8831–8843. https://doi.org/10.1021/ie500815a

Yu, J., 2012. A nonlinear kernel Gaussian mixture model based inferential monitoring approach for fault detection and diagnosis of chemical processes. Chem. Eng. Sci. 68, 506–519. https://doi.org/https://doi.org/10.1016/j.ces.2011.10.011

Yu, J., Qin, S.J., 2008. Multimode process monitoring with Bayesian inference-based finite Gaussian mixture models. AIChE J. 54, 1811–1829. https://doi.org/10.1002/aic.11515

Yu, J., Rashid, M.M., 2013. A novel dynamic bayesian network-based networked process monitoring approach for fault detection, propagation identification, and root cause diagnosis. AIChE J. 59, 2348–2365. https://doi.org/10.1002/aic.14013

Zadakbar, O., Imtiaz, S., Khan, F., 2013. Dynamic risk assessment and fault detection using a multivariate technique. Process Saf. Prog. 32, 365–375. https://doi.org/10.1002/prs.11609

Zadakbar, O., Imtiaz, S., Khan, F., 2012. Dynamic risk assessment and fault detection using principal component analysis. Ind. Eng. Chem. Res. 52, 809–816. https://doi.org/10.1021/ie202880w

Zadakbar, O., Khan, F., Imtiaz, S., 2015. Dynamic risk assessment of a nonlinear non-Gaussian system using a particle filter and detailed consequence analysis. Can. J. Chem. Eng. 93, 1201–1211. https://doi.org/10.1002/cjce.22212

Zarei, E., Azadeh, A., Aliabadi, M.M., Mohammadfam, I., 2017. Dynamic safety risk modeling of process systems using bayesian network. Process Saf. Prog. 36, 399–407. https://doi.org/10.1002/prs.11889

Zerrouki, H., Estrada-Lugo, H.D., Smadi, H., Patelli, E., 2020. Applications of Bayesian networks in chemical and process industries: A review, in: Proceedings of the 29th European Safety and Reliability Conference, ESREL 2019. pp. 3122–3129. https://doi.org/10.3850/978-981-11-2724-30914-cd

Zhang, N., Wu, L., Yang, J., Guan, Y., 2018. Naive bayes bearing fault diagnosis based on enhanced independence of data. Sensors 18, 1–17. https://doi.org/10.3390/s18020463

Zhang, Yingwei, Teng, Y., Zhang, Yang, 2010. Complex process quality prediction using modified kernel partial least squares. Chem. Eng. Sci. 65, 2153–2158. https://doi.org/10.1016/j.ces.2009.12.010

Zhang, Yingwei, Zhang, Yang, 2010. Fault detection of non-Gaussian processes based on modified independent component analysis. Chem. Eng. Sci. 65, 4630–4639. https://doi.org/10.1016/j.ces.2010.05.010

Zhang, Z., Dong, F., 2014. Fault detection and diagnosis for missing data systems with a three time-slice dynamic Bayesian network approach. Chemom. Intell. Lab. Syst. 138, 30–40. https://doi.org/10.1016/j.chemolab.2014.07.009

Zhou, N., Li, S., 2018. Nonlinear and non-Gaussian process monitoring based on simplified R-Vine copula. Ind. Eng. Chem. Res. 57, 7566–7582. https://doi.org/10.1021/acs.iecr.8b00701

Zhu, J., Ge, Z., Song, Z., Zhou, L., Chen, G., 2018a. Large-scale plant-wide process modeling and hierarchical monitoring: A distributed Bayesian network approach. J. Process Control 65, 91–106. https://doi.org/10.1016/j.jprocont.2017.08.011

Zhu, J., Yao, Y., Li, D., Gao, F., 2018b. Monitoring big process data of industrial plants with multiple operating modes based on Hadoop. J. Taiwan Inst. Chem. Eng. https://doi.org/10.1016/j.jtice.2018.05.020

Zhu, Q.X., Luo, Y., He, Y.L., 2019. Novel multiblock transfer entropy based Bayesian network and its application to root cause analysis. Ind. Eng. Chem. Res. 58, 4936–4945. https://doi.org/10.1021/acs.iecr.8b06392